Adam Mickiewicz University in Poznań

Faculty of Biology

Institute of Molecular Biology and Biotechnology

Laboratory of Human Molecular Genetics

The role of ISRE and GAS composite-containing genes in long-term IFN-I and IFN-II responsiveness

Doctoral thesis

by

Sanaz Hassani

Prepared under the supervision of

Prof. dr hab. Hans A.R. Bluyssen

Poznań 2024

Uniwersytet im. Adama Mickiewicza w Poznaniu,
Wydział Biologii
Instytut Biologii Molekularnej i Biotechnologii
Pracownia Genetyki Molekularnej Człowieka

Rola genów zawierających elementy ISRE oraz GAS w długoterminowej odpowiedzi na IFN-I i INF-II

rozprawa w języku angielskim
ze streszczeniem w języku polskim

Autor:
Sanaz Hassani

przygotowana pod kierunkiem:
Prof. dr hab. Hans A.R. Bluyssena

Poznań 2024

CONTENTS

1 Introduction

1.1 Interferons

Isaacs and Lindenmann introduced the Interferons (IFNs) as antiviral proteins to the world of science over 60 years ago. IFNs are known as a family of cytokines that perform antiviral activity. The features of the IFN-induced antiviral responses are determined by the interaction of three essential components: the virus, the host cell, and the IFNs. (Higgins, 1984; Samuel, 2001). In addition, they have an essential role in differentiation and physiological processes acting through binding cell-surface receptors (J. Hertzog et al., 1994; Sen, 2001). IFNs production can be triggered not only by viruses but also by viral intermediates like double-stranded RNA, endotoxins, certain bacteria species and other cytokines (Taylor, 2014).The interaction between IFNs and their cell surface receptors initiates a cascade of kinase activation, resulting in the dimerization of a specific group of proteins known as signal transducers and activator of transcription (STATs) including STAT1 and STAT2. Subsequently, either Interferon Stimulated Gene Factor 3 (ISGF3), composed of STAT1/STAT2/IRF9, is formed through STAT1 and STAT2 dimerization alongside interferon regulatory factor9 (IRF9) association, or Gamma Activated Factor (GAF), consisting of STAT1 homodimers, is generated. After nuclear entry, ISGF3 binds to Interferon-Stimulated Response Element (ISRE) and GAF interacts with gamma-activated sequences (GAS) in the promoter of interferon stimulated genes (ISGs) to initiate their expression, which in turn triggers antiviral responses (Heim, 1999; Michalska et al., 2018; Taylor, 2014).

1.1.1 Types And Functions

IFNs are classified into three types including IFN-I, IFN-II and IFN-III (Table 1). IFN-I comprises IFNα, IFNβ, IFNε, IFNk and IFNω and all are placed on chromosome 9 in humans (Berry et al., 2012; O. Meyer, 2009). IFN-I activates JAK-STATs signaling pathway through IFNα/β receptors (IFNAR) comprising IFNAR1 and IFNAR2 subunits. They are produced by all cell types and more potently by plasmacytoid dendritic cells (pDCs) in antiviral responses(Iversen & Paludan, 2010; E. Yang & Li, 2020). IFN-Is assume crucial functions in establishing a protective antiviral state to impede infection transmission and modifying innate immune responses by initiating the induction of ISGs. These ISGs are engaged in antiviral activities across various cell types such as natural killer (NK) cells. Additionally, they play a pivotal role in kickstarting the adaptive immune system to foster the development B cells with high affinity for antigens

(Schreiber, 2020). Accordingly, IFN-I induces the expression of activation antigens in B cells, leading to their activation and differentiation into plasma cells. Plasma cells produce antibodies with specificity for antigens (Kiefer et al., 2012).

IFN-II contains only one member named IFNγ, binds to IFNγ receptors composed of two IFNGR1 and two IFNGR2 (Resende et al., 2017). Effector T helper 1 (Th1), CD4+ T cells, cytotoxic CD8+ T cells, NK T cells and NK cells are the primary sources of IFN-γ production. It can be also produced by other cells including dendritic cells (DCs), macrophages (Mϕ), and B cells, although to a more constrained extent**.** It's notable that certain ISGs can be activated by signaling pathways triggered by both IFN-I and IFN-II. Consequently, these two types of interferons can exhibit overlapping effects (W. Liu et al., 2022)**.** The third group is called the lambda IFNs or type III IFNs which comprise IFN-λ1, -λ2, -λ3, and -λ4 and they prompt their heterodimeric receptor comprising IFNLR1 and IL10Rβ. Moreover, IFN-III can be produced by most cell types, however, their main producers are pDCs (Fensterl et al., 2015; Iversen & Paludan, 2010; Manivasagam & Klein, 2021; Stanifer et al., 2020). Similar to IFN-I**,** IFN-III can trigger a cascade through JAK-STAT signaling upon binding to its receptors. This initiates the dimerization of receptors, activating TYK2 and JAK1 kinases, which subsequently phosphorylate STAT1, leading to the formation of STAT1 homodimers, or phosphorylate STAT2, which associates with IRF9 to form ISGF3. These complexes interact with GAS and ISRE, respectively in the promoter of ISGs, inducing their expression (Lazear et al., 2019; Stanifer et al., 2020)**.** It's important to highlight the similarity between IFN-I and IFN-III in their induction mechanisms as they both activate the JAK-STAT signaling pathway and regulate ISGs via ISGF3. It has also been noted that, like IFN-I, the promoter of the IFN-III gene contains binding sites for both IRF3 and IRF7, suggesting potential co-expression with type I IFNs (Osterlund et al., 2007; Wack et al., 2015). Detecting infections by intercellular receptors induce the expression of IFNs which later activate the transcription of ISGs. These ISGs play a crucial role in combating viral and other pathogenic threats. Therefore, viruses and bacteria are potent inducer of IFNs response (Iversen & Paludan, 2010)**.** Stimulation of Pattern-Recognition Receptors (PRR) initiate producing type-I interferons as the first part of innate immune response (A. J. Lee & Ashkar, 2018; Raftery & Stevenson, 2017)**.** Accordingly, different host cell types such as pDCs can recognize the exogenous nucleic acids such as bacterial or viral DNA or RNA via their PRR which initiates the activation of different signaling cascades leading to the induction of IFN-I (Bowie & Unterholzner, 2008)**.** On the other

hand, NK cells as one of the main producers of type II interferons can be activated by different cytokines such as IFN-I, Interleukin 12, 15, 18 (IL-12, IL-15, and IL-18) (A. J. Lee & Ashkar, 2018).

The majority of therapeutic IFNs are generated via genetic engineering. IFNα, being the initial approved biotherapeutic, set the stage for the subsequent development of numerous biotherapeutics, indicating effective options for immune-related disease (Pestka et al., 2004).

IFN type	Subgroups	Receptors	Cell producers
IFN-I	IFNα, IFNβ, IFNε, IFNk and IFNω	IFNAR1, IFNAR2	Plasmacytoid dendritic cells, Fibroblasts, Epithelial cells, Leukocytes, Macrophages
IFN-II	IFN-γ	IFNGR1, IFNGR2	Activated T cells, NK cells, NK T cells
IFN-III	IFN-λ1, IFN-λ2, -IFN-λ3, and IFN-λ4	IFNLR1, IL10Rβ	Plasmacytoid dendritic cell, Epithelial cells

Table1. Interferon classification based on type, receptors and cells producers (Maher et al., 2007; Odendall & Kagan, 2015).

1.1.2 Interferon Production

Pathogen-associated molecular patterns (PAMPs) derived from microbes, such as microbial Lipopolysaccharide (LPS), viral DNA and RNA can initiate immune responses. Additionally, host inflammatory reactions can induce cellular damage, prompting the release of endogenous molecules from host cells termed damage-associated molecular patterns (DAMPs) (Jounai et al., 2012; Silva-Gomes et al., 2015)**.** Genomic DNA or mRNA, Heat Shock Proteins (HSPs) and ATP are examples of DAMPs (Garg et al., 2013)**.** Generally, PRRs like Toll-like receptors (TLRs), retinoic acid-inducible gene-I (RIG-I)-like receptors (RLRs) and melanoma differentiation-associated gene 5 (MDA5) are present in DCs, Mϕ and even fibroblasts, recognize DAMPs and PAMPs, and initiate the immune response (Colonna et al., 2002; Takeuchi & Akira, 2010). In humans, TLRs are receptors found either on the cell surface such as TLR1, TLR2, TLR4, TLR5, TLR6, and TLR10 or on the endosome membrane including TLR3, TLR7, TLR8, and

TLR9 (Kawasaki & Kawai, 2014; Mielcarska et al., 2020). In contrast, RIG-I and MDA5 serve as prominent cytoplasmic receptors (G. Li et al., 2024). pDCs are considered as main IFN-I producers that can be activated after recognition of viral RNA and DNA by TLR7, TLR8 and TLR9. subsequently, TLR7 and TLR9 employ the adaptor protein myeloid differentiation primary response protein 88 (MyD88) to their intracellular Toll/Interleukin-1 Receptor (TIR) domains. MyD88 then acts as an adaptor that recruits other signaling molecules such as tumor necrosis factor receptor-associated factor 6 (TRAF6) to the TLR7 and 9. Consequently, TRAF6 promotes the IRF5 and IRF7 polyubiquitination which is a necessary step for their activation and nuclear entry. After nuclear entrance of IRF5 and IRF7 they bind to promoter of IFNα and IFNβ and induce their expression. Through a positive feedback loop, IFNβ and IFNα activates JAK-STAT pathway by binding to their receptors on the cell surface and induce the expression of IRF7 and IRF5 respectively. (Figure1) (Balkhi et al., 2008; Fitzgerald-Bocarsly & Feng, 2007; Negishi et al., 2006).

Mϕ have the capability to generate IFN-I not only through TLRs but also via RIG-I and MDA5, akin to fibroblasts. When RIG-I detects short viral double-stranded RNA (dsRNA), MDA5 identifies long genomic dsRNAs (Reikine et al., 2014). These receptors transmit their signal through the mitochondrial antiviral-signaling protein (MAVS). The caspase activation and recruitment domain (CARD) situated at the N-terminal of MAVS associates with the CARD domain of RIG-I or MDA5, resulting in MAVS activation. Activated MAVS, triggers the involvement of TANK-binding kinase 1 (TBK1) and inhibitor of κB kinase (IKKϵ), resulting in the phosphorylation of IRF3 and IRF7. These phosphorylated factors then translocate to the nucleus, initiating the expression of IFNα and IFNβ genes. (Ali et al., 2019; Balkhi et al., 2008; Cham et al., 2012; Kawai & Akira, 2006; Pitha, 2007; Reikine et al., 2014; Wu et al., 2023)**.** Furthermore, cDCs can undergo activation subsequent to the identification of viral double-stranded DNA by cyclic GMP-AMP synthase (cGAS) (Kaushal, 2023). This process leads to the production of cyclic guanosine monophosphate–adenosine monophosphate (cGAMP), which in turn causes the activation of stimulator of interferon genes (STING). Upon activation, STING induces autophosphorylation of TBK1 leading to the subsequent phosphorylation of IRF3. Phosphorylated IRF3 then relocates to the nucleus, initiating the expression of IFN-I gene (Decout et al., 2021; G. Li et al., 2024). As mentioned above**,** DAMPs and PAMPs are recognized by PRRs. PRRs are also expressed by classical antigen-presenting cells (APCs) including Mϕ and

DCs (Gaudino & Kumar, 2019). After PAMPs and DAMPs recognition, Mϕ and DCs produce IL-12 and IL-18 which activate NK and Th1 cells (Frucht et al., 2001). As a result of their activation, NK and Th1 cells stimulate the T-box transcription factor TBX21, also known as T-bet, which directly promotes the expression of the IFN-II gene (Oh & Hwang, 2014; R. Yang et al., 2020). Moreover, Mϕ and DCs process and present antigens to naïve T cells via major histocompatibility complex (MHC) molecules. This interaction leads to the activation and differentiation of naïve T cells into Th1 cells which produce IFN-II (Figure 1) (Gaudino & Kumar, 2019).

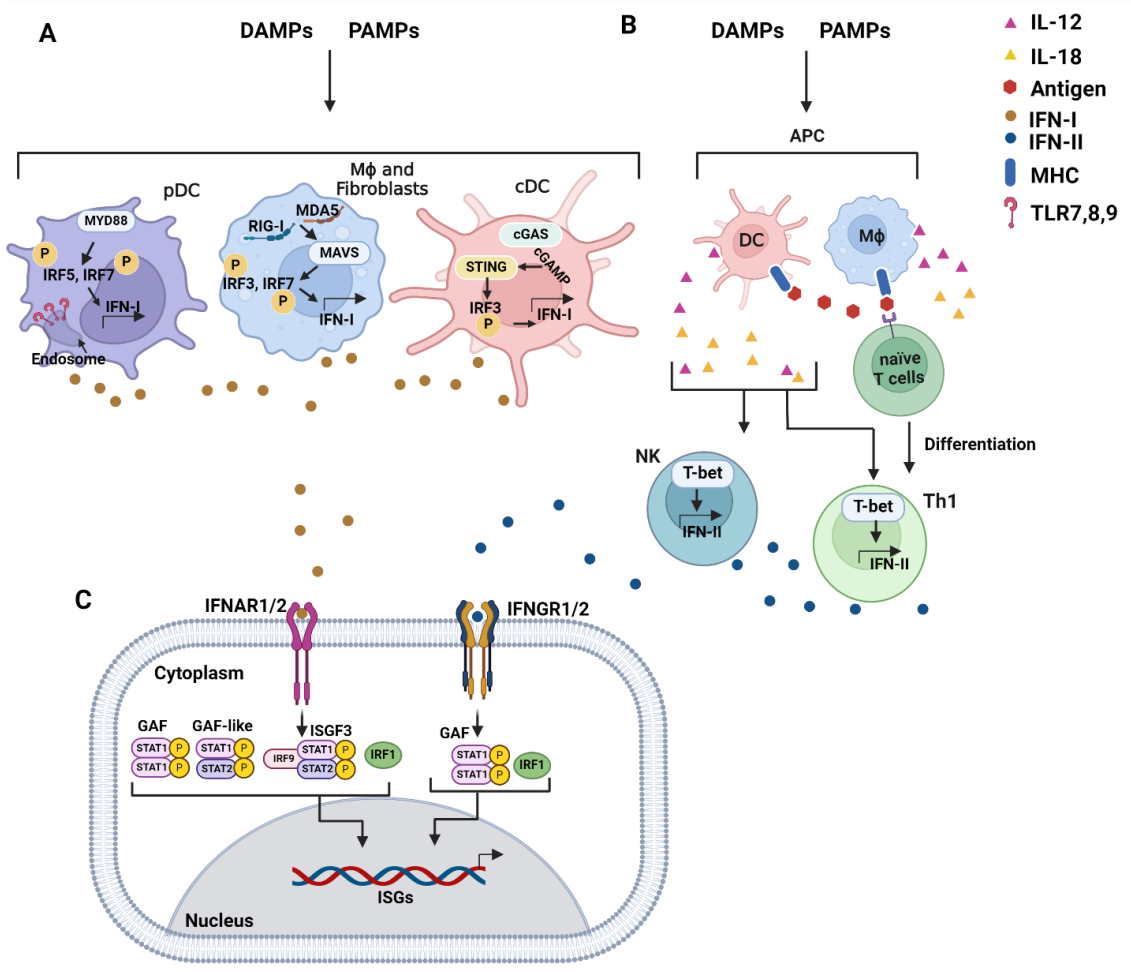

Figure 1. A streamlined schematic representation of IFN-I and IFN-II production. (Description continues on the next page)

Immune response is initiated through PAMPs or DAMPs that activate different immune cells. **(A).** DAMPs and PAMPs are detected by PRRs such as TLRs in pDCs, as well as RIG-I and MDA5 in Mϕ and fibroblasts, along with cGAS in cDCs. In pDCs , MyD88 pathway is activated through TLR7 and 9 and subsequently, IRF5 and IRF7 are phosphorylated and trigger the induction of IFN-I gene. IFN-I production is also triggered in fibroblasts and Mϕ through the activation of RIG-I and MDA5 receptors. These receptors engage MAVS, leading to the activation of IRF3 and IRF7. Through the activation of cGAS receptors, cDCs initiate IFN-I production. This activation results in the generation of cGAMP, which in turn activates IRF3 via the subsequent activation of STING. **(B).** Antigen presenting cells such as DCs and Mϕ recognize DAMPs and PAMPs through PRRs and produce IL-12 and IL-18. Also, DCs and Mϕ cells present antigen to naïve T cells leading to their differentiation to Th1 cells. IL-12 and IL-18 activate NK and Th1 to produce IFN-II via T-bet**. (C)** The produced IFN-I and IFN-II binds to their receptors (IFNARs and IFNGRs) leading to GAF,GAF-like, ISGF3 and IRF1 formation in response to IFN-I and GAF and IRF1 after IFN-II stimulation. Subsequently, after nuclear entry, ISGF3 and IRF1 target ISRE site, and GAF and GAF-like interact with GAS elements in the promoter of ISGs and trigger gene expression (G. Li et al., 2024; Reikine et al., 2014; R. Yang et al., 2020).

1.2 Type I And II Interferon Signaling Pathways

As previously mentioned, IFN-I and IFN-II induce the expression of ISGs through the JAK–STAT pathway. In this pathway (Figure 2), JAKs phosphorylate STAT1 and STAT2 proteins. IRFs also play crucial roles in regulating ISGs during IFN signaling. STAT1 (Tyr701) and STAT2 (Tyr690) are phosphorylated by JAK1 and TYK2 in the canonical IFN-I pathway. These proteins then heterodimerize and associate with IRF9 to form the ISGF3 complex which translocates to the nucleus, binds the ISRE in ISG promoters, and activates transcription of over 300 ISGs (e.g., ISG15, OAS1-3, IFIT1-3, MX1, MX2) essential for antiviral activity. IFN-II specifically induces STAT1 phosphorylation via JAK1 and JAK2. STAT1 then forms the GAF complex through homodimerization. Subsequently, GAF activates ISGs by interacting with GAS in their promoters. GAF is also present in the IFN-I pathway, inducing ISGs. The STAT1/STAT2 heterodimers (GAF-like) can also target GAS elements in ISG promoters in response to IFN-I. IRF1 is a key regulator of ISGs induced by both IFN-I and IFN-II. It targets GAAA and ISRE sites in the promoter of ISGs. It also acts as an active transcription factor, providing protective functions at the basal level (Feng et al., 2021; Kalvakolanu, 2003; X. Li et al., 1996; Michalska et al., 2018; Paul et al., 2018; L. Xu et al., 2016).

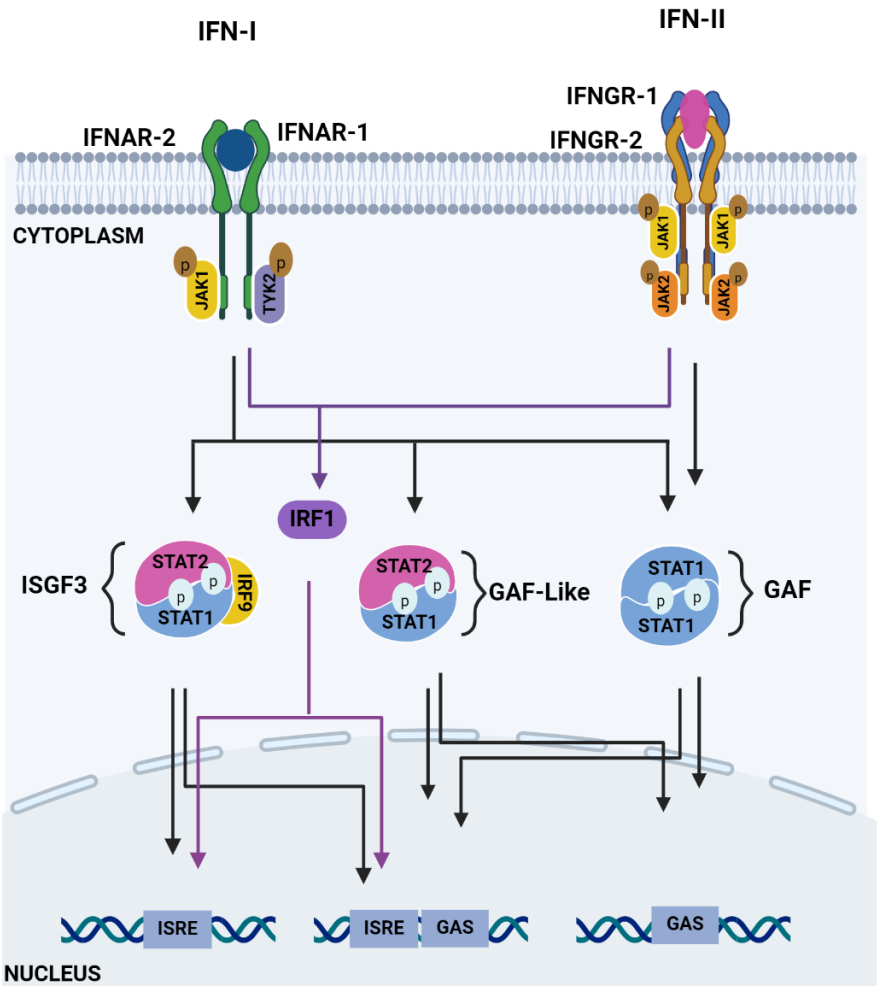

Figure 2. A general schematic Model of IFNα and IFNγ Signaling Pathways.

IFNAR serves as the receptor for IFN-I, while IFNGR acts as the receptor for IFN-II. Upon interaction between IFN and their respective receptors, a signaling cascade is initiated, leading to the phosphorylation of Janus kinases (JAK) and subsequently resulting in the phosphorylation and dimerization of STATs. Upon stimulation by IFN-I, heterodimers of STAT1 and STAT2 associate with IRF9 and form the ISGF3 complex. In addition to ISGF3, GAF, GAF-like and IRF1 are other transcription activators in the IFN-I signaling pathway. Conversely, after stimulation by IFN-II, STAT1/STAT1 homodimers form the GAF complex which along with IRF1, triggers the induction of ISGs. Subsequently, after nuclear entry, ISGF3 and IRF1 target ISRE element present in the promoter of ISGs and induce them, while GAF and GAF-like interact with GAS element. Thereby, these ISGF3, IRF1, GAF and GAF-like together with ISRE+GAS composite genes can explain functional overlap of IFN-I and IFN-II (Michalska et al., 2018).

1.3 Janus Kinases (JAKs)

Cytokine receptors consist of intracellular domains that are connected to the cytoplasmic Janus protein tyrosine kinase (JAKs) members (R. Morris et al., 2018). JAKs family contains four subgroups including Jak1, Jak2, Jak3, and Tyk2 which have significant roles in interfering with pathways in innate and adaptive immune response. They are characterized as proteins with

considerable size, comprising over 1000 amino acids. The structural domains within the Jak family members are composed of seven discernible Jak homology regions (JH1 to JH7) (Figure 3) (Firmbach-Kraft et al., 1990; Ghoreschi et al., 2009; Jain et al., 2021). The 4.1 protein, ezrin, radixin, and moesin FERM domain (JH7-JH6-JH5) is involved in the protein-protein interactions and their binding to the receptors occurs via JH7 and JH6. The SH2 domain (JH4-JH3) is responsible for engaging phosphotyrosine residues and facilitating STATs dimerization. The pseudokinase domain (JH2) serves a regulatory element and controls the function of the kinase domain. The kinase domain (JH1) is responsible for the phosphorylation of tyrosine on STATs proteins (Mengie Ayele et al., 2022; Nan et al., 2017; Seif et al., 2017).

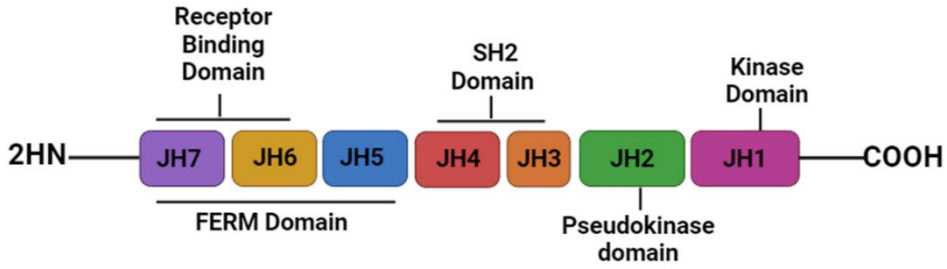

Figure 3. Illustrative diagram of the JAK proteins' structure

JAKs are characterized by seven closely related regions termed Janus homology domains (JHD) 1 through 7. The FERM domain facilitates JAK binding to the receptors. SH2 domain mediates the dimerization of STATs. JH2 domain functions as a pseudo-kinase domain, controlling the catalytic activity of JH1. JH1 is responsible for encoding the kinase function and STATs phosphorylation (Jain et al., 2021; M. Lee & Rhee, 2017; Mengie Ayele et al., 2022; Nan et al., 2017; Seif et al., 2017).

Jak1 and Jak2 can receive activation signals from a range of cytokines, including IFN-I and IFN-II. Jak3 forms a unique connection with the cytokine receptor γ chain which serves as a common element among receptors for IL-2, 4, 7, 9, and 15 (M. Chen et al., 1997). Whereas Tyk2 responds specifically to the activation induced by IFN- α/β and IL-12. Jak kinases interact with cytokine receptors using their N-terminal region. The binding of cytokines with receptors prompts receptor dimerization, facilitating the proximity of JAKs. This close proximity triggers JAK activation through transphosphorylation. Afterwards, activated JAKs phosphorylate tyrosine residues on the receptor, establishing docking sites for STAT proteins via their SH2 domains. STATs are then recruited to these docking sites on the receptor and phosphorylated by JAKs on their tyrosine residue. The STAT phosphorylation prompts STAT dimerization, nuclear entry and finally transcription activity (Leonard, 2001; Michalska et al., 2018; R. Morris et al., 2018; Seif et

al., 2017; Yeh & Pellegrini, 1999). The JAK/STAT pathway may experience negative regulation through the action of the suppressor of cytokine signaling (SOCS), which is induced by STAT proteins. This mechanism operates through a negative feedback loop: STATs elevate the expression of SOCS, which in turn inhibits the activity of JAKs, thereby exerting control over the pathway to prevent chronic inflammatory response (Kershaw et al., 2013; Nicola & Greenhalgh, 2000). Hadjadj et al. conducted a study revealing continuous phosphorylation of STAT1 in lymphocytes of patients with insufficient SOCS1. This phenomenon results in heightened activation of the STAT/JAK pathways, contributing to elevated inflammatory responses and autoimmune reactions (Hadjadj et al., 2020).

1.4 Signal Transducers And Activators Of Transcription (STAT) Proteins

STATs are transcription factors including STAT1, STAT2, STAT3, STAT4, STAT5Aa, STAT5b, STAT6 that are located in cytoplasm stimulating transcription of specific genes. They contain seven conserved regions: N-terminal domain (NTD) moderates STATs molecules interaction. This domain facilitates dimerization and oligomerization of STAT proteins (Awasthi et al., 2021; Hu et al., 2015; R. Morris et al., 2018; Nan et al., 2017). The coiled coil domain (CCD) enhances the affinity for binding to various transcription factors and enables interactions between proteins. Moreover, studies on murine STAT3 unveiled that CCD is required for tyrosine phosphorylation of STAT3 which is essential for its subsequent activation (T. Zhang et al., 2000). DNA binding domain (DBD) as a conserved domain among STAT proteins facilitates binding to the GAS site in the promoter of ISGs. Additionally, this domain contains nuclear localization signals (NLS) and nuclear export signals (NES) which are responsible for translocation of STATs between cytoplasm and nucleus. The interaction between DBD and Linker domain modulates the overall transcriptional activity of STAT proteins (Ebersbach et al., 2021; Hüntelmann et al., 2014; C.-J. Lee et al., 2020). Throughout the activation of STATs and their binding to DNA, the linker domain ensures stability and facilitates the process. Research on the STAT1 protein from Human U3A cells suggests that the linker domain serves as a site that promotes the interaction between STAT and other transcriptional complexes (Awasthi et al., 2021; E. Yang et al., 1999). Src Homology 2 domain (SH2) is another conserved domain among STATs family members. The domain interacts with regions containing phosphotyrosine, enabling interaction with other STATs and receptors (Awasthi et al., 2021). The transactivation domain (TAD) is responsible for transcriptional activation function. It also plays an important role in facilitating the degradation of

STAT proteins through the ubiquitin pathway (Ebersbach et al., 2021). Studies on the TAD domain of STAT1 protein revealed that TAD is pivotal for mediating the binding of TFs to the promoter of irf1 and irf8 genes in mice cells (Parrini et al., 2018).

STAT proteins can form both homodimers and heterodimers. During cytokine exposure, Phosphorylation of STAT proteins on a specific tyrosine allows the SH2 domain of one STAT monomer to bind to the phosphotyrosine of another STAT monomer. This phosphorylation promotes the parallel formation of STATs monomers in which both monomers have the same orientation. However, in the absence of cytokine the formation of unphosphorylated dimers occurs through an antiparallel conformation in which the two STAT monomers are aligned in opposite orientations (Begitt et al., 2023; Zhong et al., 2005). In general, after cytokine exposure, the recruitment of STATs on the receptors by JAKs occurs which in turn induces their phosphorylation at a tyrosine residue leading to STAT dimerization. These dimers then move into the nucleus, where they bind to specific DNA elements known as GAS, characterized by the consensus sequence TTTCNNNGAAA, and initiate gene expression (Ehret et al., 2001; Kang et al., 2013).

1.4.1 STAT1

Gene targeting studies provided confirmation of the indispensable role played by STAT1 in mediating the biological responses to both type I and type II IFNs. STAT1 was first characterized as a component of ISGF3 within the IFN-I signaling cascade. Later, scientists uncovered that GAF binding to GAS, is constituted by STAT1 homodimers (Schindler et al., 2007). STAT1 is a 91-kDa protein consisting of 750 amino acid residues. Like other members of the STAT family, the STAT1 protein includes the NTD, CCD, DBD, Linker domain, and SH2 domain, pY along with a C-terminal TAD domain (Figure 4) (Meng et al., 2017). NTD promotes interactions among STAT molecules and facilitates STAT dimerization and their transcriptional activity. In a study by Göder et al. involving IFN-α-treated U3C cells transfected with vectors containing NTD-mutated STAT1, it was found that alterations in STAT1 NTD led to reduced phosphorylation levels. Interestingly, these mutations did not influence the translocation of STAT1 into the nucleus (Boisson-Dupuis et al., 2012; Göder et al., 2021). The CCD aids in binding to other transcription factors like IRF9. In addition, it has been proven that the CCD plays a crucial role in both the activation of STAT1 and the regulation of DNA binding. Accordingly, mutations in the CCD of human STAT1 resulted in STAT1 hyperactivation and an augmented DNA binding

affinity. Consequently, this leads to elevated expression of target genes following IFN stimulation. DBD on the one hand is responsible for binding to GAS sequence, on the other hand, it comprises NLS and NES which are involved in nuclear import and export, respectively. Following STAT1 dimerization, the NLS becomes activated and attaches to importin-α, which subsequently binds to importin-β. This complex then undergoes translocation into the nucleus. Conversely, during nuclear export, dephosphorylation of tyrosine 701 takes place, inducing conformational changes. Afterwards, the NES interacts with exportin, facilitating the nuclear export of STAT1 (Awasthi et al., 2021; N. C. Reich, 2013; Remling et al., 2023; Tolomeo et al., 2022). The precise role of the linker in STAT1 remains partially understood; however, findings from the study of Yang et al. on IFN-γ-treated U3C cell lines indicated that mutations in the linker domain may impede STAT1's ability to bind to DNA, consequently suppressing the expression of STAT1 target genes. The SH2 domain directs its attention to phosphorylated tyrosine residues (pY 701) on STAT1, initiating STAT1 dimerization. Moreover, the SH2 domain accelerates the interaction between STAT1 and the JAK tyrosine kinases, which is crucial for the phosphorylation and activation of STAT1. The results of the study on U3-SH2mut cell lines revealed that the Arg → Gln mutation in the SH2 domain rendered STAT1 incapable of dimerizing in response to IFN-I, underscoring the significance of the SH2 domain in STAT1 dimerization. As the final domain of STAT1, TAD is accountable for interacting with other transcription factors and aiding in the recruitment of co-factors like RNA pol II to the promoters of targeted genes. Additionally, it contributes to enhancing the DNA binding capability of STAT1 by interacting with the histone acetyltransferase CBP/p300 (Gupta et al., 1996; Kim & Lee, 2007; X. Li et al., 2021; Mowen & David, 1998; E. Yang et al., 2002).

Despite STAT1 homodimers, STAT1 can form heterodimers with other STATs such as STAT1/STAT2, or STAT1/STAT2 associated with IRF9 to form ISGF3 in response to IFNα, or STAT1/STAT3 which is generated in response to IL-6 (Delgoffe & Vignali, 2013). Additionally, the STAT1/STAT2 hemi-phosphorylated dimers are another STAT1 heterodimerization that formed when STAT1 is phosphorylated but STAT2 remains unphosphorylated that forms an antiparallel conformation that makes it unable to import the nucleus. However, it is suggested that STAT1/STAT2 hemi-phosphorylated can modulate ISGF3 activity (Ho et al., 2016). In addition to the canonical phosphorylation of STAT1 at tyrosine 701 (Tyr701), phosphorylation at serine 727 (Ser727) is mediated by PI3K and Akt. This phosphorylation event is necessary for achieving

maximal activation and transcriptional activity of STAT1 in response to IFN-II (Nguyen et al., 2001). Despite the fact that pSTATs are active transcriptional factors, unphosphorylated STATs can also promote gene transcription (R. Morris et al., 2018). Hyeon Joo Cheon and colleagues demonstrated in their study that elevated levels of unphosphorylated STAT1 (Un-STAT1) can trigger gene expression in BJ fibroblasts (human fibroblasts established from skin). Although the precise mechanism remains unclear, it is proposed that a complex comprising unphosphorylated STAT1 and IRF1 engages with both the 2/γ-interferon-activated sequence (ICS-2/GAS) elements situated on a promoter of a gene called Low molecular mass peptide 2 (LMP2), thereby initiating the transcriptional activation cascade for this gene (Cheon & Stark, 2009; Chatterjee-Kishore et al., 2000). Investigation on STAT1 unveiled the significance of this protein in the activation of innate and adaptive immune responses. It is required for maturation of NK cells and their ability to destroy tumor cells or proliferation of CD8 T lymphocytes (Meissl et al., 2020; Gil et al., 2006). Reports indicate that patients with a mutated form of STAT1 experience dysfunction in the IFN pathway, rendering them susceptible to lethal viral infections (Tolomeo et al., 2022). Conversely, reports have indicated that individuals with gain-of-function (GOF) alleles in the STAT1 gene exhibit persistent phosphorylation of STAT1, leading to autoimmune manifestations (Boisson-Dupuis et al., 2012). Overall, STAT1 stands out as an essential protein needed for proper functioning of the immune system and its presence is indispensable for the orchestration of various immune responses against pathogens.

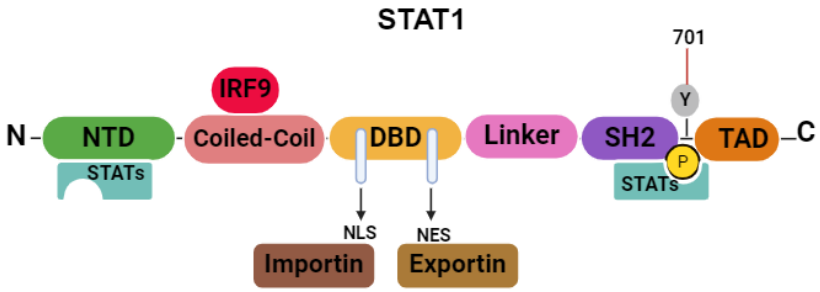

Figure 4. Structure of the STAT1 protein.

STAT1 protein consists of six domains that govern their functionality. These include the NTD, which facilitates interactions between STAT molecules; the CCD, promoting binding to other transcription factors such as IRF9. DBD is responsible for binding to specific DNA sequences. The shuttling between cytoplasm and nucleus is mediated by NLS and NES ; the linker domain, provides support during DNA binding; the SH2 and tyrosine 701 phosphorylation (pY), enabling dimerization; the TAD enables interactions with TFs, including RNA pol II (Awasthi et al., 2021; Blaszczyk et al., 2016; R. Morris et al., 2018; N. C. Reich, 2013)

1.4.2 STAT2

STAT2 plays a central role as a signaling mediator, influencing a considerable portion of the apoptotic and anti-proliferative responses triggered by IFN-α/β (Chowdhury & Farrar, 2013). STAT2, weighing 113 kDa, stands as the largest member of the STAT family. It also has similar domains as other STAT members such as NTD, CCD, DBD, linker domain , SH2 with tyrosine phosphorylation site, and TAD (Figure 5).

NTD in STAT2 comprises of eight short α-helices and it is responsible for interaction with unphosphorylated STATs. The CCD is a conserved domain among STATs and involved in the interaction with IRF9 which is required for ISGF3 formation. CCD can also interact with other proteins (Rengachari et al., 2018; Sobhkhez et al., 2014). The DBD in STAT2 protein contains NLS and NES which are responsible for nuclear import and export, respectively. Importin recognizes the NLS, enabling nuclear import, while exportin identifies the NES, promoting nuclear export. The activation of NLS/NES in DBD occurs after phosphorylation and dimerization. Despite the presence of a functional DBD in STAT2 protein no evidence is available regarding the direct DNA binding of active STAT2 homodimers. Instead, STAT2 predominantly engages in heterodimerization with STAT1 (Blaszczyk et al., 2016; HansA. R. Bluyssen & Levy, 1997; C.-J. Lee et al., 2020; N. C. Reich, 2007; Schindler et al., 2007; Steen & Gamero, 2012). The interaction between SH2 and pY is involved in the formation of the STAT1/STAT2 heterodimers. In fact, the activation of STAT2 is mediated by phosphorylation on tyrosine 690 (Y690). The STAT2 SH2 domain plays a pivotal role in mediating the interaction between STAT2 and the activated IFNα receptor. This interaction is facilitated through the recognition of phosphotyrosyl residues within the cytoplasmic domain of the IFNα receptor by the STAT2 SH2 domain. Mutations occurring in the SH2 domain of STAT2 resulted in extended tyrosine phosphorylation of both STAT1 and STAT2 upon exposure to IFN-I. Consequently, this sustained phosphorylation perpetuates their transcriptional activity within the nucleus, ultimately enhancing the apoptotic response to IFN-I (Gupta et al., 1996; Platanitis & Decker, 2018; Scarzello et al., 2007; B. Wang et al., 2020). As last domain of STAT2 protein, TAD is responsible for coordinating gene transcription through engaging transcriptional coactivators. TAD is involved in the recruitment of other co-factors such as p300/CBP, which serves as a connecting link between transcription factors and transcriptional apparatus (Awasthi et al., 2021; Duncan & Hambleton, 2021; C.-J. Lee et al., 2020; Karamouzis et al., 2007). Like DBD, it also comprises a NES. However, unlike the NES in the DBD, which is

activated after dimerization, the NES in the TAD domain remains consistently active (Blaszczyk et al., 2016).

In general, STAT2 plays a role in bringing STAT1, STAT2, and IRF9 together to form the ISGF3 complex. Furthermore, it promotes the transcriptional activation of the complex without directly binding to DNA (C.-J. Lee et al., 2020). In addition to its role in the ISGF3 complex, STAT2 has been demonstrated to form heterodimers with other STATs, such as STAT6 (STAT2/STAT6), which are induced to form by IFN-I induced B cells (Delgoffe & Vignali, 2013). Studies on IFN-α-treated U266 cells have revealed that STAT2 can dimerize with STAT3 (STAT2/STAT3) and bind to the regulatory element within the IRF1 gene. Nevertheless, the operational mechanism of STAT2/STAT3 functions remained unclear (Ghislain & Fish, 1996).

Many studies have delved into the function of STAT2 and IRF9 as a complex (STAT2/IRF9). In STAT1 knockout (STAT1KO) cells, unphosphorylated STAT2 associated with IRF9 (U-STAT2/IRF9) has been observed to shuttle between the cytoplasm and nucleus, maintaining basal expression of ISGs. Upon stimulation with IFNα, phosphorylation of STAT2 initiates the formation of STAT2/IRF9 complexes, which bind to ISRE motifs of ISGs with lower affinity as compared to ISGF3. Steen and his team provided more information regarding STAT2 Ser287 phosphorylation. Their findings uncovered that mutating STAT2 at Ser287 to alanine (S287A) increased IFNα-mediated biological effects by prolonging ISG expression and provided better protection against VSV compared to wild-type cells. They also reported that STAT2 Ser734 phosphorylation negatively regulates IFNα's antiviral response. Mutating Ser734 to alanine resulted in higher induction of ISGs like IFIT2, IFIT3, and OASL, enhancing antiviral responses. Moreover, Wang and colleagues found that mutating mice STAT2 at Thr404 (T404) to alanine prevents its phosphorylation, maintaining the anti-parallel conformation of U-STAT2 and U-STAT1 without IFN-I stimulation. Upon IFN-I stimulation, STAT2 Thr404 phosphorylation increased ISGF3's affinity for ISRE elements by accelerating the tyrosine phosphorylation of both STAT2 and STAT1 (Fink & Grandvaux, 2013; Steen & Gamero, 2013; Steen et al., 2013; Y. Wang et al., 2021).

Studies on STAT2 deficiencies unveiled that STAT2 plays a significant role during viral infection and the absence of STAT2 results in severe issues such as irregularities of inflammatory pathways in macrophages (Jordan, 2023). Furthermore, it has been reported that STAT2 is

necessary for facilitating the association of STAT1 with the IFN-I receptors (IFNAR), as evidenced by the absence of STAT1 phosphorylation in cell lines with STAT2 deficiency (Hambleton et al., 2013). Research conducted by Bucciol et al. revealed that human fibroblasts immortalized by Simian Virus 40 (SV40 fibroblasts) derived from individuals with STAT2 deficiency exhibited increased susceptibility to herpes simplex virus 1 (HSV-1) infection in vitro compared to SV40 fibroblasts from healthy controls. This underscores the critical involvement of STAT2 in the immune response (Bucciol et al., 2023).

In summary, it is evident that STAT2 has a crucial impact on various aspects of the immune system, signifying its importance in directing immune responses.

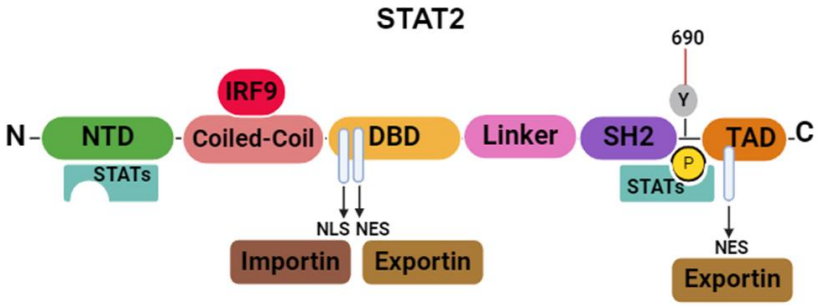

Figure 5. Structure of the STAT2 protein.

There are six domains in STAT2 protein that shares with STAT1 protein. These domains are NTD, the CCD, DBD, linker, the SH2 followed by tyrosine phosphorylation (pY) and TAD . NTD Contributes to the formation of unphosphorylated dimers with other STATs. The interaction of STAT2 and IRF9 occurs via CCD. DBD contains nuclear localization signal NLS and NES that activated after dimerization and facilitate nuclear import and export, respectively. NLS is recognized by importin and NES is recognized by exportin. SH2 and pY 690 are responsible for STAT1 and 2 dimerization. lastly, TAD domain that comprises NES binds to exportin and involved gene expression by recruiting other co-factors (R. Morris et al., 2018; Blaszczyk et al., 2016; Platanitis & Decker, 2018).

1.5 Interferon Regulatory Factors (IRFs)

IRFs were initially identified in the year 1988. IRFs serve as pivotal mediators in the signal transduction processes linked to immune response . In mammals There are 9 members of IRFs (IRF1, IRF2, IRF3, IRF4, IRF5, IRF6, IRF7, IRF8 and IRF9) that exhibit a structure with multiple domains. Recently, the identification of IRF10 and IRF11 has been reported. IRF10 was discovered in fish and birds, whereas IRF11 was identified only in fish . All nine members of IRFs share N-terminal DBD with a helix-turn-helix motif that comprises five conserved tryptophan repeats. While, C terminal domain shows diversity and plays a role in IRFs interaction with other IRF family members and non-IRF proteins. it consists of IRF association domain 1 or 2 (IAD1 , IAD2). All IRF family members except IRF1 and IRF2 possess IAD1, while IAD2 is found in

only IRF1 and IRF2. The functionality of each IRF member is tailored by the IADs, which aid protein-protein interactions and impart distinct roles and functions. Moreover, IADs mediate dimerization and activation of IRFs and their binding to co-activators like CBP/p300 which acts as a bridge between IRFs and transcriptional machinery (Antonczyk et al., 2019; Jefferies, 2019; Paul et al., 2018; Alsamman & El-Masry, 2018; W. Chen & Royer, 2010). Besides their involvement in ISGs expression through IFN-I signaling cascades, they also have crucial roles in the development of Th2 cells or Th differentiation. IRFs abnormalities are associated with different diseases including multiple sclerosis (IRF1 polymorphisms), susceptibility to systemic lupus erythematosus (SLE) (IRF3 , IRF7, IRF8 polymorphisms), Rheumatoid arthritis (IRF4 and IRF5 polymorphisms) (Kaur & Fang, 2020; Matta et al., 2017).

DBD of IRF1 and IRF2 identify the consensus sequence G(A)AAAG/CT/CGAAAG/CT/C, referred to IRF-E. Conversely, IRF9 targets a similar sequence known as ISRE, represented by A/GNGAAANNGAAACT. Notably, IRF1 and IRF2 distinctly recognize the sequence GAAA by the presence of five tryptophan repeats within their DBDs (R. Zhang et al., 2012; Takaoka et al., 2008; Shah & Choi, 2016)**.** Structural studies on IRF3 and IRF7 uncovered that phosphorylation of IRFs triggers their conformational changes which subsequently lead their dimerization. IRFs interact with DNA through the formation of homodimers, such as IRF1/IRF1 and IRF3/IRF3, or heterodimers like IRF3/IRF7. They also engage in complex formation with various transcriptional regulators, including STATs (e.g., ISGF3, STAT2/IRF9, STAT1/IRF9, STAT2/STAT6/IRF9), PU1 (IRF/PU1), and NF-κB (NF-κB/IRF). These complexes subsequently initiate the transcription of ISGs (W. Chen & Royer, 2010; Antonczyk et al., 2019).

1.5.1 IRF9

Discovered as a constituent of the ISGF3 complex, IRF9, also recognized as ISGF3γ or p48, which is part of the broader IRFs family (Suprunenko & Hofer, 2016). Similar to other IRFs, IRF9 protein (Figure 6) comprises a conserved DBD which includes five tryptophan residues that are responsible for interacting with DNA. NLS is located in the DBD and is recognized by importin enabling the nuclear import of IRF9. NLS comprises basic amino acids KGKYK and KTRLR which are separated by 10 amino acids**.** Following DBD, there is a linker juxtaposed with IAD1. The linker mediates the connection between the IAD and DBD domains. IAD1 is required to

interact with STAT1 and 2 proteins to form ISGF3, STAT2/IRF9 and STAT1/IRF9 complexes which are able to bind DNA through ISRE (A/GNGAAANNGAAACT) recognition by DBD of IRF9. While IRF9 can also interact with STAT1, its affinity for STAT1 is noticeably lower compared to STAT2.

In a study conducted by Paul et al. it has shown that IRF9 undergoes phosphorylation at residues S252 and S253 following IFNβ stimulation, and at residue R242 in the absence of IFN stimulation. All three residues are located at the IAD1. Introducing mutations in S252 and S253 decreased the expression of ubiquitin-specific peptidase 18 (USP18) as an ISG upon IFNβ treatment. These observations pointed out the functional dynamics of ISGF3, unphosphorylated ISGF3 (U-ISGF3) or STAT2-IRF9 complex (Paul et al., 2018; Arnold et al., 2013; El Fiky et al., 2008; Blaszczyk et al., 2016; Kumar et al., 2000; Rengachari et al., 2018; Paul et al., 2023).

While IRF9 is a component of ISGF3 complex, the promoter region of IRF9 gene itself includes both ISRE and GAS motifs and its expression is induced by both IFN-I and IFN-II through ISGF3 and GAF complexes (Michalska et al., 2018). IRF9 contributes significantly to enhancing the expression of the majority of ISGs by initiating the formation of ISGF3 and STAT2/IRF9 following IFN-I stimulation and STAT1/IRF9 following IFN-II stimulation (Suprunenko & Hofer, 2016). It has been reported that IRF9 role in the expression of ISGs with antiviral activities is essential. Kimura et al. conducted a study demonstrating the significant antiviral function of IRF9. They investigated the role of IRF9 in murine EF cells derived from IRF9-deficient mice. Their results disclosed that the absence of IRF9 led to diminished IFNα and IFNγ responses in the murine EF cells, along with compromised antiviral activity against HSV and VSV (Kimura et al., 1996).

Although IRF9 is known for its role in the IFN response, it also has a pivotal role in other biological aspects. For example**,** it has a significant function in the gut microbiome. Research on mice lacking IRF9, has uncovered a distinctive gut profile in their gut, characterized by heightened levels of T cells and neutrophils suggesting a plausible involvement of IRF9 in maintaining homeostasis within the gut environment (Suprunenko & Hofer, 2016)**.** Moreover, It was also suggested that IRF9 has a regulatory role in the Neointima formation. A study conducted by Zhang unveiled the role of IRF9 in the formation of the neointima (the inner layer of the blood vessels) by promoting cell growth and migration. Accordingly, they found that in the irf9-/- mice with artery injuries, the inner layer of the blood vessels was thinner, and there was less growth of muscle

cells. Interestingly, the migration of cells to the injuries was also reduced in these mice, which was associated with the suppression of matrix metalloproteinase-9 (MMP9) expression which is a proliferation- and migration-related gene (S.-M. Zhang et al., 2014). On the contrary, It has been reported that IRF9 affects liver damage caused by ischemia/reperfusion injury via suppressing sirtuin 1 (SIRT1) gene known for its protective effects on tissues. Subsequently, the inhibition of SIRT1 expression leads to heightened levels of p53 acetylation which has apoptotic function in hepatocytes (P.-X. Wang et al., 2015).

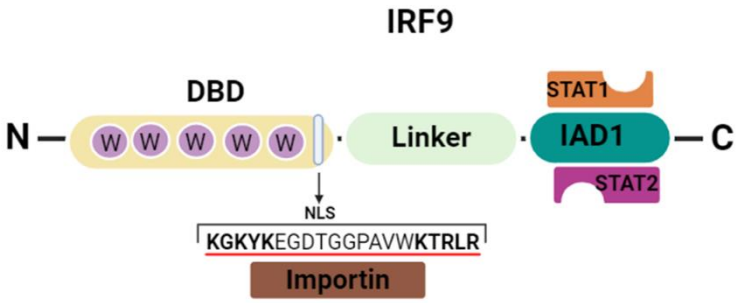

Figure 6. Structure of the IRF9 protein.

IRF9 protein structure has three domains including DBD, linker and IAD1. The preserved tryptophan residues play a crucial role for interacting between IRF9 and DNA. The entrance of IRF9 to the nucleus occurs by NLS which is located in the DBD domain. The basic amino acids of NLS are indicated in bold. The connection between the IAD and DBD domains is facilitated by a linker. The IAD1 domain mediates interactions between IRFs and other STATs (Paul et al., 2018; Arnold et al., 2013; Blaszczyk et al., 2016).

1.5.2 IRF1

IRF1 is identified as the first member of IRFs family. Similar to IRF9, It features a conserved DBD containing five tryptophan residues, enabling it to specifically bind to the GAAA sequence. Following this region, the NLS is positioned, regulating IRF1's entry into the nucleus by recognition of importin. Subsequently, a linker region is located that provides a connection between DBD and IAD2 domains, then the C-terminal IAD2 is found, which governs IRF1's interaction with other IRFs including IRF2 and IRF8 and non-IRF proteins such as NF-κB (Figure 7). It is evident that IRF1 can be phosphorylated by GSK3β at Thr181 and Ser185 residues marking it for degradation through ubiquitination which subsequently regulates IRF1 level, impacting its ability to modulate gene expression in immune responses (Feng et al., 2021; Antonczyk et al., 2019; Sundararaj & Casarotto, 2021; Garvin et al., 2019). In general, the IRF1 is a gene that contains GAS element in its promoter that is potentially targeted by STAT1/STAT1 (in response to IFN-I and IFN-II) and STAT1/STAT2 (in response to IFN-I). IRF1 can activate the expression

of ISGs by targeting the ISRE sequence within their promoter upon stimulation with IFN-I and IFN-II (Figure 8). ISGF3 and IRF1 exhibit functional overlaps due to their shared ability to target ISRE elements in the promoters of ISGs (Michalska et al., 2018). It's worth noting that the IRF1 gene is expressed at the basal levels in an IFN-independent manner, supporting the expression of ISRE-containing genes such as MX Dynamin Like GTPase 1 (MX1) and 2'-5'-Oligoadenylate Synthetase 2 (OAS2) at the basal level (Michalska et al., 2018; Yamane et al., 2019). In IRF1KO BEAS-2B cell lines, initial phosphorylation of TBK1 and subsequent activation of IRF3 were reduced. Since IRF3 is pivotal for early ISG expression, IRF1 supports early ISG expression through IRF3. Knocking down IRF1-dependent genes such as OAS2 in BEAS-2B cells and then infecting with VSV, increased viral susceptibility, highlighting IRF1-depending genes role in antiviral defense. IRF1KO BEAS-2B cells also showed reduced H3K4me1 at promoters/enhancers of these genes, indicating IRF1's role in modulating histone modifications. Additionally, IRF1-deficient mice showed increased virus susceptibility due to impaired NK cell development and insufficient IFNγ production (Panda et al., 2019; Rosain et al., 2023).

In addition to IRF1’s functions in the immune antiviral response, it also halts cell growth and division upon detecting DNA damage and plays a role as a tumor suppressor. Studies have indicated that in the absence of IRF1, mouse embryonic fibroblast (MEF) cells encounter difficulty in halting their cycle in response to DNA damage. Consequently, these cells may persist in growth and division despite DNA damage, potentially resulting in errors and heightened tumor risk (Tanaka et al., 1996).

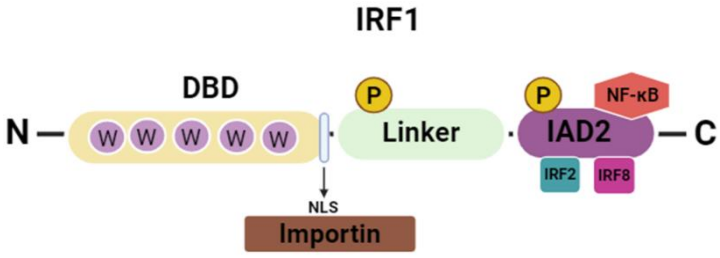

Figure 7. Structure of the IRF1 protein.

IRF1 contains three domains including DBD, linker and IAD2. Helix-turn-helix motif in DBD contains five tryptophan (w) residues and it is responsible for DNA sequence recognition . The nuclear import of IRF1 is assisted by the NLS. linker is responsible for connection domains. IAD2 participates in the interaction between IRF1,other IRFs and non-IRF proteins (Feng et al., 2021; Antonczyk et al., 2019; Sundararaj & Casarotto, 2021; Meraro et al., 1999)

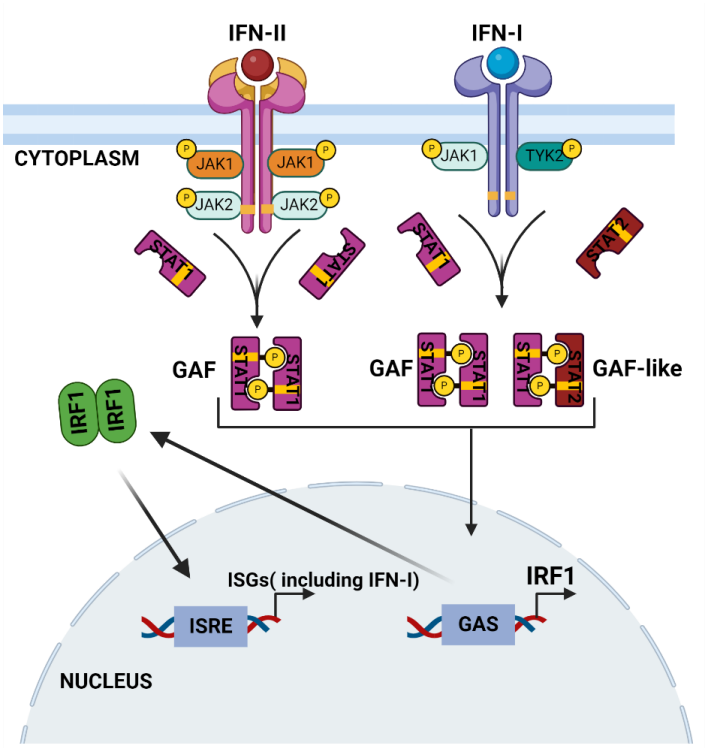

Figure 8. IRF1 in IFN-dependent host defenses.

After binding to the IFN receptors, IFN-I and IFN-II initiate the activation of Janus kinases (JAKs), leading to the subsequent phosphorylation and dimerization of STAT1 and STAT2, forming GAF and GAF-like (IFN-I) and GAF (IFN-II). These complexes then relocate into the nucleus, inducing the expression of the IRF1 gene, thereby establishing a positive feedback loop that enhances the induction of ISGs including IFN genes (Feng et al., 2021; Escalante et al., 1998).

1.6 Different Complexes Involved In IFNα And IFNγ Signaling Pathways (Canonical, Phosphorylated)

1.6.1 Interferon Stimulated Gene Factor 3 (ISGF3)

As mentioned before, after the interaction between IFN-I and its receptors, the JAK/STAT signaling pathway is activated, which in turn leads to the dimerization of STAT1/STAT2. Subsequently, STAT1/STAT2 heterodimers combine with IRF9 to create the ISGF3 complex. This complex then moves into the nucleus, where it triggers the expression of ISRE-containing genes like IFIT1, USP18, and ISG20. Maintaining the stability of ISGF3 depends on critical interactions between IRF9, STAT1 and STAT2 (Au-Yeung et al., 2013; Majoros et al., 2017; Michalska et al., 2018)**.** In the general paradigm, the ISGF3 complex is constituted by STAT1 phosphorylated on Tyr701 and STAT2 which undergoes phosphorylation at Tyr690. Additional studies suggest a possible role of serine phosphorylation of STAT1 and STAT2. For example, after cellular exposure to both IFNγ and PDGF, phosphorylation of STAT1 Ser 272 takes place through the MAP kinase pathway (Wen et al., 1995). Alternatively, in response to IFNI, this phosphorylation occurs via a kinase known as protein kinase C delta (Pkc-δ). This phosphorylation event on STAT1 Ser 272 is essential for the complete transcriptional activity of GAF and ISGF3 complexes (Pilz et al., 2003). On the other hand, evidence suggests that the activity of the ISGF3 complex is negatively regulated by the phosphorylation of STAT2 at Ser287 (Steen et al., 2013).

Scientists have discovered that STAT2 interacts with IRF9 or STAT1 even without DNA binding, and this interaction seems to be crucial for ISGF3 formation following IFN-I stimulation (Martinez-Moczygemba et al., 1997). U-STAT2/IRF9 and U-ISGF3 are able to shuttle between cytoplasm and nucleus and target ISRE- containing genes to sustain their expression at the basal level in the absence of IFN-I. On the contrary, U-STAT1/STAT2 lacks the potency to translocate into the nucleus. However, upon IFN-I stimulation, the active ISGF3 can be formed from U-STAT2/IRF9 in the nucleus or STAT1/STAT2 are phosphorylated and moves to the nucleus where form an active ISGF3 on the ISRE motifs of ISGs. The IFN-I stimulation can also promote the formation of active ISGF3 from U-ISGF3 in the cytoplasm which moves to the nucleus and initiates the expression of ISRE-containing ISGs (Blaszczyk et al., 2016; Platanitis et al., 2019)**.** Following the ISGF3-DNA interaction, the regulation of a diverse set of ISGs initiates antiviral activities in the immune system to combat viral infections (Au-Yeung et al., 2013; Majoros et al., 2017).

Previous investigations demonstrated that in response to IFN-I, the formation of ISGF3 occurs quickly because of the existence of ISGF3 components including STAT1 and STAT2 in the cytoplasm (Levy et al., 1989). Matsumoto et al. investigated the response of mouse embryonic fibroblasts (MEFs) to IFNγ, finding that both STAT1 and STAT2 underwent phosphorylation and subsequent dimerization. Together with IRF9, they form the ISGF3 complex, however, the level of ISGF3 generated in response to IFNγ was markedly lower as compared to the response triggered by IFNα (M. Matsumoto et al., 1999). Furthermore, the presence of ISGF3 in response to IFNγ was suggested by findings from the study on IFNγ-treated mice VSMC. ChIP-seq analysis revealed the binding of phosphorylated STAT2, STAT1 together with IRF9 on the promoters of ISRE-containing genes such as C-X-C Motif Chemokine Ligand 10 (Cxcl10), indicating the involvement of ISGF3 upon IFNγ stimulation (Piaszyk-Borychowska et al., 2019). Additionally, recent ChIP data from a study on mouse bone marrow-derived macrophages (BMDM) cells affirmed the transient binding of ISGF3 components to the promoters of ISRE-containing ISGs such as Isg20 and Ube216, highlighting ISGF3's role in their early induction upon IFNγ stimulation (Ravi Sundar Jose Geetha et al., 2024). While evidence suggests the presence of ISGF3 in mice upon IFNγ exposure, support for the existence of this complex in human cells in response to IFNγ is lacking.

1.6.2 ISGF3 Like Complexes : STAT2/IRF9 And STAT1/IRF9 And Others

As it was mentioned above, in response to IFN-I, STAT2/IRF9 can be phosphorylated in a STAT1-independent manner and move to the nucleus to express the expression of ISRE-containing genes (Steen & Gamero, 2012). Initially, Bluyssen and his research team proposed the existence of the STAT2/IRF9 complex following investigations conducted on STAT1KO U3A cells. Their pioneering work disclosed that STAT2 as a homodimer with IRF9 association, generates STAT2/IRF9 complex which can targets ISRE motif in the promoter of ISGs, however, its DNA-binding affinity is lower as compared to ISGF3 (HansA. R. Bluyssen & Levy, 1997). After dedicating years to studying STAT2/IRF9, scientists have uncovered additional insights into this complex. Fink and her team elucidated the elevated expression of Dual Oxidase 2 (DUOX2) and dual oxidase maturation factor 2 (DUOXA2) in Sendai virus (SeV)-infected airway epithelial cells (AEC). Their study on AEC cells illustrated that the infection stimulates the production of IFNβ/TNFα by AEC, initiating the formation of STAT2/IRF9. These proteins then bind to ISRE elements within the DUOX2 and DUOXA2 promoter, prompting their expression (Fink et al., 2013). Moreover, Nowicka and her colleagues investigated the role of STAT2/IRF9 complex in

the IFNα-treated STAT1KO Huh7.5 cells and the results showed that in the absence of STAT1, STAT2/IRF9 can prolong the expression of ISRE-containing ISGs (Nowicka et al., 2023). Additionally, the results of the study conducted by Yamauchi et al. have indicated the significant role of STAT2 in antiviral response. Their examination of the hepatitis C virus (HCV)-infected STAT2KO Huh 7.5 cells revealed that the absence of STAT2, rather than STAT1, resulted in the complete abolition of IFN-α-induced interference with HCV replication (Yamauchi et al., 2016).

While ISGF3 has been extensively studied and many insights have been gained, there remains a significant need for further investigation into the STAT1/IRF9 complex formed by the phosphorylation of STAT1 in conjunction with IRF9. Approximately three decades ago, early research proposed the involvement of STAT1/IRF9 complex in the absence of STAT2 and when both IRF9 and STAT1 levels are elevated in response to IFNγ, then it subsequently targets ISRE sequences to provoke the expression of ISGs (A. R. Bluyssen et al., 1996). Rauch and colleagues investigated the noncanonical effects of interferon regulatory factor 9 (IRF9) in response to IFNγ. Their ChIP-seq analysis in mouse macrophages unveiled the potential involvement of the STAT1/IRF9 complex in regulating cxcl10 gene expression after IFNγ treatment (Rauch et al., 2015)**.** Moreover, the results from Sekrecka's study indicated that the absence of IRF1 in human Huh7.5 cells resulted in elevated recruitment of STAT1 and IRF9 to the promoters of ISRE-containing genes following treatment with IFNγ. This suggests a potential role for the STAT1/IRF9 complex as a transcriptional factor in regulating gene expression in response to IFNγ stimulation in human cells (Sekrecka et al., 2023)**.** Finally, research conducted on A549 cells showed that upon stimulation with IFNγ, an ISGF3-like complex can be formed, termed $ISGF3^{II}$, where STAT2 remains unphosphorylated. This $ISGF3^{II}$ complex interacts with the ISRE sequence and induces the expression of IFN-responsive genes . However, it should be highlighted that that this interaction is relatively transient and leads to the early expression of ISGs as compared to the conventional ISGF3 complex (Morrow et al., 2011).

1.6.3 GAF And GAF-like Complexes

Earlier research demonstrated that the regulation of a set of ISGs in response to IFN-I and IFN-II occurs via the formation of STAT1 homodimers (GAF).

IFN-II initiates the signaling cascades by interacting with its receptors known as α chain receptors (2×) and β chain receptors (2×) on the cell surface (Randal & Kossiakoff, 2001). Subsequently, it starts transphosphorylation and activation of JAK1 and JAK2. These JAKs phosphorylate STAT1 which consequently leads to STAT1 homodimerization known as GAF. Studies on the guanylate binding protein (GBP) gene have found the GAS element in its promoter region which was bound by the GAF complex in response to IFN-II (Michalska et al., 2018; Strehlow et al., 1993). Later, it was shown that STAT1 homodimers can also induce the expression of GAS-containing genes including IRF1, IRF8 and intercellular adhesion molecule 1 (ICAM1) in response to IFNα and the homodimers was named AAF (Seegert et al., 1994; Decker et al., 1997; Michalska et al., 2018; Müller et al., 1993). In addition to the existence of GAF in response to IFN-I, it has been also reported that GAS-containing genes can be activated by another complex which is formed by STAT1/STAT2 heterodimer known as GAF-like (Brierley & Fish, 2005; Darnell, 1997; Levy & Darnell, 2002; Au-Yeung et al., 2013). However, the amount of IFN-I-induced GAF and GAF-like is lower as compared to ISGF3 which compete with these complexes due to higher potency of IRF9. Nevertheless, the GAF complex remains the principal transcriptional activator and exhibits greater potency in response to IFN-II as compared to IFN-I-induced GAF. This is due to the absence of STAT2 phosphorylation in response to IFN-II (Stewart et al., 2002; Sekrecka et al., 2023). Besides ISRE-only or GAS-only containing genes, another category of ISGs is characterized by the presence of both ISRE and GAS elements in their promoters. Examination of the GBP gene promoter, (where GAS was previously identified), revealed the presence of an ISRE which was targeted by ISGF3 in response to IFN-I. later, subsequent evidence has demonstrated that both ISRE and GAS elements are necessary for the complete induction of GBP (Strehlow et al., 1993; Decker et al., 1991).

1.7 IRF1 And Its Role In Transcriptional Regulation

Similar to ISGF3, GAF and GAF-like, IRF1 is another TF that plays a role in the regulation of ISGs in response to both IFN-I and IFN-II. In the absence of cytokine stimulation, IRF1 remains susceptible to basal level induction and preserves the expression of ISGs under basal conditions. The results of the study conducted by Yamane et al. provided evidence for this, as it revealed a

decrease in the basal expression of ISRE-containing genes in IRF1KO PH5CH8 (Immortalized human hepatocytes) and Huh7.5 cell lines in the absence of IFNs (Taniguchi et al., 1997; Yamane et al., 2019; Forero et al., 2019)**.** In terms of expression kinetics, while the expression of certain ISGs, such as MX1, persists up to 24 hours, the expression of IRF1 gene is characterized by rapid and robust dynamics, reaching its peak at 2 hours (Novatt et al., 2016).

As it was mentioned before, IRF1 possesses a single GAS site in its promoter, therefore its induction more potently relies on the GAF in response to IFN-II than GAF-like in response to IFN-I, primarily due to the lower abundance of these complexes triggered by IFN-I (Stewart et al., 2002)**.** Similar to ISGF3**,** IRF1 has the capacity to induce the expression of ISRE-containing genes, then they both contribute to the regulation of the overlapping set of ISGs (Taniguchi et al., 1997).

1.8 Regulation Of IFNα and IFNγ Signaling Pathways: A Negative Perspective

While IFNs play an essential role in bolstering the host immune system against viral infections, it's imperative to acknowledge that their dysregulation can lead to a spectrum of disorders, including autoimmune conditions such as SLE (Di Domizio & Cao, 2013; Golding et al., 1986). This underscores the delicate balance required in modulating IFN responses to maintain immune homeostasis. Various inhibitory mechanisms contribute to controlling IFN responses. Among these, the degradation of IFN-I receptors regulates type I IFN responses. Accordingly, PRR signaling pathways initiate the expression of IFN-I which in turn activates the p38 kinase that subsequently phosphorylates the IFNAR1 on Ser532. This leads to the internalization of IFNAR1 and its degradation via ubiquitylation and protect the cells from toxicity effects of IFN-I. (Ivashkiv & Donlin, 2014; Qian et al., 2011). Another common mechanism acts through SOCS. SOCS1, SOCS3 and CIS are among SOCS proteins that inhibit cytokines pathways such as IFNs. Both SOCS1 and SOCS3 inhibit JAKs activity. The kinase inhibitory region of SOCS1 inhibits the catalytic activity of Jak2 and SOCS3 blocks JAKs activity by binding to the IFN receptors. On the other hand, CIS hinders the activation of STATs by binding to IFN receptors and blocking STATs recruitment. Moreover, SOCS proteins promote the degradation of STATs and JAKs through their interaction with the ubiquitination machinery (Figure 9). It's notable that SOCS expression is also provoked by IFNs, given their classification ISGs. Consequently, when IFN signaling cascades are inhibited by SOCS, it highlights the role of SOCS in a negative feedback loop, where their induction serves to modulate immune responses and ensure proper regulation of the signaling

pathways. This intricate regulatory mechanism emphasizes the dynamic interplay between IFNs and SOCS in fine-tuning immune activation and maintaining homeostasis (D. Zhou et al., 2017; Alexander, 2002; Nicholas & Lesinski, 2011; Adams et al., 1998; A. Matsumoto et al., 1997; Naka et al., 1997). Beyond SOCS, members of the protein inhibitors of activated STATs (PIAS) family, such as PIAS1, PIAS2, PIASx, and PIASy, constitute another set of suppressors of the IFN signaling pathway. These proteins serve as inhibitors, impeding the binding of STATs to DNA (Schmidt & Müller, 2002; Coccia et al., 2002). Moreover, PIAS family members exhibit E3 ligase activity, facilitating the addition of ubiquitin-like molecules such as small ubiquitin-related modifier (SUMO) into their substrates like STATs in the SUMOylation process, thus initiating their degradation (Rogers et al., 2003; Shuai, 2006). Another regulators are PTPs that negatively regulate the IFN pathway by dephosphorylating STATs (T. Meyer & Vinkemeier, 2004; Haspel & Darnell, 1999). For example, Src homology region 2 domain-containing phosphatase-2 (SHP-2) plays a role in suppressing the IFN pathway by dephosphorylating and deactivating STAT1 (You et al., 1999; D. Xu & Qu, 2008). In addition to the mechanisms outlined above, another method of regulating IFN-I responses involves the downregulation of IFNAR. This process is assisted by protein kinase D2 (PKD2), which triggers the ubiquitination of IFNAR1 by phosphorylating Ser535 on IFNAR1. This action leads to the recruitment of the E3 ubiquitin ligase on IFNAR1, resulting in its ubiquitination and subsequent degradation. Unlike PKD2, which primarily impacts IFNAR1, the IFN-inducible protein USP18 operates differently by exerting a negative regulatory effect on IFN-I production through its interaction with IFNAR2. In this process, USP18 modulates IFN-I signaling by inhibiting the binding of JAK1 to the receptor complex, leading to subsequent downregulation of IFN-I signaling pathways (Figure 9) (Arimoto et al., 2018; Zheng et al., 2011).

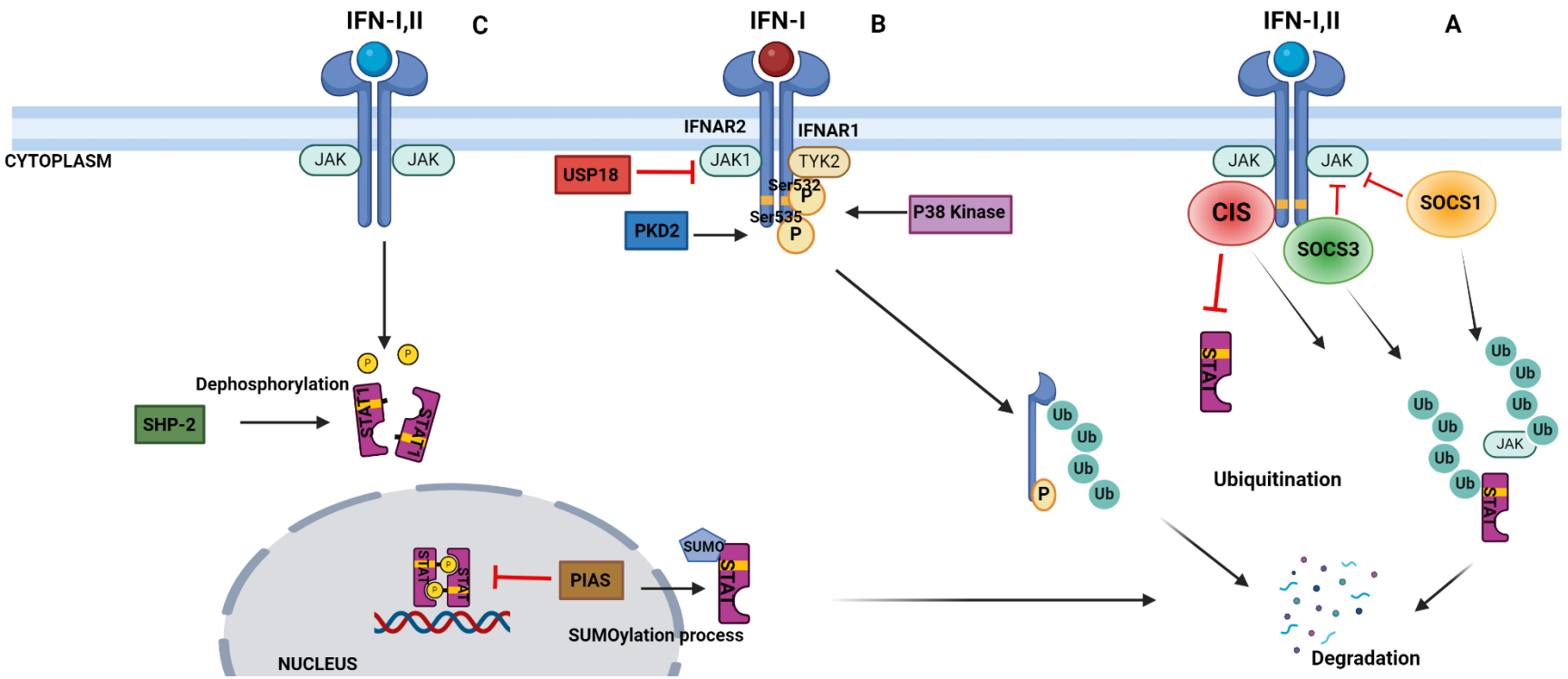

Figure 9. Negative regulation of IFN signaling pathway.

(A) The inhibition of IFN signaling cascades occurs through SOCS proteins. Specifically, SOCS1 and 3 dampen JAK activity, whereas CIS acts as an inhibitor of STAT activation. Additionally, SOCS proteins have the capability to induce the degradation of STATs and JAKs through the process of ubiquitination that is mediated by ubiquitinating machinery. **(B)** Following activation by IFN-I, the p38 kinase phosphorylates IFNAR1 on Ser532, prompting the internalization of IFNAR1 and its degradation through ubiquitylation. While, PKD2 phosphorylates Ser535 on IFNAR1 that triggers the E3 ubiquitin ligase recruitment on the receptor leading receptors's ubiquitination followed by degradation. On the other hand, USP18 adjusts IFN-I signaling by impeding the binding of JAK1 to the IFNAR2 and negatively regulates the IFN-I production. **(C)** SUMO molecules are added to the STATs protein by PIAS via their E3 ligase activity which in turn causes the STATs degradation and additionally, it inhibits the binding of STATs to the DNA. SHP-2 dephosphorylates the STAT1 proteins, and prevents the formation of ISGF3, GAF and GAF-like (Alexander, 2002; D. Zhou et al., 2017).

1.9 Unphosphorylated STAT1, STAT2 And ISGF3 In IFN-Dependent Response

Studies have shown that U-STAT1 and U-STAT2 are present within cell nuclei after exposure to IFN stimulation. This occurrence stems from the expression of STAT1 and STAT2 genes activated by IFNs-induced phosphorylated STATs which elevate their concentration that sustain their presence for several days. This phenomenon extends the duration of ISG induction, including genes like OAS1, OAS2, and MX1, STAT1 and STAT2 themselves. These findings highlight the importance of U-STATs in sustaining the expression of antiviral genes (Cheon & Stark, 2009; Cheon et al., 2013; Morrow et al., 2011). Another study was conducted by Lou et al. in which they observed the formation of a U-STAT2/IRF9 complex, capable of binding to the ISRE sequence in the promoter of retinoic acid-induced gene G (RIG-G) via a STAT1-independent manner. This process occurs following the treatment of NB4 acute promyelocytic leukemia cells with all-trans retinoic acid (ATRA), which triggers the induction of IRF1. Consequently, IRF1 induces the expression of IFNα gene, leading to the formation of the U-STAT2/IRF9 complex. Then, U-STAT2/IRF9 prompts sustained expression of RIG-G (Lou et al., 2009).

In addition to the formation of U-STAT1 homodimers and U-STAT2/IRF9 heterodimers, there are additional findings indicating that U-STAT1 and U-STAT2 can combine with IRF9 to create U-ISGF3. This occurs particularly when cells are subjected to continuous stimulation by low levels of IFNs. Cheon et al. reported in their study that extended exposure of cells to IFNβ leads to the accumulation of U-STAT1, U-STAT2, and IRF9, resulting in the formation of U-ISGF3. This complex, in turn, maintains the expression of a subset of antiviral genes, thereby sustaining the antiviral response. The results of the study conducted by Sung et al. unveiled that cell exposure to IFNλs and IFNβ promotes the formation of U-ISGF3 at high concentrations which consequently prolongs the expression of a subset of ISGs. Furthermore, they have also documented that HCV-infected Huh-7–TLR3 cells induce the production of endogenous IFN-λs and -β, initiating the generation of U-ISGF3, which consequently sustains the expression of ISGs (W. Wang et al., 2017; Cheon et al., 2013; Sung et al., 2015). However, findings of the study led by Nowicka and her team challenged these observations. Their ChIP-seq data showed that the formation of U-ISGF3 occurs in a IFN-independent manner which disagrees with the concept suggesting that U-ISGF3 or U-STAT2/IRF9 could substitute for ISGF3 or STAT2/IRF9 to sustain the prolonged expression of U-ISGs upon IFN-I stimulation (Nowicka et al., 2023).

1.10 Unphosphorylated STAT1, STAT2 And ISGF3 In IFN-Independent Response

Previous research has demonstrated that U-STAT2/IRF9 complex possesses the capability to move between the nucleus and cytoplasm using its NLS and NES regions. This mobility allows it to initiate the expression of a specific group of ISGs at a basal level, independently of IFN stimulation (Martinez-Moczygemba et al., 1997; Blaszczyk et al., 2016). Additionally, studies have indicated that the expression of specific ISGs containing GAS motifs can be maintained by the U-STAT1 complex even in the absence of IFN stimulation (Ma et al., 2019; Cheon & Stark, 2009; Braunstein et al., 2003). Wang et al.'s exploration of human intestinal and liver organoids, and liver tissues revealed compelling findings. They detected the presence of U-STAT1, U-STAT2, and IRF9, which then assembled into U-ISGF3 independently of IFN stimulation. Once formed, U-ISGF3 plays a crucial role as a transcription factor, maintaining the continuous expression of ISGs at basal levels to counter viral infections, including those caused by HCV and the hepatitis E virus (HEV) (W. Wang et al., 2017). Seven years later, Nowicka et al. embarked on a series of experiments involving cells that overexpressed all the components of ISGF3 (ST1-ST2-IRF9-U3C) and overexpressing STAT2+IRF9. Their findings reaffirmed the role of U-ISGF3 and U-STAT2/IRF9 in the IFN-independent induction of ISRE-containing ISGs such as OAS2, IFIT1, and IFI27 at basal levels which then provided cell protection against VSV infection (Nowicka et al., 2023)**.** In a study published by Platanitis and her colleagues, it was shown that pre-existing STAT2–IRF9 complex autonomously regulates the basal expression of numerous ISGs in mouse BMDMs, independent of IFN-I receptor signaling. Upon IFN treatment, there is a switch transition from the STAT2–IRF9 complex to the canonical ISGF3 complex, resulting in an acceleration of ISG transcription in mouse cells (Platanitis et al., 2019). Nevertheless, in a study conducted by Sekrecka et al. the ChIP data analysis on human Huh7.5 cells did not yield evidence regarding the formation of U-ISGF3 and U-STAT2/IRF9 at the basal level and also not after IFN treatment (Sekrecka et al., 2023).

These findings shed light on an alternative pathway for ISG expression regulation beyond traditional IFN-dependent mechanisms and highlight its significance in antiviral responses.

1.11 Interferon-Stimulated Genes – ISG

Since the action of IFNs is carried out through ISGs, gaining insights into the functions of these genes could pave the way significant advancements in antiviral treatments (Borden & Williams, 2011). An ISG represents any gene that undergoes induction as a result of IFN response including IFN-I , IFN-II and IFN-III. Their activation is mediated by specific DNA elements, such as GAS, ISRE, or IRE, which are known as IFN-responsive elements. It has been proven that some ISGs can be induced at basal conditions and in response to IFNs, while others are induced only in the presence of IFN stimulation. In addition to protein-coding ISGs, there are non-coding ISGs, such as those that generate long non-coding RNAs (lncRNAs) in response to IFNs or viral infection (Tsukahara et al., 2006; Schoggins, 2019; Mostafavi et al., 2016; Josset et al., 2014)**.** ISGs play a multifaceted role in antiviral activities, encompassing various mechanisms such as impeding viral protein function and suppressing viral replication. Furthermore, their production also contributes to processes like apoptosis or cell growth regulation. For instance, the apoptotic function of ISG15 was examined in HeLa cells, revealing its capability to enhance the expression of P53 which consequently prevents cell growth, promotes apoptosis, and exerts its anti-tumor effects (Perng & Lenschow, 2018; Tan & Katze, 1999; M.-J. Zhou et al., 2017).

Over time, the repertoire of introduced ISGs has expanded. Microarray analysis of human and murine cells treated with both IFN-I and IFN-II revealed the identification of over 300 ISGs. Later, meta-analysis across various mammalian cell types identified over 450 ISGs induced by IFNα. Similarly, microarray analysis of human peripheral blood mononuclear cells (PBMCs) resulted in identification of 950 ISGs that were activated in response to IFNα. Additionally, in IFNα-treated mouse hematopoietic cells, 975 ISGs were recognized (Schoggins et al., 2011; Lanford et al., 2006; Mostafavi et al., 2016; de Veer et al., 2001). In addition to IFNα responsive ISGs, there are many ISGs that are induced in response to IFNγ. Accordingly, more than 200 IFNγ-responsive genes were reported around 30 years ago, and this number is increasing over time. Thus far, based on Interferome v2.01 online database, IFNγ is associated with modifications of over 9,000 human genes, while IFNα is linked to alterations in around 7,000 human genes (Rusinova et al., 2013). Generally, ISGs can be grouped based on the existence of ISRE or GAS elements in their promoters. Accordingly, three distinct ISGs are recognized including ISRE-only containing genes (i.e. MX1) GAS-only containing genes (i.e. ICAM1) and the third group comprises ISGs

that have both ISRE and GAS in their promoters (i.e. GBP) (RONNI et al., 1998; Tessitore et al., 1998; Strehlow et al., 1993).

ISGs act as antiviral genes through different steps including inhibition of viral attachment and entry, nuclear entry, mRNA and protein synthesis, replication and viral assembly and they also participate in the degradation of viral genome. Each step of antiviral functions can be performed by different ISGs (Figure 10). For example, ISG-like cholesterol-25-hydroxylase (CH25H) as a GAS-only containing gene impedes the attachment of viruses to host cells and viral entry. CH25H synthesizes 25-hydroxycholesterol (25HC), which exerts catalytic effects, altering the lipid composition and fluidity of cellular membranes. Consequently, this disrupts membrane fusion between viruses and host cells (T. Xie et al., 2019; S.-Y. Liu et al., 2013).

MX1 as an ISRE-only containing gene prevents the nuclear import of viral genomes. The interaction of MX1 with components of the viral replication complex prompts its oligomerization, resulting in mis-localization and the inhibition of nuclear translocation of viral genomes (Layish et al., 2023). Interferon-gamma inducible protein 16 (IFI16) as an ISRE+GAS composite gene interacts with viral RNA and RIG-I which triggers the viral RNA ubiquitination and degradation and subsequently inhibits viral mRNA synthesis. However, poly(ADP-Ribose) polymerase family member 12 (PARP12) as an ISRE-only containing gene directly interacts with polysomes and blocks viral protein synthesis (Trapani et al., 1994; Welsby et al., 2014; Jiang et al., 2021). Another example of ISRE-only containing genes are IFI6 and ISG20. IFI6 prevents viral genome replication by binding to the promoter region and suppressing its activity, while ISG20 has exonuclease activity that degrades the viral nucleic acids. Finally, GBP5, a composite gene, functions to hinder viral assembly by inhibiting the proteolytic activity of the host protease furin, which plays a crucial role in activating the viral envelope glycoproteins (Schoggins, 2019; Sajid et al., 2021; Imam et al., 2020; Olszewski et al., 2006; R. Zhang et al., 2021).

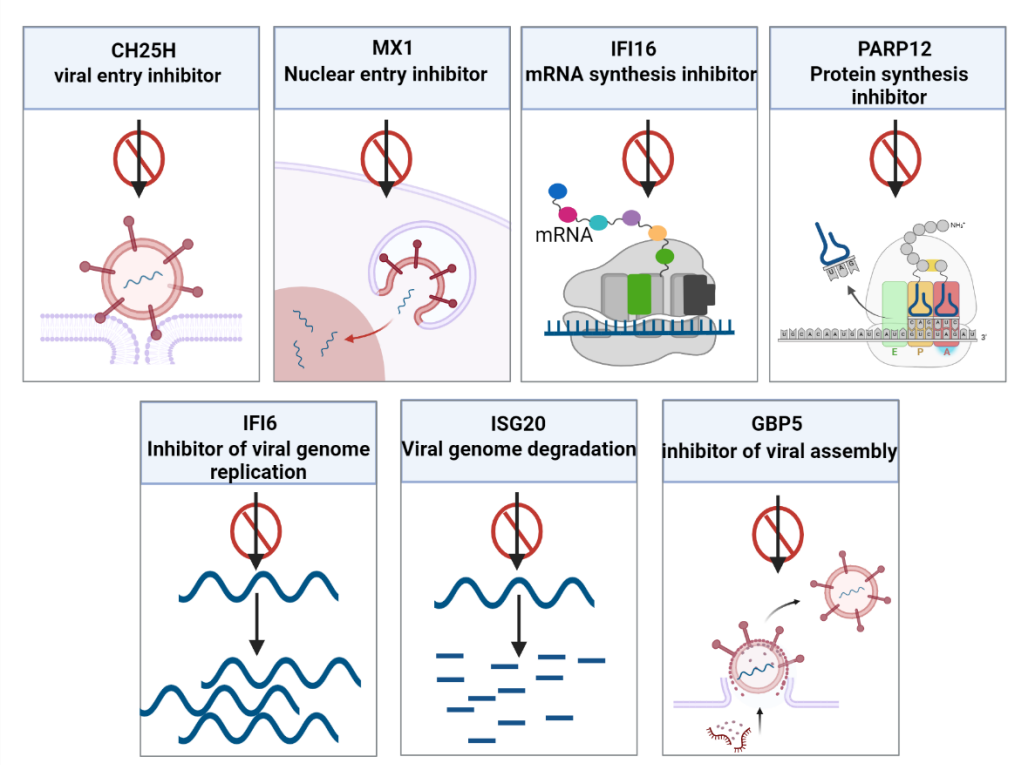

Figure 10. Inhibition of viral replication steps by diverse ISGs.

Various ISGs target distinct stages of viral replication. For instance, CH25H hinders viral entry into host cells, while MX1 impedes nuclear entry. IFI16 inhibits viral mRNA synthesis, and PARP12 suppresses viral protein synthesis. IFI6 blocks the replication of viral genome, whereas, ISG20 is responsible for degrading viral genome. GBP5 is involved in inhibition of viral assembly (Schoggins, 2019; Blondel et al., 2015).

While ISGs are predominantly recognized for their antiviral properties, emerging research suggests they also possess the capacity to exhibit antibacterial activity. This dual functionality underscores the complexity of ISGs in modulating immune responses and highlights their potential as versatile agents in combating various pathogens, extending beyond their conventional antiviral role. For example, research has shown that increased expression of IFITM3 hampers the growth of mycobacterium tuberculosis (MTb) in infected monocytic cells by augmenting endosomal acidification within these cells (Ranjbar et al., 2015).

To sum up, using high-throughput technology can aid scientists in discovering new ISGs and gaining insights into how they function and understand their transcriptional regulation in connection to the functional overlap and diversity of IFNα and IFNγ (Schoggins & Rice, 2011).

1.12 Comprehensive Exploration Of STAT1, STAT2, IRF9, And IRF1 Binding Across The Genome: Impact On ISRE And GAS-Dependent Transcription Regulation

In the late 1980s, pioneering research discovered the ISRE, a conserved DNA sequence motif in ISG promoters, crucial for the cellular response to interferon. Later, it was found that IFN-γ induced specific genes through the GAS element in their promoters. In 1997, Gao et al. identified genes with both ISRE and GAS motifs, showing how their combined action contributes to a robust interferon response, enhancing our understanding of the interferon signaling pathway (Gao et al., 1997).

1.12.1 Interferon-Dependent

ChIP (Chromatin Immunoprecipitation) technology has been crucial in deciphering the complex molecular mechanisms that regulate the expression of ISGs after IFN treatment. A series of studies have employed ChIP-seq and ChIP-chip technologies to elucidate the involvement of key transcription factors in this process, namely STAT1, STAT2, IRF9, and IRF1. The results of ChIP-chip data conducted on IFNα and IFNγ-treated HeLaS3 cells uncovered the characterization profile of STAT1 and STAT2 binding to a region on chromosome 22 that comprises GAS or ISRE sites. In addition, the binding of STAT1 and STAT2 in response to IFNα in this region leads to the recognition of non-conserved GAS sites. Nevertheless, certain binding sites exclusively interacted with STAT2, suggesting the potential for different mechanisms to modify the specificity of STAT1 binding (Hartman et al., 2005).

In 1996, Xiaoxia's team characterized the STAT1 and STAT2 binding following IFN treatment. They found that in the in U2A cells, which lack IRF9, STAT1 as a homodimer and also with STAT2 association forms STAT1/STAT2 heterodimer in response to IFN-α and interacts with the GAS element at the upstream of IRF1 gene and provoke its expression (X. Li et al., 1996). Several years later, a study on IFNα-treated human U266 cells corroborated these findings. Using monoclonal antibodies to STAT1 and STAT2, and Immunoprecipitation of protein-DNA complexes revealed a binding profile of STAT1 and STAT2 to a palindromic sequence, wherein a single residue differed within the core of the palindromic consensus GAS in the IRF1 gene (Ghislain et al., 2001).

Data obtained from studies utilizing whole-genome methodologies are currently archived in accessible databases, providing global accessibility for scientists. The encyclopedia of DNA

elements (ENCODE) project is an example (The ENCODE Project Consortium, 2012). According to this project, ChIP-seq data from IFNα and IFNγ-treated K562 cell lines, exposed to IFNs for 30 minutes and 6 hours, were analyzed. In IFNα-treated cells, antibodies targeting STAT1, STAT2, and IRF1 were used, whereas antibodies for STAT1 and IRF1 were employed for IFNγ-treated cells. In 2018, Michalska and her colleagues implemented data from the ENCODE project. The team conducted an analysis of the ChIP-seq data to introduce TF binding sites. Her team has characterized various ISGs, categorizing them into GAS-only, ISRE-only, or GAS/ISRE composite-containing genes. These genes possess target elements for GAF/GAF-like, ISGF3, and IRF1. Furthermore, analysis of ChIP-seq data from IFNγ-treated HeLa S3 cells identified 1,441 STAT1 target genes, but only 194 were upregulated, highlighting STAT1's complex regulatory mechanisms (Michalska et al., 2018). Platanitis and colleagues recently conducted a study involving BMDM treated with either IFNβ or IFNγ. The ChIP-seq results, employing STAT1, STAT2, and IRF9, revealed the formation of ISGF3 in response to both IFNβ and IFNγ, with subsequent binding to genes containing ISREs. Interestingly, in irf9KO cells, no binding of STAT1 and STAT2 to ISRE-containing genes was observed (Platanitis et al., 2019). ChIP-seq analysis of IFNβ-treated mouse embryonic stem cells (ESCs) and MEFs showed varying STAT1 and STAT2 binding profiles on ISG promoters. More binding peaks were found in MEFs than in ESCs, and protein levels of STAT1 and STAT2 were lower in ESCs both before and after IFNβ stimulation. This suggested distinct cell-type-specific mechanisms regulating the IFNβ response (Muckenhuber et al., 2023). In addition, Sekrecka et al. analyzed STAT1, STAT2, IRF9, and IRF1 binding after IFNα treatment, and STAT1 and IRF1 binding after IFNγ treatment in Huh 7.5 cells. In IFNα-treated WT cells, early recruitment of phosphorylated STAT1 and STAT2 aligned with early GAS-only gene expression, confirming the role of GAF and GAF-like complexes. Conversely, IFNγ treatment showed prolonged STAT1 recruitment and delayed GAS-only gene expression. IRF1 recruitment lagged behind STAT1 and STAT2 for both IFNs. Likewise, ISRE-only gene induction correlated with delayed IRF1 and ISGF3 recruitment. They also identified ISGs with both ISRE and GAS sites, sharing binding characteristics of both elements. Investigation of STAT1KO Huh 7.5 cells disclosed delayed STAT2 and IRF9 binding to ISRE-containing genes, correlating with prolonged gene induction. Similarly, prolonged STAT1 and IRF9 binding in IFNγ-treated IRF1KO Huh 7.5 cells shed light on the potential role of STAT1/IRF9 in ISRE-containing gene expression (Sekrecka et al., 2023). Nowicka et al.'s study provided insights into

ISRE gene expression involving ISGF3 and STAT2/IRF9 complexes. Time-dependent IFNα responses in WT 2fTGH and Huh7.5 cells showed early, transient STAT1 and STAT2 binding in both cell lines, however WT Huh7.5 cells exhibited prolonged expression of ISRE-containing genes as compared to 2fTGH cells, correlating with ISGF3 recruitment. Conversely, STAT1KO ST2-U3C and Huh7.5 cells displayed prolonged STAT2 and IRF9 binding, confirming the role of STAT2/IRF9 in prolonged ISRE gene expression, consistent with Sekrecka et al.'s findings (Nowicka et al., 2023)**.**

The existence of ISRE and GAS elements in the distal regulator region of some ISGs such as STAT1 gene have been reported to facilitate the transcriptional regulation through chromatin looping between the proximal promoter and the distal region. Several ISGs, including SOCS1, interferon-induced transmembrane protein1,2 and 3 (IFITM1, IFITM2, IFITM3) have been identified in addition to the STAT1 gene that their transcriptional regulation involves chromatin looping between the proximal promoter and distal regulatory regions (P. Li et al., 2017; Abou El Hassan et al., 2017).

1.12.2 Interferon-Independent

The basal induction of ISGs is vital in maintaining cellular antiviral defenses, contributing to the rapid response to pathogen attacks and establishing a state of readiness for the immune system. Contrary to the conventional understanding that STATs operates as monomers until activated by tyrosine phosphorylation, emerging scientific evidence questions this concept. According to reports by Cheon et al, the elevated U-STAT1 levels achieved through transfection with a STAT1-encoding vector can maintain the expression of certain ISGs, such as OAS2, IFI27, and STAT1 itself in BJ fibroblasts in the absence of IFN stimulation (Cheon & Stark, 2009). Confirming these findings, analyzing the ChIP-seq data from GM12878 cells (human lymphoblastoid cell lines) sourced from the ENCODE ChIPseq Experiment Matrix database and Gene Expression Omnibus uncovered that, in the absence of IFN stimulation, STAT1 binds to the promoters of 186 out of 350 ISGs (W. Wang et al., 2017)**.**

In addition to U-STAT1, there are several studies reporting the involvement of U-STAT2 in the expression of ISGs at the basal conditions. Accordingly, In the study conducted by Testoni et al, the integration of ChIP and expression analysis unveiled STAT2's autonomous influence on the expression of ISGs in Huh7 cell lines, regardless of its phosphorylation status. Prior to IFNα

treatment, research indicated that STAT2 is pre-associated with 62% of the examined human target promoters, constituting the majority of ISGs (Testoni et al., 2011). These findings correlated with the results of the study conducted by Platanitis et al, suggesting STAT2, in association with IRF9, interacts with the promoter regions of ISRE containing ISGs independently of IFN stimulation in mouse BMDM. The STAT2/IRF9 complex then sustains gene expression at basal levels. Additionally, it was also noted that STAT2/IRF9 contributes to maintaining chromatin accessibility, potentially facilitating ISGF3 binding upon IFNα or IFNγ stimulation (Platanitis et al., 2019). However, ChIP-seq results from untreated Huh7.5 cells, showed the absence of STAT2 basal binding on ISG promoters, contrasting Testoni's and Platanitis' findings (Sekrecka et al., 2023). In a study conducted by Nowicka and her team, based on ChIP-seq data, it was found that under basal conditions, STAT1, STAT2, or IRF9 did not bind to the promoter of ISRE-containing genes across various cell lines, including 2fTGH, Huh7.5, ST2U3C, and STAT1KO Huh7.5, consistent with findings that published by Sekrecka et al. However, the research experiments provided further insights into the role of U-ISGF3 in the basal expression of ISRE-containing genes in untreated ST1-ST2-IRF9-U3C cells, where components of ISGF3 (STAT1, STAT2, and IRF9) were found to be overexpressed (Nowicka et al., 2023).

IRF1 is another TF that is induced at basal level and maintains the expression of ISRE/IRE-containing ISGs at the basal condition. In research led by Chatterjee-Kishore and colleagues, it has been evidenced that IRF1, along with U-STAT1, targets the promoter of LMP2 in Hela cells without IFN treatment, thereby maintaining its expression at basal levels (Chatterjee-Kishore et al., 2000; Feng et al., 2021). The genome-wide binding analyses of IRF1 yielded further understanding of its involvement in the basal induction of ISGs. In ChIP-chip experiments performed on untreated and IFNγ-treated HeLa cells, only 2 STAT1 peaks were observed, while 28 IRF1 peaks were identified in the untreated condition, indicating its role in driving ISG expression at basal levels (Abou El Hassan et al., 2017). Supporting these results, analysis of RNA-seq data from untreated BEAS-2B cells, which are respiratory epithelial cells with constitutive IRF1 expression, revealed the basal expression of a subset of IRF1-dependent ISGs such as MX1, BST2, and OAS2. The involvement of IRF1 in sustaining the expression of these genes was validated by observing reduced expression levels in IRF1KO BEAS-2B cells (Panda et al., 2019).

The discovery of unphosphorylated complexes, such as U-STAT1, U-ISGF3, U-STAT2/IRF9 and IRF1, has expanded our understanding of the antiviral activity exhibited by ISGs at their basal expression levels. This newfound knowledge sheds additional light on the intricate mechanisms underlying the basal antiviral response mediated by ISGs.

1.13 A Positive Feedback Regulation Of STAT1, STAT2, IRF9 And IRF1, And The Role Of The GAS and ISRE

The regulation of STAT1, STAT2, IRF9, and IRF1 genes in response to IFN-I and IFN-II via ISRE and GAS-dependent mechanisms is a critical aspect of the positive feedback loop within the IFN signaling pathway.

STAT1, as a pivotal mediator in cytokine-triggered gene expression, along with other STATs, undergoes activation in response to both IFN-I and IFN-II. The possible elucidation for the priming effect of type I IFN resides in the initiation of STAT1 expression, given its status as an ISG (Gough et al., 2010). STAT1 gene has been reported to have ISRE elements in its proximal promoter (Yuasa & Hijikata, 2016). Moreover, the additional analysis of the human STAT1 gene uncovered the existence of an (IRF-E)/GAS/IRF-E (IGI) motif located in the intron 1/exon 2 region (Wong et al., 2002)**.** Chip-seq experiments on the human STAT1 gene confirmed the presence of proximal ISRE, and both ISRE and GAS elements 5.5-kb upstream of human STAT1 gene, bound by ISGF3, IRF1, GAF, and GAF-like complexes. Similarly, Yuasa and colleagues found distal regulatory elements approximately 5.5-kb upstream of the mouse stat1 gene containing ISRE and GAS motifs that enhance stat1 promoter activity. A chromosome conformation capture (3C assay) in mouse fibroblasts (RGB3T3-5 cells) showed a physical link between the 5.5URR of stat1 and its proximal promoter, suggesting autoregulation of STAT1. Upon exposure to IFN-I and IFN-II, STAT1 homodimers bind to the distal GAS site at the 5.5URR of the stat1 gene and at the promoter of other ISGs like STAT2 and IRF9, stimulating their expression. In addition, ISGF3 complex, activates stat1 expression by binding to the ISRE motif in the 5.5URR region (Yuasa et al., 2012; Yuasa & Hijikata, 2016). Yuasa and the team utilized the NCBI GenBank mouse and human genome databases for conducting bioinformatics analyses. Their research has identified GAS-like and ISRE/IRF-E motifs within the proximal promoter of the mouse Stat2 gene, as well as a GAS site in the proximal promoter of both human and mouse IRF9 (Yuasa & Hijikata, 2016). Later, ChIP-seq data analysis exhibited STAT1, STAT2, IRF9 and IRF1 binding to the proximal promoter of both STAT2 and IRF9 genes after IFNα and IFNγ

which confirmed the binding of ISGF3 and IRF1 to ISRE, GAF and GAF-like to the GAS element presented in the promoter of these genes. Subsequent RNA-seq experiments confirmed the expression of STAT2 and IRF9 genes by IFN-responsive complexes in response to IFNα and IFNγ (Michalska et al., 2018; Sekrecka et al., 2023).

IRF1 as a complex interacts with the ISRE site and induces the expression of ISGs in response to both IFN-I and IFN-II. However, IRF1 is a gene that possesses a GAS element in the proximal promoter region which is recognized by GAF in response to IFN-I and IFN-II and GAF-like in response to IFN-I (Au-Yeung et al., 2013; Michalska et al., 2018; X. Li et al., 1996). Following IFN-I and IFN-II stimulation, the STAT1 and STAT2 genes exhibit a robust response, leading to a substantial production of the GAF and GAF-like proteins. Subsequently, GAF in response to both IFN-I and IFN-II and GAF-like in response to IFN-I target the GAS site in the promoter of IRF1 and govern its expression (Sekrecka et al., 2023). Consequently, IRF1 complexes as a part of the positive feedback loop, prolong the expression of ISRE-containing ISGs such as STAT1, STAT2 and IRF9**.** Following IFN-I and IFN-II stimulation, the STAT1 and STAT2 genes exhibit a robust response, leading to a substantial production of the GAF and GAF Like proteins. Subsequently, GAF in response to both IFN-I and IFN-II and GAF-like in response to IFN-I target the GAS site in the promoter of IRF1 and regulates its expression. Consequently, IRF1 complexes as a part of positive feedback loop, prolong the expression of ISRE containing ISGs such as STAT1, STAT2 and IRF9.

Collectively, these observations provided a better understanding of the important roles played by STAT1, STAT2, IRF9, and IRF1 as part of complexes involved in the positive feedback regulation of themselves as ISRE+GAS composite (STAT1,STAT2, IRF9), or GAS-only containing genes (IRF1), as well as in the long-term IFN responses of other ISGs. Moreover, This knowledge uncovers the complex processes behind how cells respond to interferons and it also helps in developing targeted treatments for viral infections and other immune disorders.

1.14 Modulation Of IFN Response Over Time

The cumulative knowledge of IFN response regulation has deepened our understanding of how STAT1, STAT2, IRF9, and IRF1 are pivotal in triggering antiviral responses by activating ISGs. Generally, in response to IFNα (Figure 11) and IFNγ (Figure 12), ISGF3, IRF1, GAF and GAF-like interact with ISRE and GAS sites in the promoter of GAS-only, ISRE-only and ISRE+GAS composite ISGs in a time-dependent manner (Sekrecka et al., 2023). Following the interaction between IFNα and IFNARs (Figure 11), a cascade initiates wherein STAT1 and STAT2 undergo phosphorylation and dimerization. This leads to the formation of both STAT1/STAT1 homodimers and STAT1/STAT2 heterodimers which then translocate to the nucleus to stimulate the expression of genes by targeting GAS site in the promoter of GAS-only containing and ISRE+GAS composite genes. In addition to these homodimers and heterodimers, STAT1 and STAT2 with IRF9 altogether generates ISGF3 that binds to the ISRE element in the promoter of ISRE-only and ISRE+GAS composite genes after nuclear entry. Moreover, in response to IFNα, STAT2/IRF9 (in the absence of STAT1) and IRF1 are another complexes that regulates the expression of ISGs by interacting with ISRE element. On the contrary, Upon IFNγ binding to IFNGRs (Figure 12), the phosphorylation and dimerization of STAT1 occur, which form the STAT1/STAT1 homodimer that subsequently binds to the GAS elements located in the promoter of ISRE+GAS composite and GAS-only containing genes including IRF1 gene. Consequently, IRF1 is recruited to the ISRE motif and induces the expression of ISRE-only or ISRE+GAS composite genes in response to IFNγ. Additionally, following IFNγ stimulation, STAT1 together with IRF9 generate STAT1/IRF9 complex which targets ISRE site in the promoter of ISRE-only or ISRE+GAS composite genes.

Therefore, STAT1,STAT2 and IRF9 as ISRE+GAS composite genes are induced by STAT2/IRF9 (in the absence of STAT1), ISGF3, IRF1, GAF and GAF-like in response to IFNα, and GAF, STAT1/IRF9 and IRF1 upon IFNγ stimulation. While, IRF1 as a GAS-only containing gene is expressed by GAF and GAF-like after IFNα treatment, and by GAF in response to IFNγ. Thus, these TFs as components of the positive feedback loop maintain the long-term IFNα and IFNγ response (Sekrecka et al., 2023). Nevertheless, STAT1, STAT2, IRF9, and IRF1 also play a pivotal role in sustaining the expression of ISGs at basal levels even in the absence of IFN stimulation. Accordingly, under basal conditions, IRF1, U-ISGF3, STAT1/IRF9 and U-STAT2/IRF9 complexes support the expression of genes containing ISREs, while U-STAT1

sustains the expression of GAS-containing ISGs and composite genes can be expressed at basal levels by all forms of complexes. However, stimulation by IFNα and IFNγ induces alterations in the cellular milieu, facilitating rapid antiviral responses (Figure 11-12). To sustain the long-term IFN response, unphosphorylated complexes cooperate with phosphorylated ones in the positive feedback loop. Clearly, ISRE-only containing genes can be induced by STAT2/IRF9 (in the absence of STAT1), ISGF3 and IRF1 in response to IFNα and IRF1 and STAT1/IRF9 in response to IFNγ. On the other hand, the induction of GAS-only containing genes occurs via GAF and GAF-like after IFNα stimulation, while only GAF is involved in response to IFNγ. GAS+ISRE composite genes are the novel group of composite genes that can be regulated by all complexes including STAT2/IRF9 (in the absence of STAT1), ISGF3, IRF1, GAF and GAF-like in response to IFNα and GAF, STAT1/IRF9 and IRF1 upon IFNγ stimulation. This suggests that composite genes, by integrating signals from multiple types of interferons, could be instrumental in shaping the cellular response to diverse IFN stimuli. It underscores the intricate interplay and potential crosstalk between the signaling pathways activated by IFNα and IFNγ, which may contribute to the versatility and adaptability of the immune system in combating viral infections. Despite extensive research efforts dedicated to unraveling the intricacies of the IFNα and IFNγ signaling pathways and the regulatory complexes governing IFN-responsive genes, there are still some aspects that remain not fully understood, particularly regarding the nuanced functions of ISRE+GAS composite genes. For example, what precise mechanisms underlie the functionality of ISRE+GAS composite genes in their response to IFNs? How are these genes regulated in non-canonical IFN signaling pathways? What factors govern their precise regulation in diverse biological contexts? How does the distance between ISRE and GAS sites from the transcription start site (TSS) impact the regulation of composite genes? Moreover, IFN signaling interacts with various other signaling pathways, such as those implicated in inflammation, cell proliferation, and immune regulation. Further research is needed to elucidate the extent of the crosstalk between these pathways and the IFN-driven control of ISRE+GAS composite genes, along with the functional implications of these interactions. Additionally, exploring the functional significance of these composite genes in orchestrating immune responses to viral infections will contribute to a comprehensive understanding of host defense mechanisms mediated by interferons.

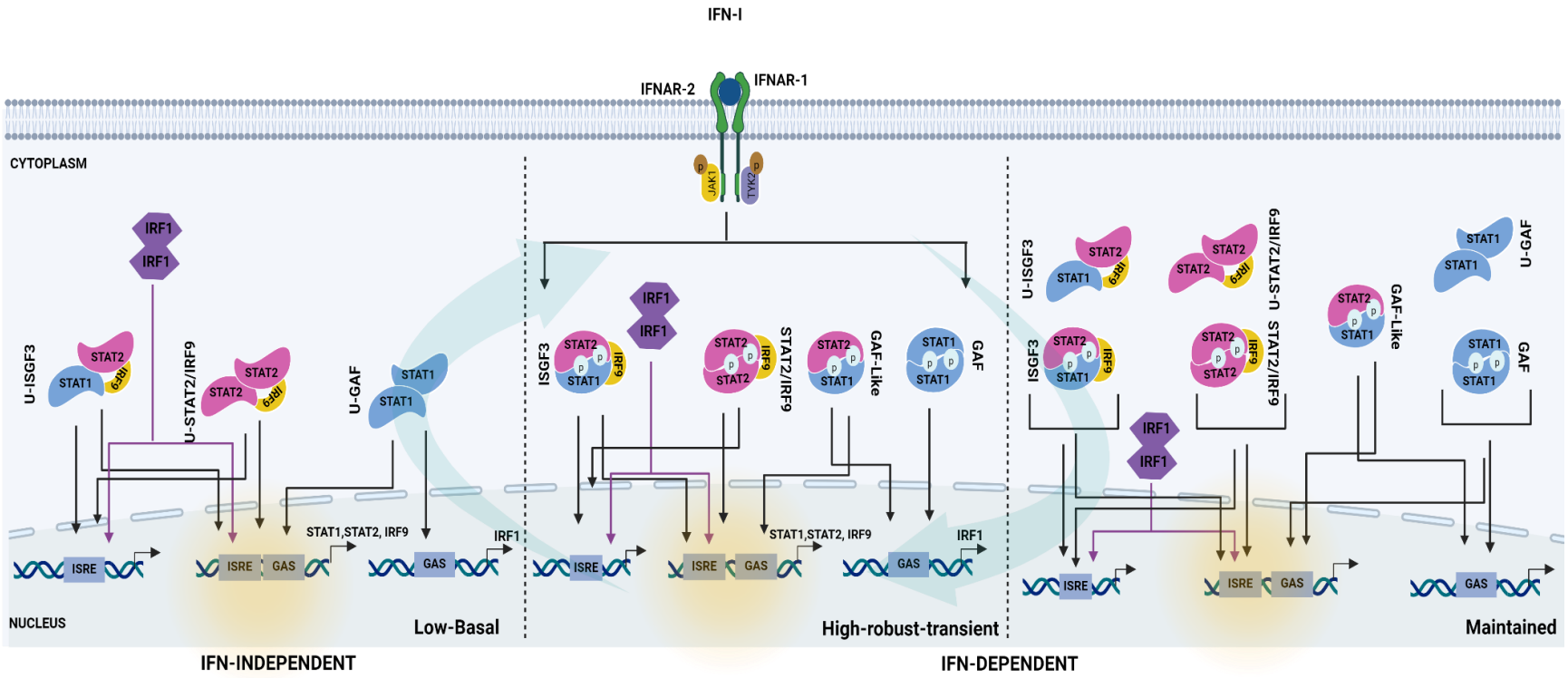

Figure 11. Transcription of ISGs in IFN-I-independent and IFN-I-dependent pathways.

In the absence of IFN-I stimulation (basal condition), the basal expression of ISRE-only containing genes is mediated by U-ISGF3, U-STAT2/IRF9 and IRF1 , while GAS-only containing genes are basally expressed by U-GAF. However, ISRE+GAS composite genes (indicated by glow yellow color) can be expressed at basal levels by all four complexes including U-ISGF3, U-STAT2/IRF9, IRF1 and U-GAF indicating their potential role in immune response. In response to IFN-I, JAK1 and TYK2 mediate the STAT1 and STAT2 phosphorylation leading the formation of STAT1 homodimers (GAF), heterodimers (GAF-like) binding to GAS and STAT1/STAT2/IRF9 (ISGF3), STAT2/IRF9 (in the absence of STAT1) and IRF1 interacting with ISRE sites and initiate a transient and robust gene expression. As a consequence, there is a swift buildup of freshly produced STAT1, STAT2, IRF9, and IRF1 proteins in the cytoplasm. The reduction in the levels of phosphorylated proteins allows the unphosphorylated complexes to supplement the function of phosphorylated complexes along with IRF1 in maintaining the expression of ISGs (maintained phase). The big transparent green arrows indicate the positive feedback loop (Michalska et al., 2018).

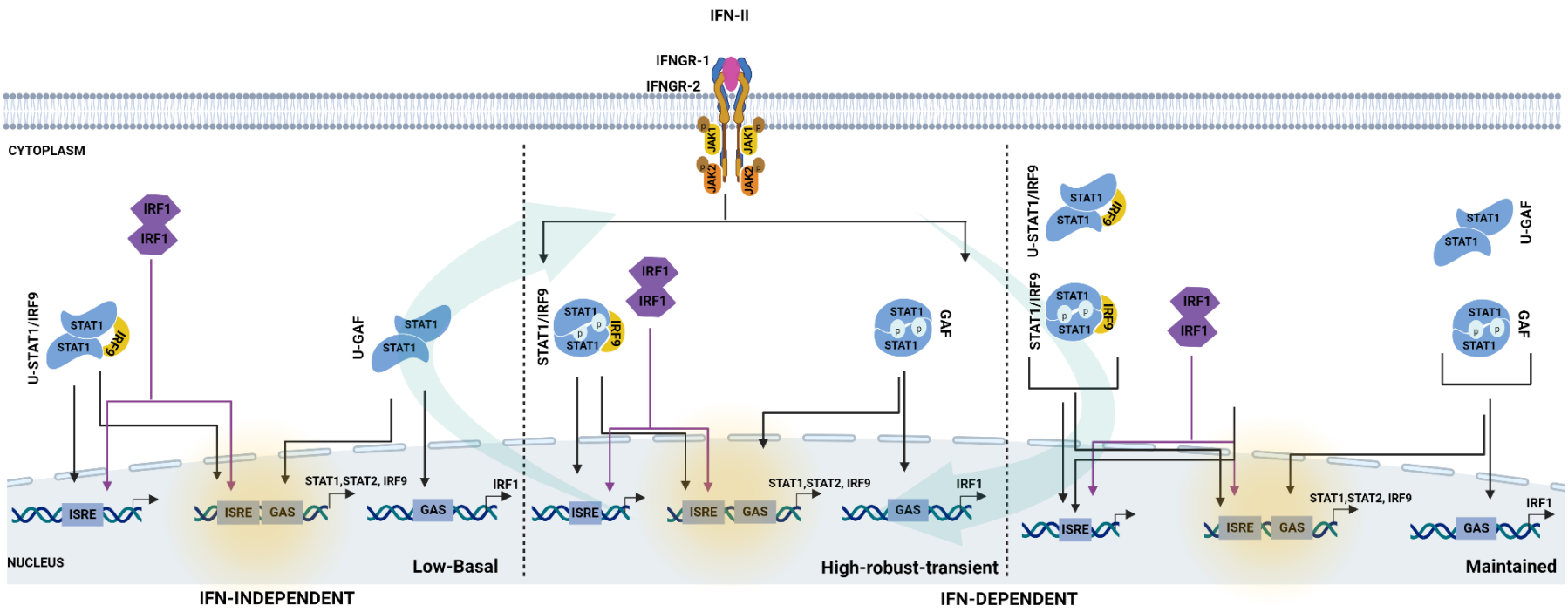

Figure 12. Transcription of ISGs in IFN-II-independent and IFN-II-dependent pathways.

In the absence of IFN-II stimulation (basal condition), the basal expression of ISRE-only containing genes is mediated by U-STAT1/IRF9 and IRF1 , while GAS-only containing genes are basally expressed by U-GAF. However, ISRE+GAS composite genes (indicated by glow yellow color) can be expressed at basal levels by all three complexes including U-STAT1/IRF9, IRF1 and U-GAF indicating their potential role in immune response. In response to IFN-II, JAK1 and JAK2 mediate the STAT1 phosphorylation leading the formation of GAF, binding to GAS and IRF1 interacting with ISRE sites and initiate a transient and robust gene expression. As a consequence, there is a swift buildup of freshly produced STAT1 and IRF1 proteins in the cytoplasm. Diminished phosphorylated protein levels enable unphosphorylated complexes, together with IRF1, to support the function of phosphorylated complexes in sustaining ISG expression. (maintained phase). The big transparent green arrows signify the presence of a positive feedback loop (Michalska et al., 2018).

2 Hypothesis And Objectives

Hypothesis

IFN-I and IFN-II dependent transcription of composite genes depends on ISRE and GAS composition and differential binding of ISGF3, IRF1, STAT1/IRF9, GAF and GAF-like complexes.

Objectives

- To generate a complete list of IFNα- and IFNγ-induced ISRE and GAS composite site-containing genes with their ISGF3, IRF1, GAF and GAF-like binding profile and putative biological function.
- To further characterize the genome-wide role of IFN-I and IFN-II-activated ISGF3, IRF1, GAF and GAF-like complexes in time-dependent ISG expression through ISRE and GAS composites.
- To further characterize the role of IFN-I and IFN-II-activated ISGF3, IRF1, GAF and GAF-like complexes in binding to distal ISRE and GAS-containing elements and in transcriptional regulation.
- To further characterize the IFN-I and IFN-II induced transcription of ISRE-GAS composite genes in WT, STAT1, STAT2, IRF9, IRF1 and IRF1.9dKO cell lines.
- To further understand the role of ISRE and GAS distance and organization in transcriptional regulation of ISRE+GAS composite genes in response to IFN-I and IFN-II.
- To further understand the ability of the ISRE+GAS composite site to act as a molecular switch in response to IFN-I and IFN-II.
- To further characterize the role of the GAS and ISRE sites in transcription of different classes of ISRE+GAS composite genes in response to IFN-I and IFN-II.
- To further investigate the role of ISRE+GAS composite genes in IFN-I and IFN-II mediated anti-viral activity.

3 Material And Methods

3.1 Cell Lines

Dr. Sada from the Department of Genome Science and Microbiology at the University of Fukui in Fukui, Japan generously provided human hepatocellular carcinoma cell lines: Huh7.5, Huh7.5 STAT1KO, Huh7.5 STAT2KO, and Huh7.5 IRF9KO. These cell lines lacking STAT1, STAT2, or IRF9 were generated using the CRISPR/Cas9 system, as outlined in Yamauchi et al.'study (STAT1 is essential for the inhibition of hepatitis C virus replication by interferon-λ but not by interferon-α). Furthermore, Agata Sekrecka created Huh7.5 IRF1KO and Huh7.5 IRF1.9dKO cell lines using the pZG22D03-2 plasmid from ZGene Biotech Inc.

3.1.1 Cell Culture

Huh7.5, Huh7.5 STAT1KO, STAT2KO, IRF9KO, IRF1KO and IRF1.9dKO cells were cultured in DMEM (11, IITD PAN Wrocław) supplemented with 10% FBS (10500-064,ThermoFisher Scientific(TSF)),1% L-glutamine (X0550, BioWest), 1% penicillin/streptomycin/amphotericin B (A5955, Sigma-Aldrich), and 1% MEM NEAA (TSF) to sustain their growth. (The term used for the mentioned media in material and method is "full culture media"). Cell culture was conducted in 10cm dishes at 37°C under 5% CO2 conditions, and cells were passaged when they reached approximately 90% confluency.

3.2 Interferon Treatment

To study the response of Huh7.5 and various KO cell lines to interferon alpha and gamma at different time intervals (0, 2h, 4h, 8h, 24h, and 72h) for qPCR analysis, cells were seeded in 6-well plates with complete culture media. After 24 hours, the culture medium was replaced with a starvation medium containing DMEM supplemented with 1% FBS, 1% MEM NEAA, 1% L-glutamine, and 1% penicillin/streptomycin/amphotericin B. Following an 8-hour starvation period, the cells were treated with IFNα (1000 U/ml, IF007, MERCK) or IFNγ (10 ng/ml, IF002, MERCK) for the specified durations.

3.3 RNA Isolation And Reverse Transcription

Column-based Total RNA Zol-Out™ D kit (043, A&A Biotechnology) was used following the manufacturer’s protocol to isolate total RNA from suspended cells in TRI-REAGENT (TRI118, MRC). Subsequently, nuclease-free water was used to elute total RNA and its concentration was determined using a Spectrophotometer (DeNovix). Following the

manufacturer's guidelines, the RevertAid First-Strand Synthesis Kit (K1622, TFS) was used for reverse transcription. To begin, 500 ng of isolated RNA was diluted in final volume of 8ul of nuclease-free water. Subsequently, 2 µl of a mixture containing DNase I (1 U) in reaction buffer (10x) was added to reach 10ul of final volume and incubated at 37°C for 30 minutes. After this incubation, the tubes were transferred to the ice and 1 µl of 50 mM EDTA (EN0521, TFS) was added into the tubes, followed by incubation at 65°C for 10 minutes. Next, 1 µl of Random Hexamer primers (100 µM, [SO142, TFS]) was added into the reaction tubes and incubated at 65°C for 5 minutes. As the final step, a mixture was prepared comprising of 0.75µl of 10 mM dNTPs (10297018, TFS), 9.75µl of nuclease-free water, 0.5µl of RiboLock RNase Inhibitor 40 U/µl (EO0381, TFS), 3µl of 5x RT buffer and 1µl of RevertAid Reverse Transcriptase (200 U/µl, [EP0442, TFS]) and added to the reaction tubes and then subjected to a thermal cycling program including incubation at 25°C for 10 minutes, followed by 1 hour at 42°C, and a final step of 10 minutes at 70°C using the C1000 Touch Thermal Cycler (Bio-Rad). The acquired cDNA was employed in real-time PCR experiments.

3.4 Real-Time PCR (qPCR)

The components listed below were used for the qPCR reaction, which was performed on the Bio-Rad CFX Thermal Cycler System to evaluate gene expression: Genious 2X SYBR Green Fast qPCR Mix (RK21205, ABclonal), nuclease-free water, and a combination of forward and reverse primers. The specific quantities of these reagents can be found in Table 2. PCR conditions are represented in Table 3.

Reagent	volume
Genious 2X SYBR Green Fast qPCR Mix	5µl
H2O	0,8µl
Forward + Reverse primer mix	1.2ul
cDNA (12,5x diluted)	3µl

Table 2. Description of qPCR sample preparation.

Step	Temperature	Time duration	
Initial denaturation	95°C	6 min	
Denaturation	95°C	7 sec	40 cycles
Primer annealing	Specific for designed primers	45sec	
Melting curve	Melting curve analysis was carried out using the default settings integrated into the Thermal Cycler utilizing a 1°C incremental step.		

Table 3. The conditions for the qPCR reaction.

Glyceraldehyde-3-phosphate dehydrogenase (GAPDH), a housekeeping gene, was used for the purpose of normalizing the expression level of the gene of interest. ΔΔCT formula was used for the determination of fold change and it is represented in the Table 4.

Formula	Description
$\Delta CTgene$	$CTgene$ - $CTref$ *
$\Delta CTcontrol$	$CTgene$ - $CTref$ *
$av.\Delta$CT $control$	$arithmetic\ average\ of\ \Delta$CT $control\ values$
ΔΔCT	$\Delta CTgene$ - $av.\ \Delta CTcontrol$
Q	2^(-ΔΔCT)
* Ct ref stands for the reference which is associated with the housekeeping gene.	

Table 4. ΔΔCT method for assessing fold change.

The results are displayed as the mean value along with the standard error of the mean (SEM) for two independent biological replicates unless it is specified. The graphs were generated using GraphPad Prism 6.01 software. The primer sequences utilized for Real-Time PCR are presented in the table below (Table 5).

Gene	Forward/Reverse	Sequence 5'->3'
PARP14	Forward	ACGATG AAATGA GGCGTT GTC
	Reverse	TGCCAG GTCTTG ATTCTC GG
SP110	Forward	GAAAGGGGCAGGAACGACAA
	Reverse	CAGGCTTCCAGAGATTCCATGT
GBP3	Forward	CCAGCGATCCAGCGAAAGAA
	Reverse	GGCATTGTTCTCTTGTCTGTGC
ETV7	Forward	GTGCAAGCCAGATGTGAAGC
	Reverse	TACAGGACGTCACGGAGTCT
APOL6	Forward	CGTCTT TCTCCA GCCCAG AC
	Reverse	CAAATG ATTTTC TTCTCT CCACGG
STAT2	Forward	TCGAAA CACCTG TGGAGA GC
	Reverse	GTCTTC CCTTTG GCCTGG AT
IRF9	Forward	GAGCCA CAGGAA GTTACA GACA
	Reverse	CGCCCG TTGTAG ATGAAG GT
DDX60	Forward	CCTGGGCAGAACCTCCATTT
	Reverse	CGCATACTCGGCATCCTTGA
NLRC5	Forward	CCGGGAGCTCTGAGGGAGT
	Reverse	GTCTGGGCTATGTGTGCCTT
NMI	Forward	AGGCGCTGCTGTTTTCCG
	Reverse	TTCCATGATCCCCCGCGT
DDX58	Forward	CATGTCCACCTTCAGAAGTGTCT
	Reverse	AGCAGGCAAAGCAAGCTCTA
STAT1	Forward	TGTTAT GGGACC GCACCT TC
	Reverse	AGTGAA CTGGAC CCCTGT CT
GAPDH	Forward	CAATATGATTCCACCCATGGCAA
	Reverse	GATCTCGCTCCTGGAAGATGG

Table 5. Primer sequences used in Real-Time PCR.

3.5 RNA-Seq Data Analysis

Dr. Agata Sekrecka* conducted the RNA-seq experiments, while Dr. Katarzyna Kluzek* performed the bioinformatic analysis of the RNA sequencing data. Dr. Kluzek optimized the scripts and bioinformatics pipelines to facilitate the analysis of RNA-seq data.

* *Laboratory of Human Molecular Genetics at IMBB, Adam Mickiewicz University in Poznan*

To analyze the RNA-seq data, alignment of the Fastq files was conducted against the Homo sapiens GRCh38.dna.primary_assembly genome build (release-100) using STAR version 2.7.3a,

as described by Dobin et al. in 2013 (STAR: ultrafast universal RNA-seq aligner). Quality control checks were conducted using FastQC (Andrews, 2010) and the results were consolidated using MultiQC (Ewels et al., 2016). FeatureCounts v1.6.2 with default settings (Liao et al., 2014) was used to calculate gene counts for each sample. Genes showing low counts (below 10 across all time points) were excluded to perform downstream analysis.

3.5.1 Differential Gene Expression (DEG)

DEG analysis was carried out using the DESeq2 v1.30.1 package (Love et al., 2014) in R v4.0.3 software (R Core Team, 2021). In order to discover genes responding to IFN treatment over time, the likelihood ratio test (LRT) was employed. These tests assessed the fit of count data in a "full model," which included independent variables such as time, compared to a "reduced model" that excluded these variables. DEG analysis was conducted considering the factors such as time and replicates. To classify the samples, principal component analysis (PCA) analysis was performed to distinguish the samples based on the factors including time, replicates and treatment. The statistical significance measured based on False discovery rate (FDR)-adjusted q-values (with a 5% threshold) using the Benjamini-Hochberg method. The log2FC (fold change) was calculated for each gene. Upregulated genes were defined as those with log2FC > 0.5 and adjusted p-values (padj) less than 0.05.

3.5.2 Clustering Analysis

The gene clustering was performed using K-means method implemented in iDEP (0.96) web tool (Ge et al., 2018). In this regard, the genes were normalized using mean center method with K=3 and K=2 for IFNa-responsive and IFNy-responsive genes, respectively. Then, the clustered genes were plotted in a timely manner based on the log2FoldChange extracted from our RNA-seq dataset using R ggplot2 (3.4.2)tool.

3.5.3 Heatmap Generation

Transcriptional responses to IFNα and IFNγ treatment were visualized through the generation of heatmaps, employing the pheatmap v1.0.12 (Kolde, 2019) and ComplexHeatmap v2.10.0 (Gu et al., 2016) packages. Normalized counts obtained from DESeq2 were extracted for selected genes. Row scaling with Z-scores was carried out for plotting purposes. For IFNα group, the hierarchical clustering was performed to rank the genes based on their expression pattern. However, for IFNγ group, to ensure the consistency of genes, those same genes ranked in IFNα

were selected without applying further clustering. The color scale represents the change in expression over time for each sample in comparison to the expression of the non-treated control. High expression is shown in red, while low expression is depicted by the color purple.

3.5.4 Enrichment Analysis Of Gene Ontology And KEGG Terms

The GO biological Process and KEGG enrichment analysis were carried out using enrichGO and enrichKEGG functions, respectively, available in clusterProfiler package (4.10) (Yu et al., 2012). This analysis was conducted under the settings bonferroni-adjusted pvalue cutoff < 0.05 and minimal size of genes annotated by Ontology term for testing >10 and maximal size of genes annotated for testing <500. Then, the results were visualized using dotplot function in the same R package. In both GO and KEGG enrichment, the terms are sorted based on their statistical significance, gene ratio and gene count.

3.6 Chip-Seq Data Analysis

Dr. Agata Sekrecka conducted the ChIP-Seq experiments, while Dr. Katarzyna Kluzek provided support in bioinformatic data analysis, suggesting the most suitable tools at each stage of the analysis process.

All ChIP-seq experiments were run in duplicate and evaluated against input DNA. Following quality assessment of the raw reads using FastQC (Andrews, 2010). ChIP-seq data was processed using the ENCODE Transcription Factor (Figure 13) and Histone ChIP-seq processing pipeline v3 (https://github.com/ENCODE-DCC/chip-seq-pipeline2) with the standard settings (The ENCODE Project Consortium, 2012). In summary, Bowtie2 v2.4.1 (Langmead & Salzberg, 2012) was employed to align the raw reads to the hg38 v29 genome (https://www.encodeproject.org/files/ENCFF110VAV/) with a mapping quality threshold of 30. Following this alignment, Picard Tools (http://broadinstitute.github.io/picard/) was used to mark duplicates. Subsequently, Peaks were identified using SPP with a false discovery rate (FDR) threshold of 0.01. Next, the optimal number of reproducible peaks among biological replicates was measured using the Irreproducible Discovery Rate (IDR) statistical method. It compares a pair of ranked lists of regions and sets scores showing expected probability that the peak belongs to the noise component. An IDR score threshold of 0.02 was selected to generate an optimal set of peaks. After this step, the optimal number of reproducible peaks among biological replicates was determined using the Irreproducible Discovery Rate (IDR) statistical method. Following screening

against curated blacklist of regions in the human genome provided by the ENCODE pipeline, peaks that overlapped with these regions were excluded. Using MACS2, P-value signal tracks were generated for each replicate individually and for the pooled replicates.

Quality control reports were generated at every stage of data analysis, e.g.:

• The library's complexity was assessed by calculating NRF (non-redundant fraction),

PBC1 and PBC2 (PCR bottleneck coefficient), NRF>0.9, PBC1>0.9, and PBC2>10 are recommended values.

• Normalized and Relative Strand Cross-Correlation (NSC and RSC) and Cross-Correlation Plot were used to evaluate ChIP-seq quality. According to ENCODE guidelines, RSC > 0.8 and NSC > 1.05 were recommended.

• IDR Rescue Ratio, IDR Self-Consistency Ratio and IDR Reproducibility Test were implemented for replicate consistency assessment. All samples met the quality standards, according to the thresholds established by ENCODE. A complete description of all parameters is available at: https://www.encodeproject.org/datastandards/terms/#concordance.

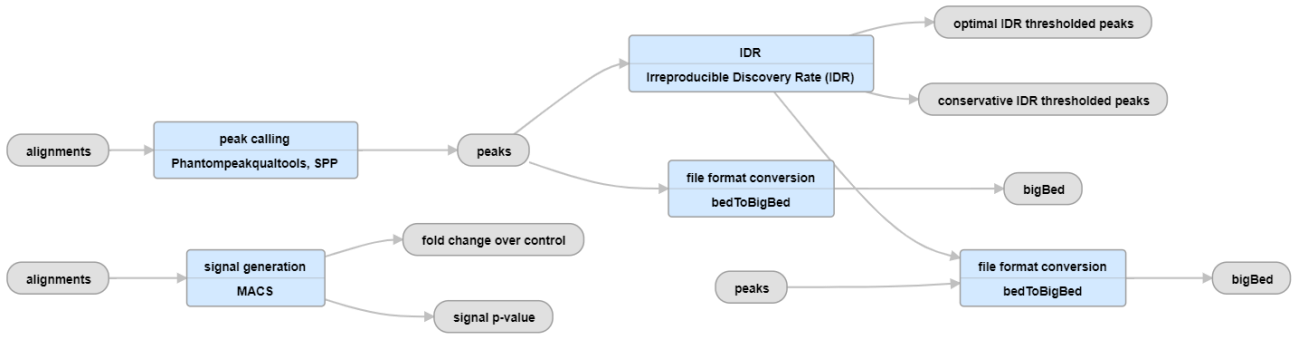

Figure 13. Workflow for processing ChIP-seq data of a transcription factor.

The graph was obtained from ENCODE: Encyclopedia of DNA Elements (Davis et al., 2018). https://www.encodeproject.org/pipelines/ENCPL138KID/

3.6.1 Selection Of Top Score Peaks

In order to ensure high-quality data, peaks with the lowest scores were filtered out from the peak list, employing a cut-off set at 10-20% of the maximum peak score of a specific antibody. Consequently, approximately 4000 peaks with the highest scores were identified for each antibody, except for IRF9. Due to the poor quality of the IRF9 ChIP, a 5% threshold was applied. To further refine this non-redundant peak list, for each antibody, irrespective of time points, peaks with the

highest scores were selected. Subsequently, all the peaks from different antibodies (pSTAT1, pSTAT2, IRF1, IRF9 in case of IFNα and pSTAT1, IRF1 and IRF9 in case of IFNγ) were merged into one list based on the maximum score of the peaks collected from different antibodies. This selection generated a short list of peaks with the highest score which then implemented for peak annotation using Homer tools.

3.6.2 Visualization In The Integrative Genomics Viewer

For visualizing ChIP-seq data in the Integrative Genomics Viewer (IGV) (Thorvaldsdóttir et al., 2013). Bowtie2 aligner v2.4.1 (Langmead & Salzberg, 2012) was used to create BAM files. These files were then converted to bigwig format with bamCoverage from deepTools2 v3.5.0 (Ramírez et al., 2016). Snapshots were then captured for presenting them in figures.

3.6.3 Binding Site Motifs Identification

Using a custom R script, a list of all peaks across samples was generated. These peaks were then analyzed for enriched transcription factor binding motifs using Hypergeometric Optimization of Motif EnRichment (HOMER) version 4.9.1 (Heinz et al., 2010). The findMotifsGenome.pl program (HOMER) was used to discover motifs, employing a standard background and setting the region size for motif discovery to 200. Subsequently, the matrices selected for the characterization of the binding elements including 4 binding elements for GAS and 3 for ISRE (Figure 14) were utilized for annotating binding sites using the annotatePeaks.pl function in HOMER package. Universalmotif package v1.12.1 was used to generated Motif logos (Tremblay, 2021).

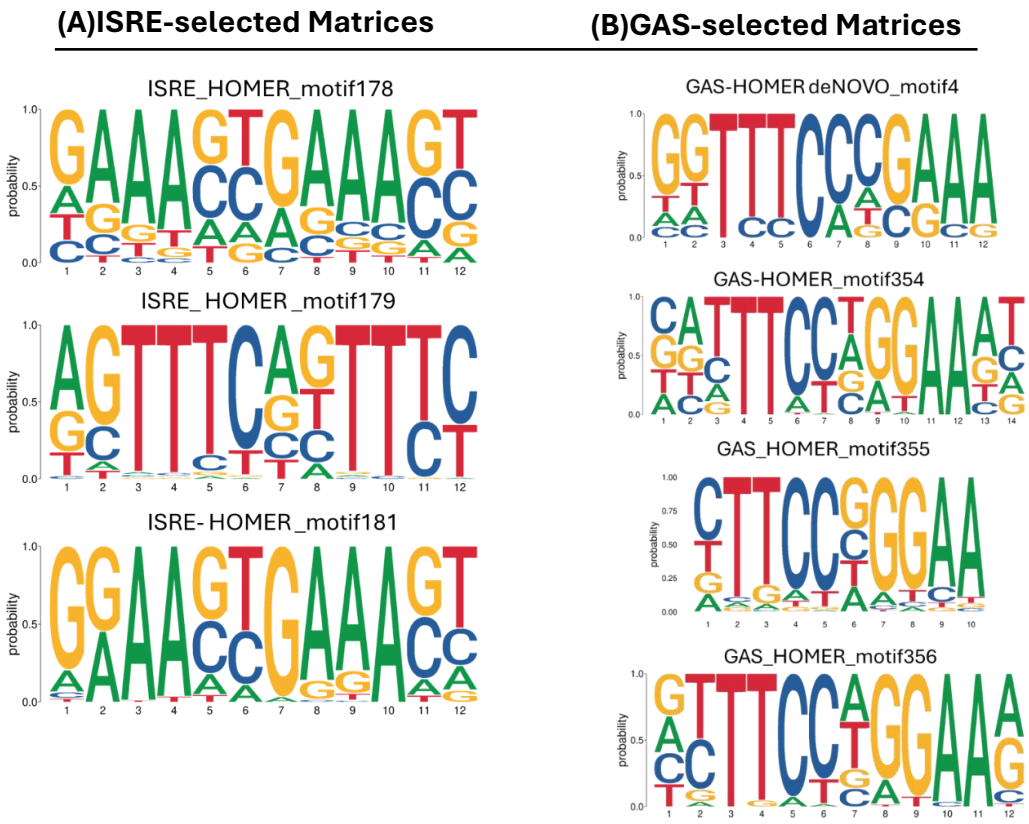

Figure 14. The selected matrices for annotating binding sites in the peak region from ChIP-seq experiments encompass both GAS and ISRE.

For both ISRE **(A)** and GAS **(B)** sites, the final set of matrices employed in annotating TF binding sites.

3.7 Luciferase Reporter Assay

The Gibson assembly methodology was employed to design primers with 15-nucleotide overhangs, which were complementary to the restriction enzyme's cleavage site, for the purpose of generating the intended constructs containing the promoter regions of selected ISGs. In our study the pXPG vector (plasmid#71248, Addgene) used as the structural framework for all luciferase constructs. In this study the pXPG vector was linearized using the SmaI (R0141S, NEB) restriction enzyme, following the manufacturer's protocol. Subsequently, the assembly of the plasmid and an insert was accomplished using the NEBuilder® HiFi DNA Assembly master mix (E2621, NEB). The amplification of the promoter regions for the pre-selected ISRE+GAS composite genes including, APOL6, DDX60, DDX58, NMI, NLRC5 and IRF1 (proximal and distal) was carried out using 70 ng genomic DNA (gDNA) sourced from Huh7.5 cells as the template. The reaction was initiated by employing PrimeSTAR GXL DNA polymerase (R050B,

Takara) (Table 6) in accordance with the manufacturer's instructions and executed using the T100 Thermal Cycler (BioRad).

Denaturation	98°C	10 sec	30-40 cycles
Annealing	60 °C	15 sec	
Extension	68°C	10sec/kb	
Soak	4°C	Indefinite	1 cycle

Table 6. PCR program using PrimeSTAR GXL DNA polymerase.

The PCR product visualization on the agarose gel was performed using Simply Safe dye. Following this, a column-based purification step was conducted on PCR product utilizing the Monarch DNA Gel Extraction Kit (T1020, NEB) according to the manufacturer's instructions. DNA fragments were assembled using NEBuilder HiFi DNA Assembly Master Mix (E2621, NEB) at a temperature of 50°C for a duration of 45 minutes. During the heat-shock process the DH5α E. Coli competent cells were transformed and plated on Agar medium (2021_1000, A&A Biotechnology) supplemented with antibiotics (ampicillin 100mg/ml, 2017-5,A&A Biotechnology) and incubated at 37°C overnight. Following the incubation period, colony PCR was conducted to screen bacterial colonies using GoTaq® G2 DNA Polymerase (M7841, Promega) (Table 7). The primers applied for colony PCR annealed to the plasmid and flank the region of interest and they were the same as those utilized for Sanger sequencing (Table 8). Subsequently, the PCR product was visualized on a 1% agarose gel to verify the presence of the insert (the promoter sequences of pre-selected composite genes) within the pXPG vector. Following the selection of positive colonies, they were inoculated into liquid bacterial culture medium (LB, 2020-1000, A&A Biotechnology) and allowed to incubate overnight at 37°C. Afterwards, plasmids were extracted using the column-based Monarch® Plasmid Miniprep Kit (T1010L), NEB).

Pre- Denaturation	**95°C**	**2 min**	**20-30 cycle**
Denaturation	95°C	0:15 min	
Annealing	60°C	0:15	
Extension	72°C	1min/1kb	
Extension	72°C	5 min	1 cycle
Soak	4°C	Indefinite	1 cycle

Table 7. PCR conditions for reactions with GoTaq polymerase.

Primer name	Forward/Reverse	Sequence 5'->3'
Fluc	Forward	ATCATGTCTGGATCCAAGCTCA
	Reverse	TCTCCAGCGGTTCCATCTTC

Table 8. Primers used for colony PCR and Sanger sequencing.

After plasmid isolation they were dispatched to the Molecular Biology Techniques Laboratory at Adam Mickiewicz University in Poznan, Poland, for Sanger sequencing. The alignment of the acquired sequences was conducted using Geneious Prime software. To investigate the promoter activity of the pre-selected composite genes, a luciferase reporter assay was conducted. Initially, Huh7.5 cells, comprising WT, STAT1KO, STAT2KO, IRF9KO, IRF1KO, and IRF1.9dKO cell lines, were seeded into 96-well plates at a density of 1.8 x 103 cells per well. After 20 hours, the cells were co-transfected with 70 ng of experimental plasmids along with 30 ng of pRLRenilla luciferase control reporter vector (pRL-SV40; [E2231, Promega]) as an internal control, utilizing Lipofectamine 3000 (L3000-015, TFS) as the transfection reagent. 24 hours post transfection, cells were treated with IFNα (1000 U/ml) or IFNγ (10 ng/ml) for 8 hours. Following that, luciferase reporter assay with four technical replicates per experiment was conducted using Dual-Glo® Luciferase Assay System (E2920, Promega) in accordance with the manufacturer's guidelines and luminescence level was quantified with the SPARK® multimode microplate reader (TECAN). Firefly luciferase activity was normalized to Renilla luciferase activity within each sample to calculate the Relative Luciferase Units (RLU). Data visualization was carried out using GraphPad Prism 6.01. The flanking primers used for inserting the wild-type promoter sequences in this study are listed in Table 9.

Primer name	Forward/Reverse	Sequence 5'->3'
pXPG_APOL6	Forward	atctcgagctcggtacccAGATGCTGTGGAGGAAAGCA
	Reverse	tgccaagcttgtcgacccCAGGTGCCTAAAGCCAACCC
pXPG_NMI	Forward	atctcgagctcggtaccc ACAAGC TCCACA ACAAAA CAAGA
	Reverse	tgccaagcttgtcgaccc AGCTTG CAGTGA GCCGAG AT
pXPG_DDX60	Forward	atctcgagctcggtacccGTTTATACAGAACAGTAATCATCAGCT
	Reverse	tgccaagcttgtcgacccCTGCCCCTTGACCAGGAATA
pXPG_DDX58	Forward	atctcgagctcggtacccTTAAGAAAATGAAATGGTAAGCCACA
	Reverse	tgccaagcttgtcgacccTTCACCTCGCTGGAACTCAG
pXPG_NLRC5	Forward	atctcgagctcggtacccCATCCTGGAGGCTCTCCG
	Reverse	tgccaagcttgtcgacccGCCGGCAACTCTTCCTCC
pXPG_IRF1_Proximal	Forward	atctcgagctcggtacccATCAAGGTAGGGCTACTATT
	Reverse	tgccaagcttgtcgacccGGTCCACGCCGCGTC
pXPG_IRF1_Distal	Forward	atctcgagctcggtacccGCACAGTCCCCTCTTTCCC
	Reverse	tgccaagcttgtcgacccAAACGTTGCACTGTTATAAAATTCCT

Table 9. The primer sequences used for the integration of the promoter region of ISRE+GAS-composite genes into the pXPG plasmid. Overhangs that complement the pXPG vector are indicated in small letters.

NEBuilder® HiFi DNA Assembly Master Mix was utilized to perform site-directed mutagenesis (SDM) on the GAS and ISRE sites, following the manufacturer's instructions. Table 10 represents the flanking primers with mutations used for SDM in this study. To generate constructs containing mutated ISRE or GAS sites, a PCR reaction was initiated by employing 10ng of a plasmid containing the wild-type composite genes promoter sequence as a template, using PrimeSTAR GXL DNA polymerase (R050B, Takara). Following this, the PCR product was observed on an agarose gel and subsequently purified using column-based Monarch DNA Gel Extraction Kit. NEBuilder HiFi DNA Assembly Master Mix was used to perform plasmid ligation at a temperature of 50°C for a duration of 45 minutes. Subsequent procedures, such as bacterial transfection, colony selection, and Sanger sequencing were carried out. In order to create a double-mutant plasmid (mutated ISRE and GAS simultaneously), plasmids harboring single mutations (mutated ISRE or mutated GAS) were employed as templates for a PCR reaction.

Primer name	Forward/Reverse	Sequence 5'->3'
pXPG_PARP14_ ΔISRE	Forward	ACACTCGCGCTCGAGTCAAAGTTAGCGGCCCGG
	Reverse	CTCGAGCGCGAGTGTTTCCTGGAAAACTCCCAGGC
pXPG_PARP14_ ΔGAS	Forward	GTTACACAGACAACGAAAGCGAAAGAGTCAAAGTTAGC
	Reverse	CGTTGTCTGTGTAACTCCCAGGCCTTGGTTTCC
pXPG_PARP14_ ΔISRE/ΔGAS	Forward	ACACTCGCGCTCGAGTCAAAGTTAGCGGCCCGG
	Reverse	CTCGAGCGCGAGTGTTTCCTGGAAAACTCCCAGGC
pXPG_PARP14_ ΔpISRE	Forward	ACGAAAGCGCTCGAGTCAAAGTTAGCGGCCCGG
	Reverse	CTCGAGCGCTTTCGTTTCCTGGAAAACTCCCAGGC
pXPG_PARP14_ΔpGAS	Forward	GTTACACAGGAAACGAAAGCGAAAGAGTCAAAGTTAGC
	Reverse	CGTTTCCTGTGTAACTCCCAGGCCTTGGTTTCC
pXPG_DDX60_ ΔISRE1	Forward	GGACTCCTGCTCCCTAAGTGCTTCTGAGAGGAGAAAGG
	Reverse	AGGGAGCAGGAGTCCTTCAGCACGAATTAGGCG
pXPG_DDX60_ ΔGAS	Forward	ACTACACACACAAGTGCCTCGCCTAATTCGTGC
	Reverse	ACTTGTGTGTGTAGTTTAGCATCCTTCCCTTCAATCAG
pXPG_DDX60_ ΔISRE1/ΔGAS	Forward	ACTACACACACAAGTGCCTCGCCTAATTCGTGC
	Reverse	ACTTGTGTGTGTAGTTTAGCATCCTTCCCTTCAATCAG
STAT1_pd_distΔISRE/ΔGAS	Forward	CAGAGCTCGAGCTCGCACGTGGGGCGGCTCTTC
	Reverse	CGAGCTCGAGCTCTGCCCGGGAGCGAGAAGG
STAT1_pd_distΔISRE_proxΔISRE	Forward	TAAAGCGAGCGGCTCGGTTTCCTCTCAATCCCAGTCC
	Reverse	GAGCCGCTCGCTTTAGAGCCTGCGGGAGCAGTACG
STAT1_pd_ΔISRE/ΔISRE/ΔGAS	Forward	CAGAGCTCGAGCTCGCACGTGGGGCGGCTCTTC
	Reverse	CGAGCTCGAGCTCTGCCCGGGAGCGAGAAGG
pXPG_NMI_ ΔISRE1	Forward	TCACTCGTGCTCTTAGTTTTTTTTTCTGTTAGTGACT
	Reverse	TAAGAGCACGAGTGATTTTTAAAAAGGGGTGGTTTTGC
pXPG_NMI_ ΔGAS	Forward	TGTTACACGGACAGGGCAGGCGCGCTGGGCCTTGG
	Reverse	CCTGTCCGTGTAACAGCAGCGCCTGAAACGCC
pXPG_NMI_ ΔISRE1/ΔGAS	Forward	TGTTACACGGACAGGGCAGGCGCGCTGGGCCTTGG
	Reverse	CCTGTCCGTGTAACAGCAGCGCCTGAAACGCC

Table 10. Primer sequences for mutagenesis of composite gene promoters.

3.8 Antiviral Assay

Antiviral assays were carried out on various cell types, including WT, STAT1KO, and IF1.9dKO Huh 7.5 cell lines, with and without IFNα (WT and STAT1KO cells), IFNβ and IFNγ (WT, STAT1KO and IRF1.9dKO cells) stimulation. These collaborative antiviral experiments took place at Professor Chien-Kuo Lee's laboratory within the Graduate Institute of Immunology, College of Medicine, National Taiwan University in Taipei, Taiwan.

IFNα-treated cells:

To conduct antiviral assay, proper amount of WT, STAT1KO cells were plated in a 96-well plate. After 24 hours they were left untreated or treated following 2-fold serial dilutions of IFNα starting from 1000 U/ml. 24 hours post treatment, cells were infected by vesicular stomatitis Indiana virus (VSV) at a multiplicity of infection (MOI) of 0.1. 20 hours post-infection the medium was aspirated, and cells were then fixed with a 4% formaldehyde solution at room temperature for 20 minutes. Crystal violet (0.5%) staining was applied to visualize the cells, and any extra dye was eliminated by immersing the plate in water.

IFNβ-treated cells:

Proper amount of WT, STAT1KO and IRF1.9dKO cells were plated in a 96-well plate. After 24 hours they were left untreated or treated following 2-fold serial dilutions of IFNβ (300-02BC, Peprotech) starting from 100 U/ml. 24 and 72 hours post treatment, cells were infected by VSV at a MOI of 1.0. 20 hours post-infection the medium was aspirated, and cells were then fixed with a 10% formaldehyde solution at room temperature for 20 minutes. Crystal violet (0.5%) staining was applied to visualize the cells, and any extra dye was eliminated by immersing the plate in water.

IFNγ-treated cells, (two different amounts were applied):

1. Proper amount of WT cells were plated in a 96-well plate. After 24 hours they were left untreated or treated following 2-fold serial dilutions of IFNγ (300-02, Peprotech) starting from 4000pg/ml. 24 hours post treatment, cells were infected by VSV at a MOI of 0.1. 20 hours post-infection the medium was aspirated, and cells were then fixed with a 10% formaldehyde solution at room temperature. Crystal violet staining was applied to visualize the cells, and any extra dye was eliminated by immersing the plate in water. **2**. Proper amount of WT, STAT1KO and IRF1.9dKO cells were plated in a 96-well plate. After 24 hours they were left untreated or treated following 2-fold serial dilutions of IFNγ (300-02, Peprotech) starting from 10000 U/ml. 24 and 72 hours post treatment, cells were infected by VSV at a MOI of 1.0. 20 hours post-infection the medium was aspirated, and cells were then fixed with a 10% formaldehyde solution at room temperature. Crystal violet staining was applied to visualize the cells, and the plate was submerged into water to remove any extra dye.

4 Results

4.1 Identifying ISRE+GAS Composite Genes

To identify IFNα and IFNγ-induced composite genes we developed a composite gene selection strategy, based on previously generated ChIPseq and RNAseq data sets (Figure 15). Chromatin immunoprecipitation sequencing (ChIP-seq) experiments were performed by Agata Sekrecka on IFNα-treated WT-Huh7.5 cells utilizing antibodies against pSTAT1(phosphorylated STAT1), pSTAT2(phosphorylated STAT2), IRF9 and IRF1 at time points of 0, 0.5h, 2h, 8h, 24h, and 72h and IFNγ-treated WT-Huh7.5 cells using antibodies targeting pSTAT1 (phosphorylated STAT1), IRF9 and IRF1 at time points of 0, 0.5h, 4h, 24h, and 72h. After ChIP-seq analysis (see material and methods), as it is shown in the workflow (Figure 15) Initially, a list of ISRE+GAS-composite genes was prepared that displayed high- quality peaks (peak scores>100 for any one of the antibodies, in at least one timepoint) in response to IFNα. (The term used for the composite genes in the thesis is "ISRE+GAS-composite genes"). Only protein-coding composite genes were chosen. Subsequently, composite genes underwent filtration based on ISRE/GAS motifs present in the promoter/5'UTR regions. Following that, we examined whether the remaining composite genes showed peak scores >100 in response to IFNγ. Next, to investigate the expression level of composite genes in response to IFNα or IFNγ, we applied the analyzed data obtained from RNA-seq (see material and methods). It's noteworthy to mention that RNA-seq experiments were conducted by Agata Sekrecka on IFNα and IFNγ-treated WT-Huh7.5 cells at time points of 2h, 4h, 8h, 24h, 48h and 72h. By conducting a differential gene expression analysis (DEG), genes that indicated log2FC>0.5 and padj < 0.05 (at any one of the time points) were considered as up-regulated genes. Accordingly, composite genes that showed no expression in response to both IFNs were eliminated. In addition, in our previous study (Sekrecka et al., 2023) composite structure was identified in the distal regulatory element (-6 kb) of STAT1 gene. Moreover, in this study, we identified ISRE+GAS composite structure at the distal regulatory element (-6 Kb) of IRF1 gene. Both STAT1 and IRF1 genes displayed peak scores>100 and significantly induced in response to IFNα or IFNγ (log2FC>0.5 and padj<0.05). As a result, a list of 89 ISRE+GAS composite genes was generated (Table S1) which was broadly categorized into three gene groups including commonly IFNα and IFNγ-induced genes (Table S1-pink panel), IFNα-induced genes (Table S1-green, blue and yellow panels) and finally, IFNγ-induced genes (Table S1-orange and red panels). For further characterization of composite genes we pre-selected 30 composite genes

that revealed different ISRE/GAS distances and random organizations (Table 11). Accordingly, we performed cluster (Figure 17) and heatmap analysis (Figure 19) along with examining the binding patterns of STAT1, pSTAT1, STAT2, pSTAT2, IRF9 and IRF1 in response to IFNα and STAT1, pSTAT1, IRF9 and IRF1 in response to IFNγ in WT cells (Figure 18). Likewise, we compared the binding pattern of pSTAT2 and IRF9 in STAT1KO cells (Figure 20) to WT cells in response to IFNα. Later, to gain a deeper understanding of how composite genes are regulated transcriptionally and whether the distances and orientations of ISRE/GAS elements affect this regulation, we conducted qPCR in WT, STAT1, STAT2, IRF9, IRF1 and IRF1.9dKO cells and analyzed the detailed binding patterns of pSTAT1, pSTAT2, IRF9 and IRF1 in response to IFNα and pSTAT1, IRF9 and IRF1 after IFNγ treatment for 13 pre-selected ISRE+GAS-composite genes (Table11-genes are marked in green) from different ISRE/GAS distance groups in WT and STAT1KO cells (refer to part 4.3). Next, we performed promoter-luciferase reporter assay on IFNα and IFNγ- treated WT cells for 8 composite genes including PARP14, APOL6, DDX60, NLRC5, DDX58, NMI, STAT1 and IRF1 (refer to part 4.5) to understand the role of ISRE and GAS. Last but not least, we conducted promoter-luciferase reporter assay on IFNα and IFNγ-treated WT, STAT1, STAT2, IRF9, IRF1 and IRF1.9dKO cells for 5 composite genes including PARP14, APOL6, DDX60, NMI and STAT1(in case of STAT1 gene, luciferase assay was conducted in WT, STAT1, STAT2 and IRF1KO cells) , to understand the precise role of different complexes such as ISGF3, GAF, GAF-like, IRF1, STAT2/IRF9 and STAT1/IRF9 (refer to part 4.6).

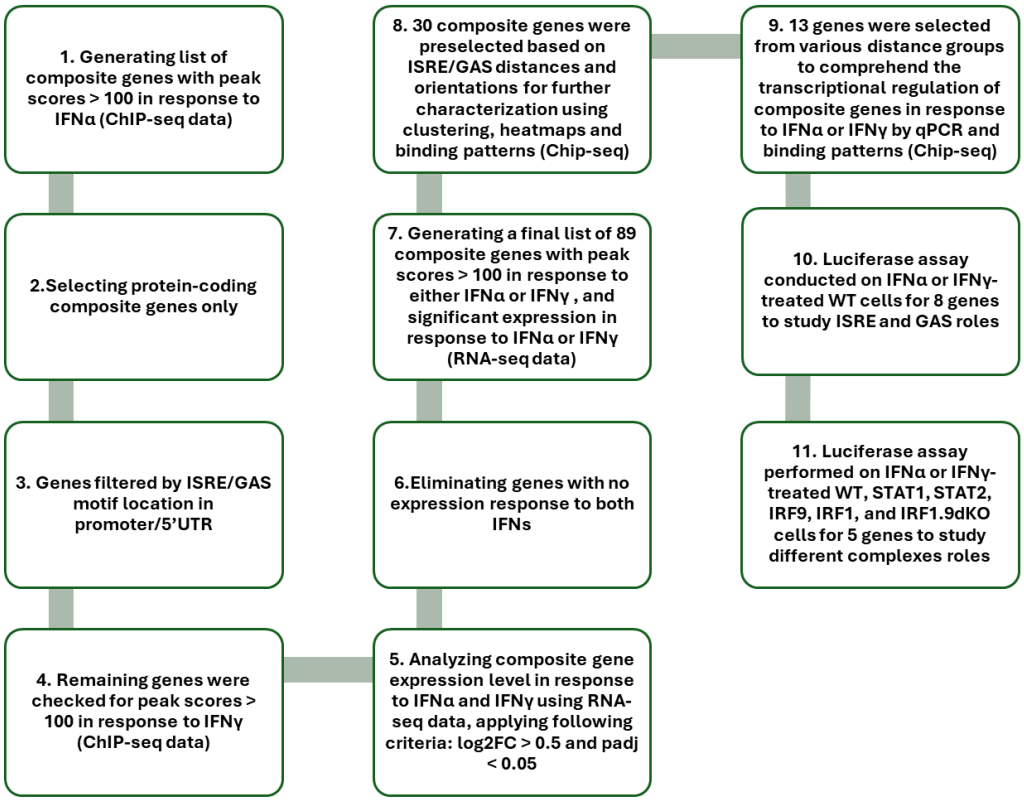

Figure 15. The workflow for generation of 89 composite gene list and pre-selection of composite genes for further analysis.

The compilation of 89 composite genes underwent an analysis for enrichment in Gene Ontology (GO) terms for Biological Processes (Figure16-A) and for KEGG (Kyoto Encyclopedia of Genes and Genomes) Pathway (Figure16-B). As shown in the figure 16 panel A, the terms related to viral response are expectedly enriched, indicating the prominent involvement of our gene set in such biological processes. Other terms also represent the immune response activity in our gene set. As illustrated in panel B, the term related to Coronavirus Disease is significantly enriched, showing the involvement of our gene set in this pathway which is related to viral infection response. In addition, other pathways reflect the contribution of our gene set in other viral infection-related pathways such as Influenza A and Epstein-Barr virus infection. In accordance with GO analysis, the primary functionality of 89 composite genes was linked to the defense response and processes within the immune system.

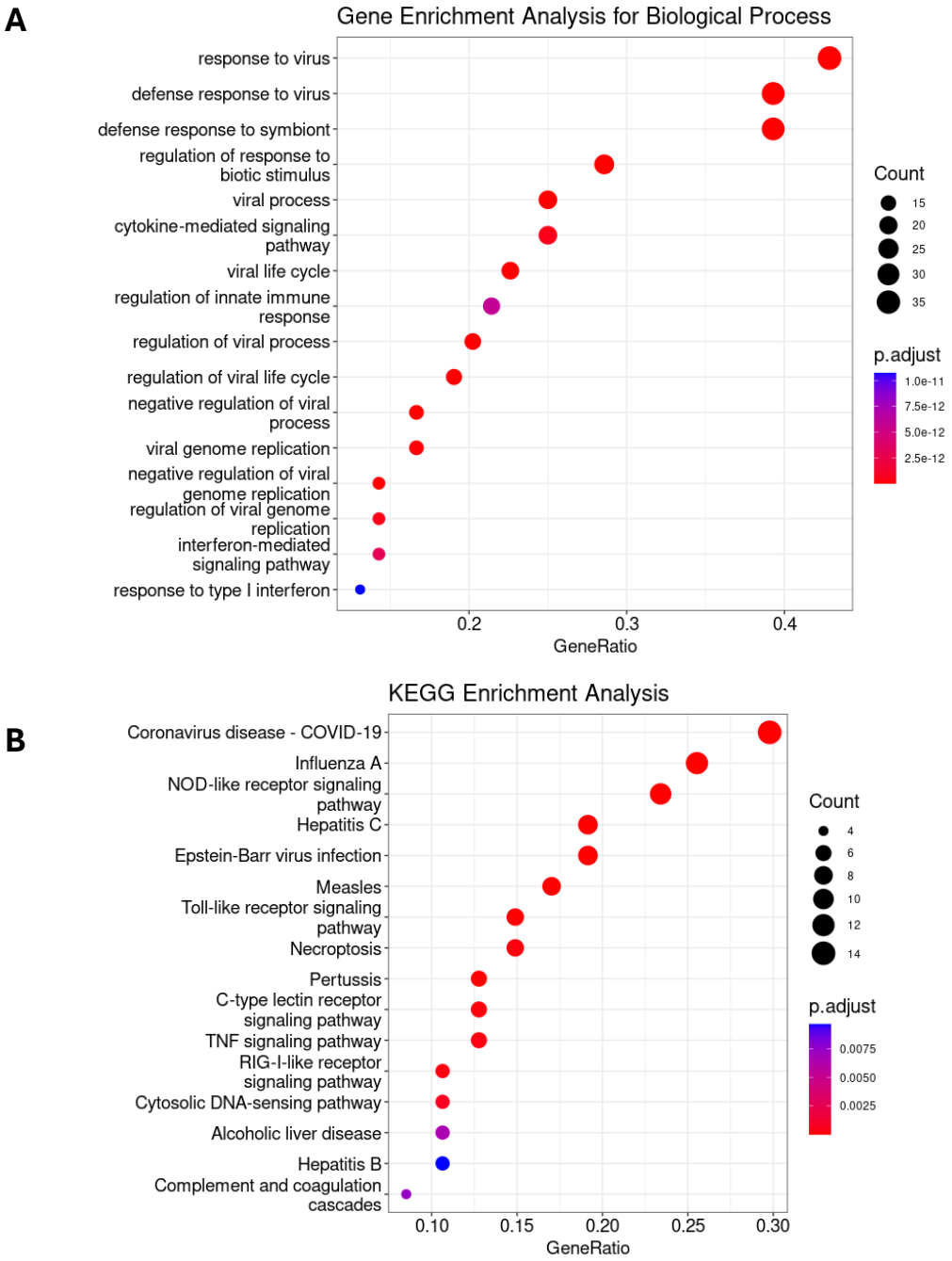

Figure 16. The enrichment analysis for Biological Processes and KEGG Pathway.

A. GO term enrichment analysis was conducted and plotted on the list of 89 IFNα or IFNγ upregulated composite genes using R package clusterProfiler (version 3.0.4). The x-axis, labeled "GeneRatio," spans from 0 to approximately 0.5, representing the ratio of genes associated with each biological process within the total gene set. The y-axis enumerates various biological processes, predominantly related to viral response and immune system activation. Each circle on the scatter plot corresponds to one of these biological processes. The size of each circle is proportional to the count of genes associated with the corresponding biological process, with sizes varying from 15 to 35. The color of the circles indicates the adjusted p-value (p-adjust) for each process, with a color gradient from purple to red. The darker the color, the lower the p adjust value, indicating a higher statistical significance. (Description continues on the next page)

B. The gene enrichment analysis was conducted and plotted using R package clusterProfiler (version 3.0.4). The x-axis represents the "GeneRatio," which ranges from 0 to 0.30, indicating the proportion of genes associated with each disease or condition within the total gene set. The y-axis enumerates various diseases and conditions. Each disease or condition is represented by a colored circle on the scatter plot. The size of each circle corresponds to the count of genes associated with the respective disease or condition, ranging from 4 to 14. The color intensity of the circles indicates the adjusted p-value for each disease or condition, with a gradient from dark purple to red representing p adjust values.

4.2 Exploring ISRE/GAS Distances And Organizations: Further Characterization Of Composite Genes

To increase our understanding of the transcriptional regulation of composite genes, a preselection process was implemented for commonly induced composite genes by IFNα and IFNγ (padj less than 0.05, log2FC > 0.5) exhibiting binding pSTAT1, pSTAT2, IRF9, and/or IRF1 after IFNα treatment, as well as binding pSTAT1 and/or IRF9 and/or IRF1 upon IFNγ treatment. This preselection specifically considered the distance between ISRE and GAS motifs and the ISRE/GAS organization as pivotal criteria to investigate whether variable distances or random organization might impact the transcriptional regulation of composite genes in response to IFNα and IFNγ. Accordingly, 30 ISRE+GAS-composite genes (Table 11) were selected which displayed different arrangements of ISRE and GAS exhibiting either ISRE-GAS (+) or GAS-ISRE (−) configurations with variable distances ranging from overlap to more than 200 base pairs. Based on the variable ISRE/GAS distance composite genes were categorized into five groups (Table 11, groups are divided by bold horizontal lines) comprising genes with I. very close ISRE/GAS (0-5 nt; i.e. PARP14), II. close ISRE/GAS distance (5-20 nt; i.e. APOL6), III. medium ISRE/GAS distance (20-100 nt; i.e. NLRC5), IV. long ISRE/GAS distance (>100 nt; i.e. NMI), VI. group of genes with distal regulatory ISRE/GAS (i.e. STAT1).

	GENE	ISRE	Linker	GAS	Orientation
	Consensus	AG-TTT-CNN-TTT-CN		-TTC-CNG-GAA-	
1	IFI35	AC-TTT-CA-TTT-CC	OVERLAP	TTC-ACG-GAA-A	-
2	EPSTI1	AG-TTT-CGG-TTT-CT	OVERLAP	TTC-TGA-GAA-A	-
3	MYD88	GC-TTT-CGC-TTT-CC	OVERLAP	TTC-TCG-GAA-A	-
4	LGALS3BP	AC-TTT-CGA-TTT-CC	OVERLAP	TTC-TG-GAA-A	-
5	**PARP14**	GC-TTT-CG-TTT-CC TC-TTT-CGC-TTT-CG	OVERLAP 1	TTC-CAG-GAA-A	-
6	**ETV7**	TC-TTT-CGT-TTT-CG	0	TTC-CCG-GAA-G	+
7	**SP110**	AC-TTT-CAC-TTT-TC	1	TTC-TCG-GAA-G	+
8	IRF2	AA-TTT-CAT-TTT-CG	2	TTC-CGA-GAA-A	+
9	TRIM22	AC-TTT-CG-TTT-CT	2	TTC-TGA-GAA-T	-
10	APOL2	AC-TTT-CAC-TTT-CC	4	TGC-TGG-GAA-G	-
11	**GBP3**	AC-TTT-CAG-TTT-CA	5	TTC-CTT-GAA-A	-
12	IFITM3	AG-TTT-CGG-TTT-CT	14	TGC-CAG-GAA-A	-
13	CXCL10	GG-TTT-CAC-TTT-CC	14	TTC-AA-GAA-A	-
14	**STAT2**	AG-TTT-CGG-TT-CC	15	TTC-TC-GAA-A	+
15	**IRF9**	AG-TTT-CAG-TT-CT	16	TTC-TGG-GAA-A	-
16	PHF11	GG-TTT-CGT-TTT-CT	16	TTC-CGG-GAT	+
17	DTX3L	AG-TTT-CGC-TT-CC	17	TGC-CGG-GAA	-
18	**APOL6**	AC-TTT-CAG-TTT-CC	18	TTC-CTG-GAA-G	+
19	**DDX60**	1-GG-TTT-CAG-TTT-CC 2-AG-TTT-CGG-TTT-CC	25 61	TTC-CAC-GAA-A	- -
20	USP18	AG-TTT-CGC-TTT-CC	37	TTC-CCC-GCA	-
21	**NLRC5**	AC-TTT-CAG-TTT-CG	48	TTC-TCG-GCA-G	-
22	PLSCR1	GG-TTT-CG-TTT-CC	52	TTC-TGA-GAA-G	+
23	CD274	AC-TTT-CTG-TTT-CA	63	TTC-ACC-GAA	+
24	CSF1	AC-TTT-CAC-TTT-CC	65	TTC-CCA-TAA-A	-
25	ACY3	GC-TTT-CGG-TTT-CT	88	TTC-CCT-GAA-G	+
26	TMEM140	AC-TTT-CG-TTT-CC	148	TTC-TG-GAA	-
27	**DDX58**	AG-TTT-CG-TTT-CC	213	TTC-CTA-TAA-A	-
28	**NMI**	1-AA-TTT-CAC-TTT-CG 2-TG-TTT-CAA-TTT-CC	274 314	TTC-CGG-GAA-G	+ -
29	**STAT1**	AC-TTT-CGC-TTTT (Distal regulatory element) AG-TTT-CGC-TTT-CC (Proximal promoter)	39 6223	TTC-CCC-GAA-A (Distal regulatory element)	+
30	**IRF1**	GG-TTT-CGG-TTT-CT (Distal)	6123 718 399 33	TTC-CCC-GAA (Proximal) TTC-CCG-GAA-A (Dist-GAS1) TTC-GCG-GAA-A (Dist-GAS2) TTC-CAG-GAAG (Dist-GAS3)	 - + +

Table 11. The selected list of 30 GAS+ISRE-composite genes with their relevant distance.

Composite genes listed presenting the sequences of both GAS and ISRE motifs with the specified orientation of ISRE and GAS(ISRE-GAS (+) or GAS-ISRE (−)) and distance between both sites indicated as the Linker. The bold horizontal lines separates the gene groups based on their ISRE/GAS proximity and marked genes in green are pre-selected composite genes for further characterization.

4.2.1 Insights Into Time-Dependent Expression Patterns And The Impact Of ISRE/GAS Distances And Organizations

The examination of the expression profile of 30 pre-selected composite genes using RNA-seq data obtained from IFNα and IFNγ treated WT Huh7.5 cells indicated various expression patterns over time (Figure 17). In response to IFNα, three distinct clusters were identified and each characterizing distinct time-dependent patterns (Figure 17-A): an early response cluster (maximum 4h, i.e.CD274, cluster A), an intermediate response cluster (maximum 8h, i.e.PARP14, cluster B) and a late response cluster (>8h, i.e.LGALS3BP cluster C). Whereas, two clusters were identified in response to IFNγ in which genes distinguished mainly intermediate (i.e. STAT1) and late (i.e. DDX60) profiles (Figure 17-B) (IRF1, the only gene expressed maximally at the early time point in response to IFNγ, was not categorized into a separate group). Some genes such as DDX60 indicated maximum expression at intermediate time points after IFNα stimulation, while in response to IFNγ it displayed maximum expression at later time points. However, genes such as PARP14 indicated intermediate responses to both IFNs. Furthermore, we observed that the majority of composite genes displayed maximum expression at 8h in response to both IFNs. However, the expression level decreased 24h after IFNα and IFNγ treatment. Genes in distinct groups with random ISRE/GAS organization and distances including PARP14, STAT2, DDX60, DDX58 and STAT1 (Table 11) exhibited comparable expression patterns in response to IFNα. Likewise, after IFNγ treatment, ETV7, APOL6, NLRC5, NMI and STAT1 displayed similar expression patterns. These observations might indicate that the expression profile of composite genes is not influenced by variations in the distance or arrangement of ISRE and GAS elements.

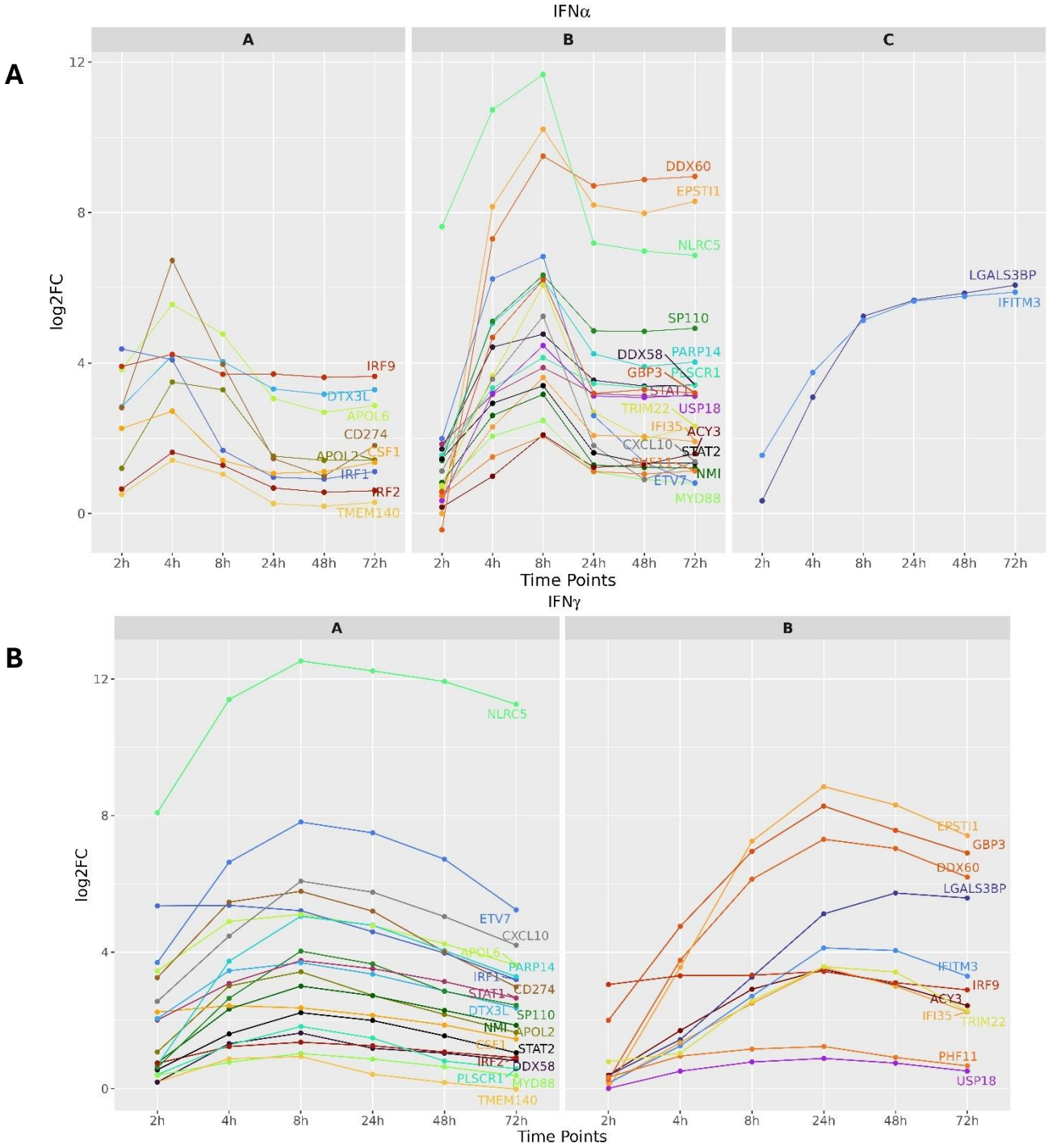

Figure 17. The clustering of the 30 composite genes obtained from RNA-seq data. Expression changes over time in WT Huh7.5 cells in response to IFNα and IFNγ.

30 composite genes were clustered in three groups in case of IFNα **(A)** and two groups in case of IFNγ **(B).** treatment based on k-means methods using iDEP (96) tool. (data presented as log2fold change) obtained from IFNα and IFNγ treated WT Huh7.5 cell lines. n=2

4.2.2 Differential Binding Of ISGF3, GAF, GAF-Like, And IRF1 Complexes To Composite Genes Is Required For Time-Dependent IFNα And IFNγ Transcriptional Responses

Upon conducting a more detailed analysis of the ChIP-seq data for the commonly induced 30 composite genes, we observed similar and strong binding pattern of STAT1, pSTAT1,STAT2 ,pSTAT2, IRF9 and IRF1 for STAT2, IFITM3, MYD88, DTX3L, USP18, TMEM140, PLSCR1, APOL6, PARP14, DDX60, DDX58, APOL2, STAT1 (Figure 18-AI), IRF2, NMI, SP110, CD274, NLRC5, PHF11 (Figure 18-AII) in response to IFNα. However, IRF9, IRF1 (Figure 18-AI), TRIM22, EPSTI1 and IFI35 (Figure 18-AII) displayed either weak or no IRF1 binding upon IFNα treatment. Likewise, following IFNα stimulation, LGALS3BP, ACY3,IFI35, CXCL10, CSF1, ETV7 and GBP3 (Figure 18-AII) exhibited weak IRF9 binding . On the other hand in response to IFNγ, comparable STAT1, pSTAT1, IRF9 and IRF1 binding was detected for STAT1, APOL6, DTX3L, STAT2, TMEM140, PARP14, PLSCR1, APOL2, IFITM3 (Figure 18-BI), DDX60, USP18, DDX58, SP110 and NLRC5 (Figure 18-BII). However either weak or no IRF9 binding was observed for NMI, MYD88, CSF1, APOL2, ETV7, CD274 (Figure 18-BI), LGALS3BP, IFI35, ACY3, GBP3, IRF2 and PHF11 (Figure 18-BII) in response to IFNγ. In addition, EPSTI1, CXCL10, TRIM22 displayed weak IRF1 and IRF9 binding upon IFNγ treatment. On the contrary, no IRF1 binding was detected for IRF1 and IRF9 genes in response to IFNγ (Figure 18-BI). This observation aligned with the occurrence of an ISRE and a GAS site located within their promoters, characterized by a random arrangement and differing distances. However, for STAT1 and IRF1 genes, ISRE and GAS composite structure was observed at distal regulatory site(Figure18-AI-BI). As it is indicated in figure, composite genes organized in a descending order based on their binding patterns, moving from stronger (Figure 18-AI-BI) to weaker (Figure 18-AII-BII), in response to IFNα or IFNγ. To visualize the binding affinity of weak binders, adjustments were made to the IGV scale. Interestingly, binding of pSTAT and STAT was still present at 72h after treatment, whereas no transition could be observed from phosphorylated STATs (pSTATs) to unphosphorylated STATs (STATs) in chromatin interaction of composite genes in response to both types of interferons. Interestingly, binding of IRF1 to certain target genes (i.e. PARP14) was detected at the basal level (Figure 18-AI-BI). Additionally, the binding of IRF9 to the promoter region of various composite genes such as APOL6 and PARP14 following IFNγ stimulation (Figure 18-BI) could suggest a possible role for STAT1/IRF9 in the transcriptional regulation of these genes (Sekrecka et al., 2023). The strong binding of all components including pSTAT1,

pSTAT2, IRF9 and IRF1 after IFNα stimulation and strong binding of pSTAT1, IRF9 and IRF1 in response to IFNγ for some genes (i.e. APOL6) could predict the involvement of ISGF3+IRF1 binding to ISRE and GAF+GAF-like binding to GAS following IFNα treatment. Additionally, it suggests the role of IRF1+STAT1/IRF9 binding to ISRE and GAF targeting GAS sites in response to IFNγ. In general, the participation of all components indicated the switch ability of ISRE and GAS in their transcriptional regulation. Furthermore, it became apparent that, despite differences in the distance and orientation of GAS and ISRE motifs, genes generally displayed similar binding profiles, whether strong or weak. This observation suggests that there is no correlation between ISRE/GAS distances or orientation and binding patterns.

AI

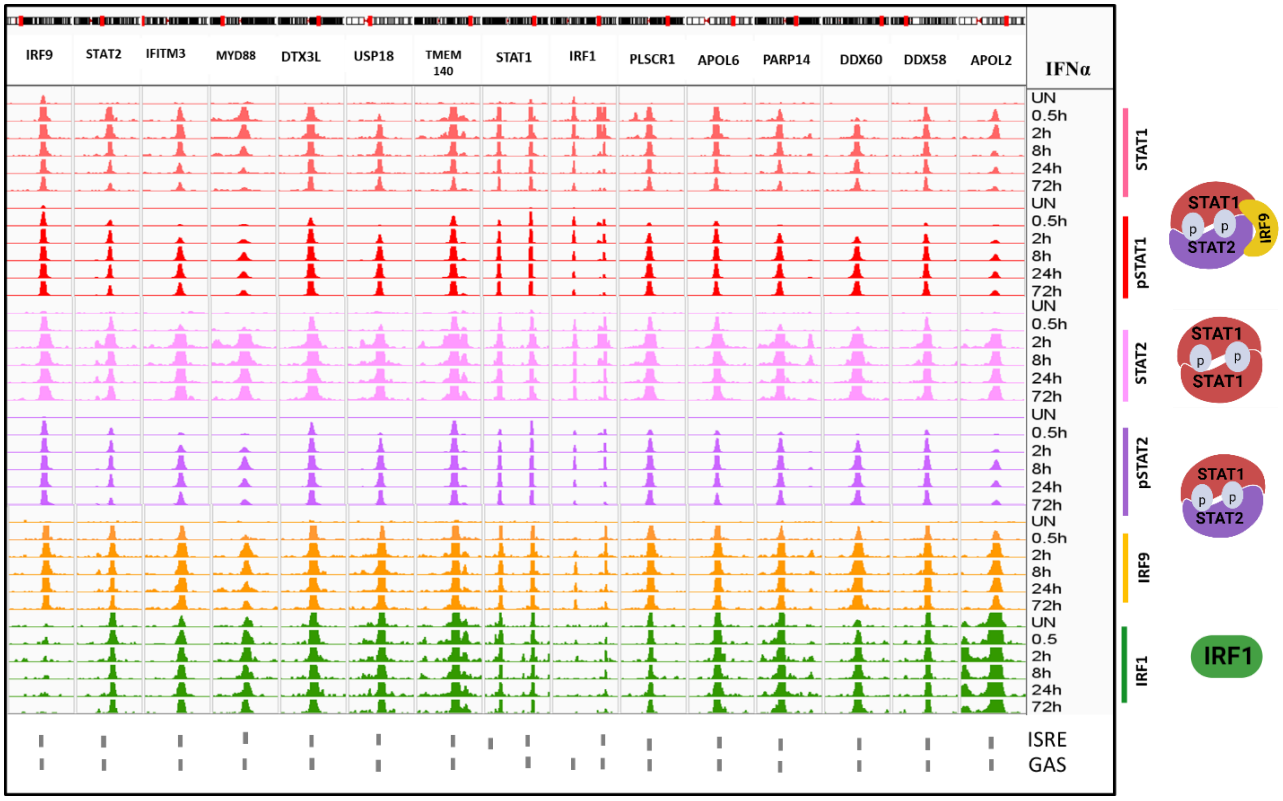
IRF9
STAT2
IFITM3
MYD88
DTX3L
USP18
TMEM 140
STAT1
IRF1
PLSCR1
APOL6
PARP14
DDX60
DDX58
APOL2
IFNα
UN
0.5h
2h
8h
24h
72h
0.5
ISRE
GAS
STAT1
pSTAT1
STAT2
pSTAT2
IRF9
IRF1
STAT1
STAT2
IRF9
IRF1

AII

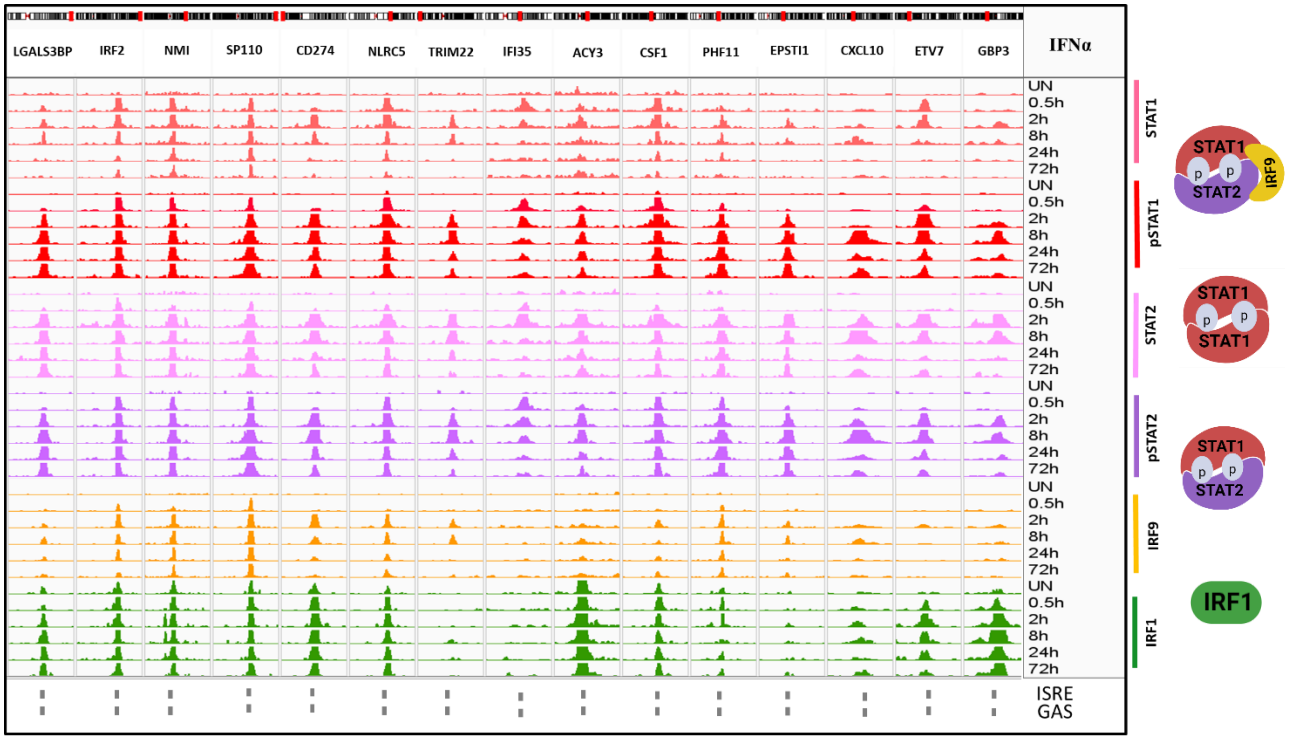
LGALS3BP
IRF2
NMI
SP110
CD274
NLRC5
TRIM22
IFI35
ACY3
CSF1
PHF11
EPSTI1
CXCL10
ETV7
GBP3
IFNα
UN
0.5h
2h
8h
24h
72h
ISRE
GAS
STAT1
pSTAT1
STAT2
pSTAT2
IRF9
IRF1
STAT1
STAT2
IRF9
IRF1

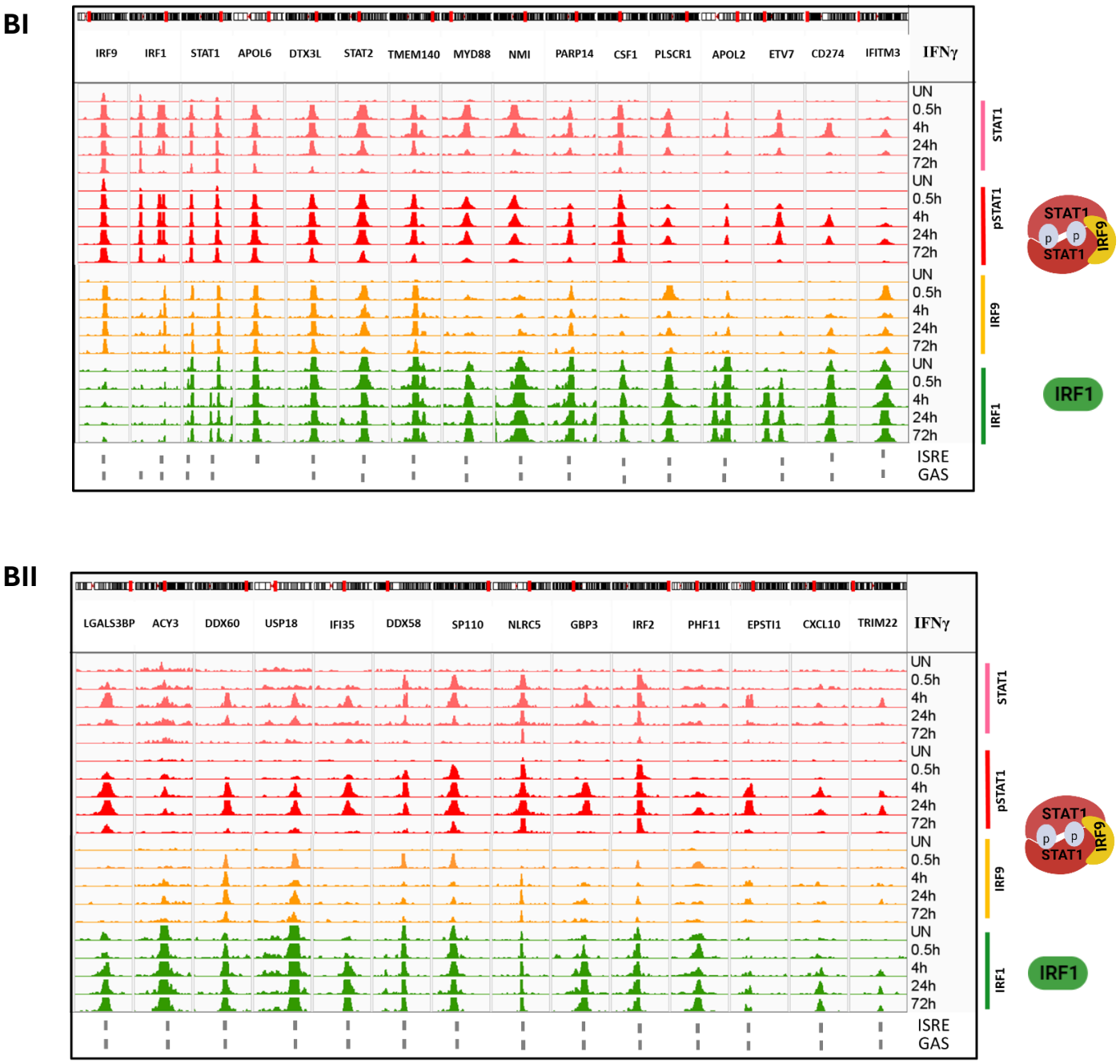

Figure 18. Illustrative representations of the ChIP-seq peaks identified in the promoter regions of 30 composite genes after IFNα(A) and IFNγ (B) treatment in WT cells.

AI-AII. ChIP-seq peaks detected in the promoter regions of 30 composite genes in both untreated and IFNα-treated conditions illustrated through representative views. The tracks correspond to various time points, arranged from top to bottom for each antibody: UN(untreated cells), 0.5h,2h,8h,24 and 72h. Scale of strong binders (AI): pSTATs 0-2000, STATs 0-100, IRFs 0-80 and weak binders (AII): pSTATs 0-100, STATs 0-40, IRFs 0-80. The complexes on the right side of the figures show the possible combinations of different components in WT cells.(Description continues on the next page)

BI-BII. ChIP-seq peaks detected in the promoter regions of 30 composite genes in both untreated and IFNγ-treated conditions illustrated through representative views. The tracks correspond to various time points, arranged from top to bottom for each antibody: UN(untreated cells), 0.5h,4h,24 and 72h. Scale of strong binders (BI): pSTATs 0-500, STATs 0-100, IRFs 0-80 and weak binders (AII): pSTATs 0-100, STATs 0-40, IRFs 0-80. The complexes on the right side of the figures show the possible combinations of different components in WT cells. For all four figures (AI, AII, BI and BII) the IGV genome browser was used to visualize peak locations, which were all aligned to the human reference genome hg38.

4.2.3 Comparative Analysis Of Transcriptional Responses Of 30 Composite Genes To IFNα And IFNγ In WT, STAT1, STAT2, IRF9, IRF1 And IRF1.9dKO Cell Lines

The expression patterns of 30 composite genes following exposure to both IFNα and IFNγ were examined using heatmaps. In response to IFNα the expression pattern of 30 composite genes in WT cells indicated that the majority of these genes exhibited maximum expression at intermediate time points (8h). However, the expression patterns shifted to later time points in STAT1KO cells in response to IFNα (Figure 19-A) which was in agreement with the prolonged pSTAT2/IRF9 binding obtained from ChIP-seq data in STAT1KO cells after IFNα treatment (Figure 20). In IFNα-treated STAT2KO cells, genes are still expressed, however the expression is delayed and weaker as compared to WT cells. This could point to the role of IRF1 and GAF complexes. In IRF1KO cells, either a notable induction or reduction in the expression of composite genes was observed indicating the role of ISGF3, GAF and GAF-like in response to IFNα. Interestingly, similar to STAT2KO cells the expression of composite genes reduced in IRF9KO and IRF1.9dKO cells after IFNα stimulation highlighting the main role of ISGF3 complex. However, the slight gene expression in IFNα-treated IRF9KO cells, predicted the involvement of IRF1, GAF and GAF-like complexes. Likewise, in IFNα-treated IRF1.9dKO cells, the minimal gene expression suggested the potential involvement of GAF and GAF-like complexes (Figure 19-A). On the other hand, In response to IFNγ, composite genes exhibited maximum expression at 8 and 24h in WT, STAT2, IRF1 and IRF9KO cells (Figure 19-B). Briefly, IRF1, GAF and possibly STAT1/IRF9 are suggested to be involved complexes upon IFNγ treatment in WT and STAT2KO cells. The expression of the genes was still observed in IRF1KO cells, pointing to the possible role of STAT1/IRF9 and GAF in response to IFNγ (Sekrecka et al., 2023). Genes were induced in IRF9KO and slightly in IRF1.9dKO cells. This pointed to the role of GAF and IRF1 in IRF9KO, and only GAF in IRF1.9dKO cells following IFNγ stimulation. These findings served as evidence supporting the significant role of STAT1, STAT2, IRF9 and IRF1 components in the expression of composite genes. Moreover, these findings point to the involvement of both ISRE and GAS motifs in the transcriptional regulation of composite genes in WT cells. In addition, the induction

of these genes in knockout cell lines suggests their potential ability to switch between GAS and ISRE binding sites during transcriptional activation.

Subsequently, the distribution of peaks was examined in Huh7.5 STAT1KO cells using STAT2, pSTAT2, and IRF9 antibodies following IFNα stimulation. ChIp-seq was conducted on IFNα-treated cells for 2, 24 and 72 hours. As illustrated in figure 20, genes are arranged in descending order based on their binding patterns from stronger such as IRF9 (Figure 20-A) to weaker such as TRIM22 (Figure 20-B). Composite genes exhibited a prolonged binding pattern for STAT2, pSTAT2, and IRF9 antibodies and no transition from phosphorylated STAT2 (pSTAT2) to unphosphorylated STAT2 (STAT2) was detected in long term chromatin interaction of composite genes in response to IFNα. For the majority of composite genes, there was an absence of basal binding for STAT2, pSTAT2, and IRF9, while minimal binding was noted at 2h. Moreover, the binding profile is shifted towards later time points (24-72h) in STAT1KO cells as compared to WT cells in response to IFNα. In the absence of STAT1, the significant contribution of STAT2/IRF9 complex in prolonged composite gene expression is highlighted following IFNα treatment. Notably, this complex distinctly prioritizes the targeting of ISRE over ISGF3 in response to IFNα in the absence of STAT1 (Blaszczyk et al., 2015). This observation also highlights a shift from a mechanism dependent on both ISRE and GAS in WT to a mechanism solely reliant on ISRE in STAT1KO upon IFNα stimulation.

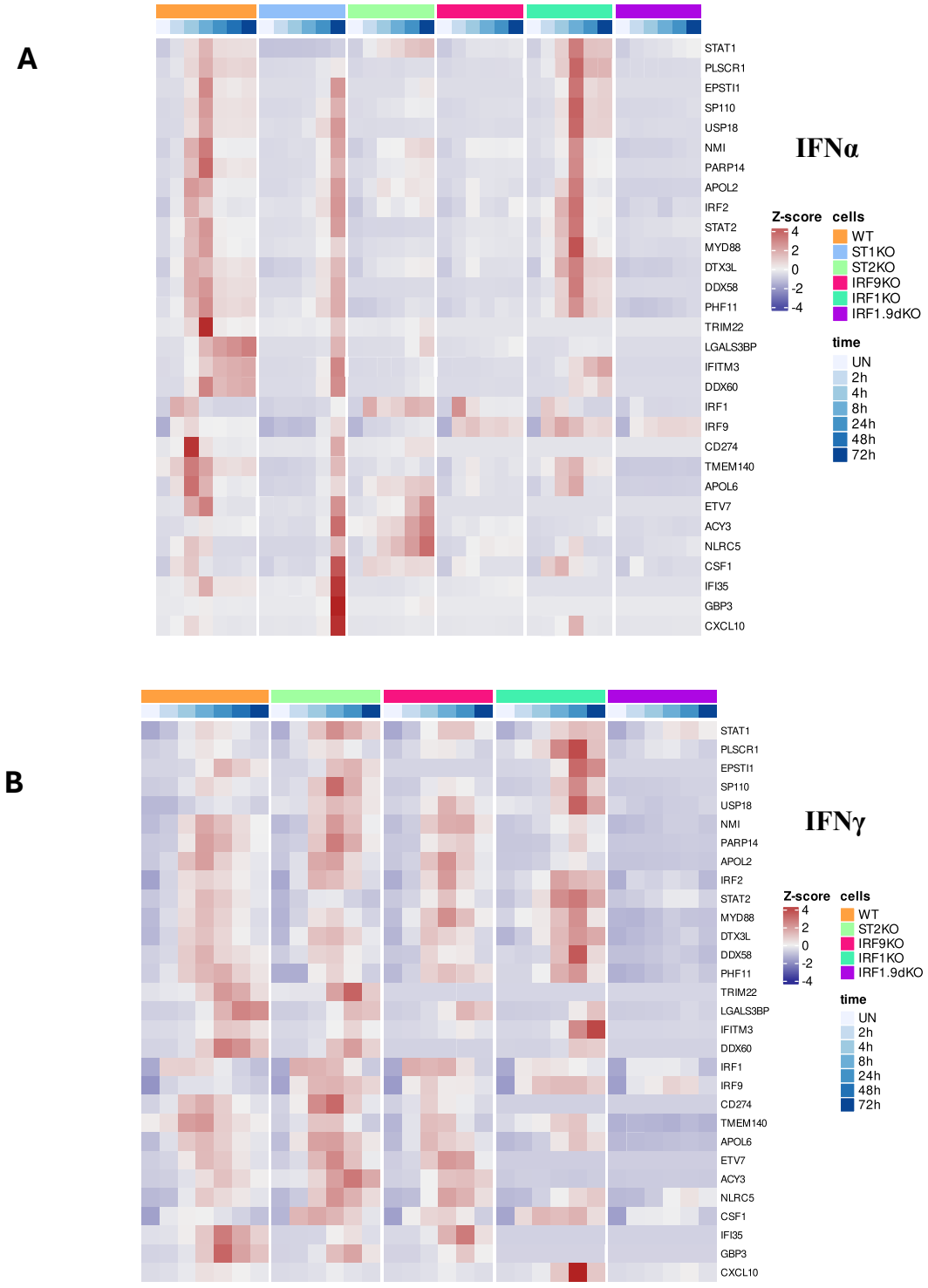

Figure 19. Analyzing the transcriptional response triggered by IFNα and IFNγ stimulation in both WT and mutant Huh7.5 cell lines for comprehensive characterization of composite genes.

The final composite list containing 30 genes was used to generate Heatmaps. Normalization of counts across all cell lines was conducted using z-score. The cell types are arranged vertically, while genes are displayed horizontally. WT cells were treated with IFNα **(A)** and IFNγ **(B)** for 2, 4, 8, 24, 48 and 72h, while KO cell lines were exposed to IFNα and IFNγ (except STAT1KO) for 2, 4, 8, 24 and 72h. High expression is demonstrated in red and low expression is indicated in purple.

Figure 20. Illustrative representations of the ChIP-seq peaks identified in the promoter regions of 30 composite genes after IFNα treatment in STAT1KO cells.

ChIP-seq peaks detected in the promoter regions of 30 composite genes in both untreated and IFNα-treated conditions illustrated through representative views. The tracks correspond to various time points, arranged from top to bottom for each antibody: UN(untreated cells), 2h, 24 and 72h. Scales of strong binders **(A):** pSTATs and STATs 0-200, IRF9 0-80 and weak binders **(B):** pSTATs 0-100, STATs 0-80, IRF9 0-80. The IGV genome browser was used to visualize peak locations, which were all aligned to the human reference genome hg38. The complex on the right side of the figures show the main possible combination of components in STAT1KO cells in response to IFNα.

4.3 Exploring Recruitment Of STAT1, STAT2, IRF9, And IRF1 To Regulatory Regions Of ISRE+GAS Composite Genes Upon Stimulation With IFNα Or IFNγ

For a deeper comprehension of the correlation between ISRE/GAS distance, pSTATs/IRFs binding patterns, and the varied expression of composite genes in WT, STAT1, STAT2, IRF9, IRF1 and IRF1.9 mutant cells, we conducted a thorough analysis of 13 pre-selected composite genes across different distance groups. This analysis involved examining the ISRE/GAS binding interactions of pSTAT1, pSTAT2, IRF9, and IRF1 using zoom-in screenshots from both WT Huh

7.5 cells treated with IFNα (1000 U/ml) and IFNγ (10 ng/ml), and STAT1KO cells treated with IFNα (1000 U/ml) only, across different time points (0-72h). Additionally, gene expression profiles were assessed using qPCR to compare WT and KO cells after exposure to IFNα and IFNγ also at different time points spanning from 0 to 72 hours.

Group1-PARP14,ETV7, SP110 and GBP3 : Very close ISRE/GAS distance (0-5nt)

The promoters of PARP14, SP110, ETV7and GBP3 (Figure21) exhibit a GAS site positioned in close proximity to the ISRE, with variations ranging from 0 to 5 nucleotides, oriented as (GAS-ISRE), (ISRE-GAS), (ISRE-GAS), and (GAS-ISRE), respectively. In WT cells, all 4 genes displayed a time-dependent pSTAT1, pSTAT2 and IRF1 and IRF9 binding pattern upon IFNα treatment and pSTAT1, IRF1 and IRF9 in response to IFNγ. Upon IFNα treatment, PARP14 and SP110 (Figure 21,A-B) exhibited stronger pSTAT1, pSTAT2, IRF1, and IRF9 binding as compared to ETV7 and GBP3 (Figure 21,C-D). Only Minimal IRF9 binding was observed for ETV7 and GBP3 in response to IFNα. This suggested that ISGF3+IRF1 bind to ISRE and GAF+GAF-like binding to GAS in response to IFNα. Likewise, pSTAT1/IRF9+IRF1 bind to ISRE and GAF binds to GAS in response to IFNγ for PARP14 and SP110 in WT cells. While for ETV7 and GBP3 after IFNα treatment, the involved complexes could include IRF1 binding to ISRE and GAF+GAF-like interacting with GAS. And after IFNγ treatment, the complexes might involve IRF1 binding to ISRE and GAF targeting GAS in WT cells. Interestingly, PARP14 and SP110 exhibited broader pSTATs binding than IRFs upon IFNα in WT cells. This observation could agree with the fact that pSTATs contact both GAS and ISRE sites and IRFs target only the ISRE site. However, pSTATs/IRFs binding to ETV7 and GBP3 in response to IFNα appeared weaker, making it more challenging to detect this broader pSTATs binding. This may also elucidate the difficulty in detecting IRF9 binding for ETV7 and GBP3. As it is shown in the figure 21,both ISRE and GAS sites are located under the peak summit of pSTATs and IRFs (dotted line in the Figure). The binding patterns correlated with close proximity of both sites and that both ISRE and GAS are potentially occupied. In STAT1KO cells, in all four genes, a prolonged pSTAT2/IRF9 binding was detected. Therefore, the binding profile is shifted towards later time points in STAT1KO cells as compared to WT cells. Nevertheless, PARP14 and SP110 exhibited stronger binding of pSTAT2 and IRF9 in comparison to ETV7 and GBP3 .Additionally, the fact that both pSTAT2 and IRF9 exclusively bind to the ISRE (as STAT2/IRF9) rather than the GAS

site is consistent with the comparable width of pSTAT2 and IRF9 binding. This suggested the potential involvement of both ISRE and GAS sites for these composite genes in WT cells in response to both IFNs, while only the ISRE site appears to be involved in STAT1KO cells in response to IFNα. Next, the investigation of expression profiles (Figure 22) revealed that in WT cells all four genes showed maximum expression at 8h in response to IFNα. PARP14 and SP110 (Figure 22,A-B) displayed maximum response at 8h in response to IFNγ, while, GBP3 and ETV7 displayed maximum expression at 24h in WT cells (Figure 22,C-D). In general, this correlated with the expression profiles in response to IFNα and IFNγ observed in our cluster analysis (Figure 17). Treatment of STAT1KO cells with IFNα resulted in maximal expression for all four genes at 72 hours matching to the role of pSTAT2/IRF9 binding to ISRE. As expected, no gene expression was observed in STAT1KO cells following IFNγ stimulation. Likewise, in the STAT2KO cells the profile for all genes in response to IFNα has also become prolonged. However, in response to IFNγ, they all showed similar expression profile in STAT2KO cells compared to WT cells. No gene expression was detected in IRF9, IRF1 and IRF1.9dKO cells for ETV7 and GBP3 in response to IFNα and in response to IFNγ, gene induction was not observed in IRF1 and IRF1.9dKO. In contrast, in IRF9KO cells similar to WT cells, in response to IFNα, PARP14 showed a maximum response at 8h, while for SP110 there is a prolonged response. In IFNγ-treated IRF9KO cells PARP14 and SP110 showed maximum response at 8h, while maximum expression for ETV7 and GBP3 is at 8h and 24h, respectively. For all four genes IFNγ-treated IRF9KO exhibited comparable expression profile as WT cells. In IRF1KO cells, both PARP14 and SP110 indicated maximum expression at 8h upon IFNα stimulation, whereas in response to IFNγ, they both exhibited a maximum expression at 24h. Prolonged expression was detected for PARP14 and SP110 after IFNα and IFNγ treatment in IRF1.9dKO cells (Figure 22). The binding patterns of pSTAT1, pSTAT2, IRF1, and IRF9, as well as the qPCR data for PARP14 and SP110 in WT cells (Figure 21 and 22, A-B), enabled us to anticipate the involvement of related complexes in KO cells. For example, in response to IFNα, In STAT1KO cells, pSTAT2/IRF9 interacts with ISRE. In STAT2KO cells, IRF1 binds ISRE while GAF targets GAS; in IRF9KO, there is interactions between IRF1 and ISRE, alongside GAF+GAF-like binding to GAS; likewise, in IRF1KO cells, ISGF3 targets ISRE and GAF+GAF-like recruits GAS. Finally, in IRF1.dKO cells, GAF+GAF-like targets GAS. In response to IFNγ, IRF1+pSTAT1/IRF9 binds ISRE and GAF targets GAS in STAT2KO cells. While IRF1 recruits ISRE and GAF interacts with GAS in IRF9KO; Moreover,

pSTAT1/IRF9 binds ISRE and GAF recruits GAS in IRF1KO, and in IRF1.9dKO cells, GAF binds GAS. Together, for PARP14 and SP110, this clearly pointed to a shift from ISRE+GAS dependent mechanism in WT, STAT2, IRF9 and IRF1KO cells to a GAS-only dependent mechanism in IRF1.9dKO cells in response to both types of IFNs. On the other hand, the absence of ETV7 and GBP3 expression (Figure 22) in IRF9KO and IRF1KO cells, but not in STAT2KO cells following IFNα treatment, suggested the potential involvement of IRF9 and IRF1 targeting ISRE as IRF9/IRF1 complex in STAT2KO cells. In STAT1KO cells, pSTAT2/IRF9 interacts with ISRE. Consequently, GAF+GAF-like complexes bind to GAS in IRF9, IRF1, and IRF1.9dKO cells, but the lack of expression in these cell lines may indicate the low potency of GAF +GAF-like complexes. Contrastingly, in response to IFNγ, ETV7 and GBP3 were expressed in STAT2 and IRF9KO cells but not in IRF1 and IRF1.9dKO cells. This might point to the role of IRF1 targeting ISRE and GAF targeting GAS in STAT2 and IRF9KO cells. However, the absence of expression in IRF1.9dKO cells could confirm that GAF is not potent enough to induce ETV7 and GBP3 in response to IFNγ. These results could indicate the possible shift from ISRE+GAS dependent mechanism in WT cells to ISRE-only dependent mechanism in KO cells for ETV7 and GPB3 in response to both IFNs. Furthermore, following IFNα stimulation, there is a transition from a mechanism reliant on both ISRE and GAS in WT cells to one solely dependent on ISRE in STAT1KO cells for PARP14 , SP110, ETV7 and GBP3.

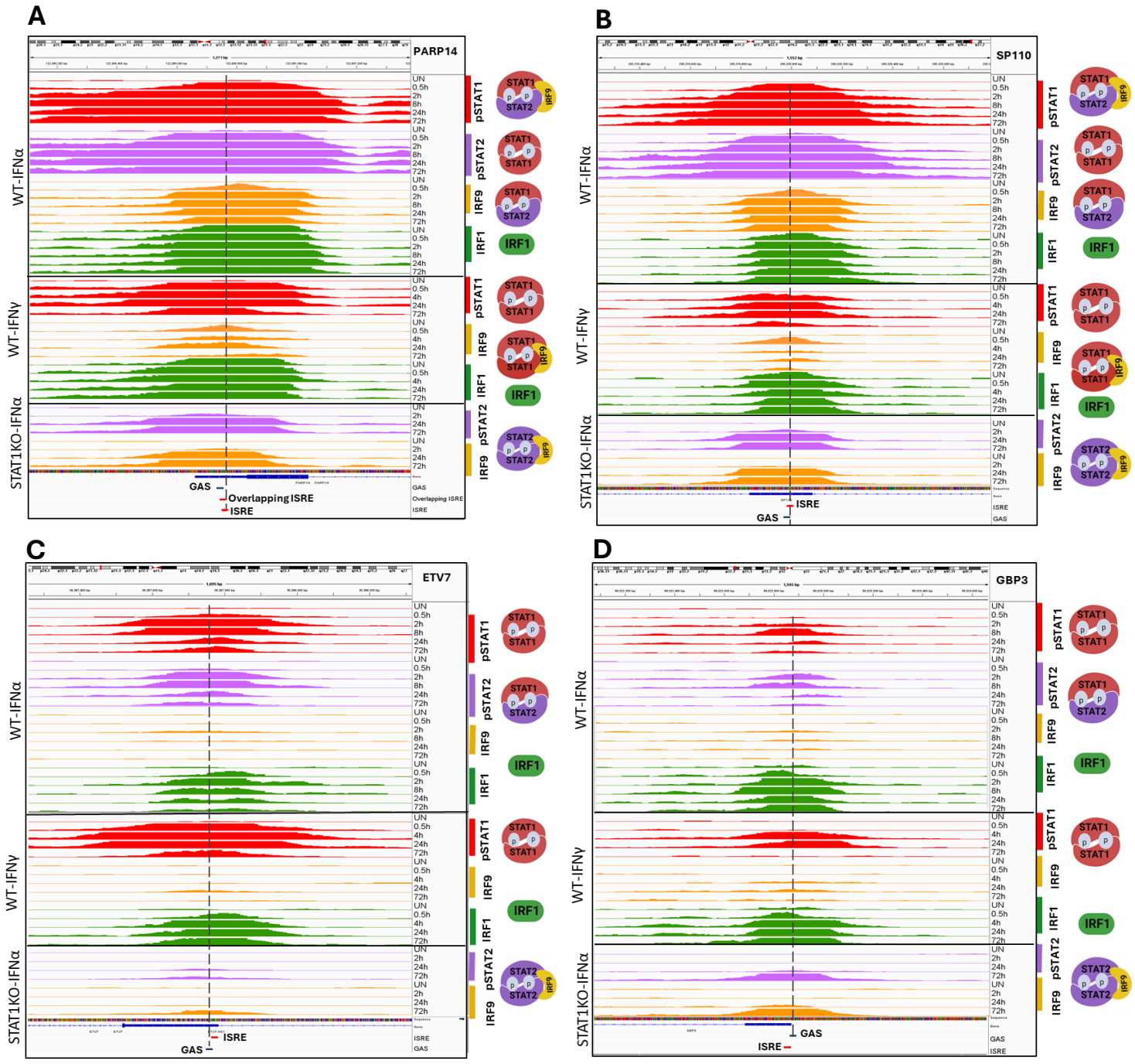

Figure 21. Analyzing the recruitment of pSTAT1, pSTAT2, IRF9, and IRF1 to the regulatory regions of PARP14, SP110, ETV7 and GBP3 in response to IFNα or IFNγ . The figures were separately generated as IGV screenshots for each cell line and each IFN type.

Zoom-in screenshot of pSTAT1, pSTAT2, IRF9 and IRF1 binding profile in WT Huh7.5 cells as well as pSTAT2/IRF9 binding in STAT1KO cells for PARP14 **(A)** and SP110 **(B),** ETV7 **(C)** and GBP3 **(D).** WT cells were left untreated or treated with IFNα for 0.5, 2, 8, 24 and 72h and with IFNγ for 0.5, 4, 24, 72h. STAT1KO cells were left untreated or treated with IFNα for 2, 24, and 72h. The IGV genome browser was used to visualize peak locations, which were all aligned to the human reference genome hg38. Scale: pSTATs 0-100, IRFs 0-80. (Description continues on the next page)

The complexes on the right side of the figures show the possible combinations of different components. ISRE and GAS sites are indicated at the bottom of each figure with red and blue color, respectively. The dotted line illustrates the coverage of ISRE and GAS by the peak summit.

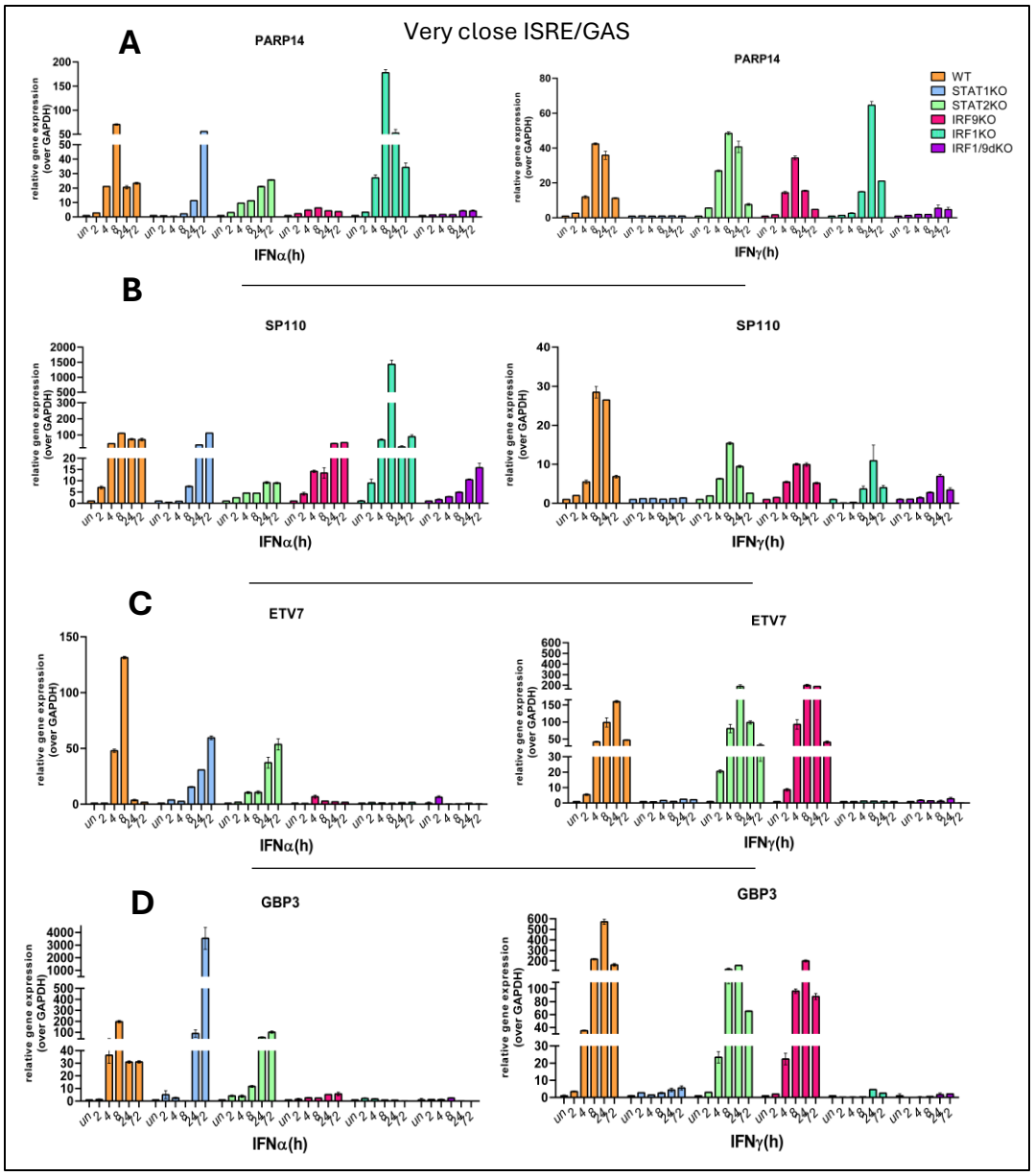

Figure 22. The expression profile of PARP14, SP110, ETV7 and GBP3 genes in WT as compared to KO cells in response to IFNα or IFNγ.

Analysis of the expression profile of PARP14 **(A),** SP110 **(B),** ETV7 **(C)** and GBP3 **(D)** was determined using qPCR. Different Huh7.5 cell lines including WT, STAT1KO, STAT2KO, IRF9KO, IRF1KO and IRF1.9dKO were left untreated or treated with IFNα (1000 U/ml) or IFNγ (10 ng/ml) for the specified time points. GAPDH was used as a housekeeping gene to measure the relative expression. n=2, mean +/- SEM (except for SP110,ETV7 and GBP3 n=1 in WT and STAT1KO).

Group2-STAT2, IRF9, APOL6: Close ISRE/GAS distance (5-20nt)

As it is observed in figure 23, the promoter of STAT2, APOL6 and IRF9 is defined by the presence of a GAS and an ISRE varying from 5 to 20 nucleotides arranged in different orientations including (ISRE-GAS), (ISRE-GAS) and (GAS-ISRE) for each gene, respectively. In WT cells, STAT2 and APOL6 (Figure 23, A-B) displayed similar time-dependent pSTAT1, pSTAT2 and IRF1 and IRF9 binding patterns in response to IFNα and pSTAT1, IRF1 and IRF9 in response to IFNγ. For IRF9 (Figure 23-C), no IRF1 binding was detected after treatment with both types of IFNs. This pointed that in transcriptional regulation of APOL6 and STAT2 in WT cells, IFNα triggers ISGF3+IRF1 to bind ISRE and GAF+GAF-like to target GAS. In contrast, IFNγ stimulates IRF1+pSTAT1/IRF9 interaction with ISRE and GAF recruitment to the GAS. In case of the IRF9 gene, in WT cells, ISGF3 interacts with ISRE and GAF+GAF-like bind to GAS in response to IFNα. Upon IFNγ stimulation, pSTAT1/IRF9 binds to ISRE and GAF targets GAS. Additionally, all three genes exhibited broader pSTATs binding than IRFs upon IFNα and also after IFNγ treatment in WT cells. This pointed that pSTATs interact with both GAS and ISRE sites, whereas IRFs exclusively target the ISRE site. In the figure 23, it is demonstrated that for all three genes both ISRE and GAS sites are situated beneath the peak summit of pSTATs and IRFs, as indicated by the dotted line. The binding patterns correlate with the close proximity of both sites, suggesting that both ISRE and GAS sites in STAT2, APOL6 and IRF9 are potentially occupied in WT cells. Treatment of STAT1KO cells with IFNα led to a prolonged binding pattern of pSTAT2 and IRF9, exhibiting comparable peak width while interacting with only ISRE element. Similar to PARP14, SP110, ETV7 and GBP3 (Figure 21), this could point to the participation of both ISRE and GAS sites in STAT2, APOL6 and IRF9 gene regulation in WT cells upon exposure to both IFNs, while only the ISRE site is implicated in STAT1KO cells following IFNα stimulation. The examination of the expression profiles unveiled that STAT2 and APOL6 (Figure 24, A-B) exhibited maximum expression at 8h after IFNα treatment in WT cells. However, STAT2 and APOL6 showed maximum response to IFNγ at 24h and 8h, respectively. IRF9 (Figure 24-C) indicated maximum expression at later times after IFNα in WT cells. Nevertheless, our cluster (Figure 17-A) and heatmap analysis (Figure 19-A) revealed that the maximum response of IRF9 to IFNα occurred at early time points (4h) in WT cells. IFNγ-treated WT cells exhibited the highest response for the IRF9 gene at 24h which is correlated with our cluster and heatmap analysis. IFNα-treated STAT1KO cells resulted in maximum expression at

72h for all three genes matching the role of pSTAT2/IRF9. As expected, IFNγ stimulation did not induce any of the three genes in STAT1KO cells. In STAT2KO cells, STAT2, APOL6 and IRF9 showed prolonged expression in response to IFNα. Whereas, after IFNγ treatment in STAT2KO cells, APOL6 gene displayed highest expression at 8h, IRF9 showed maximum expression at 4-24h, and STAT2 maximally expressed at 4-8h. In IRF9KO cells, STAT2 and APOL6 exhibited highest expression at 8h and IRF9 showed prolonged expression profiles upon IFNα stimulation. The peak response for all three genes in IFNγ-treated IRF9KO cells occurred at 8 hours. In the absence of IRF1, STAT2, APOL6 and IRF9 genes reached maximum expression at 8h after IFNα stimulation. Whereas, in response to IFNγ, the peak response occurred at 24h. In IRF1.9dKO cell, upon IFNα treatment, all three genes exhibited peak expression at later time points (24-72h). Similar to IFNγ-treated WT cell lines, IRF1.9dKO cells treated with IFNγ exhibited peak expression at 8 and 24h for STAT2. Likewise, maximum response was observed at 8h in IFNγ-treated IRF1.9dKO cells for IRF9. While, delayed response was detected for APOL6 after IFNγ treatment in IRF1.9dKO cells (Figure 24). Based on our findings regarding the binding patterns of pSTAT1, pSTAT2, IRF9, and IRF1, as well as the qPCR results (Figure 23-24) in WT cells, we predicted the complexes involved in KO cells for regulation of STAT2, APOL6 and IRF9 genes after IFNα and IFNγ stimulation. Consequently, the prolonged expression of all three genes in STAT1KO cells confirmed the involvement of pSTAT2/IRF9 targeting ISRE in response to IFNα. In STAT2 and APOL6 genes in response to IFNα, IRF1 and GAF target ISRE and GAS in STAT2KO cells, respectively. Likewise, in IRF9KO cells, IRF1 binds ISRE, and GAF/GAF-like targets GAS. In IRF1KO, ISGF3 binds ISRE and GAF/GAF-like interacts with GAS. Moreover, in IRF1.9dKO cells, GAF/GAF-like recruit GAS. However, in response to IFNγ, in STAT2KO cells, IRF1+pSTAT1/IRF9 and GAF bind ISRE and GAS, respectively. Similarly, IRF1 binds ISRE, and GAF targets GAS in IRF9KO cells. In IRF1KO cells, pSTAT1/IRF9 and GAF bind ISRE and GAS, respectively, whereas in IRF1.9dKO group, GAF complex binds GAS. For the STAT2 and APOL6 genes, this observation could point to a shift from the ISRE+GAS dependent mechanism observed in WT, STAT2, IRF9 and IRF1KO cells to GAS-only mechanism in IRF1.9dKO cells after treatment with both IFNs. For the IRF9 gene, the engaged complexes in response to IFNα are predicted as follows: pSTAT2/IRF9 interacts with ISRE in STAT1KO cells. While, GAF targets GAS in STAT2KO cells. In IRF9KO and IRF1.9dKO groups, GAF+GAF-like bind GAS. in IRF1KO group, ISGF3 is recruited to the ISRE and GAF+GAF-like target GAS.

On the other hand, in response to IFNγ, pSTAT1/IRF9 binds to ISRE and GAF interacts with GAS in STAT2KO and IRF1KO. Likewise, in IRF9KO and IRF1.9dKO cells, GAF is recruited to the GAS. This observation might suggest a potential transition from the ISRE+GAS dependent mechanism observed in WT, and IRF1KO cells to GAS-only dependent mechanism in IRF9, IRF1.9dKO in response to both IFNs for IRF9 gene. Additionally, after IFNα stimulation, all three genes show a transition from a mechanism dependent on ISRE+GAS in WT cells to one reliant solely on ISRE in STAT1KO cells.

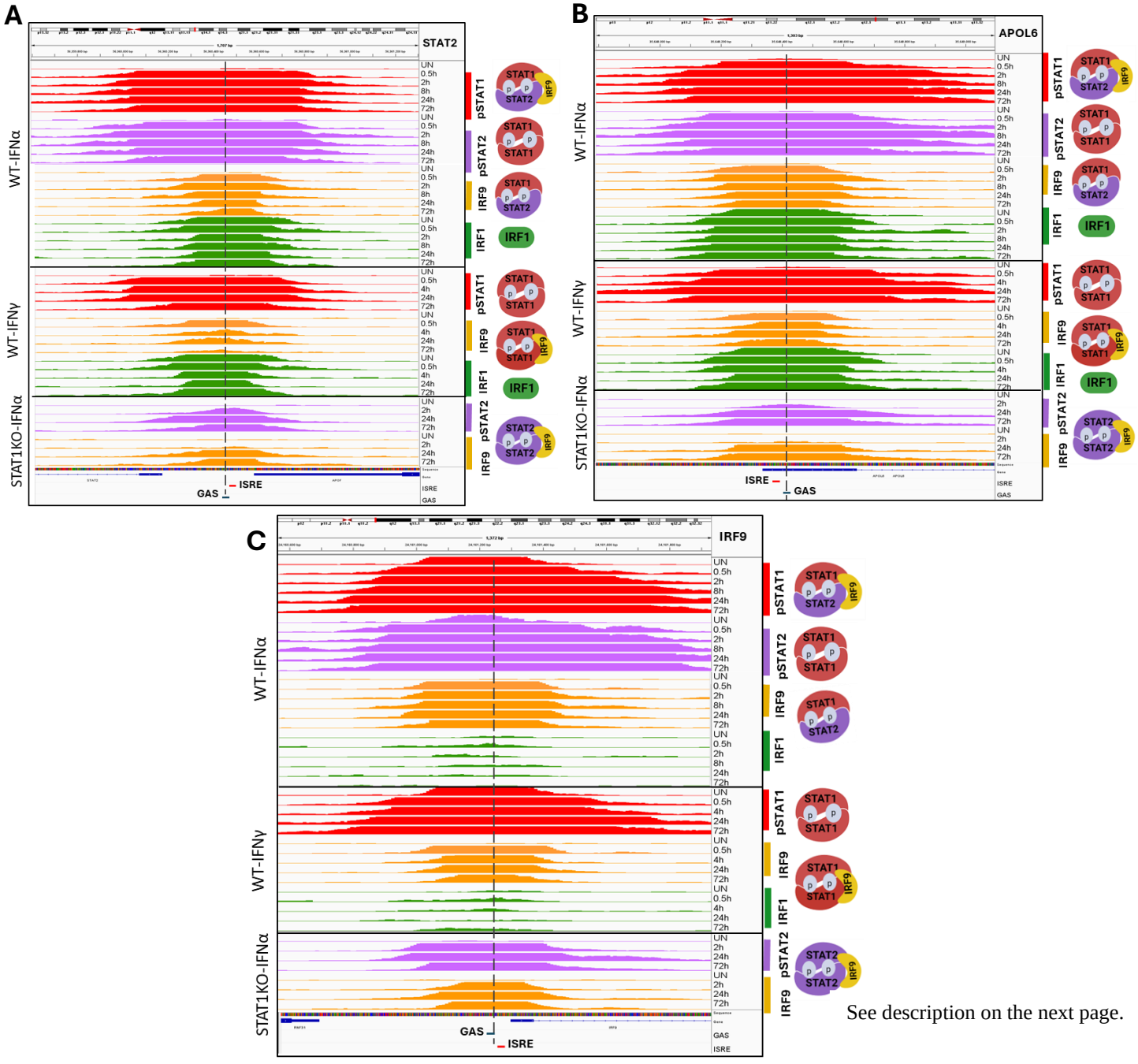

See description on the next page.

Figure 23. Analyzing the recruitment of pSTAT1, pSTAT2, IRF9, and IRF1 to the regulatory regions of STAT2,IRF9 and APOL6 in response to IFNα or IFNγ . The figures were separately generated as IGV screenshots for each cell line and each IFN type. Description continues on the next page.

Zoom-in screenshot of pSTAT1, pSTAT2, IRF9 and IRF1 binding profile in WT Huh7.5 cells as well as pSTAT2/IRF9 binding in STAT1KO cells for STAT2 **(A)** and APOL6 **(B)** and IRF9 **(C).** WT cells were left untreated or treated with IFNα for 0.5, 2, 8, 24 and 72h and with IFNγ for 0.5, 4, 24, 72h. STAT1KO cells were left untreated or treated with IFNα for 2, 24, and 72h. The IGV genome browser was used to visualize peak locations, which were all aligned to the human reference genome hg38. Scale: pSTATs 0-100, IRFs 0-80. The complexes on the right side of the figures show the possible combinations of different components. ISRE and GAS sites are indicated at the bottom of each figure with red and blue color, respectively. The dotted line illustrates the coverage of ISRE and GAS by the peak summit.

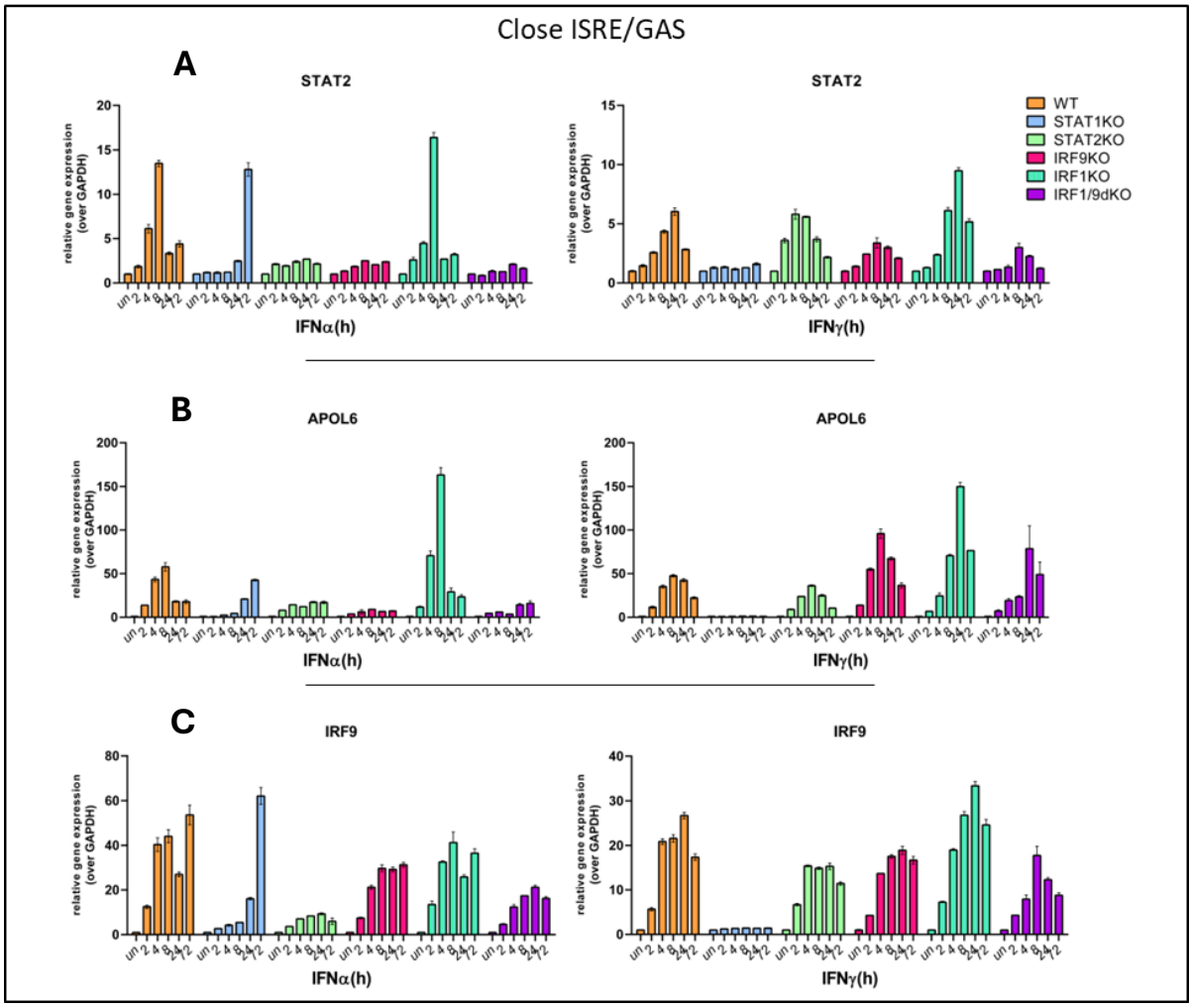

Figure 24. Expression profile of STAT2, IRF9 and APOL6 in WT as compared to KO cells in response to IFNα or IFNγ.

Analysis of the expression profile of STAT2 **(A),** APOL6 **(B),** IRF9 **(C)** was determined using qPCR. Different Huh7.5 cell lines including WT, STAT1KO, STAT2KO, IRF9KO, IRF1KO and IRF1.9dKO were left untreated or treated with IFNα (1000 U/ml) or IFNγ (10 ng/ml) for the specified time points. GAPDH was used as a housekeeping gene to measure the relative expression. n=2, mean +/- SEM.

Group3-DDX60 and NLRC5 :medium ISRE/GAS distance(20-100nt)

The promoter of DDX60 contains two ISRE sites [ISRE(1) and ISRE(2)] and one GAS site. The GAS site is positioned 25 base pairs away from ISRE(1) and 61 base pairs away from ISRE(2) (Figure 25-B). On the other hand, the promoter of NLRC5 features a GAS and an ISRE, with a 48-nucleotide gap between them (Figure 25-A). For both genes ISRE and GAS are arranged in a negative orientation (GAS-ISRE). In WT cells, both genes displayed a time-dependent pSTAT1, pSTAT2 and IRF1 and IRF9 binding pattern in response to IFNα and pSTAT1, IRF1 and IRF9 in response to IFNγ. This suggested that for both genes in WT cells during IFNα stimulation, ISGF3 along with IRF1 bind to ISRE while GAF and GAF-like target GAS. On the other hand, during IFNγ stimulation, IRF1+pSTAT1/IRF9 interact with ISRE, whereas, GAF binds to GAS. Similar to PARP14, SP110 (group1) (Figure 21) and genes in group2 (Figure 23) , NLRC5 showed a broader binding of pSTATs compared to IRFs in response to both IFNs. This could indicate that pSTATs interact with both GAS and ISRE sites, while IRFs solely target the ISRE site. Despite exhibiting broader pSTAT1 and pSTAT2 binding than IRFs in response to IFNα for DDX60, no broader pSTAT1 binding was observed compared to IRFs after IFNγ treatment. This could point that GAS is not occupied by pSTAT1 upon IFNγ treatment in DDX60. In STAT1KO cells, NLRC5 and DDX60 exhibit prolonged STAT2 and IRF9 binding exclusively to the ISRE sites after IFNα stimulation, similar to genes in groups 1 and 2. However, DDX60 exhibited stronger pSTAT2 and IRF9 binding to ISRE(1) and (2) as compared to NLRC5 in STAT1KO cells which could be connected to the presence of two adjacent ISRE sites in the promoter of DDX60. According to the expression profiles in WT cells, both genes (Figure 26) indicated maximum expression at 8h in response to IFNα. In response to IFNγ, DDX60 (Figure 26-B) showed maximum response at 24h, while NLRC5 (Figure 26-A) reached its highest expression at 8h in WT cells. This observation is in agreement with heatmap (Figure19) and cluster analysis (Figure 17). Treatment of STAT1KO cells with IFNα resulted in both genes exhibiting their peak response at 72h consistent with the involvement of pSTAT2/IRF9. As anticipated, no gene expression was observed for NLRC5 and DDX60 in IFNγ-treated STAT1KO cells. In STAT2KO cells, a prolonged expression profile was observed upon IFNα stimulation for both genes. While, after IFNγ treatment, NLRC5 displayed highest response at 8h, while DDX60 reached its peak expression at 24h. In IRF9KO cells, after IFNα stimulation, NLRC5 and DDX60 exhibited maximum response at 4h and 8h, respectively. On the contrary, upon IFNγ stimulation,

NLRC5 showed peak response at 8h and DDX60 displayed maximum expression at 24h. NLRC5 and DDX60 showed maximum expression at 8 hours and 72 hours, respectively in IFNα-treated IRF1KO cells. However, both genes exhibited maximum response at 24h in IFNγ-treated IRF1KO cells. In IRF1.9dKO cells, no gene expression was observed for DDX60 in response to both IFNs, while NLRC5 displayed maximum response at later time points (Figure 26). Analyzing the binding patterns of pSTAT1, pSTAT2, IRF9 and IRF1 alongside qPCR results (Figure 25-26) for DDX60 and NLRC5 in WT cells allowed us to predict the complexes involved in the expression of these genes in WT and KO cells. Despite the binding pattern of pSTAT1 and pSTAT2 observed in WT cells for DDX60 (Figure 25-B) The lack of gene induction for DDX60 in IRF1.9dKO cells in response to both IFNs suggested that GAF+GAF-like upon IFNα stimulation and GAF upon IFNγ stimulation may not have a dominant role to induce gene expression. Thus, in WT cells, the main transcriptional regulatory complexes for DDX60 are ISGF3+IRF1 binding to ISRE(1) and (2) in response to IFNα and IRF1+pSTAT1/IRF9 interacting with ISRE(1) and (2) in response to IFNγ. This could point to the potent role of the ISRE site in DDX60. Delayed expression of both genes in STAT1KO cells after IFNα treatment pointed the involvement of pSTAT2/IRF9 binding ISRE. In response to IFNα, for DDX60, the main complex in STAT2 and IRF9 knockout cells is IRF1 binding ISRE(1) and (2). Conversely, in IRF1KO cells, the primary contributor is ISGF3 targeting ISRE(1) and (2) in response to IFNα. However, upon IFNγ stimulation, in STAT2KO cells, IRF1+pSTAT1/IRF9 bind ISRE(1) and (2). Likewise, IRF1 binds ISRE(1) and (2) in IRF9KO cells. Whereas, in IRF1KO cells, pSTAT1/IRF9 interacts with ISRE(1) and (2). These observations likely pointed to the participation of an ISRE-only mechanism in WT cells as well as KO cell lines in DDX60. For NLRC5 in WT cells, during IFNα stimulation, ISGF3+IRF1 bind ISRE and GAS is targeted by GAF+GAF-like. While, IRF1 and GAF target ISRE and GAS, respectively in STAT2KO cells. Likewise, in IRF9KO cells, IRF1 binds ISRE, and GAF/GAF-like binds GAS. Moreover, in IRF1.9dKO cells, GAF/GAF-like targets GAS. In contrast, following IFNy treatment, ISRE is targeted by IRF1+pSTAT1/IRF9, and GAS is interacting with GAF in WT cells. Whereas, in STAT2KO cells, IRF1+pSTAT1/IRF9 and GAF bind ISRE and GAS, respectively. Similarly, IRF1 binds ISRE, and GAF targets GAS in IRF9KO cells. In IRF1KO cells, pSTAT1/IRF9 and GAF target ISRE and GAS, respectively, whereas in IRF1.9dKO cells, GAF complex recruits GAS. For the NLRC5 gene, similar to PARP14, SP110 (group1), STAT2 and APOL6 (group2) this clearly pointed to a shift from ISRE+GAS dependent

mechanism in WT, STAT2, IRF9 and IRF1KO cells to a GAS-only dependent mechanism in IRF1.9dKO cells in response to both types of IFNs. In addition, the findings confirmed a transition from ISRE+GAS dependency in WT to ISRE dependency in STAT1KO cells in response to IFNα for both genes.

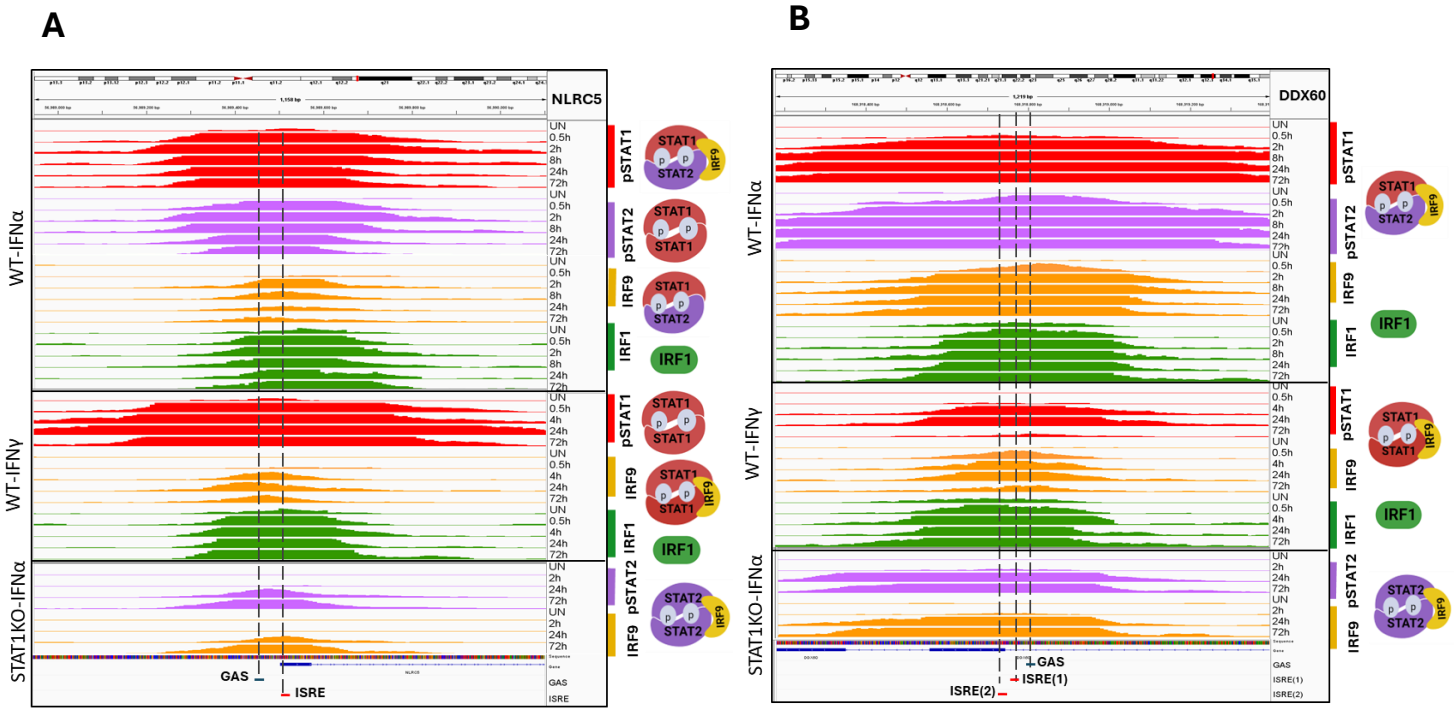

Figure 25. Analyzing the recruitment of pSTAT1, pSTAT2, IRF9, and IRF1 to the regulatory regions of NLRC5 and DDX60 in response to IFNα or IFNγ . The figures were separately generated as IGV screenshots for each cell line and each IFN type.

Zoom-in screenshot of pSTAT1, pSTAT2, IRF9 and IRF1 binding profile in WT Huh7.5 cells as well as pSTAT2/IRF9 binding in STAT1KO cells for NLRC5 **(A)** and DDX60 **(B).** WT cells were left untreated or treated with IFNα for 0.5, 2, 8, 24 and 72h and with IFNγ for 0.5, 4, 24, 72h. STAT1KO cells were left untreated or treated with IFNα for 2, 24, and 72h. The IGV genome browser was used to visualize peak locations, which were all aligned to the human reference genome hg38. Scale: pSTATs 0-100, IRFs 0-80. The complexes on the right side of the figures show the possible combinations of different components. ISRE and GAS sites are indicated at the bottom of each figure with red and blue color, respectively. The dotted line illustrates the coverage of ISRE and GAS by the peak summit.

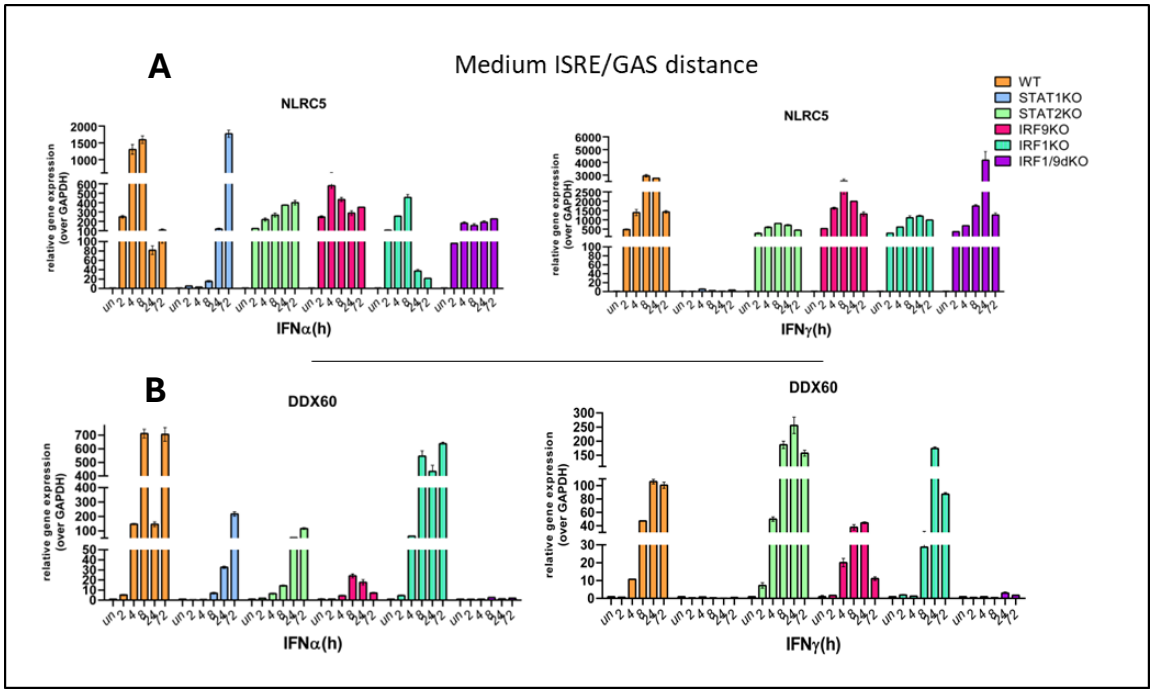

Figure 26. Expression profile of NLRC5 and DDX60 in WT as compared to KO cells in response to IFNα or IFNγ.

Analysis of the expression profile of NLRC5 **(A)** and DDX60 **(B)** was determined using qPCR. Different Huh7.5 cell lines including WT, STAT1KO, STAT2KO, IRF9KO, IRF1KO and IRF1.9dKO were left untreated or treated with IFNα (1000 U/ml) or IFNγ (10 ng/ml) for the specified time points. GAPDH was used as a housekeeping gene to measure the relative expression. n=2, mean +/- SEM.

Group4-DDX58 and NMI: long ISRE/GAS distance, (>100)

The promoter of DDX58 gene (Figure 27-A) contains a GAS and an ISRE site with a 213 nt separation and negative orientation (GAS-ISRE). In contrast, promoter of NMI (Figure 27-B) characterized by the presence of one GAS and two ISRE marked as ISRE(1) and ISRE(2) with a 274-nucleotide separation between the ISRE(1) and GAS and 314-nucleotide separation between the ISRE(2) and GAS. ISRE(1) and GAS oriented positively (ISRE-GAS), while GAS and ISRE(2) oriented negatively (GAS-ISRE) in NMI. In WT cells, both genes displayed comparable time-dependent binding pattern of pSTAT1, pSTAT2, IRF1, and IRF9 in response to IFNα. However, in response to IFNγ, no IRF9 binding was observed for NMI. This observation could predict the possible involvement of ISGF3+IRF1 binding to ISRE and GAF+GAF-like targeting GAS in response to IFNα for both genes. However, upon IFNγ stimulation, for DDX58 , the involved factors could be IRF1+pSTAT1/IRF9 binding to ISRE and GAF interacting with GAS. For NMI, the main

complexes might include IRF1 targeting ISRE and GAF recruiting GAS in response to IFNγ. Similar to genes from group1(except GBP3) (Figure 21) , group2 (Figure 23) and group3 (Figure 25), DDX58 and NMI both exhibited a wider range of pSTATs binding as compared to IRFs after IFNα and IFNγ treatment in WT cells. This might align with the concept that pSTATs interact with both GAS and ISRE sites, while IRFs target solely the ISRE site. As it is shown in figure, the summit of IRF1 and IRF9 peaks notably shifts towards the ISRE site in DDX58 and towards ISRE(1) in NMI. However, for NMI we observed weak IRF1 binding to ISRE(2) in response to both IFNs and weak IRF9 binding to ISRE(2) only in response to IFNα. This suggested the presence of a less potent or inactive ISRE(2) site in the NMI promoter. On the other hand, as the distance increases between ISRE and GAS in the promoter region of NMI, a more distinguishable binding pattern was observed for GAF+GAF-like binding to GAS and IRF1 and IRF9 targeting ISRE. In IFNα-treated STAT1KO cells, prolonged and comparable peak width of pSTAT2 and IRF9 binding solely to the ISRE for DDX58 was observed. Similarly, for NMI, strong pSTAT2/IRF9 interacting ISRE(1) and weak pSTAT2/IRF9 binding ISRE(2) was detected. Based on gene expression profiles, DDX58 (Figure 28-A) and NMI (Figure 28-B) displayed maximum response at 8h after treatment with both IFNs In WT cell lines. This observation is in line with our heatmap and cluster analysis. In STAT1KO cells, prolonged expression pattern in response to IFNα is in agreement with the involvement of pSTAT2/IRF9 for both genes. As expected, no gene expression was detected in response to IFNγ in STAT1KO cells. In STAT2KO group, after IFNα stimulation, the expression pattern has also become prolonged for both genes. In contrast, upon IFNγ treatment, DDX58 and NMI exhibited maximum response at 8h in. In IRF9KO cells, maximum expression was observed at 4h for DDX58, while, for NMI the expression was prolonged following IFNα stimulation. On the contrary, after IFNγ treatment, peak response was observed at 8h for both genes in IRF9KO cells. In IRF1KO cell lines, DDX58 and NMI showed maximum response at 8 and 24h in response to IFNα and IFNγ, respectively. Lastly, in IRF1.9dKO cell lines, in case of IFNα, DDX58 showed highest expression at 8h. Whereas, NMI displayed maximum response at 24h. However, unlike WT cells, in response to IFNγ, for both genes the peak expression was observed at 72h (Figure 28). By examining the binding patterns and qPCR results (Figure 27-28) for DDX58 and NMI , we were able to predict the complexes that play a role in the expression of these genes in WT and KO cells. Hence, due to the low expression of DDX58 in STAT2KO, it is predicted that IRF1, GAF and GAF-like are not potent enough in

response to IFNα and ISGF3 is the main complex that binds to ISRE in WT cells. In contrast, in response to IFNγ for DDX58, IRF1+pSTAT1/IRF9 targets ISRE and GAF interacts with GAS. Subsequently, in WT cells for NMI, ISGF3+IRF1 interacts with ISRE and GAF+GAF-like are recruited to GAS in response to IFNα . However, in response to IFNγ, the main contributors in WT cells for NMI are as follows: IRF1 binds ISRE and GAF targets GAS. In STAT1KO cells, pSTAT2/IRF9 interacts with ISRE in response to IFNα for both DDX58 and NMI. For DDX58 gene after IFNα stimulation, in STAT2KO cells, IRF1 and GAF target ISRE and GAS, respectively. Likewise, in IRF9KO group, IRF1 binds ISRE, and GAF+GAF-like interact with GAS. In IRF1KO, ISGF3 recruits ISRE and GAF+GAF-like bind GAS. Moreover, in IRF1.9dKO cells, GAF+GAF-like target GAS. On the contrary, upon IFNy treatment, IRF1+pSTAT1/IRF9 interact with ISRE and GAF binds GAS in STAT2KO cells. Similarly, IRF1 binds ISRE, and GAF targets GAS in IRF9KO cells. In IRF1KO cells, pSTAT1/IRF9 and GAF bind ISRE and GAS, respectively, whereas in IRF1.9dKO group, GAF complex binds GAS. As it was mentioned earlier, IRF1, GAF and GAF-like complexes are not potent enough to significantly induce the expression of DDX58 in STAT2, IRF9 and IRF1.9dKO cells in response to IFNα. For NMI, the predicted complexes in response to IFNα are as follows: IRF1 and GAF target ISRE and GAS, respectively in STAT2KO cells. IRF1 binds ISRE and GAF+GAF-like interact with GAS in IRF9KO. ISGF3 targets ISRE and GAF+GAF-like bind to GAS in IRF1KO. Lastly, GAF+GAF-like recruit GAS in IRF1.9dKO cells. In contrast, in response to IFNγ, IRF1 binds ISRE and GAF targets GAS in STAT2KO and IRF9KO cells. Likewise, in IRF1KO group, GAF interacts with GAS. Finally, GAF binds GAS in IRF1.9dKO. This clearly pointed to a shift of ISRE+GAS-dependent mechanism in WT, STAT2, IRF9 to a GAS-only dependent mechanism IRF1.9dKO cells in response to both types of IFNs for DDX58 and NMI in response to IFNα. Similarly, there is a shift from an ISRE+GAS-dependent mechanism in WT, STAT2, and IRF9 cells to a GAS-dependent mechanism in IRF1KO and IRF1.9dKO cells in response to IFNγ for NMI. However, a notable decrease in DDX58 expression levels in response to IFNγ might indicate an ISRE-exclusive mechanism.

Additionally, there is a shift from ISRE+GAS dependent mechanism in WT cells to the ISRE-only mechanism in STAT1KO cells in response to IFNα for both genes.

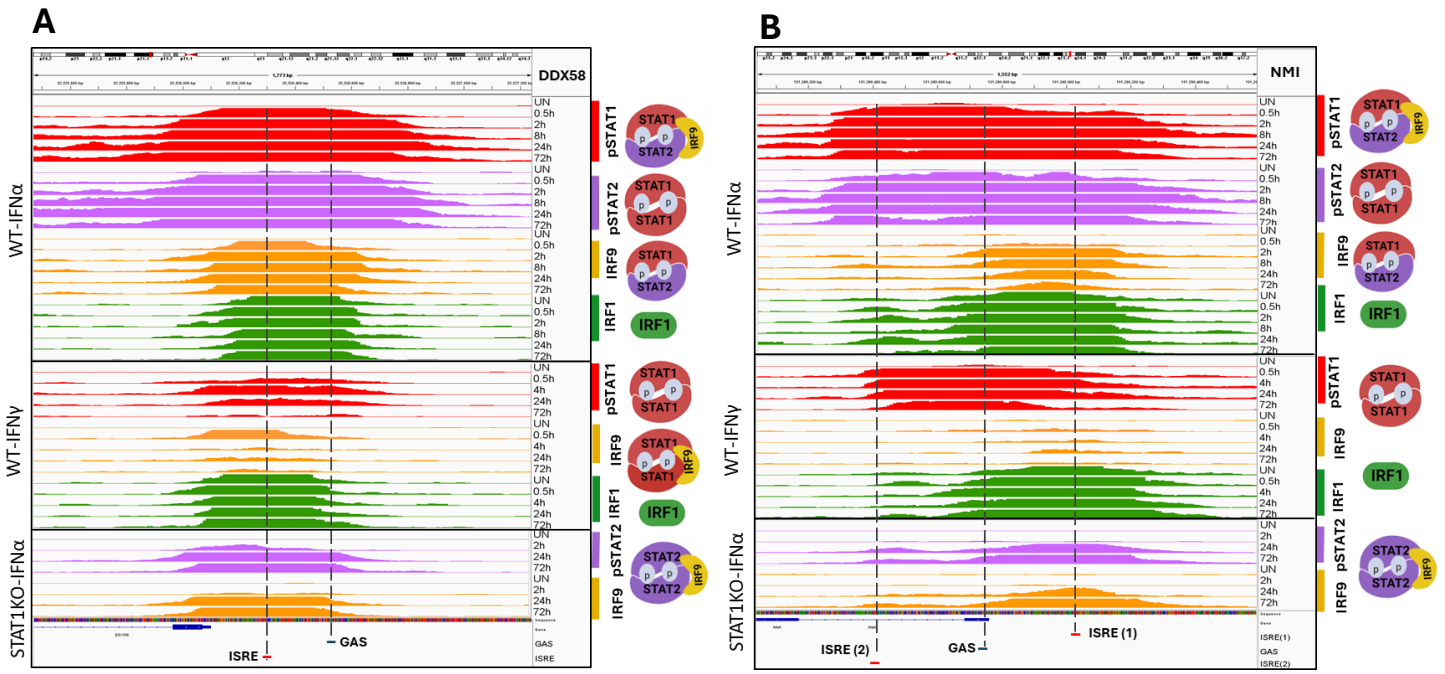

Figure 27. Analyzing the recruitment of pSTAT1, pSTAT2, IRF9, and IRF1 to the regulatory regions of DDX58 and NMI in response to IFNα or IFNγ . The figures were separately generated as IGV screenshots for each cell line and each IFN type.

Zoom-in screenshot of pSTAT1, pSTAT2, IRF9 and IRF1 binding profile in WT Huh7.5 cells as well as pSTAT2/IRF9 binding in STAT1KO cells for DDX58 **(A)** and NMI **(B).** WT cells were left untreated or treated with IFNα for 0.5, 2, 8, 24 and 72h and with IFNγ for 0.5, 4, 24, 72h. STAT1KO cells were left untreated or treated with IFNα for 2, 24, and 72h. The IGV genome browser was used to visualize peak locations, which were all aligned to the human reference genome hg38. Scale: pSTATs 0-100, IRFs 0-80. The complexes on the right side of the figures show the possible combinations of different components. ISRE and GAS sites are indicated at the bottom of each figure with red and blue color, respectively. The dotted line illustrates the coverage of ISRE and GAS by the peak summit.

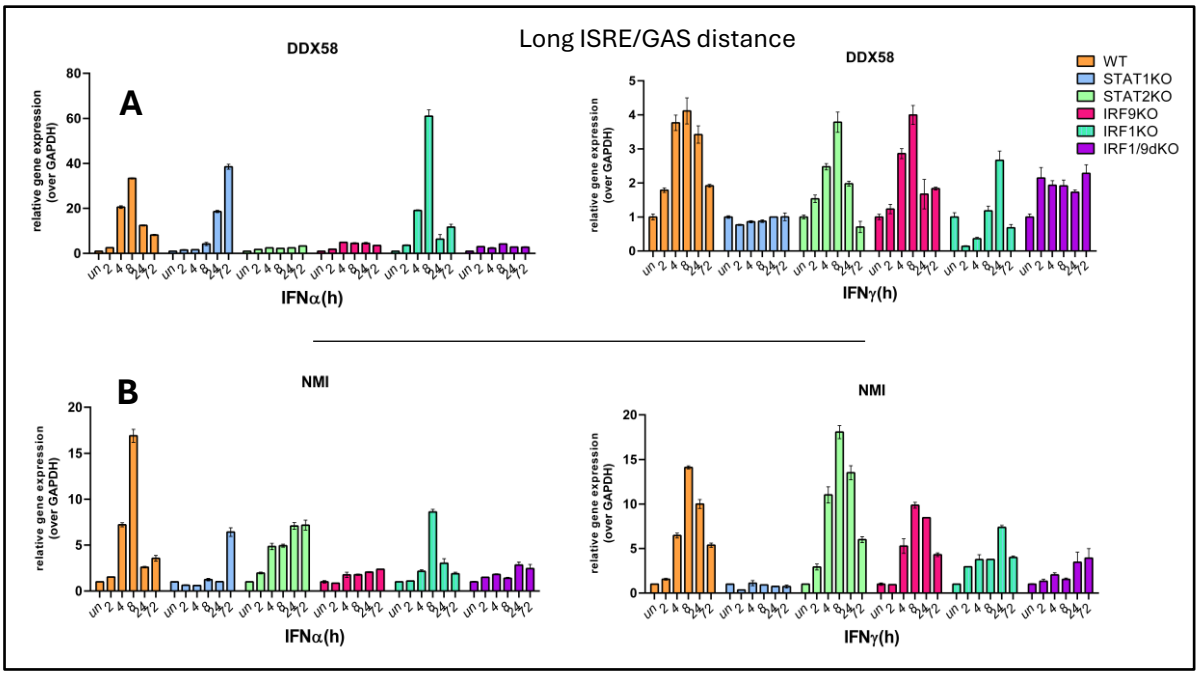

See description on the next page

Figure 28. Expression profile of DDX58 and NMI in WT as compared to KO cells in response to IFNα or IFNγ.

Analysis of the expression profile of DDX58 (A) and NMI **(B)** was determined using qPCR. Different Huh7.5 cell lines including WT, STAT1KO, STAT2KO, IRF9KO, IRF1KO and IRF1.9dKO were left untreated or treated with IFNα (1000 U/ml) or IFNγ (10 ng/ml) for the specified time points. GAPDH was used as a housekeeping gene to measure the relative expression n=2, mean +/- SEM.

Group5-STAT1 and IRF1: Distal regulatory ISRE/GAS

The STAT1 and IRF1 genes exhibit a composite structure comprising ISRE and GAS elements in the distal region, situated approximately 6kb away from the proximal promoter (Figure 29). In the distal regulatory region of STAT1(Figure 29-A), the ISRE and GAS elements are separated by 39 nt in a positive orientation (ISRE-GAS).In the distal regulatory region of IRF1(Figure 29-B), three GAS sites are identified: GAS(1) positioned 718 nt away from ISRE with negative orientation (GAS-ISRE), GAS(2) positioned 399 nt away from ISRE with a positive orientation (ISRE-GAS), and GAS(3) positioned 33 nt away from ISRE with a positive orientation (ISRE-GAS). Notably, while STAT1 features an ISRE only in its proximal promoter, IRF1 is distinguished by the presence of a single GAS element in its proximal promoter. In WT cells, STAT1 displayed time-dependent pSTAT1, pSTAT2 and IRF1 and IRF9 binding pattern in response to IFNα and pSTAT1, IRF9 and IRF1 in response to IFNγ at both proximal promoter and distal composite sites. Similar to IRF9 gene (Figure23-C), the IRF1 gene exhibited a binding pattern involving pSTAT1, pSTAT2 and IRF9 but not IRF1 at distal region in response to IFNα. Likewise, in response to IFNγ, it exhibited pSTAT1 and IRF9 binding, but no IRF1 binding at the distal composite site. Additionally, following IFNα treatment, there was no IRF1 binding and only weak IRF9 binding was observed at the proximal promoter of the IRF1 gene. However, pSTAT1 and pSTAT2 binding was observed at the proximal promoter of the IRF1 gene. On the other hand, In response to IFNγ, pSTAT1 binding was observed, while there is no IRF1 or IRF9 binding at the proximal promoter of IRF1 gene. This is in agreement with the presence of a GAS site and the absence of an ISRE at the proximal promoter of IRF1 gene. For the STAT1 gene, this observation suggested the potential involvement of ISGF3+IRF1 binding to the distal and proximal ISRE and GAF+GAF-like targeting the distal GAS, in response to IFNα in WT cells. On the other hand, upon IFNγ stimulation, potential complexes could include IRF1+pSTAT1/IRF9 interacting with proximal and distal ISRE and GAF binding to the distal GAS. For the IRF1 gene, during IFNα treatment, potential complexes include ISGF3 binding to the distal ISRE, and GAF+GAF-like interacting with the distal GAS (1) and (3) and proximal GAS elements. Conversely, after IFNγ

treatment, predicted complexes involve pSTAT1/IRF9 targeting the distal ISRE, and GAF targeting both the distal GAS(1) and (3) and proximal GAS elements in WT cells. Both genes exhibited broader pSTATs binding than IRFs at distal region upon IFNα and IFNγ treatment in WT cells. Despite the absence of GAS in the proximal promoter of STAT1 gene, still broader pSTATs binding than IRFs was observed. Similarly, for the IRF1 gene, IRF9 binding was detected at the proximal promoter despite the absence of ISRE. This finding implied the existence of a chromatin looping mechanism that links proximal and distal regions of both STAT1 and IRF1 genes. In the IRF1 gene, the significant distances between GAS(1), GAS(2), and GAS(3) at distal region led to broad and discernible pSTAT1 and pSTAT2 binding patterns (in case of IFNα) and pSTAT1 binding (in case of IFNγ). This contrasts with IRFs' exclusive targeting of ISRE at distal region. The observation suggested potential activity of GAS(1) and GAS(3), covered by pSTATs peak summit in response to both IFNα and IFNγ (Figure 29-B). In IFNα-treated STAT1KO cells, pSTAT2 and IRF9 show extended binding specifically to ISRE at the proximal and distal regions of STAT1 gene pointing to the presence of ISRE. In contrast, for IRF1 gene, the binding of pSTAT2 and IRF9 was detected at the distal region, while at the proximal promoter the binding of only pSTAT2 (possibly as homodimers) was observed. The STAT1 gene (Figure 30-A) showed maximum expression at 8h in response to both IFNs, while IRF1(Figure 30-B) displayed maximum expression at early time points (2-4h) in response to both types of IFN in WT cells. These findings were in line with our heatmap (Figure 19) and cluster (Figure 17) analysis. IFNα-treated STAT1KO cells resulted in maximum response at 72h for both genes pointing to the role of pSTAT2/IRF9. As expected, neither STAT1 nor IRF1 are induced in STAT1KO cells upon IFNγ stimulation. In all KO cells, IRF1 gene showed peak expression at 2-4h time points in response to both IFNs. However, in STAT2KO cells, STAT1 gene exhibited maximum response at 72 and 8h to IFNα and IFNγ, respectively. In IRF9KO cells, after treatment with both IFNs, STAT1 gene displayed maximum expression at later time points. For STAT1 gene, IFNα-treated IRF1KO cells resulted in maximum response at 8h while IFNγ-treated IRF1KO cells showed maximum expression at 24h. STAT1 demonstrated late response (24h) to both IFNs in IRF1.9dKO group (Figure 30). Using ChIP-seq and qPCR data from WT cells (Figure 29-30), we derived the complexes likely involved in other cell lines. Accordingly, for STAT1 gene following IFNα treatment, pSTAT2/IRF9 interacts with proximal and distal ISRE in STAT1KO cells. IRF1 binds proximal and distal ISRE, and GAF targets distal GAS in STAT2KO cell. Likewise, in IRF9KO

cell lines, IRF1 interacts with proximal and distal ISRE, and GAF/GAF-like binds distal GAS. Whereas, in IRF1KO cells, ISGF3 targets proximal and distal ISRE, and GAF+GAF-like are recruited to distal GAS. Lastly, in IRF1.9dKO group, GAF binds distal GAS. Conversely, after IFNγ stimulation for STAT1 gene, IRF1+pSTAT1/IRF9 interact with proximal and distal ISRE and GAF binds distal GAS in STAT2KO cells. Similarly, IRF1 targets proximal and distal ISRE, and GAF binds distal GAS in IRF9KO cells. In IRF1KO cells, pSTAT1/IRF9 interacts with proximal an distal ISRE, and GAF binds distal GAS. Finally, in the IRF1.9dKO cells, the GAF solely binds distal GAS. For STAT1 gene, this clearly pointed to a shift of ISRE+GAS- dependent mechanism in WT, STAT2, IRF9 and IRF1KO cells to a GAS-dependent mechanism in IRF1.9dKO cells in response to both types of IFNs. Subsequently, for the IRF1 gene, after IFNα treatment in STAT1KO cells, pSTAT2/IRF9 binds distal ISRE with possible subsequent targeting of proximal and distal GAS by STAT2 homodimer. Likewise, GAF binds to distal GAS(1,3) and proximal GAS in STAT2KO cells. Moreover, In IRF9 and IRF1.9dKO cells, GAF+GAF-like target distal GAS(1,3) and proximal GAS. Whereas, in IRF1KO cells, ISGF3 interacts with distal ISRE and GAF+GAF-like bind to distal GAS(1,3) and proximal GAS. On the contrary, following IFNγ stimulation for IRF1 gene, pSTAT1/IRF9 binds distal ISRE and GAF targets distal GAS(1,3) and proximal GAS in STAT2 and IRF1KO cells. In IRF9 and IRF1.9dKO groups, GAF interacts with distal GAS(1,3) and proximal GAS. Similar to IRF9 gene, for IRF1, this observation may indicate a potential shift from the ISRE+GAS-dependent mechanism in WT and IRF1KO cells to a GAS-only dependent mechanism in IRF9 and IRF1.9dKO cells in response to both IFNs. Moreover, there is a shift from ISRE+GAS- dependent mechanism in WT cells to ISRE-only dependent mechanism in STAT1KO cells after IFNα treatment for STAT1 gene. Surprisingly, Given that the possible binding of STAT2 homodimers to the proximal and distal GAS sites and pSTAT2/IRF9 binds to distal ISRE, a possible ISRE+GAS dependent mechanism is anticipated for IRF1 in IFNα-treated STAT1KO cells.

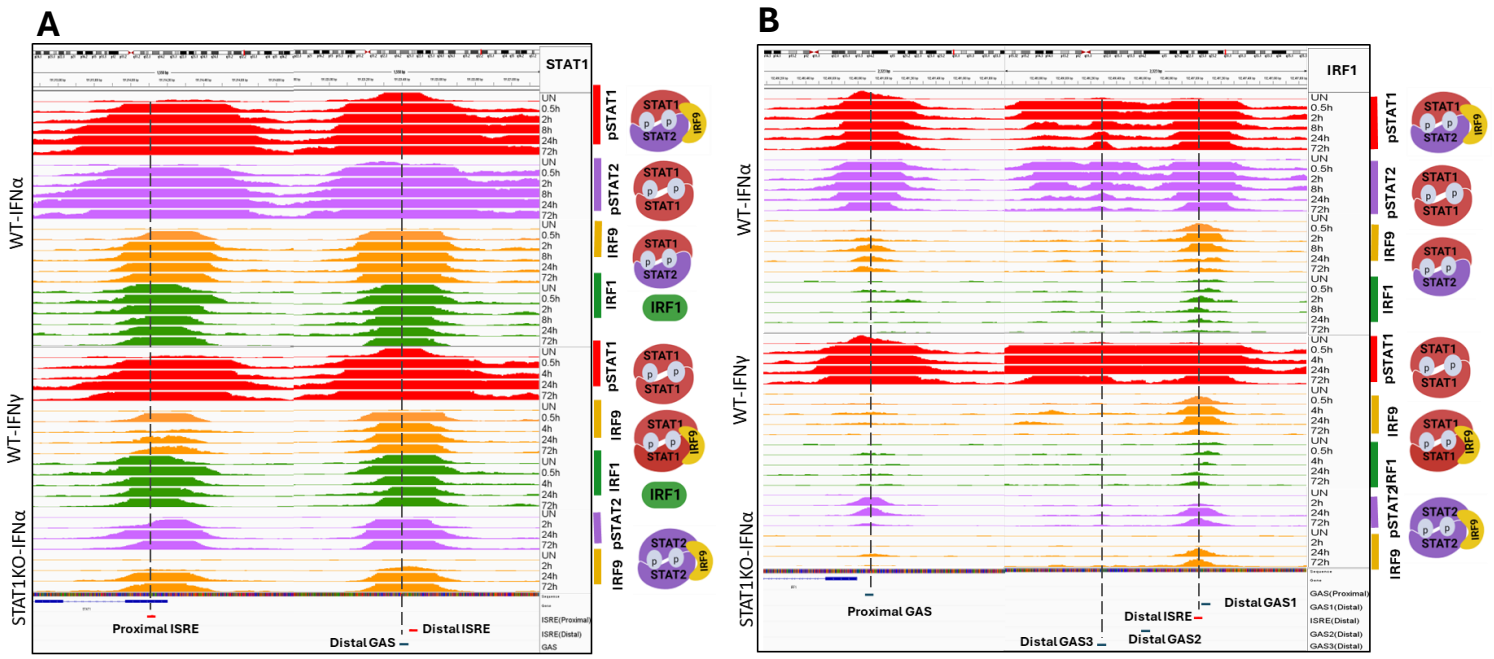

Figure 29. Analyzing the recruitment of pSTAT1, pSTAT2, IRF9, and IRF1 to the regulatory regions of STAT1 and IRF1 in response to IFNα or IFNγ . The figures were separately generated as IGV screenshots for each cell line and each IFN type.

Zoom-in screenshot of pSTAT1, pSTAT2, IRF9 and IRF1 binding profile in WT Huh7.5 cells as well as pSTAT2/IRF9 binding in STAT1KO cells for STAT1 **(A)** and IRF1 **(B)**. WT cells were left untreated or treated with IFNα for 0.5, 2, 8, 24 and 72h and with IFNγ for 0.5, 4, 24, 72h. STAT1KO cells were left untreated or treated with IFNα for 2, 24, and 72h. The IGV genome browser was used to visualize peak locations, which were all aligned to the human reference genome hg38. Scale: pSTATs 0-100, IRFs 0-80. The complexes on the right side of the figures show the possible combinations of different components. ISRE and GAS sites are indicated at the bottom of each figure with red and blue color, respectively. The dotted line illustrates the coverage of ISRE and GAS by the peak summit.

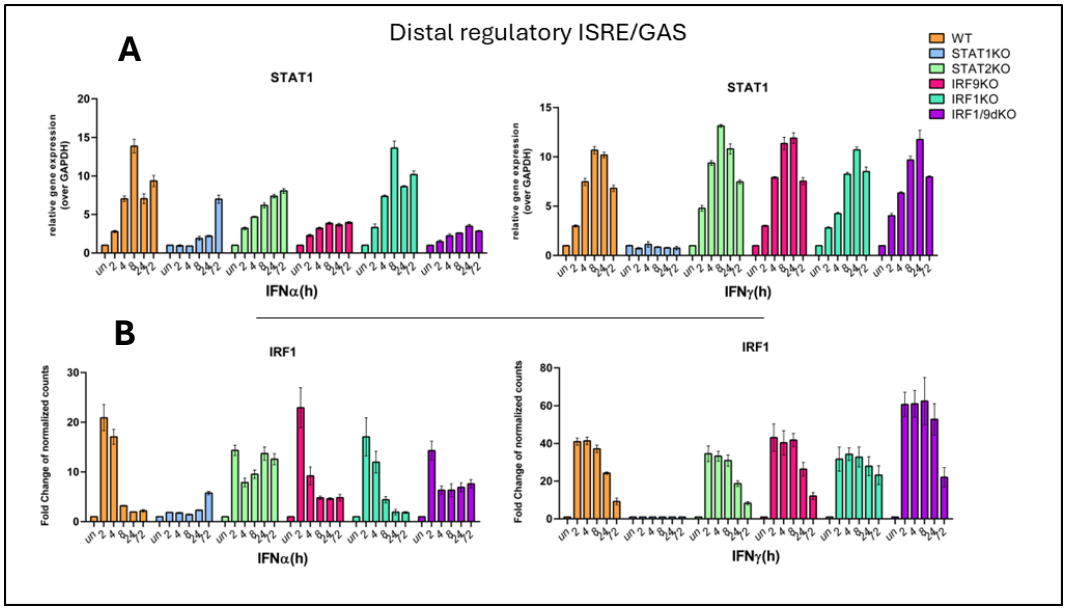

See description on the next page.

Figure 30. Expression profile of STAT1 and IRF1 in WT as compared to KO cells in response to IFNα or IFNγ.

Analysis of the expression profile of STAT1 **(A)** and IRF1 **(B)** was determined using qPCR and RNA-seq respectively. Different Huh7.5 cell lines including WT, STAT1KO, STAT2KO, IRF9KO, IRF1KO and IRF1.9dKO were left untreated or treated with IFNα (1000 U/ml) or IFNγ (10 ng/ml) for the specified time points. GAPDH was used as a housekeeping gene to measure the relative expression n=2, mean +/- SEM.

In general, these findings offer additional evidence demonstrating the functionality of both ISRE and GAS sites within composite genes across varying distance groups. They can be effectively utilized in conjunction through co-binding of transcription factors or independently. Overall, the expression of pre-selected composite genes in WT cells as well as KO cells further proved the switch ability of ISRE and GAS in transcriptional regulation of composite genes. The results additionally confirmed that there is no correlation between the distance or orientation of ISRE/GAS sites and the binding or expression profiles of composite genes.

4.4 The Application Of Site-Directed Mutagenesis Alongside The Assessment Of Promoter-Luciferase Expression

To gain a more precise understanding of the functionality of the ISRE and GAS sites in a selection of previously analyzed composite genes from different distance groups including PARP14 (very close ISRE/GAS), APOL6 (close ISRE/GAS), DDX60 and NLRC5 (medium ISRE/GAS distance), NMI (long ISRE/GAS distance), STAT1 and IRF1 (distal regulatory ISRE/GAS) initially, site-directed mutagenesis (SDM) and promoter-luciferase expression analysis were conducted in WT cells. Subsequently, to further delineate the involvement of ISGF3, IRF1, STAT2/IRF9, STAT1/IRF9, GAF, and GAF-like factors in the transcriptional regulation of PARP14, APOL6, DDX60, NMI and STAT1 in response to IFNα and IFNγ, we performed SDM combined with promoter-luciferase assays in WT and KO cells. Table (12) presents data on the size of the cloned promoter fragments of pre-selected composite genes, along with the constructs used in this study, which include wild-type (WT) and mutated ISRE and GAS sites. Table (13) provides further details on the ISRE/GAS distances, orientation and WT and mutated nucleotides of the ISRE/GAS sites. Constructs including PARP14_WT, APOL6_ΔISRE, APOL6_ΔGAS and APOL6_ΔISRE/ΔGAS, STAT1_ WT_prox/dist , STAT1_pd_ distΔISRE, STAT1_pd_ distΔGAS, STAT1_pd_ proxΔISRE (marked in red in Table 12) were already prepared in the lab previously (more details are available in Sekrecka et al., 2023).

4.4.1 Generation And Validation Of Cloned Fragments Into The Vector (pXPG)

Obtaining genomic DNA from Huh7.5 cells enabled the amplification of proximal promoters of PARP14, APOL6, DDX60,NLRC5, DDX58, NMI, and distal regulatory regions of STAT1 and IRF1. Generally, the subsequent steps were carried out for all genes. Initially, PCR gradient was conducted to optimize the conditions. Accordingly, the optimal annealing temperature for all fragments was 66℃ for all genes. In the next step, gel electrophoresis was conducted and the bands corresponding to the fragments were cut out and purified utilizing a Gel-out kit in the subsequent step. Subsequently, the concentration of DNA samples, ranging between 30-60 ng/µL, was determined using a Nanodrop spectrophotometer. In order to clone the DNA fragments in the following step, pXPG vector (containing Firefly luciferase) was used as the backbone of the constructs. Consequently, the pXPG underwent cleavage and linearization through the use of the SmaI restriction enzyme under the following conditions: 30°C for 2h. By employing a negative control (undigested pXPG) which displayed three distinct plasmid shapes, including supercoiled, open-circular (oc), and linear configurations, the digestion resulted in the production of linear pXPG, sized at 6087 base pairs. Subsequently, Using the NEBuilder HiFi DNA Assembly Master Mix, ligation of the promoter fragments with the digested pXPG vector was performed. Following that, the samples underwent a 45-minute incubation at 50°C in a thermoblock.

Gene Name	Promoter fragment size	Constructs
PARP14	1500	PARP14_WT PARP14_ΔISRE PARP14_ΔGAS PARP14_ΔpGAS PARP14_ ΔpISRE PARP14_ΔGASΔISRE
APOL6	607	APOL6_WT APOL6_ ΔISRE APOL6_ ΔGAS APOL6_ ΔISRE ΔGAS
DDX60	1430	DDX60_WT DDX60_ΔISRE(1) DDX60_ΔGAS DDX60_ΔGASΔISRE(1)
NLRC5	711	NLRC5_WT
DDX58	1153	DDX58_WT
NMI	1130	NMI_WT NMI_ΔISRE NMI_ΔGAS NMI_ΔGAS/ΔISRE
IRF1 (proximal promoter)	1175	IRF1-proximal-WT
IRF1(Distal region)	1698	IRF1-distal-WT
STAT1(proximal-distal)	1745	STAT1_prox/dist_WT STAT1_pd_distΔISRE STAT1_pd_distΔGAS STAT1_pd_proxΔISRE STAT1_pd_distΔISRE/ΔGAS STAT1_pd_distΔISRE_proxΔISRE STAT1_pd_ΔISRE/ΔISRE/ΔGAS

Table12. Overview of pre-selected ISRE+GAS-composite genes, corresponding promoter fragment sizes, and constructs prepared and used in this study.

Constructs marked in red were generated in the lab previously (More details are available in (Sekrecka et al., 2023)). pd stands for the proximal and distal regions. Prox is the abbreviation of proximal and dist is the abbreviation of distal.

Gene	ISRE(WT) ΔISRE	LINKER(bp)	GAS(WT) ΔGAS	Orientation
PARP14	GAAAGCGAAAGA ACTCGCGCTCGA 3'ΔISRE: GAAAGCGCTCGA	1	TTCCAGGAAA ACACAGACAA 5'ΔGAS: ACACAGGAAA	-
APOL6	AGGAAACTGAAAGT AGAGGACTGCCCGT	18	TTTCCTGGAA TGGACTGACC	+
DDX60	GAAACTGAAACC ACTCCTGCTCCC	25	TTTCCACGAAAG TACACACACAAG	-
NLRC5	ACTTTCAGTTTC	48	GATTTCTCGGCAGC	-
DDX58	GGAAACGAAACT	213	TTTCCTATAAAG	-
NMI	GAAAGTGAAATT ACTCGTGCTCTT	274	GTTTTCCGGGAAGG GTTACACGGACAGG	+
IRF1 (proximal)	-	-	TTCCCCGAA	NA
IRF1 (distal)	GGTTTCGGTTTCT	718 399 33	TTCCCGGAAA TTCGCGGAAA TTCCAGGAAG	- + +
STAT1(Proximal-Distal)	Proximal: AGTTTCGCTTTCC AAGCGCGCGCGCC Distal: ACTTTCGCTTTT AAGCGAGCGGCT	6223 39	 Distal: GTTTCCCCGAAA GAGCTCGAGCTC	 +

Table13. Overview of WT and mutated ISRE and GAS sites (including distances and orientation) of pre-selected ISRE+GAS-composite genes promoters.

Nucleotides highlighted in red indicate mutations in the ISRE or GAS sites. The term "Linker" refers to the distance between ISRE and GAS. NA: not applicable

4.4.2 Confirmation Of Successful Cloning Through Colony PCR

The utilization of bacterial transformation resulted in the creation of bacterial clones containing the desired construct. A bacterial plate was employed as a negative control, with digested pXPG used to verify the adequacy of pXPG digestion. After overnight, the bacteria plates were analyzed. The transformed bacterial plates exhibited a higher number of bacterial colonies (30-40) in comparison to the negative control, where typically 5-6 bacterial colonies were observed. Next, 8 bacterial colonies were selected to perform colony PCR to discern the clones possessing the desired constructs containing the targeted DNA fragment. Particular primers, Fluc_F and Fluc_R (Table 8, same primers used for sanger seq), were employed in colony PCR to anneal to the plasmid and flank the region of interest, ensuring the precision of the cloning procedure. Following colony PCR, gel electrophoresis was performed to screen the bands with the

exact size of the DNA fragments of APOL6, DDX60, NLRC5, DDX58, NMI and IRF1 genes that cloned into the pXPG. Upon confirming the presence of bands corresponding to the size of the cloned DNA fragments, the constructs were sent for Sanger sequencing.

4.4.3 Verification Of Cloned Fragment Integrity Using Sanger Sequencing

Sanger sequencing was undertaken to validate the accuracy and integrity of the cloned fragments within the constructs generated in this study, including PARP14, APOL6, DDX60, NLRC5, DDX58, NMI, STAT1 and IRF1 (Figure S1). Accordingly, the primers Fluc_F and Fluc_R utilized to encompass the flanking region of the fragment, were applied. As it mentioned before, the constructs containing WT promoter of PARP14 (PARP14_WT) and WT proximal and distal regulatory sites (STAT1_prox/dist_WT) were generated in the lab and sequenced previously and the Sanger sequencing results are not shown in figure S1. As it is shown in figure S1-A, the wild-type ISRE and GAS sites of promoter of APOL6 remained their wild-type state. Additionally, the WT promoter of DDX60 possessing wild-type ISRE and GAS were inserted into the vector successfully (Figure S1-B). Due to the considerable distance between ISRE and GAS in DDX58 (Figure S1, D(I) and D(II)), as well as in NMI (Figure E(I)-E(II) and E(III)), the figure of sequenced fragments were segmented, with all ISRE and GAS elements in both genes maintaining their wild-type status. Similarly, for IRF1 (Figure S1,F), the figure of sequenced fragments were divided into segments. As depicted in Figure S1, F(I), (II), (III), (IV), and (V), the sequence of the ISRE and GAS sites are preserved in their wild-type condition.

4.4.4 Implementing Mutations In ISRE And GAS Elements Through A Site-Directed Mutagenesis Approach

To examine the function of ISRE and GAS elements and assess the impact of nucleotide alterations in their sequences, a site-directed mutagenesis (SDM) approach was employed for PARP14, APOL6, DDX60, NMI and STAT1 genes. This approach requires PCR reactions using designing specific primers to introduce the nucleotide modifications in ISRE and GAS elements. Generally, During PCR reaction, the constructs containing WT proximal promoters of PARP14, APOL6, DDX60, NMI and WT distal regulatory region of STAT1 gene were used as the template. Subsequently, gel electrophoresis was performed, and the specific band corresponding to the desired construct size was excised from the gel. After the subsequent step, the nick generated in the constructs during SDM was repaired using NEBuilder HiFi DNA assembly master mix, followed by incubation of the constructs at 50°C for 45 minutes. During bacterial transformation,

the constructs containing mutations in ISRE and/or GAS (Table 13) were transformed into the bacteria. Next, 8 bacterial colonies were selected to conduct colony PCR to screen the positive clones containing the desired construct with introduced mutations in their ISRE and/or GAS. Primers Fluc_F and Fluc_R were employed in the colony PCR to bind to the plasmid backbone. Following the assessment of bands corresponding to the desired constructs on the electrophoresis gel, the constructs underwent Sanger sequencing to validate the successful implementation of nucleotide modifications.

4.4.5 Verification Of Site-Directed Mutagenesis Using Sanger Sequencing

Sanger sequencing was conducted by Fluc_F and Fluc_R primers (Table 8) for validation of the precision and efficiency of the site-directed mutagenesis procedure on constructs containing individual mutated ISRE, mutated GAS and simultaneous mutated ISRE/GAS in the promoters of PARP14, APOL6, DDX60, NMI, and STAT1 genes (Figure S2). As it was mentioned before, constructs including APOL6_ΔISRE, APOL6_ ΔGAS and APOL6_ ΔISRE/ΔGAS, STAT1_pd_ distΔISRE, STAT1_pd_distΔGAS, STAT1_pd_proxΔISRE were generated in the lab and sequenced previously and the Sanger sequencing results are not shown in figure S2. In figure S2-A, complete mutated ISRE(ΔISRE) (AI), complete mutated GAS (ΔGAS)(AII), partial mutated ISRE (ΔpISRE) (AIII), partial mutated GAS (ΔpGAS) (AIV) and simultaneous ΔISRE/ΔGAS (AV) of PARP14 are shown. Likewise, figure S2-B illustrates mutated ISRE(1) (BI), mutated GAS (BII), and ISRE(1)/GAS mutated DDX60 (BIII). In figure S2-C, mutated constructs of the NMI promoter are depicted. Exch construct is distinguished by various border colors. For instance, the red border (CI) signifies mutations in ISRE(1), while ISRE(2) and GAS remain unaffected. The green border (CII) denotes mutations in GAS, while ISRE(1) and (2) remain unchanged. Lastly, the blue one (CIII) indicates mutations in ISRE(1) and GAS sites, with ISRE(2) remaining unaltered. Similarly, figure S2-D represents mutated constructs of the STAT1 gene. The orange border (DI) indicates mutated distal ISRE and distal GAS sites with no changes in proximal ISRE in the promoter of the STAT1 gene (the Sanger results for unaltered proximal ISRE is not shown). The purple (DII) shows mutations in both distal and proximal ISRE, with the distal GAS site remaining unchanged. Finally, simultaneous mutations in distal ISRE/GAS and proximal ISRE are represented by the yellow border (DIII).

4.5 Further Characterization Of The ISRE And GAS Elements Within Composite Genes In Wild-Type Cells Using Site-Directed Mutagenesis

First, to understand the exact role of ISRE and GAS, we compared the promoter activity of PARP14, APOL6, DDX60, NLRC5, NMI, DDX58, STAT1 and IRF1 in WT cells. For instance, promoters of PARP14 and APOL6 (very close and close ISRE/GAS distance, respectively) displayed high luciferase activity in WT constructs after IFNα treatment (Figure 31,A-B). However, constructs containing WT promoter of APOL6 (Figure 31-B) exhibited higher response in response to IFNγ as compared to WT constructs of PARP14 (Figure 31-A). This was in line with the observed comparative binding patterns of ISGF3, GAF, GAF-like and IRF1. This observation correlated with low gene expression levels of PARP14 after IFNγ as compared to IFNα (Figure 22-A). Additionally, this finding is in agreement with the similar gene expression levels of APOL6 in response to both IFNs (Figure 24-B). The distinctive feature of the composite site in the PARP14 gene lies in the direct adjacency of a GAS site to the ISRE. For PARP14, mutations in the ISRE (ΔISRE) led to a significant decrease in response to both IFNα and IFNγ, while mutations in the GAS (ΔGAS) site showed less effects, with the remaining ISRE exhibiting greater sensitivity to IFNα as compared to IFNγ. Simultaneous mutations in both regulatory elements (PARP14_ΔISRE/ΔGAS) of the PARP14 gene resulted in a total loss of promoter's ability to respond to both IFNα and IFNγ. The proximity of the GAS and ISRE in PARP14 suggests the existence of an overlapping ISRE site (Figure S2-AI). Intriguingly, implementing mutations solely in the 3′ half of the ISRE site (PARP14_ΔpISRE) led to a partial response to both types of IFNs, indicating the functional significance of this overlapping ISRE. Conversely, mutations in the 5′ half of the GAS site (PARP14_ΔpGAS) had no significant impact on IFNα and IFNγ response, suggesting a more potent role of the ISRE site (Figure 31-A). Subsequently, for APOL6 (Figure 31-B), the constructs containing mutated ISRE (APOL6_ΔISRE) responded more to IFNγ. While GAS mutated APOL6 (APOL6_ΔGAS) responded more to IFNα. Simultaneous mutations in both regulatory elements (APOL6_ΔISRE/ΔGAS) caused the total abolishment of promoter activity in response to both IFNα and IFNγ pointing to the functional ISRE and GAS in the promoter of APOL6. WT constructs of DDX60 (Figure 31-C) and NLRC5 (Figure 31-D) (medium ISRE/GAS distance) showed promoter activity in response to both IFNs. However, in contrast to NLRC5, where the WT promoter showed a stronger response to IFNγ, DDX60 promoter tended to respond more to IFNα. This could point to the potent role of GAS in NLRC5 in response to IFNγ. Nevertheless, we did not conduct site-directed mutagenesis targeting the ISRE and GAS

sites for NLRC5 gene, preventing us from examining the specific role of ISRE and GAS in its promoter region. For DDX60, constructs with mutated GAS (DDX60_ΔGAS) still displayed high luciferase activity as compared to constructs with mutated ISRE(1) (DDX60_ΔISRE1) in response to IFNα. This could point to the more potent ISRE site than GAS. However, because of the shorter distance between ISRE1 and GAS, we opted to introduce mutations specifically in ISRE(1) not ISRE(2). Furthermore, similar promoter activity was detected in both WT and constructs containing mutated GAS (DDX60_ΔGAS) in response to IFNγ confirming that GAS is not as potent as ISRE(1) site. Interestingly, luciferase activity was still detected in response to both types of IFNs where both ISRE and GAS sites were simultaneously mutated (DDX60_ΔISRE/ΔGAS) potentially correlating with the presence of an active ISRE(2) in the DDX60 promoter. Next, we assessed the promoter activity of NMI (Figure 31-E) and DDX58 (Figure 31-F) as they both belong to long ISRE/GAS distance group. While the promoter of NMI exhibited luciferase activity in response to both IFNs, the promoter of DDX58 only responded to IFNα. This could correlate with strong IFNα and very weak IFNγ-induced gene expression of DDX58 (Figure 28-A). The weak IRF1 binding to ISRE(2) in response to both IFNs and weak IRF9 binding to ISRE(2) only in response to IFNα suggested the presence of a less potent or inactive ISRE(2) site in the promoter of NMI (Figure 27-B). Consequently, we refrained from conducting site-directed mutagenesis targeting the ISRE(2) site in the NMI promoter. ISRE Mutated NMI (NMI_ΔISRE(1)) partially responded to both IFNα and IFNγ. Conversely, mutations in the GAS (NMI_ΔGAS) site tended to enhance the response to both types of IFNs. This pointed to the predominant role of the ISRE site in the promoter of NMI and it is predicted that GAS might have an inhibitory effect on the ISRE site (Figures 31-E). Unfortunately, we did not perform site-directed mutagenesis targeting ISRE and GAS for DDX58, therefore, we were not able to determine the precise roles of ISRE and GAS in its promoter. Finally, we performed the luciferase assay to examine the promoter activity of STAT1 and IRF (Distal regulatory ISRE/GAS). Regarding STAT1 (Figure 31-G), both proximal and distal regions were simultaneously cloned into the pXPG vector. Mutations solely in the proximal ISRE (ST1_pd_ ΔISRE_prox) or mutations in both distal ISRE and GAS composite sites (ST1_pd_ ΔISRE/ΔGAS_dist) for STAT1 led to a partial response to both IFNs. This confirmed that achieving optimal promoter activity in response to IFNα and IFNγ requires both the proximal ISRE site and the distal composite sites. However, the mutations introduced in both proximal and distal ISRE simultaneously (ST1_ΔISRE/ΔISRE) resulted in low response to both IFNs as

compared to constructs that one of the ISRE elements is available including ST1_ΔGAS_dist, ST1_ ΔISRE_dist, ST1_ ΔISRE_prox and ST1_ΔISRE/ ΔGAS _dist. This could point to the importance of ISRE site in the proximal promoter and distal regulatory region. A total cessation of STAT1 promoter activity in response to both IFNα and IFNγ was observed when mutations were introduced simultaneously in all three regulatory elements (ST1_pd_ ΔISRE/ΔISRE/ΔGAS). Concerning IRF1 (Figure 31-H), the outcomes demonstrate constructs where the proximal promoter and distal ISRE and GAS composite sites were individually inserted into the pXPG vector, and site-directed mutagenesis results are not available. In comparison to constructs featuring WT distal ISRE and GAS composite sites (IRF1_Distal), the one containing the proximal GAS site (IRF1_Proximal) exhibited a greater response to both IFNα and IFNγ. However, constructs containing distal ISRE and GAS composite sites (IRF1_Distal) exhibited very weak response to both IFNs. This observation suggested similar to STAT1 gene, the distal composite sites of IRF1 gene are active and could play a role in IFN-induced transcription. Nevertheless, our failure to conduct site-directed mutagenesis for the IRF1 gene complicates the investigation into the precise functions of ISRE and GAS.

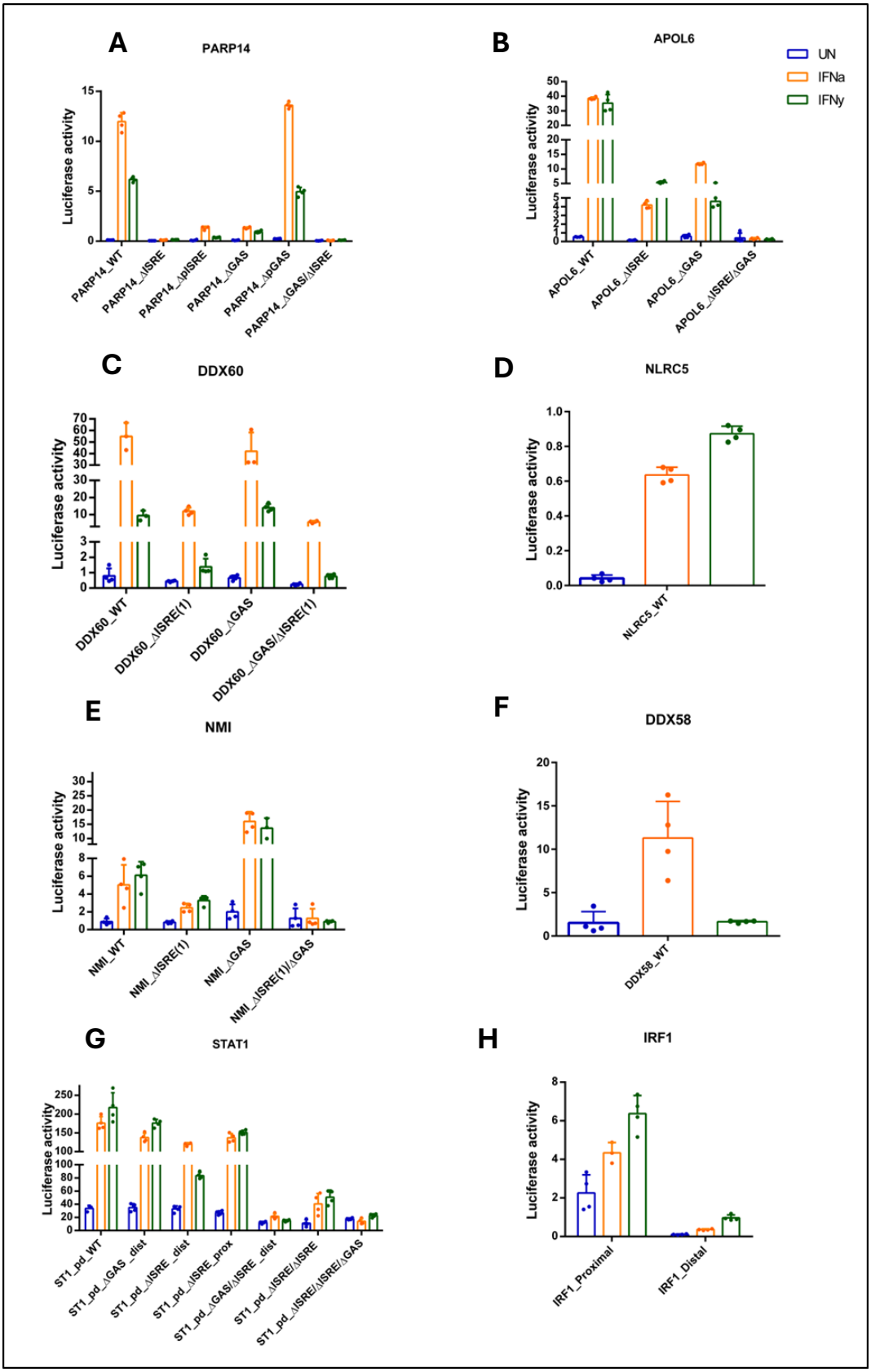

See description on the next page.

Figure 31. Characterization of promoter activity of composite genes in IFNα- and IFNγ-stimulated WT cell line.

The luciferase-based reporter assay results for PARP14 **(A),** APOL6 **(B),** DDX60 **(C),** NLRC5 **(D)**, NMI **(E),** DDX58 **(F),** STAT1 **(G)** and IRF1 **(H).** pXPG containing WT Promoter regions or mutated (Δ)GAS and/or ISRE sequences were used (for DDX58 and NLRC5 only the wild-type promoters were utilized). Firefly luciferase (pXPG) and Renilla luciferase (pRLSV40) vectors were co-transfected into Huh7.5 WT cells. Cells were left untreated and treated with IFNα and IFNγ for 8h. The level of fluorescence of Firefly and Renilla was measured after cell lysis. Bars illustrate the promoter activity of the samples. mean +/- SEM, n=2 (except for DDX58, NLRC5, and IRF1, where n=1).

4.6 Comparative Analysis Of ISGF3, IRF1, GAF, And GAF-Like Functions In Composite Genes In KO Cell Lines Using Site-Directed Mutagenesis

To delve deeper into the precise involvement of ISGF3, IRF1, GAF, and GAF-like in the transcriptional regulation of composite genes, site-directed mutagenesis was employed in combination with luciferase assay in STAT1, STAT2, IRF9, IRF1 and IRF1.9dKO cells. In this context, among the genes analyzed for the roles of ISRE and GAS in section 4.5, five genes from different ISRE/GAS distance groups including PARP14(very close ISRE/GAS), APOL6 (close ISRE/GAS), DDX60 (medium ISRE/GAS distance) , NMI (long ISRE/GAS distance) and STAT1 (Distal regulatory ISRE/GAS) were selected.

PARP14 (Very close ISRE/GAS distance):

To further characterize the role of ISRE and GAS site in PARP14, luciferase activity was studied in different cell lines using constructs containing WT and mutated ISRE (PARP14_ ΔISRE) or/and GAS (PARP14_ΔGAS) (Figure 32). In STAT1KO cells, constructs containing WT promoter (PARP14_WT) showed partial luciferase activity in response to IFNα (Figure 32, A and at a smaller scale in A(I)). This could point to the lower potency of pSTAT2/IRF9 in response to IFNα or the short-term IFNα treatment. And as expected, it remained unresponsive to IFNγ as compared to WT cells. These observations correlated with qPCR data (Figure 22-A). Individually ISRE mutated PARP14 (PARP14_ΔISRE) and GAS mutated PARP14 (PARP14_ΔGAS) did not respond to both IFNs (Figure 32-A(I)). Even though in the GAS mutated PARP14 (PARP14_ΔGAS) ISRE is present and targeted by pSTAT2/IRF9 in STAT1KO cells, still no promoter activity was detected following IFNα stimulation. This suggested the importance of overlapping ISRE (Figure S2-AI), which is altered by mutations introduced in the GAS site. In STAT2KO and IRF9KO cells (Figure 32) the WT constructs displayed lower response to IFNα as compared to WT cells pointing to the importance of ISGF3. However, IFNγ response was still detected in WT constructs indicating the role of IRF1 complex. Likewise, similar to WT cells, GAS mutated PARP14 (PARP14_ΔGAS) responded to the IFNγ in both STAT2KO and IRF9KO

cells. However, no promoter activity was detected in mutated ISRE PARP14 (PARP14_ΔISRE) upon both IFNs treatment confirming the significance of ISRE. IRF1KO cells, expressing WT constructs showed higher promoter activity in response to IFNα as compared to IFNγ. Nevertheless, the promoter activity in WT constructs is lower in IRF1KO cells as compared to WT cells pointing the role of IRF1 complex. Mutation individually introduced into the ISRE (PARP14_ΔISRE) resulted in complete loss of promoter activity after both IFNα and IFNγ treatment in IRF1KO cells. Additionally, in response to IFNγ, despite the presence of ISRE which is targeted by pSTAT1/IRF9, GAS mutated PARP14 (PARP14_ΔGAS) showed no promoter activity in IRF1KO cells. This highlighted the vital contribution of the overlapping ISRE that is mutated by introducing mutations in GAS site. In IRF1.9dKO cells, constructs containing WT promoter, individually mutated ISRE (PARP14_ΔISRE) and mutated GAS (PARP14_ΔGAS) did not respond to both IFNs. This confirmed the importance of overlapping ISRE which was mutated by introducing mutation in ISRE or GAS sites. Moreover, in IRF1.9dKO cells, in WT constructs, neither GAF nor GAF-like exhibits significant potency in stimulating promoter activity in response to IFNα, similarly, GAF lacks potency in inducing promoter activity following IFNγ treatment. This is in consistent with low expression of PARP14 in IRF1.9dKO cells after IFNα and IFNγ stimulation (Figure 22-A). A complete loss of promoter activity was observed in simultaneously mutated ISRE and GAS in PARP14 (PARP14_ΔISRE/_ΔGAS) across all cell lines. These findings confirmed the significance of overlapping ISRE in the promoter of PARP14. Based on the findings we have outlined a transcriptional mechanism for PARP14 (Figure 33). Accordingly, we proposed a dominant overlapping ISRE mechanism in which an overlapping ISRE is the main transcriptional element in the promoter of PARP14 in response to both IFNα and IFNγ. However, we confirmed the presence of an active GAS site with a less dominant role. Additionally, ISGF3 displayed higher potency than IRF1, GAF and GAF-like in response to IFNα, while, IRF1 exhibited greater potency than GAS following IFNγ treatment. Moreover, consistent with the binding of IRF9 in WT cells upon exposure to IFNγ (Figure 21-A), we can infer the limited involvement of pSTAT1/IRF9 following IFNγ treatment (Figure 33).

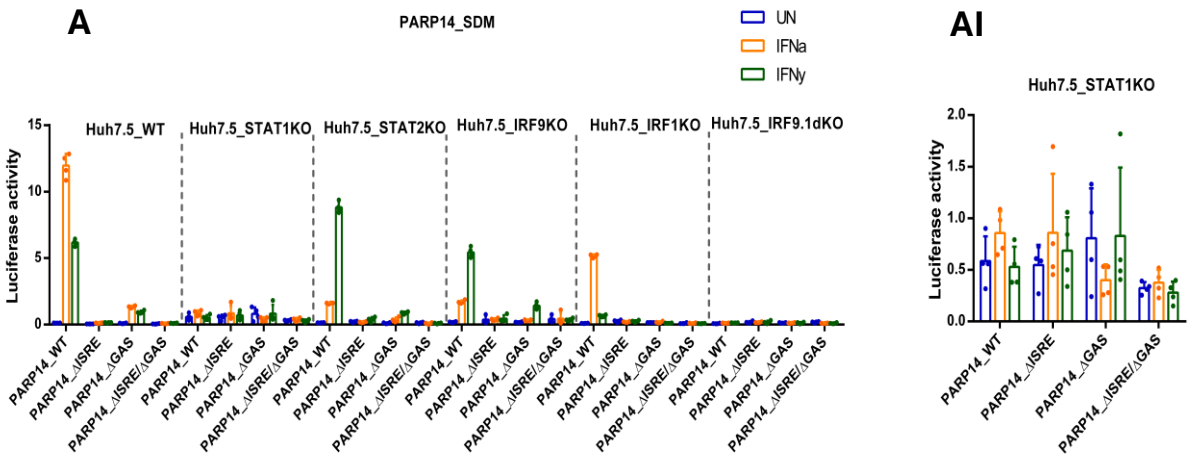

Figure 32. Characterization of promoter activity of IFNα and IFNγ-stimulated PARP14 in WT Huh7.5 as compared to KO cell lines.

A. The luciferase-based reporter assay results for PARP14 in WT, STAT1, STAT2, IRF9, IRF1 and IRF1.9dKO cells. **A(I).** The luciferase-based reporter assay results for PARP14 in STAT1KO cells. The pXPG vector was used to clone WT sequence or mutated (Δ)GAS and/or ISRE sequence of promoter. Firefly luciferase (pXPG) and Renilla luciferase (pRLSV40) vectors were co-transfected into Huh7.5 WT, STAT1, STAT2, IRF9, IRF1 and IRf1.9dKO cells. Cells were left untreated and treated with IFNα and IFNγ for 8h. The level of fluorescence of Firefly and Renilla was measured after cell lysis. Bars illustrate the promoter activity of the samples. Mean +/- SEM , n=2

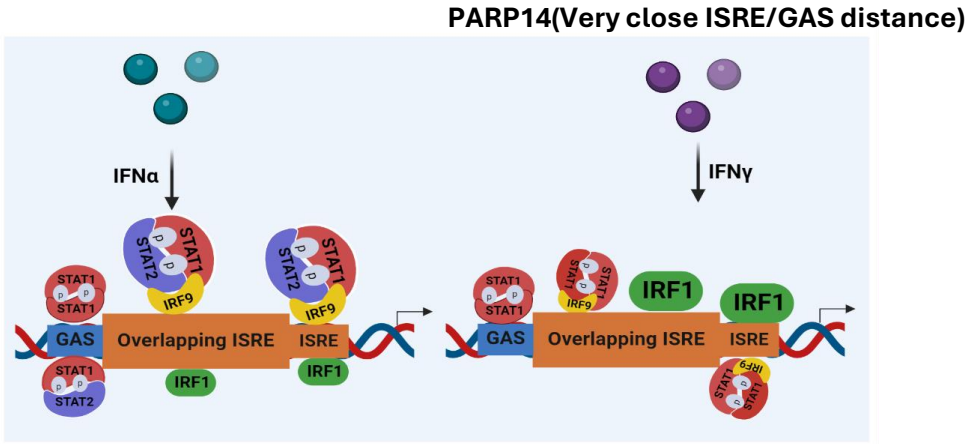

Figure 33. PARP14's predictive transcriptional regulatory mechanism in the presence of ISRE and GAS elements, alongside all transcriptional components such as pSTAT1, pSTAT2, IRF9, and IRF1, in response to IFNα and IFNγ.

According to this model, dominant overlapping ISRE mechanism is predicted. GAS site is indicated by blue box and ISREs are shown by orange box. As it is shown in the figure, GAS and ISREs are oriented negatively (GAS- ISRE). Overlapping ISRE is the dominant regulatory motif in the promoter of PARP14 in response to both IFNs. However the active GAS is less potent as compared to the ISRE after IFNα and IFNγ treatment. The increased size of overlapping ISRE is indicative of its primary role in response to both IFNs. The diminished dominance of GAS is reflected in its reduced size. (Description continues on the next page)

ISGF3 is the main TF as demonstrated by bigger size, while, GAF, GAF-like and IRF1 are the less potent TFs as indicated by their smaller size in response to IFNα. On the other hand, upon IFNγ stimulation, IRF1 is the key TF indicated by increased size, while GAS and pSTAT1/IRF9 displays reduced potency, indicated by its decreased size.

APOL6 (Close ISRE/GAS distance):

In STAT1KO cells (Figure 34), constructs containing WT promoter (APOL6_WT) and mutated GAS (APOL6_ ΔGAS) partially responded to IFNα pointing to the role of pSTAT2/IRF9 binding the ISRE. However, the promoter activity is lower in these constructs in STAT1KO cells as compared to WT cell lines. Luciferase activity was entirely abolished in the mutated ISRE (APOL6_ΔISRE) construct in response to IFNα treatment. As anticipated, no response was detected after IFNγ stimulation for WT (APOL6_WT), ISRE mutated (APOL6_ΔISRE) and GAS mutated APOL6 (APOL6_ ΔGAS) constructs. These observations are in line with qPCR results in STAT1KO cells after IFNα and IFNγ treatment (Figure 24-B). In STAT2 and IRF9KO cells, WT constructs (APOL6_WT) responded to IFNα. However, this response is lower in IRF9KO cells as compared to WT and STAT2KO cells. This emphasized the significance of ISGF3. For both STAT2 and IRF9KO cells, WT constructs displayed higher promoter activity in response to IFNγ. In both STAT2 and IRF9KO cells, the luciferase activity significantly reduced in ISRE mutated APOL6 (APOL6_ΔISRE) and GAS mutated APOL6 (APOL6_ΔGAS) constructs in response to IFNα. Nevertheless, both constructs responded to IFNγ. This indicated the contribution of GAF binding GAS in ISRE mutated APOL6 (APOL6_ΔISRE) and IRF1 targeting ISRE in GAS mutated APOL6 (APOL6_ΔGAS) in response to IFNγ. In IRF1KO cells, luciferase activity was observed for the constructs containing WT promoter (APOL6_WT) in response to both IFNs. However, this response was lower in IRF1KO cells as compared to WT cells pointing to the role of IRF1 complex. In ISRE mutated APOL6 (APOL6_ ΔISRE) promoter activity was observed after IFNα and IFNγ treatment in IRF1KO cells explaining the existence of an active GAS site targeted by GAF/GAF-like upon stimulation with IFNα and GAF following treatment with IFNγ. In contrast, constructs containing mutated GAS (APOL6_ ΔGAS) responded to IFNα in IRF1KO cells, while it remained unresponsive to IFNγ despite the presence of ISRE targeted by pSTAT1/IRF9 after IFNγ. This suggested that pSTAT1/IRF9 lacks the potency to induce promoter activity in GAS mutated APOL6 (APOL6_ΔGAS) in IRF1KO cells. Lastly, in IRF1.9dKO cells, for WT construct no luciferase activity was observed in response to IFNα, while in response to IFNγ promoter activity was still detected indicating the role of GAF targeting GAS site. This was confirmed by detecting promoter activity in construct containing mutated ISRE (APOL6_ ΔISRE). On the contrary, GAS mutated APOL6 (APOL6_ΔGAS) remained unresponsive to both IFNs as compared to WT constructs in IRF1.9dKO cells (Figure 34). This observation was in agreement

with APOL6 gene expression in IRF1.9dKO cells in response to IFNγ (Figure 24-B). No promoter activity was detected in response to IFNα and IFNγ in all cell lines (Figure 34), when mutations were introduced simultaneously in both ISRE and GAS (APOL6_ΔISRE/ΔGAS), further confirming the involvement of active ISRE and GAS elements. These findings provide additional confirmation of the crucial involvement of ISGF3 in IFNα response, and of IRF1 and GAF in IFNγ response. ISRE is a crucial element in the promoter of APOL6 with more potency compared to GAS in response to IFNα, while in response to IFNγ, both sites might be potent. Collectively, a combined mechanism is predicted (Figure 35)for APOL6 in which both ISRE and GAS elements are functionally active in the promoter of APOL6. In addition, ISGF3 exhibited higher potency than IRF1, GAF and GAF-like upon IFNα treatment. Whereas, both IRF1 and GAF complexes are the main TFs in response to IFNγ. Furthermore, in agreement with the binding of IRF9 in response to IFNγ (Figure 23-B) a minor role is predicted for pSTAT1/IRF9 upon IFNγ stimulation (Figure 35).

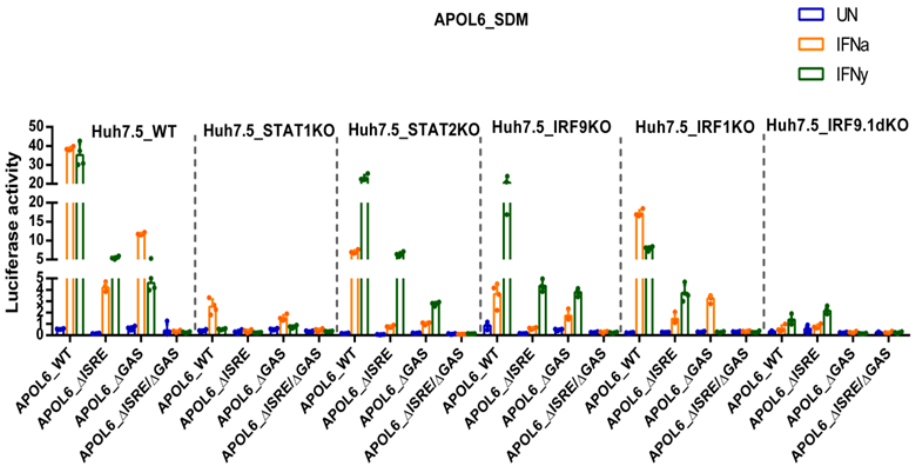

Figure 34. Characterization of promoter activity of IFNα and IFNγ-stimulated APOL6 in WT Huh7.5 as compared to KO cell lines.

The luciferase-based reporter assay results for APOL6 in WT, STAT1, STAT2, IRF9, IRF1 and IRF1.9dKO cells. The pXPG vector was used to clone WT sequence or mutated (Δ)GAS and/or ISRE sequence of promoter. Firefly luciferase (pXPG) and Renilla luciferase (pRLSV40) vectors were co-transfected into Huh7.5 WT, STAT1, STAT2, IRF9, IRF1 and IRF1.9dKO cells. Cells were left untreated and treated with IFNα and IFNγ for 8h. The level of fluorescence of Firefly and Renilla was measured after cell lysis. Bars illustrate the promoter activity of the samples. Mean +/- SEM. n=2

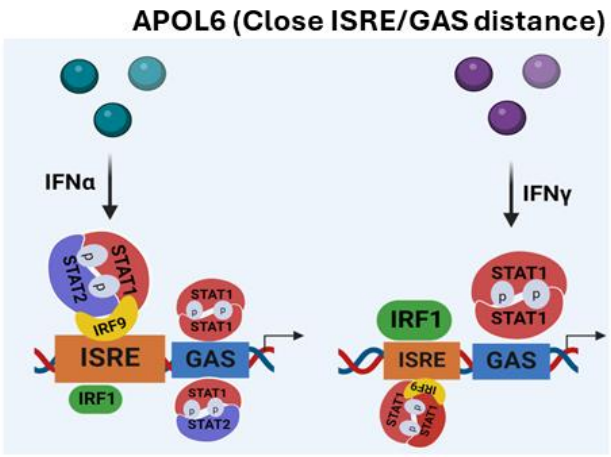

Figure 35. APOL6's predictive transcriptional regulatory mechanism in the presence of ISRE and GAS elements, alongside all transcriptional components such as pSTAT1, pSTAT2, IRF9, and IRF1, in response to IFNα and IFNγ.

According to this model, a combined mechanism is predicted for APOL6 wherein both ISRE and GAS elements are functional, however, ISRE is more potent than GAS in response to IFNα as evidenced by its bigger size in response to IFNα. In response to IFNγ both ISRE and GAS are equally potent as it is indicated by their identical sizes. GAS site is indicated by blue boxes and ISRE is shown by orange boxes. As it is shown in the figure, GAS and ISRE are oriented positively (ISRE-GAS). Following IFNα treatment, ISGF3 is the Primary TF as demonstrated by its enlarged size. Whereas, GAF, GAF-like, and IRF1 exhibit lower potency, as shown by their smaller sizes. Upon IFNγ treatment, both IRF1 and GAF complexes are the key TFs as illustrated by their larger sizes, whereas, pSTAT1/IRF9 has a minor role indicated by its small size.

DDX60 (medium ISRE/GAS distance):

In STAT1KO cells (Figure 36), the response to IFNα was partial in constructs containing WT promoter (DDX60_WT) and mutated GAS (DDX60_ΔGAS) as compared to WT cells, indicating the involvement of pSTAT2/IRF9 binding to ISRE. However, this response was lower in mutated GAS (DDX60_ΔGAS) construct in comparison with WT promoter (DDX60_WT). Surprisingly, mutated ISRE(1) (DDX60_ΔISRE1) and ISRE(1)/GAS DDX60 (DDX60_ΔISRE1/ ΔGAS) exhibited no response to IFNα in STAT1KO cells despite the presence of ISRE2. As expected, WT promoter, mutated ISRE(1) (DDX60_ΔISRE1) and mutated GAS (DDX60_ΔGAS) constructs remained unresponsive to IFNγ in STAT1KO cells. These results correlated with qPCR data for DDX60 in STAT1KO cells in response to IFNα and IFNγ (Figure 26-B). In STAT2 and IRF9KO cells, the promoter activity is significantly reduced in WT constructs (DDX60_WT) in response to IFNα as compared to WT cells demonstrating the role of ISGF3. Conversely, promoter activity was still detected in WT constructs (DDX60_WT) in response to IFNγ in both STAT2 and IRF9KO cells. Likewise, ISRE(1) mutated DDX60 (DDX60_ΔISRE1) showed no response to IFNα despite the presence of GAS in STAT2 and IRF9KO cells. This suggested the presence of

an inactive GAS site. This was confirmed by abolished IFNγ response for ISRE(1) mutated DDX60 (DDX60_ΔISRE1) construct in STAT2 and IRF9KO cells. In contrast, no or very low IFNα response was detected in constructs containing mutated GAS (DDX60_ΔGAS). While after IFNγ treatment, promoter activity was still detected for GAS mutated DDX60 (DDX60_ΔGAS) indicating the role of IRF1complex binding to ISRE in STAT2 and IRF9KO cells. In IRF1KO cell lines, lower promoter activity was observed for WT constructs (DDX60_WT) in response to IFNα as compared to WT cells. The promoter activity for WT constructs of DDX60 after IFNγ treatment in IRF1KO cells suggested the participation of the pSTAT1/IRF9 complex rather than GAF. This was confirmed by loss of promoter activity of WT constructs in response to IFNγ in IRF1.9dKO cells. No IFNα and IFNγ response was observed for ISRE(1) mutated DDX60 (DDX60_ΔISRE1) in IRF1KO cells. Whereas, GAS mutated DDX60 (DDX60_ΔGAS) responded only to IFNα pointing the role of ISGF3 binding ISRE. Finally, in IRF1.9dKO cells, all constructs including WT, DDX60_ΔISRE1 and DDX60_ΔGAS remained unresponsive to both IFNs as compared to WT cells suggesting the presence of an inactive GAS in the promoter of DDX60 (Figure 36). This observation was consistent with the absence of DDX60 gene expression in IRF1.9dKO cells (Figure 26-B). Introducing mutations in both ISRE(1) and GAS elements simultaneously led to the total abolition of DDX60 promoter activity in response to both IFNα and IFNγ across all KO cell lines. No promoter activity was detected for mutated ISRE(1) (DDX60_ΔISRE1) and ISRE(1)/GAS DDX60 (DDX60_ΔISRE1/ΔGAS) in response to IFNα in all KO cells despite the presence of ISRE(2) (Figure 36). Based on the results, we suggested one element mechanism for DDX60 (Figure 37). Accordingly, the presence of an inactive GAS is predicted. Furthermore, ISGF3 serves as the primary transcription factor in response to IFNα, while IRF1 and pSTAT1/IRF9 emerges as the predominant complexes following IFNγ treatment. Moreover, both ISRE(1) and (2) are required for optimal expression of DDX60 in WT cells, however ISRE(1) is more potent than ISRE(2).

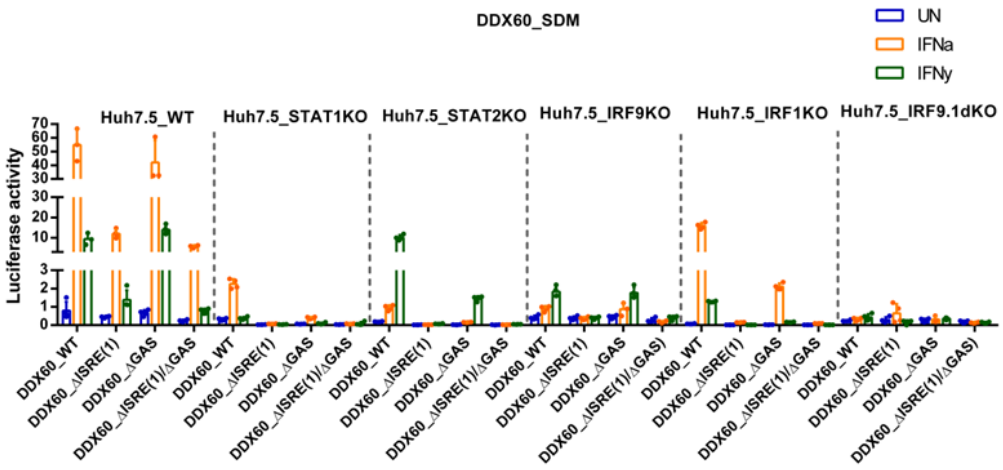

Figure 36. Characterization of promoter activity of IFNα and IFNγ-stimulated DDX60 in WT Huh7.5 as compared to KO cell lines.

The luciferase-based reporter assay results for DDX60 in WT, STAT1, STAT2, IRF9, IRF1 and IRF1.9dKO cells. The pXPG vector was used to clone WT sequence or mutated (Δ)GAS and/or ISRE sequence of promoter. Firefly luciferase (pXPG) and Renilla luciferase (pRLSV40) vectors were co-transfected into Huh7.5 WT, STAT1, STAT2, IRF9, IRF1 and IRF1.9dKO cells. Cells were left untreated and treated with IFNα and IFNγ for 8h. The level of fluorescence of Firefly and Renilla was measured after cell lysis. Bars illustrate the promoter activity of the samples. Mean +/- SEM, n=2

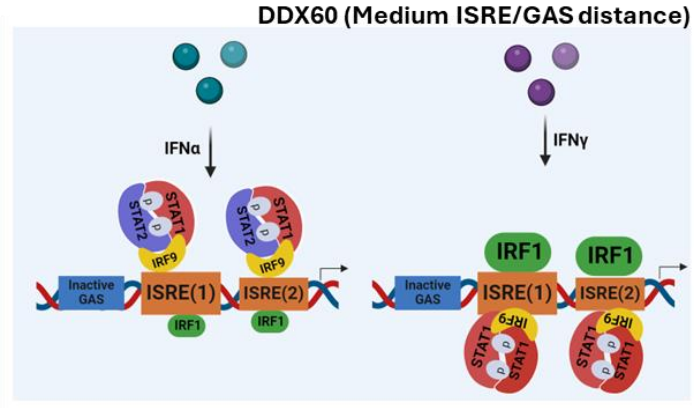

Figure 37. DDX60's predictive transcriptional regulatory mechanism in the presence of ISRE and GAS elements, alongside all transcriptional components such as pSTAT1, pSTAT2, IRF9, and IRF1, in response to IFNα and IFNγ.

According to this model, one element mechanism is proposed for DDX60 wherein GAS site is not active. GAS site is indicated by blue box and ISREs are shown by orange boxes. As it is shown in the figure, GAS and ISREs are oriented negatively (GAS-ISRE). ISRE(1) is more potent element than ISRE(2) in response to both IFNs indicated by its enlarged size. After IFNα treatment, ISGF3 is the key contributor as demonstrated by increased size, while IRF1 is less potent TF illustrated by its smaller size. Upon IFNγ stimulation, IRF1and pSTAT1/IRF9 stand as the principal TFs responsible for regulating the expression of DDX60 as demonstrated by their bigger sizes.

NMI (long ISRE/GAS distance):

In STAT1KO cells as it is shown in figure 38-A and at a smaller scale in A(I), in comparison to WT cells, constructs containing the WT promoter (NMI_WT) and mutated GAS (NMI_ΔGAS) exhibited partial response to IFNα, implicating the participation of pSTAT2/IRF9 binding to the ISRE. No IFNα response was detected in ISRE(1) mutated NMI (NMI_ΔISRE1). As expected, no IFNγ response was observed in constructs including NMI_WT, NMI_ΔISRE1 and NMI_ΔGAS. This observation is in line with expression of NMI after IFNα and the absence of gene expression in response to IFNγ in STAT1KO cells (Figure 28-B). In STAT2KO cells, WT constructs (NMI_WT) displayed partial promoter activity in response to IFNα as compared to WT cells, while in IRF9KO cells, WT promoter remained unresponsive to IFNα pointing to the main role of ISGF3. However, in both STAT2 and IRF9KO cells, WT_NMI exhibited lower but still detectable promoter activity after IFNγ stimulation as compared to WT cells. ISRE(1) mutated NMI (NMI_ΔISRE1) remained unresponsive to IFNα, whereas after IFNγ treatment, promoter activity was still observed in both STAT2 and IRF9KO cells. This could point to the role of GAF binding GAS in response to IFNγ. In both cell lines, GAS mutated NMI (NMI_ ΔGAS) exhibited comparable promoter activity to the WT constructs in response to both IFNs. These observations In STAT2 and IRF9KO cells, indicated the significant role of ISGF3 and IRF1 binding to ISRE in response to IFNα and IFNγ, respectively. In IRF1KO cells, lower IFNα and IFNγ response was detected for WT constructs (NMI_WT) as compared to WT cells. However, WT_NMI tended to respond more to IFNα than to IFNγ. The promoter activity was observed for ISRE(1) mutated NMI (NMI_ΔISRE1) confirming the presence of an active GAS site which is targeted by GAF/GAF-like upon IFNα stimulation and GAF after IFNγ treatment in IRF1KO cells (Figure 38-A). Similar to APOL6 (Figure 34) and DDX60 (Figure 36), NMI exhibited promoter activity for constructs containing mutated GAS (NMI_ΔGAS) in response to IFNα, but not to IFNγ in IRF1KO cells. This could point to the absence of pSTAT1/IRF9 in response to IFNγ which is in line with the lack of IRF9 binding in WT cells after IFNγ treatment for NMI (Figure 27-B). Lastly, in IRF1.9dKO cells , no luciferase activity was observed for constructs including NMI_WT, NMI_ΔISRE1 and NMI_ΔGAS upon IFNα treatment compared to WT cells. In contrast, NMI_WT , NMI_ ΔISRE1 constructs partially responded to IFNγ indicating the existence of an active GAS site. However, GAS mutated NMI (NMI_ΔGAS) remained unresponsive to IFNγ in IRF1.9dKO cells (Figure 38-A). These observations correlated with the expression of NMI in IRF1.9dKO in response to IFNγ

(Figure 28-B). Simultaneous mutations in ISRE(1) and GAS (NMI_ ΔISRE1/ ΔGAS) resulted in a complete loss of promoter activity in all cell lines (Figure 38-A). The results for NMI further confirm the potent role of ISGF3 in response to IFNα and IRF1 in response to IFNγ. Nevertheless, GAF and GAF-like (in case of IFNα) and GAF (in case of IFNγ) might play a minor role. The abolished promoter activity in constructs including NMI_ΔISRE1 and NMI_ ΔISRE1/ΔGAS in STAT1, STAT2, IRF9 and IRF1.9dKO in response to IFNα cells could point to the presence of an inactive of ISRE(2) in the promoter of NMI. Based on the results from WT and KO cells, an inhibitory mechanism is predicted for NMI (Figure 39). According to this mechanism GAS site might have an inhibitory effect on the ISRE site in response to both IFNs. Likewise, both ISRE1 and GAS are active in the promoter of NMI. However, ISRE is more significant than GAS element in response to both IFNs. ISGF3 is the main TF after IFNα treatment, while, IRF1 is the key complex in response to IFNγ. Furthermore, in agreement with the absence of IRF9 binding in response to IFNγ in WT cells, it is predicted that pSTAT1/IRF9 has no role in transcriptional regulation of NMI after IFNγ stimulation. In addition, correlating with weak IRF1 binding to ISRE(2) in response to both IFNs, no pSTAT1 binding after IFNγ treatment, and weak IRF9 binding to ISRE(2) only in response to IFNα in WT cells (Figure 27-B), the ISRE(2) is not potentially active in the promoter of NMI (Figure 39).

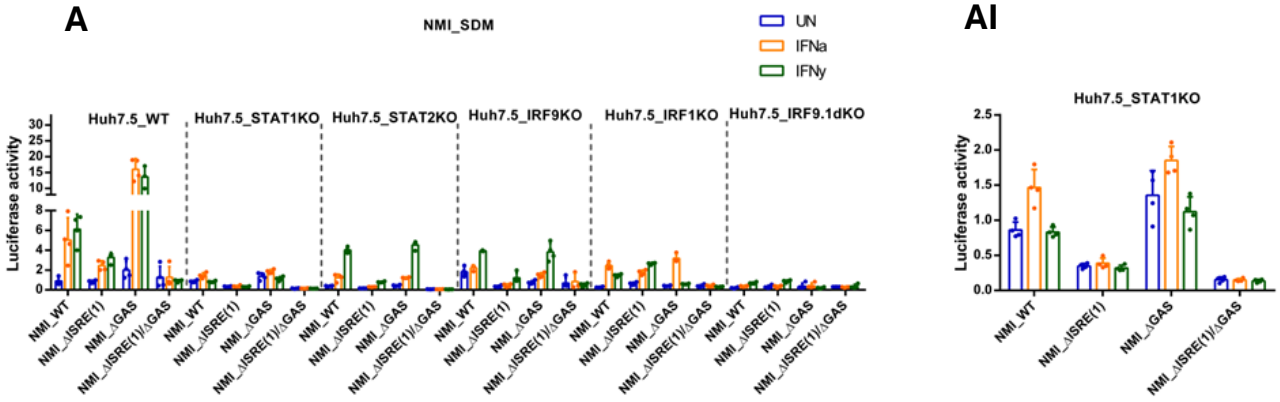

Figure 38. Characterization of promoter activity of IFNα and IFNγ-stimulated NMI in WT Huh7.5 as compared to KO cell lines.

A. The luciferase-based reporter assay results for PARP14 in WT, STAT1, STAT2, IRF9, IRF1 and IRF1.9dKO cells. **A(I).** The luciferase-based reporter assay results for NMI in STAT1KO cells. The pXPG vector was used to clone WT sequence or mutated (Δ)GAS and/or ISRE sequence of promoter. Firefly luciferase (pXPG) and Renilla luciferase (pRLSV40) vectors were co-transfected into Huh7.5 WT, STAT1, STAT2, IRF9, IRF1 and IRF1.9dKO cells. Cells were left untreated and treated with IFNα and IFNγ for 8h. The level of fluorescence of Firefly and Renilla was measured after cell lysis. Bars illustrate the promoter activity of the samples. Mean +/- SEM. n=2

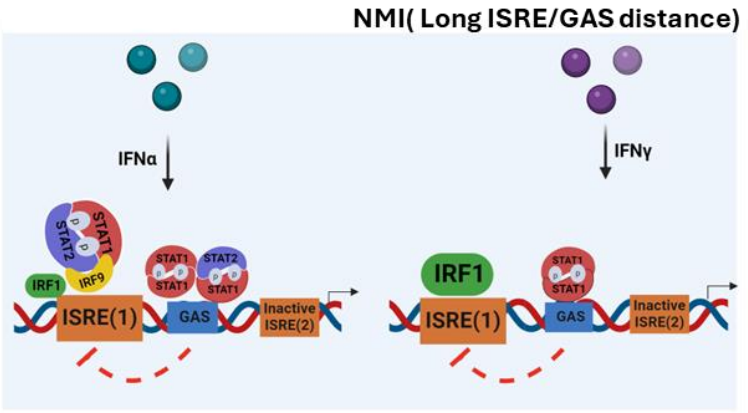

Figure 39. NMI's predictive transcriptional regulatory mechanism in the presence of ISRE and GAS elements, alongside all transcriptional components such as pSTAT1, pSTAT2, IRF9, and IRF1, in response to IFNα and IFNγ.

According to this model, an inhibitory mechanism is anticipated for NMI where GAS may exert an inhibitory effect on ISRE(1), depicted by a dashed red line. GAS site is indicated by a blue box and ISREs are shown by orange boxes. As it is shown in the figure, GAS and ISRE(1) are oriented positively (ISRE-GAS), while, GAS and ISRE (2) are oriented negatively (GAS-ISRE). While ISRE(2) remains inactive, ISRE(1) emerges as the predominant site, as evidenced by its larger size compared to GAS. In response to IFNα, ISGF3 is the primary TF, evident from its larger size, however, GAF, GAF-like and IRF1 are less potent as indicated by their decreased sizes. Upon IFNγ treatment, IRF1 is the main TF illustrated by its enlarged size, while GAF has less potency as demonstrated by its smaller size.

STAT1(Distal regulatory ISRE/GAS):

In STAT1KO cells (Figure 40-A and at a smaller scale in A(I)), lower promoter activity was detected in WT constructs (ST1_pd_WT) in response to IFNα compared to WT cells. This confirmed the role of pSTAT2/IRF9 binding to the ISRE in response to IFNα in STAT1KO cells. However, no IFNα response was observed for constructs containing mutated distal GAS (ST1_pd_ ΔGAS_dist) despite the existence of proximal and distal ISRE in STAT1KO cells. Constructs containing mutated proximal and/or distal ISRE including ST1_pd_ΔISRE_dist, ST1_pd_ ΔISRE_prox, ST1_pd_ ΔGAS/ΔISRE_dist and ST1_pd_ ΔISRE/ΔISRE did not respond to IFNα in STAT1KO cells. As expected, all constructs remained unresponsive after IFNγ stimulation in STAT1KO cells. These observations correlated with weak STAT1 gene expression in STAT1KO cells upon IFNα and the absence of gene expression in response to IFNγ (Figure 30-A). In STAT2KO cells, WT constructs (ST1_pd_WT) showed partial response to both IFNs in comparison to WT cells indicating the role of IRF1 and GAF in response to IFNα and IRF1,GAF and pSTAT1/IRF9 in response to IFNγ (Figure 40-A). This was in line with STAT1 gene expression in STAT2KO cells after IFNα and IFNγ stimulation (Figure 30-A). Nonetheless, the response to IFNα was lower than that to IFNγ, underscoring the importance of ISGF3 in response

to IFNα. Constructs containing mutated distal GAS (ST1_pd_ΔGAS_dist) showed comparable response as mutated proximal ISRE (ST1_pd_ΔISRE_prox) after IFNα or IFNγ treatment in STAT2KO cells. This indicated the role of IRF1 in response to both IFNs in ST1_pd_ ΔGAS_dist constructs and the role of GAF and IRF1 in response to both IFNs in ST1_pd_ ΔISRE_prox constructs. However, IFNα and IFNγ response in distal ISRE mutated STAT1 (ST1_pd_ ΔISRE_dist) and (ST1_pd_ ΔISRE/ΔISRE) significantly reduced. This could suggest the significance of distal ISRE. This was confirmed by complete loss of promoter activity in distal ISRE/GAS mutated STAT1 (ST1_pd_ΔGAS/ΔISRE_dist). In IRF1KO cells, WT constructs (ST1_pd_WT) displayed similar promoter activity as compared to WT cells in response to IFNα and IFNγ pointing to the presence of ISGF3 complex. Constructs harboring mutated distal GAS (ST1_pd_ΔGAS_dist) demonstrated comparable promoter activity to those with mutated proximal ISRE (ST1_pd_ ΔISRE_prox) following treatment with either IFNα or IFNγ. This showed the role of ISGF3 and pSTAT1/IRF9 in response to IFNα and IFNγ, respectively in ST1_pd_ΔGAS_dist constructs. While in ST1_pd_ΔISRE_prox constructs, ISGF3, GAF and GAF_like are the involved complexes upon IFNα treatment and in response to IFNγ, GAF and pSTAT1/IRF9 play the role in IRF1KO cells (Figure 40-A). This observation correlated with our qPCR results in IRF1KO cells (Figure 30-A). For constructs including ST1_pd_ ΔISRE_dist and ST1_pd_ ΔISRE/ΔISRE lower but still detectable promoter activity was observed in response to both IFNs as compared to WT constructs in IRF1KO cells again pointing to the importance of distal ISRE. This was again confirmed by the significantly reduced response upon IFNα and complete loss of promoter activity in response to IFNγ for mutated distal ISRE and GAS (ST1_pd_ΔISRE/ΔGAS) construct in IRF1KO cells. Simultaneous mutations in all three elements (ST1_pd_ ΔISRE/ΔISRE/ ΔGAS) led to a total loss of response to both IFNs in WT and all KO cell lines. Luciferase assay was not performed for STAT1 constructs in IRF9KO and IRF1.9dKO cells and we were unable to explore the involvement of GAF and GAF-like in the response to IFNα, as well as GAF's role in the response to IFNγ in IRF1.9dKO cells (Figure 40-A). However, based on STAT1 gene expression analysis in IRF9 and IRF1.9dKO cells (Figure 30-A), we can predict that the distal GAS is functionally active and GAF plays the key role in response to IFNγ. Our findings suggest the presence of a looping mechanism through TFs within the STAT1 gene, linking the proximal promoter and distal regulatory sites, facilitating the optimal expression of STAT1 following IFN stimulation (Figure 41). Accordingly, consistent with ISGF3 binding upon IFNα exposure and

IRF1 binding in response to both IFNs, targeting distal and proximal ISREs in WT cells, along with pSTAT2/IRF9 binding in STAT1KO cells following IFNα treatment (Figure 29-A), a looping mechanism mediated by transcription factors connects proximal promoter and distal regulatory sites. However, the distal regulatory sites play a crucial role in this mechanism. Furthermore, ISGF3 exhibited significant potency in response IFNα, whereas, upon IFNγ treatment, GAF and pSTAT1/IRF9 are the main TFs (Figure 41).

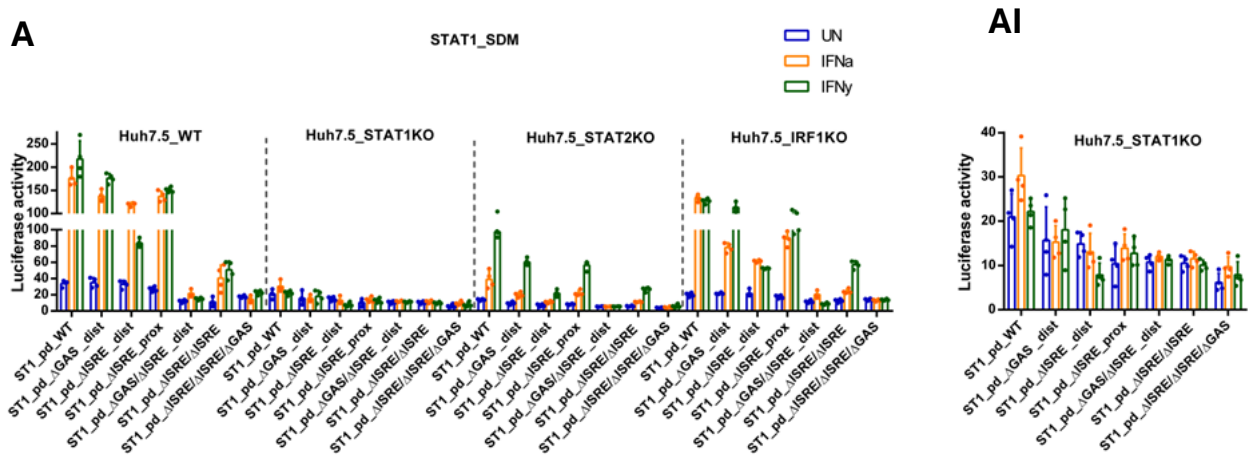

Figure 40. Characterization of promoter activity of IFNα and IFNγ-stimulated STAT1 in WT Huh7.5 as compared to KO cell lines.

A. The luciferase-based reporter assay results for STAT1 in WT, STAT1, STAT2, IRF1KO cells. **A(I).** The luciferase-based reporter assay results for STAT1 in STAT1KO cells. The pXPG vector was used to clone WT sequence or mutated (Δ)GAS and/or ISRE sequence of promoter. Firefly luciferase (pXPG) and Renilla luciferase (pRLSV40) vectors were co-transfected into Huh7.5 WT, STAT1, STAT2 and IRF1KO cells. Cells were left untreated and treated with IFNα and IFNγ for 8h. The level of fluorescence of Firefly and Renilla was measured after cell lysis. Bars illustrate the promoter activity of the samples. Mean +/- SEM. n=2

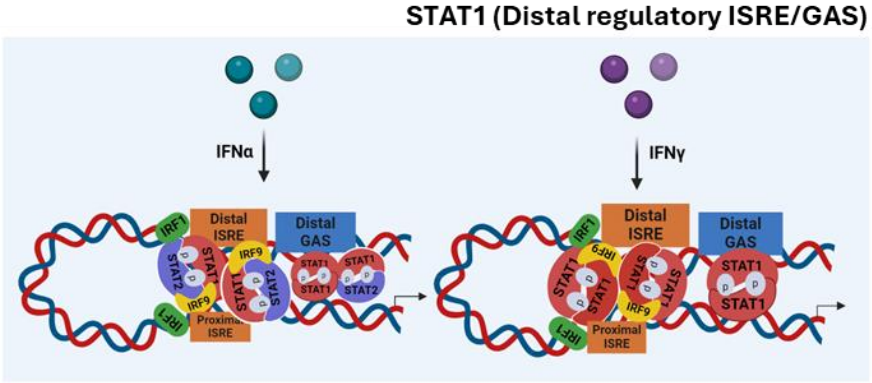

Figure 41. STAT1's predictive transcriptional regulatory mechanism in the presence of ISRE and GAS elements, alongside all transcriptional components such as pSTAT1, pSTAT2, IRF9, and IRF1, in response to IFNα and IFNγ.

Based on this model, a looping mechanism is proposed for STAT1 by which proximal promoter and distal regulatory sites are interconnected, enabling the optimal expression of STAT1. The blue boxes indicate the distal GAS site, while the orange boxes represent the proximal and distal ISREs. The greater significance of the distal ISRE and GAS sites compared to the proximal ISRE is demonstrated by their larger sizes. (Description continues on the next page)

In response to IFNα, ISGF3 is the key regulatory TF as illustrated by its larger size, while GAF, GAF-like and IRF1 are less potent TFs indicated by decreased sizes. Following IFNγ treatment, GAF and pSTAT1/IRF9 are the primary transcription factors evident from their larger sizes, while IRF1 is the less potent TF as demonstrated by its smaller size.

According to the findings, we have determined that composite genes can undergo transcriptional regulation through distinct mechanisms, which are based on the presence of active ISRE and GAS elements, and co-binding of ISGF3, IRF1, GAF, and/or GAF-like complexes in response to IFNα, as well as IRF1, pSTAT1/IRF9, and/or GAF complexes in response to IFNγ. Additionally, we have observed no correlation between the mechanisms of transcriptional regulation and the distances or orientations of ISRE/GAS elements. This suggests that GAF, GAF-like, ISGF3, STAT1/IRF9, and IRF1 complexes work closely together without directly interacting.

4.7 The Viral Protection Capacity Of WT, STAT1 And IRF1.9dKO Cells Following IFNβ And IFNγ Stimulation

Antiviral Assay

In our investigation of IFNα and IFNγ-dependent composite gene expression in section 4, coupled with the evaluation of the ISRE/GAS role through Site-directed mutagenesis in section 5, comparing WT cells to KO cells, we observed that composite genes are typically activated in WT cells by both IFNs through an ISRE+GAS dependent mechanism. Moreover, in WT cells, ISRE emerges as the predominant element in response to IFNα, while in general, both ISRE and GAS become the predominant motifs in response to IFNγ. However, the contribution of the GAS and ISRE site also depends on the composition of the composite site. In STAT1KO cells, gene activation occurs solely in response to IFNα via an ISRE-dependent mechanism. In IRF1.9dKO cells, composite genes are induced in response to IFNγ through a GAS-dependent mechanism. To couple the IFNα or IFNγ dependency of composite genes in WT, STAT1, IRF1.9dKO cells to whether these cells are able to combat viral infection in response to IFNα and IFNγ, antiviral assays were conducted in collaboration with Yu-ling from the lab of Professor Chien-Kuo Lee within the Graduate Institute of Immunology, College of Medicine, National Taiwan University in Taipei, Taiwan. An initial antiviral assay was conducted on WT and STAT1KO cells. Accordingly, 25000 cells were seeded and left for 24h. Subsequently, both WT and STAT1KO cells were left untreated or treated for 24h with a 2-fold serial dilution of IFNα starting from 1000U/ml (Figure 42-A). Likewise, WT cells were left untreated or treated for 24h with a 2-fold serial dilution of IFNγ

starting from 4000pg/ml (Figure 42-B). 24h post-treatment, cells were infected with Vesicular stomatitis Indiana virus (VSV) at a MOI of 0.1 and left for 20h. On the plate, the leftmost row wells contain untreated and infected cells as positive control, while the rightmost row wells contain untreated and uninfected cells as negative control. As it is shown in figure 42 the black wells indicate the presence of viable cells. Unexpectedly, despite employing a high concentration of IFNα, we observed an inadequate antiviral response, with only a minimal number of wells exhibiting viable cells in both WT and STAT1KO cells after IFNα treatment. The minimum concentration of IFNα demonstrating an effect on cell viability in IFNα-treated WT cells was 62.5 U/ml, indicated by the red border. In contrast, IFNα-treated STAT1KO cells exhibited viable cells at a concentration of 250 U/ml. The remaining wells with added IFNα exhibit similarity to the positive control (the leftmost row), where no IFNα was added. Overall, the viral protection in WT cells persisted longer than in STAT1KO cells after IFNα stimulation. Contrary to our expectations of observing viability (indicated by black wells) of WT cells treated with IFNγ, we did not detect any viral protection upon IFNγ stimulation. This was confirmed by the absence of cell viability in wells infected with VSV, regardless of whether IFNγ was applied or not. This finding may suggest that the low concentration of IFNγ failed to trigger the expression of ISGs.

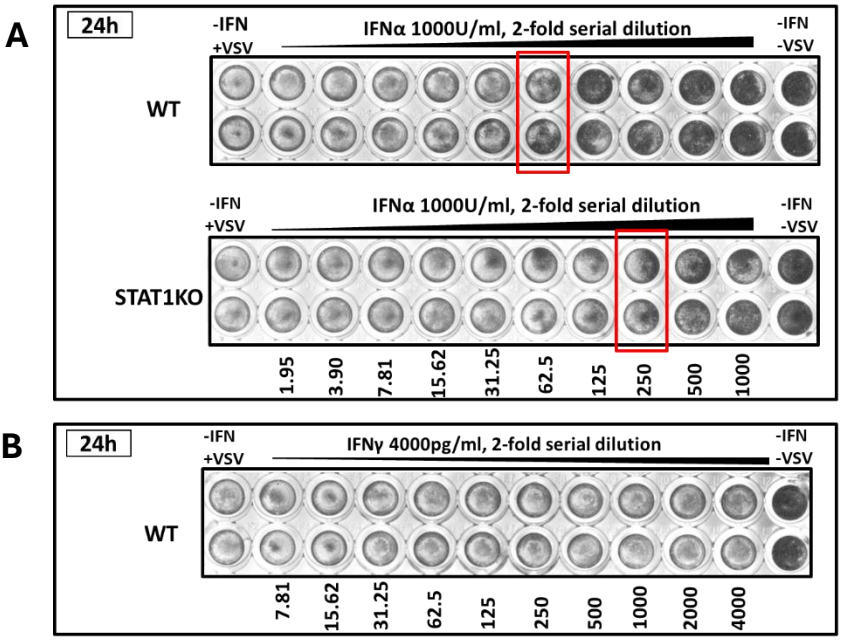

Figure 42. Antiviral response triggered by IFNα and IFNγ stimulation.

A. WT and STAT1KO Huh7.5 cells were subjected to a pre-treatment with a two-fold serial dilution of IFNα starting from 1000 U/ml and incubated for 24h. **B.** WT cells were treated with a two-fold serial dilution of IFNγ starting from 4000 pg/ml and incubated for 24h. (Description continues on the next page)

Subsequently, cells were exposed to VSV infection at a MOI of 0.1 for 20 hours. On the plate, the leftmost row consists of untreated cells, while the rightmost row consists of uninfected cells. Following that, the outcomes were observed through crystal violet staining, with the black wells indicating the presence of viable cells. For every concentration, there are two replicates represented by two rows for each cell line. The red borders indicate the wells with the least concentration showing the effect of IFNα on cell viability. The numbers beneath the wells represent the concentration of IFNs (U/ml for IFNα and pg/ml for IFNγ).

Due to unexpected results, we decided to replace the IFNα with fresh IFNβ. IFNβ interacts with the same receptor and triggers the same signaling pathway as IFNα, resulting in the induction of similar ISGs. Likewise, we increased the concentration of IFNγ to obtain viral protection in WT cells. Additionally, enhancing the MOI of VSV was undertaken to achieve total lysis of cells lacking protection against VSV, especially those located in the center of the wells.

Consequently, we proceeded with conducting the antiviral experiments on cell lines including WT, STAT1, and IRF1.9dKO cells. Additionally, Due to the delayed pSTAT2/IRF9 binding and a shifted expression pattern towards 72h in IFNα-treated STAT1KO cells, we decided to conduct the assay at this time point as well. Accordingly, 25000 cells were seeded and left for 24h. Then WT, STAT1KO, and STAT1.9dKO cell lines were left untreated or treated with a 2-fold serial dilution of IFNβ starting from 100 U/ml (Figure 43,A-B) and IFNγ starting from 10000U/ml (Figure 43,C-D) for both 24 hours and 72 hours. The cells were subsequently infected with VSV at a MOI of 1.0 and left for another 20h. Viral protection was noted in a dose-dependent manner in WT cells following treatment with both IFNs, as well as in STAT1KO cells following IFNβ stimulation. As indicated by the red borders in WT cells, the minimal IFNβ concentration providing viral protection for 24 hours was 0.39 U/ml (Figure 43-A). However, by 72 hours, the required IFNβ concentration for cell protection against the virus increased to 3.12 U/ml (Figure 43-B). Thus, WT cells exhibited enhanced antiviral efficacy at 24h as opposed to 72h after IFNβ treatment. Likewise, in WT cells, a minimal concentration of 625 U/ml of IFNγ was required to confer viral protection for 24 hours (Figure 43-C). Whereas, no antiviral response was detected in 72h IFNγ-treated WT cells (Figure 43-D). Thus, IFNβ-treated WT cells indicated more efficient antiviral response as compared to IFNγ-treated WT at 24h. Reduction in antiviral response after 72h in IFNβ-treated WT cells correlated with reduced expression of ISGs (Sekrecka et al., 2023) and reduced expression of ISRE+GAS-composite genes observed after 72h in this study (Figure 19-A). In IFNβ-treated STAT1KO cells, the assay yielded an antiviral response after both 24 and 72 hours, but with a slight decreased efficiency at 72h. This was verified by applying a minimal concentration of 3.12 U/ml of IFNβ to confer protection against the virus for 24 hours, contrasted

with 12.5 U/ml at 72 hours (as indicated by the red borders) (Figure 43, A-B). This observation was correlated with prolonged expression of composite genes in IFNα-treated STAT1KO cells (Figure 19-A) and expression of ISRE-only containing genes (Sekrecka et al., 2023). Similar to previous experiments that IFNα was utilized (described above), WT cells exhibited extended viral protection compared to STAT1KO cells upon IFNβ treatment at both 24 and 72-hour time points (Figure 43,A-B). A lack of response in IFNγ-treated STAT1KO cells at both 24 and 72 hours post-treatment was detected (Figure 43, C-D). This is in agreement with the absence of induction of ISGs including composite genes in STAT1KO cells following IFNγ treatment (Sekrecka et al., 2023). Furthermore, IRF1.9dKO cells treated with either IFNβ or IFNγ did not exhibit a significant antiviral response at both 24 and 72 hours.

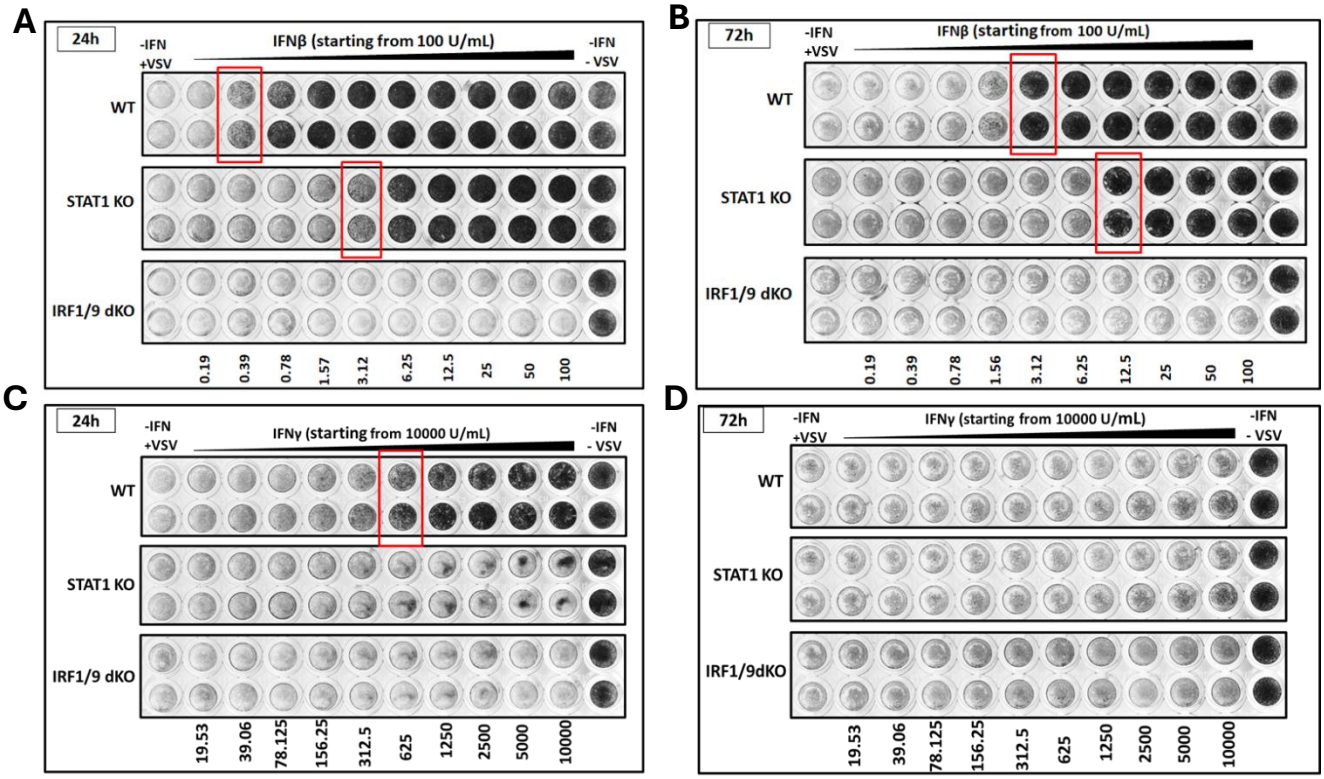

Figure 43. Antiviral response triggered by IFNβ and IFNγ stimulation.

A-B. WT, STAT1KO and IRF1.9dKO Huh7.5 cells were subjected to a pre-treatment with a two-fold serial dilution of IFNβ starting from 1000 U/ml and incubated for 24h (A) and 72h(B). **C-D**. WT, STAT1KO Huh7.5 cells were subjected to a pre-treatment with a two-fold serial dilution of IFNγ starting from 10000 U/ml and incubated for 24h (C) and 72h(D). Subsequently, cells were exposed to VSV infection at a MOI of 1.0 for 20 hours. On the plate, the leftmost row consists of untreated cells, while the rightmost row consists of uninfected cells. Following that, the outcomes were observed through crystal violet staining, with the black wells indicating the presence of viable cells. For every concentration, there are two replicates represented by two rows for each cell line. The red borders indicate the wells with the least concentration showing the effect of IFNβ or IFNγ on cell viability. The numbers beneath the wells represent the concentration of IFNs (U/ml).

Based on the findings, the prolonged viral protection observed in IFNβ/α-treated WT cells, in contrast to IFNβ/α-treated STAT1KO cells, suggest that the combined use of ISRE+GAS motifs in WT cells is more effective in inducing adequate ISGs. Consequently, this leads to long-term protection against viruses compared to the presence of only the ISRE motif in STAT1KO cells. The antiviral response in IFNβ-treated STAT1KO correlated with the involvement of pSTAT2/IRF9 in expression of ISRE containing genes. The stronger antiviral response observed in WT cells treated with IFNβ compared to those treated with IFNγ might indicate that IFNγ is less potent to induce ISGs required for effective viral protection. Moreover, the absence of antiviral response in IFNγ-treated STAT1KO cells correlated with the lack of transcriptional response of ISGs including ISRE+GAS-composite genes in response to IFNγ in STAT1KO cells (Figure 22, 24, 26, 28, 30). The deficiency of antiviral response in IRF1.9dKO cells following treatment with IFNβ and IFNγ confirmed that the GAS-dependent mechanism of composite genes fails to induce the necessary ISGs essential for a potential antiviral response. However, this also suggests that GAS-only containing genes, which are also expressed under these conditions be involved in other functions rather than antiviral response.

5 Discussion

The human body's defense system, known as the immune system, has a significant role in protecting against invading pathogens such as viruses, bacteria, and fungi. When the body faces pathogens, the immune system mounts a coordinated response, initiating processes such as inflammation, during which inflammatory cells generate cytokines such as Interferons, including IFNα and IFNγ (Kopitar-Jerala, 2017). Interferons, a group of signaling proteins, are crucial in orchestrating the body's defense against viral infections. These molecules are among the first immune pathways activated upon viral invasion and are essential for controlling viral replication and spread (Walker et al., 2021).

Interferons serve as initiators of signaling cascades after binding to their corresponding receptors, thereby agitating a series of molecular events that culminate in the transcriptional activation of genes pivotal in anti-pathogenic responses. Despite considerable advancements in understanding the role of interferons in immune regulation and host defense, ongoing research endeavors continue to unveil novel insights into the complexity of the immune system and the involvement of interferons therein. While significant strides have been made in elucidating the functions of interferons, the quest to unravel the full extent of their immunomodulatory effects and therapeutic potential remains an active area of investigation in contemporary immunology.

Throughout this thesis, our specific attention was directed towards a novel group of ISGs, known as ISRE+GAS-containing genes where we delved into elucidating the transcriptional regulatory mechanisms governing their expression in response to IFNα and IFNγ spanning from untreated conditions to 72 hours of stimulation.

5.1 Time-Dependent Role Of Different Complexes In The Expression Of ISRE+GAS- Containing Genes

According to previous studies, IFN-I primarily activates ISRE-containing genes via ISGF3 and IRF1 complexes, whereas IFN-II mainly induces GAS-containing genes through the GAF complex. However, the involvement of GAF-like for the expression of GAS-only containing genes in response to IFN-I and IRF1 for induction of ISRE-only containing genes upon IFN-II treatment pointed out the functional overlap of IFN-I and IFN-II (Odendall et al., 2014; Miyamoto et al., 1988; Decker et al., 1997; Sekrecka et al., 2023; Michalska et al., 2018). To understand the transcriptional mechanisms of ISRE+GAS-composite genes in response to IFNα and IFNγ, we

developed a gene selection strategy. ISGs with both ISRE and GAS elements in their promoters were classified as ISRE+GAS-composite genes. Using ChIP-seq data, we selected ISGs with peak scores over 100 for pSTAT1, pSTAT2, IRF9, and IRF1 in WT Huh7.5 cells after IFNα treatment. We then identified protein-coding composite genes with ISRE and GAS sites in the promoter/5'UTR and distal regulatory region. These genes were further examined for peak scores over 100 for pSTAT1, IRF9, and IRF1 following IFNγ treatment. We assessed expression levels of specific composite genes using RNA-seq data, applying criteria of log2FC > 0.5 and padj < 0.05. A list of 89 composite genes was compiled, all with peak scores >100 and significant induction by either IFNα or IFNγ, or common expression after both IFNs (Table S1). This selection revealed different types of composite genes with variations in ISRE+GAS organization, distance, and orientation. As previous studies have highlighted the role of composite genes in viral infection (Barrat et al., 2019; Schoggins, 2014) our GO and KEGG analysis (Figure 16) of 89 IFNα or IFNγ-induced composite genes further proved the primary functions of these ISRE+GAS composite genes were related to immune responses. This observation aligns with the findings of the study conducted by Sekrecka et al, where GO analysis of ISRE-only, GAS-only and ISRE+GAS composite-containing genes was linked to the defense response. However, functional differences appear to exist among the various gene groups, particularly for GAS-only-containing genes which are also involved in the RNA biosynthetic process (Sekrecka et al., 2023).

To further examine the regulation of ISRE+GAS composite genes, we pre-selected 30 commonly IFNα and IFNγ-induced composite genes which exhibited random ISRE+GAS organization (ISRE-GAS (+) or GAS-ISRE (−)) and the ISRE+GAS distances varied between overlap and more than 200 base pairs (Table 11). The cluster analysis (Figure 17) obtained from RNA-seq data of WT IFNα and IFNγ-treated Huh7.5 cells unveiled the time-dependent expression of ISRE+GAS-composite genes. Accordingly, they were grouped into three categories in response to IFNα including early, intermediate and late expression. However, following IFNγ stimulation, two groups of genes were categorized comprising intermediate and late response. Based on these categories, we identified composite genes that mostly showed intermediate expression (8h) in response to both IFNs such as NLRC5, PARP14, STAT1 and STAT2 (Figure 17). On the other hand, there are genes that exhibited different time-dependent expression after IFNα or IFNγ stimulation. For instance, IRF9 showed early expression (4h) in response to IFNα (Figure 17-A), while after IFNγ treatment, it displayed late expression (24h) (Figure 17-B). Or DDX60

demonstrated intermediate expression (8h) after IFNα treatment, whereas, it exhibited late response (24h) to IFNγ. These observations correlated with the phosphorylation of STAT1 and STAT2 (in the case of IFNα) and STAT1 (in the case of IFNγ) obtained from western blot analysis in the study conducted by Sekrecka et al. Furthermore, the early phosphorylation of STAT1 (Sekrecka et al., 2023) is consistent with the early expression (4h) of IRF1 in response to both IFNs. The expression of STAT1, STAT2, IRF9 and IRF1 genes (part of positive feedback loop) (Figure 17) correlated with the potential involvement of GAF and GAF-like at early time points in response to both IFNs which is followed by prolonged recruitment of IRF1 and ISGF3 in response to IFNα and IRF1 and STAT1/IRF9 after IFNγ treatment (Sekrecka et al., 2023). These findings were further confirmed by ChIP-seq data analysis of 30 pre-selected composite genes (Figure 18). Another example is the early expression of APOL6 (Figure 17-A) which is consistent with the early phosphorylation of STAT1 and STAT2 in response to IFNα and the intermediate response (Figure 17-B) of the gene corresponds with the early to intermediate phosphorylation of STAT1 upon IFNγ treatment (Sekrecka et al., 2023). In our previous study, GAS-only containing genes displayed early expression, while ISRE-only containing genes showed late response to both IFNs (Sekrecka et al., 2023). Our discovered set of ISRE+GAS-composite genes exhibited a diverse expression pattern in response to both types of IFN that showed both early (like GAS-only genes) and late (like ISRE-only genes) induction following IFNα and IFNγ stimulation.

The ChIP-seq data analysis (Figure 18,AI-AII) confirmed the simultaneous recruitment of pSTAT1, pSTAT2, IRF9, and IRF1 pointing to the involvement of ISGF3, IRF1, GAF and GAF-like in response to IFNα. In contrast, after IFNγ treatment (Figure 18,BI-BII), pSTAT1 and IRF1 were recruited, with IRF9 appearing less frequently which pointed to the role of GAF, IRF1 and STAT1/IRF9. Among ISRE+GAS-composite genes STAT1, STAT2, IRF9 and IRF1 are part of a positive feedback loop. STAT1 and STAT2 (Figure 17) as composite genes displayed maximum expression at 4-8h in response to both IFNs which correlates with the pSTAT1 and pSTAT2 phosphorylation at early time points following IFNα and IFNγ treatment shown in the study conducted by Sekrecka et al (Sekrecka et al., 2023). While, the early induction of IRF9 (Figure 17-A) correlates with pSTAT1 and pSTAT2 phosphorylation at early time points after IFNα stimulation, the late expression of IRF9 in response to IFNγ (Figure 17-B) is consistent with the later IRF1 protein expression according to the results of our recent publication by Sekrecka et al (Sekrecka et al., 2023). In addition to STAT1, STAT2 and IRF9, IRF1 is another component of

positive feedback loop which was considered as a GAS-only containing gene. The maximum expression of IRF1 at 4h aligns (Figure 17, A-B), with the early phosphorylation of STAT1and STAT2 in response to IFNα and only STAT1 following IFNγ treatment that was shown in the study led by Sekrecka et al (Sekrecka et al., 2023; Cheon et al., 2013; Nowicka et al., 2023). According to the literature, GAS-only containing genes such as IRF8 and ICAM1 exhibited early expression which is in line with the transient binding of GAF (pSTAT1) and GAF-like (pSTAT1/pSTAT2) upon IFNα treatment. However, in response to IFNγ, the delayed expression of GAS-only containing genes correlated with the more prolonged binding of GAF complex. Moreover, the ChIP-seq data analysis obtained from K562 cells (http://www.encodeproject.org) following IFNα stimulation, the binding of GAF-like complex was also suggested to drive the expression of GAS-only containing genes. On the other hand, the expression of ISRE-only containing genes was late and it was supported by ISGF3 and IRF1 recruitment in response to IFNα, or IRF1 and infrequently by pSTAT1/IRF9 following IFNγ stimulation (Sekrecka et al., 2023; Michalska et al., 2018; Yamane et al., 2019; Decker et al., 1997; Ehret et al., 2001). In addition to IFN treatment, the binding of IRF1 to ISRE-containing genes has been reported at the basal condition to sustain the expression of ISGs. For example, IRF1 knockout impairs basal expression of certain ISGs in BEAS-2B cells, suggested a role for IRF1 in maintaining basal ISG levels (Panda et al., 2019; Abou El Hassan et al., 2018).

Our recent novel ISRE+GAS-composite genes that contain both ISRE and GAS motifs showed diverse expression patterns in response to both IFNs meaning they possess binding characteristics that merge features from GAS-only and ISRE-only containing genes. This response mirrors the behavior of GAS-only (early) and ISRE-only (later) containing genes. In case of ISRE+GAS composite genes, after IFNα treatment, ISGF3, IRF1, GAF, and GAF-like binding occurs, while IFNγ stimulation leads to GAF, IRF1 binding. Likewise, IRF9 binds to the ISRE site of a number of composite genes (i.e.APOL6, STAT2 and DTX3L) in WT Huh7.5 cells in response to IFNγ (Figure 18). This suggests a potential role for the STAT1/IRF9 complex. This is consistent with the findings of a study published by Bluyssen et al, on fibrosarcoma cells lacking ISGF3 components showing that STAT1 and IRF9 are required to express the ISRE-containing genes in response to IFNγ. Moreover, ChIP-PCR analysis conducted in mouse macrophages uncovered the potential role of the STAT1/IRF9 complex in controlling the expression of the cxcl10 gene in response to IFNγ (H. A. Bluyssen et al., 1995; Rauch et al., 2015). These interactions collectively

reflect the combined binding characteristics of ISRE+GAS-composite genes. Similar to ISRE-only-containing genes, IRF1 binding was observed for composite genes at basal conditions (Figure 18) which highlights a multifaceted involvement of IRF1 in ISRE-containing genes. It is suggested a mechanism where IRF1 recruits at the basal level, and upon IFNα stimulation, ISGF3 co-binds, indicating a molecular switch from IRF1 to ISGF3 in the transcriptional regulation of ISRE-only and ISRE+GAS-composite containing genes in response to IFN. Moreover, the basal binding of IRF1 may promote the quick binding of ISGF3, GAF or IRF1 after IFN stimulation to provide a strong antiviral response (Sekrecka et al., 2023).

Nevertheless, ISGF3 bound to the ISRE of composite genes earlier and stronger than it does to genes that contain only the ISRE in response to IFNα. The early binding of GAF and GAF-like corresponded with the early and transient expression of composite genes after IFNα treatment (Figure 18-A) However, correlating with the study here, composite genes showed a later response to IFNα as compared to GAS-only-containing genes. And following IFNγ treatment, they exhibited earlier response than ISRE-only containing genes. The long-term transcriptional responses of composite genes activated by IFNγ relied on both GAS and ISRE sites, with the time-dependent recruitment of pSTAT1 (GAF) and IRF1 playing a crucial role (Sekrecka et al., 2023; Michalska et al., 2018). A study on the promoter of gbp2 gene has shown that STAT1 contributes by creating a chromatin environment conducive to transcription, while IRF1 facilitates the recruitment of RNA PolII-containing complexes (Ramsauer et al., 2007). The initial and early recruitment of GAF (Figure 18-B) aligns with the earlier expression of ISRE+GAS-composite genes upon IFNγ stimulation. This is subsequently followed by a more sustained binding of IRF1, which maintains the expression of composite genes in response to IFNγ (Figure 17-B). The absence of pSTAT2 binding for the ISRE+GAS-composite genes after IFNγ treatment correlates with the lack of STAT2 phosphorylation obtained from western blot analysis in our earlier published study (Sekrecka et al., 2023).

As described in the literature, U-ISGF3 and U-GAF may play roles in the long-term IFN response (Cheon et al., 2013; Sung et al., 2015)**.** Accordingly, the expression of ISRE-containing genes is prolonged by U-ISGF3 and IRF1, and prolonged induction of GAS-only-containing genes happens through the binding of U-GAF (Blaszczyk et al., 2016; Michalska et al., 2018). However,

our recent publications contradict these findings, as ChIP-seq data showed no U-ISGF3 or U-GAF binding in response to IFNs (Sekrecka et al., 2023; Nowicka et al., 2023).

In the case of ISRE+GAS composite genes, a switch from ISGF3 and GAF to U-ISGF3 and U-GAF could be imagined. However, based on our ChIP-seq data (Figure 18-A), even after 72 hours, pSTAT1 and pSTAT2 levels remained detectable in response to IFNα challenging the model that U-ISGF3 and U-GAF sustain the expression of composite genes. This persistence supports the idea that ISGF3 (comprising pSTAT1, pSTAT2, and IRF9) plays a role in both early and sustained composite gene expression in response to IFNα. Similarly, GAF, a homodimer of pSTAT1, is essential for timely responses to IFNγ agreeing with the findings of the study conducted by Sekrecka and her team (Sekrecka et al., 2023). Since in the study here we observed no shift from phosphorylated STATs (pSTATs) to unphosphorylated STATs (U-STATs) in chromatin interaction of composite genes in response to both types of interferons at later time points, these observations disagree with switch model by which ISGF3 and GAF are replaced by U-ISGF3 and U-GAF to drive the prolonged expression of ISRE and GAS containing genes. While, these findings are in agreement with the results of Sekrecka and Nowicka's studies on ISRE-only and GAS-only containing genes in which no U-ISGF3 and U-GAF binding was detected upon IFN treatment (Morrow et al., 2011; Megger et al., 2017; Sekrecka et al., 2023; Nowicka et al., 2023; Cheon et al., 2013). Nevertheless, the time-dependent activation of ISRE+GAS composite genes via ISGF3 and IRF1 binding to ISRE, alongside GAF and GAF-like interactions with GAS sites upon IFNα stimulation, as well as IRF1 and STAT1/IRF9 targeting ISRE and GAF binding to GAS in response to IFNγ clearly point out the transcriptional and functional overlap of both types of IFN.

Based on the literature, STAT2/IRF9 plays a role in the STAT1 deficient cells and it was proposed that STAT2/IRF9 can take over the role of ISGF3 in WT cells (Blaszczyk et al., 2016). In accordance with this, Bluyssen et al, showed that in the absence of STAT1, phosphorylated STAT2 formed a homodimer that associated with IRF9 generated STAT2/IRF9 complex which triggered the induction of ISRE-containing gene following IFNα treatment (HansA. R. Bluyssen & Levy, 1997). This is in line with the prolonged expression of ISRE-containing genes in the Huh7.5 and ST2-U3C lacking STAT1 (Sekrecka et al., 2023; Nowicka et al., 2023; Blaszczyk et al., 2015). Moreover, Yamauchi an colleagues demonstrated that IFNα induces ISRE gene

transcription and inhibits HCV replication in HCV-infected Huh-7.5 cells. This mechanism is based on STAT2 but did not involve STAT1 (Yamauchi et al., 2016). However, it has been reported that compared to ISGF3, the STAT2/IRF9 complex has a lower affinity for DNA, which necessitates higher concentrations of STAT2 and IRF9 proteins. This requirement leads to an extended duration of pSTAT2/IRF9 activity, which induces ISRE-containing genes in response to IFNα (Blaszczyk et al., 2015)**.** In line with these observations, our ChIP-seq data revealed a delayed binding profile of pSTAT2 and IRF9 to the ISRE site of ISRE+GAS-composite genes in IFNα-treated STAT1KO Huh7.5 cells and no transition from phosphorylated STAT2 (pSTAT2) to unphosphorylated STAT2 (U-STAT2) was observed in the long-term chromatin interaction of composite genes in response to IFNα (Figure 20). Furthermore, this extended binding pattern of pSTAT2 and IRF9 corresponded with a delayed expression of composite genes, as demonstrated by our RNA-seq analysis (Figure 19-A). These findings are in agreement with Nowicka's study in which no switch from pSTAT2IRF9 to U-STAT2/IRF9 was detected at later time points (Nowicka et al., 2023).

5.2 The Expression Of ISRE+GAS-Composite Containing Genes Depends On The Availability Of Transcription Factors, A Molecular Switch Model

To further clarify the association between ISRE/GAS distance, pSTATs/IRFs binding patterns, and the varied expression of ISRE+GAS-composite genes in WT, STAT1, STAT2, IRF9, IRF1 and IRF1.9 mutant cells, we performed an extensive examination of 13 pre-selected composite genes spanning various distance groups including very close, close, medium, long, and distal regulatory regions.

We observed overlapping binding complexes among different distance groups, such as PARP14-SP110 (group 1) (Figure 21, A-B), STAT2-APOL6 (group 2) (Figure 23, A-B), NLRC5 (group 3) (Figure 25-A) and STAT1 (group 5) (Figure 29-A). In these genes the cooperation of ISGF3+IRF1 binding to ISRE and GAF+GAF-like targeting GAS in response to IFNα was observed. However, in response to IFNγ, there is a collaboration between pSTAT1/IRF9+IRF1 interacting with ISRE and GAF binding to GAS. However, minor distinctions were noted among the genes across distance groups, including instances of either no or very weak IRF9 binding in response to both IFNs in WT cells (ETV7, GBP3 in group 1) (Figure 21, C-D), or exclusively in response to IFNγ (NMI in group 4) (Figure 27-B). Similarly, there were cases of either no or very weak IRF1 binding in response to both IFNs (IRF9 in group 2) (Figure 23-C), (IRF1 in group 5)

(Figure 29-B). Despite these minor variations, the expression levels and profiles of these ISRE+GAS-composite genes remained unaffected in WT cells (Figure 22 (C-D), Figure 24 (C), Figure 28 (B), Figure 30 (B)), indicating that both ISRE and GAS sites are functionally accessible. The variations might be attributed to the ISRE/GAS composition, but further investigation is necessary to confirm this. Moreover, these observations highlighted that there is no correlation between varying distances between ISRE and GAS and complexes involved in the transcriptional regulation of composite genes.

Generally, in WT cells responding to IFNα (Figure 21-23-25-27-29), broader peaks of pSTAT1 and pSTAT2 compared to IRFs (except GBP3 and ETV7) were observed. Likewise, in response to IFNγ broader peaks of pSTAT1 compared to IRFs (except DDX60, PARP14 and SP110) were detected. This indicates pSTAT1 and pSTAT2 target ISRE as part of ISGF3 components and bind to GAS as components of GAF and GAF-like complexes in the case of IFNα. following IFNγ treatment, pSTAT1 interacts with ISRE as part of pSTAT1/IRF9 and targets GAS as GAF complex. However, IRFs exclusively target the ISRE site. Despite this, distinguishing binding to GAS and ISRE separately remains challenging in closer distance group (i.e. PARP14) (Figure 21-A) in WT cells. Whereas in longer distance groups (i.e. NMI) (Figure 27-B) the peaks broaden, facilitating clearer differentiation of binding of GAF+GAF-like to GAS and ISGF3+IRF1+pSTAT1/IRF9 to ISRE sites. On the other hand, In IFNα-treated STAT1KO cells, (Figure 21-23-25-27-29) the binding profile of STAT2 and IRF9 shifted towards later time points as compared to WT cells. Moreover, both pSTAT2 and IRF9 target ISRE site correlating with the comparable width of pSTAT2 and IRF9 binding as compared to WT cells where broader peaks of pSTAT1 and pSTAT2 were observed in contrast with IRFs, indicating the involvement of both ISRE and GAS. Nevertheless, there were slight variations in the binding of pSTAT2 and IRF9. For instance, PARP14 displayed stronger pSTAT2/IRF9 binding (Figure 21-A) whereas ETV7, belonging to the same distance group as PARP14, exhibited weaker binding (Figure 21-C). Likewise, in group3, DDX60 showed wider pSTAT2/IRF9 binding (Figure 25-B) as compared to NLRC5 (Figure 25-A). Furthermore, all 13 pre-selected ISRE+GAS-composite genes across different distance groups displayed prolonged expression in STAT1KO cells in response to IFNα (Figure 22-24-26-28-30) correlating with the delayed binding of pSTAT2/IRF9. These observations additionally affirmed the lack of correlation between transcriptional regulation of composite genes and divergent ISRE/GAS distance or orientation.

In addition, akin to the binding pattern observed in the proximal promoter of STAT1 gene that comprises an ISRE (group5) (Figure 29-A), a distal regulatory region (~6kb) exhibited a combined recruitment of STAT1, STAT2, IRF9 and IRF1 which is a further proof for the presence of a composite structure at the distal regulatory region in the human STAT1 gene (Sekrecka et al., 2023). This finding was in agreement with the results of the study conducted by Yuasa et al, in which an ISRE+GAS composite structure was observed at the 5.5-kb upstream of the mouse STAT1 gene (Yuasa & Hijikata, 2016). Likewise, the investigation of ChIP-seq data analysis obtained from IFNα or IFNγ-treated K562 cells (http://www.encodeproject.org) is also in line with the hypothesis of the existence of distal ISRE/GAS structure (Michalska et al., 2018). More interestingly, our recent study identified a distal regulatory ISRE/GAS structure approximately 6 kb upstream of the human IRF1 gene. This region exhibited binding of STAT1, STAT2, and IRF9, confirming the presence of both ISRE and GAS elements. In contrast, the proximal promoter of the human IRF1 gene (Figure 29-B) demonstrated binding of only STAT1 and STAT2, indicating the presence of solely a GAS site. These findings correlated with the transcriptional regulation of STAT1 which showed more prolonged expression following IFNα and IFNγ stimulation as compared to the IRF1 gene which possesses only GAS site in its proximal promoter and exhibited an early response to both IFNs similar to other GAS-only containing genes. Moreover, this data indicates the operation of an active chromatin looping mechanism that links both proximal and distal regulatory regions in both STAT1 and IRF1 genes (Sekrecka et al., 2023; Michalska et al., 2018).

Various expression levels of ISRE+GAS-composite genes in different mutant cell lines showed that different IFN signaling components are responsible for gene expression and switching between ISRE and GAS. However, slight differences were noted, such as the lack of ETV7 and GBP3 expression (Figure 22, C-D) in IRF9, IRF1, and IRF1.9dKO cells after IFNα treatment, and in IRF1 and IRF1.9dKO cells after IFNγ treatment. Likewise, no DDX60 gene expression (Figure 26-B) was detected in IRF1.9dKO cells after treatment with either IFNα or IFNγ. Generally, there was a shift from an ISRE+GAS-dependent mechanism in WT, STAT2, IRF9, and IRF1KO cells to a GAS-only dependent mechanism in IRF1.9dKO cells in response to both IFNs. Additionally, The WT Huh7.5 cells showed ISGF3, IRF1 binding to ISRE and GAF and GAF-like targeting GAS in response in response to IFNα, and after IFNγ stimulation, IRF1 and STAT1/IRF9 binds to ISRE and GAF interacts with GAS site. Therefore there is an ISRE+GAS mechanism in response

to both IFNs in WT cells. However, there is a shift from ISRE+GAS mechanism in WT cells to an ISRE-only mechanism in IFNα-treated STAT1KO cells where only ISRE is involved and bound by pSTAT2/IRF9. In the case of ETV7 and GBP3 (Figure 22, C-D) there is a transition from ISRE+GAS in WT cells to an ISRE-only mechanism in KO cells. This was indicated by the possible role of IRF1/IRF9 dimer binding ISRE in STAT2KO cells in response to IFNα and the main contribution of IRF1 targeting ISRE in STAT2 and IRF9KO cells after IFNγ stimulation. While the individual roles of IRF1 and IRF9 in regulating ISG expression have been well-documented, the specific role of an IRF1/IRF9 dimer has not been addressed in the existing literature.

Interestingly, for DDX60 (Figure 26-B), ISRE was the main element in WT as well as in KO cells. This was confirmed by main role played by ISGF3+IRF1 binding to ISRE in response to IFNα and IRF1+pSTAT1/IRF9 interacting with ISRE upon IFNγ treatment in WT cells. Subsequently, in STAT2 and IRF9KO groups IRF1 binds to ISRE after IFNα stimulation. Likewise, IRF1+pSTAT1/IRF9 targets ISRE in STAT2KO and IRF1 interacts with ISRE in IRF9KO cells in response to IFNγ treatment. In IRF1KO, ISGF3 targeting ISRE is the involved complex in response to IFNα while after IFNγ stimulation pSTAT1/IRF9 binds to ISRE site in the promoter of DDX60 gene. Similar expression patterns in response to IFNα and/or IFNγ were observed among ISRE+GAS-composite genes across different distance groups such as PARP14 (Figure 22-A), APOL6 (Figure 24-B) and NMI (Figure 28-B) validating the lack of correlation between ISRE/GAS distances/orientation and expression profiles.

The ability of ISRE+GAS-composite genes to be induced by IFNs in different mutant cell lines (Figure 19) indicates their greater flexibility in transcriptional response to both IFNα and IFNγ compared to ISGs containing only ISRE or GAS elements. This observation suggests that ISRE+GAS-composite genes can dynamically switch between utilizing ISRE and GAS elements based on the availability of specific transcription factors over time. Moreover, the change in the expression profile in different KO cell lines as compared to WT is a reflection of the adaptive characteristics of ISRE+GAS-composite genes (Figure 44). This adaptability might confer a regulatory advantage, allowing them to maintain an effective antiviral response even under varying conditions and enhancing the overall immune defense strategy (Sekrecka et al., 2023; Abdul-Sater et al., 2015; Ramachandran & Horvath, 2009).

In general, based on ChIP-seq data, promoter analysis of a set of 13 pre-selected ISRE+GAS-composite genes revealed the presence of both ISRE and GAS binding sites. Accordingly, the proximal promoter showed random ISRE and GAS organization (ISRE-GAS or GAS-ISRE) that are located in a variable distance from 0 to more than 200bp (Table 11). Although the observed variation in orientations and distances between GAS and ISRE sites within these ISRE+GAS-composite genes had no effect on transcriptional regulation of composite genes. Based on the differences in binding patterns in WT cells (i.e. IRF9 and PARP14) and expression profiles (i.e. GBP3 and APOL6) in different KO cells, potential different mechanisms could be proposed for transcriptional regulation of composite genes. This is further supported by the promoter activity results obtained from the luciferase assay.

These mechanisms likely involve the coordinated activity of GAF, GAF-like, ISGF3, IRF1 and STAT1/IRF9 complexes, functioning without direct molecular interaction. Nevertheless, IFNα response of ISRE+GAS-composite genes is mostly ISRE driven, whereas IFNγ response involves both GAS and ISRE sites (possibly in a time-dependent manner) (Piaszyk-Borychowska et al., 2019; Sekrecka et al., 2023). Several studies have reported the co-binding of STAT and IRF and their role in the transcriptional regulation of ISGs. For instance, the Chip-seq data analysis performed on K562 cells unveiled the co-binding of STAT1 and IRF1 after cell treatment with IFNγ (D. Xie et al., 2013). Moreover, it has been shown that the transcriptional regulation of gbp2 required the co-binding of STAT1 and IRF1 (Ramsauer et al., 2007). Likewise, research by Kumatori et al. revealed the cooperative role of STAT1 and IRF1 in regulating gp19 transcription in IFNγ-treated U937 cells (Kumatori et al., 2002). Furthermore, it has been demonstrated that the co-binding of STAT1 and IRF1 is essential for the induction of the human CIITA gene in response to IFNγ (A. Morris et al., 2002). In addition, the significance of the co-binding of STATs and non-IRF complexes was demonstrated by scientific reports. For example, the transcriptional activation of pro-inflammatory genes is facilitated by the co-binding of STAT1-containing complexes and NFκB (which were triggered in response to IFN-I or IFN-II) in conjunction with LPS (Piaszyk-Borychowska et al., 2019). Furthermore, it has been evident that the collaborative interaction between NFκB and STAT1 is essential for the activation of specific ISGs like Isg15, gbp, and

Stat1 for the transcriptional response of infected macrophages to Listeria monocytogenes (Farlik et al., 2010; Wienerroither et al., 2015; Platanitis & Decker, 2018).

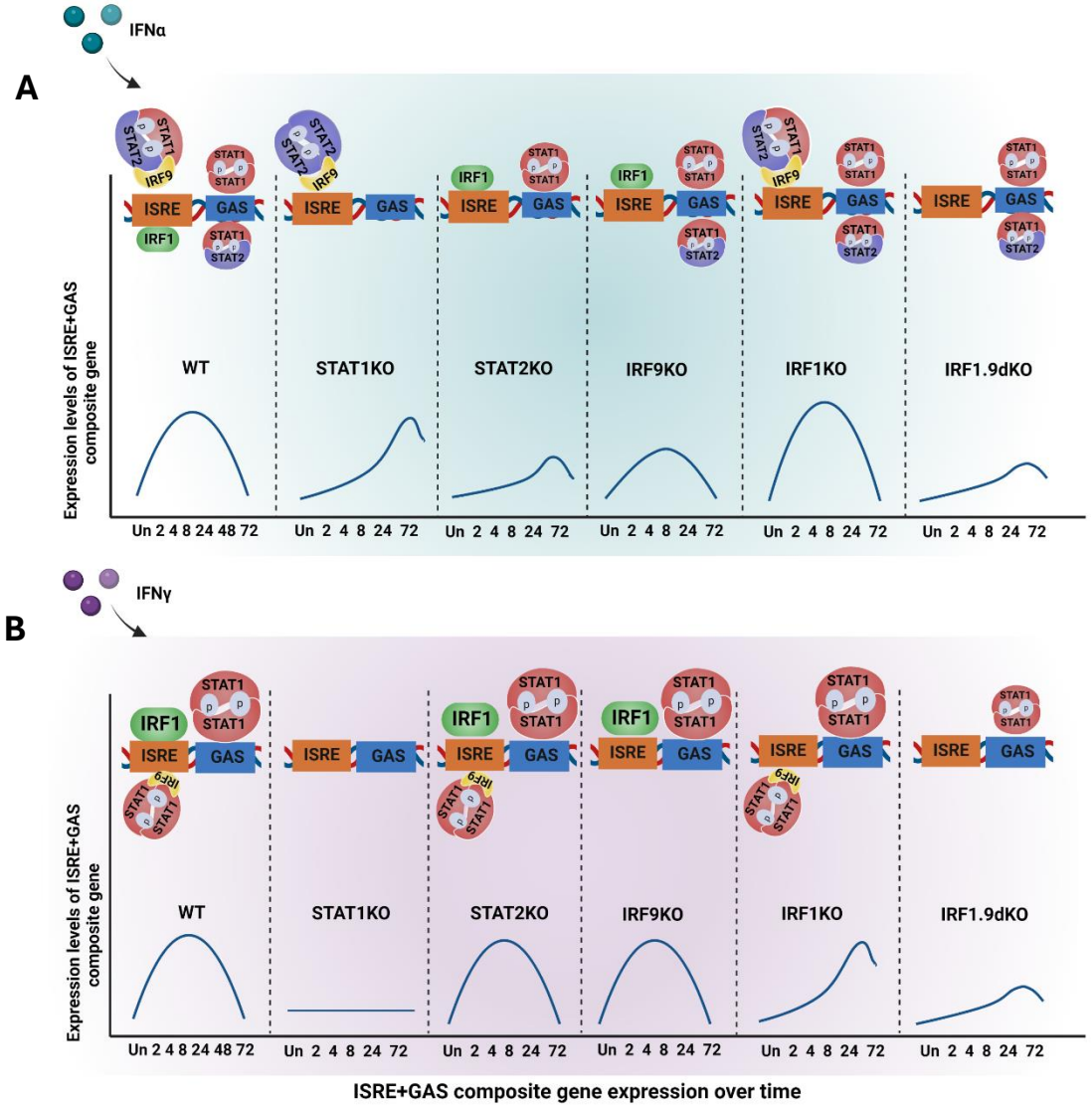

Figure 44. A simplified illustrative model of the ISRE and GAS switching mechanism in diverse cell lines after IFNα and IFNγ stimulation.

The graphs display the expression patterns of ISRE+GAS composite genes in various cell lines, with the transcription factors involved in response to IFNα **(A)** and IFNγ **(B)** indicated above each graph. The more potent complexes are depicted with larger sizes in response to both IFNs. The larger size of ISRE in response to IFNα indicates its greater potency compared to GAS. The horizontal and vertical lines demonstrate the typical ISRE+GAS-composite gene expression over time and expression levels of composite genes, respectively. The cell lines are separated by dash lines.

5.3 ISRE+GAS-Composite Genes Are Induced In Response To IFNα And IFNγ Through Different Mechanisms

As understood, TFs regulate gene expression by binding to transcription binding sites, which vary in size and may possess consensus motifs or not. Additionally, the regulation of gene expression in eukaryotic cells entails the coordination of multiple transcription binding sites within their promoters (Bilu & Barkai, 2005). ISRE+GAS composite genes are a group of IFN-induced genes whose expression could be controlled by different ISRE and GAS sites. In the present study, eight ISRE+GAS-composite genes including PARP14, APOL6, DDX60, NLRC5, DDX58, NMI, STAT1 and IRF1 were pre-selected from various distance groups to elucidate the precise roles of GAS and ISRE in the transcriptional regulation of these composite genes in WT cells. Then, five genes out of eight were chosen including PARP14, APOL6, DDX60, NMI and STAT1 to investigate the role of ISGF3, IRF1, STAT2/IRF9, STAT1/IRF9, GAF and GAF-like. By further investigation of the ISRE+GAS-composite genes we found that these genes are regulated through different mechanisms such as a dominant overlapping ISRE mechanism , a combined mechanism, a one-element mechanism, an inhibitory mechanism and a looping mechanism. In addition, ISRE+GAS-composite genes can also utilize various transcriptional mechanisms depending on the composition of ISRE and GAS. This includes genes with a single ISRE and GAS in their promoter, such as APOL6, IRF9, STAT2, SP110, GBP3, ETV7, NLRC5, and DDX58. And genes with multiple ISRE and GAS elements in their promoter including PARP14, DDX60, and NMI, as well as genes with a distal ISRE/GAS organization, such as STAT1 and IRF1.

Accordingly, we found APOL6 (Figure 35) possessing one ISRE and one GAS in its proximal promoter region that both elements are functionally active and a combined use of ISRE and GAS is required for optimal induction in response to IFNα and IFNγ. However, ISRE is more potent than GAS in response to IFNα which is predicted to be targeted by ISGF3 more potently after IFNα stimulation. In response to IFNγ, IRF1 strongly binds to ISRE and GAF potently targets GAS motif. In addition to APOL6, SP110, STAT2 and NLRC5 have single ISRE and GAS and based on the binding profiles (Figure 21(B), 23(A), 25(A)) in WT cells and expression profiles in WT and KO cells (Figure 22(B), 24(A), 26(A)) it is predicted that in response to both IFNs, SP110 and STAT2 are using the same mechanism as APOL6 for transcriptional regulation (Figure 45), while, according to luciferase assay results using the WT NLRC5 promoter in WT cells (Figure 31-D), GAS is predicted to have greater potency than ISRE in response to IFNγ. However, upon

IFNα stimulation, NLRC5 can be regulated by the same mechanism as APOL6 (Figure 45). Nevertheless, more experiments need to be provided for further proof. Unlike the other pre-selected composite genes, GBP3 and ETV7 are anticipated to not require ISGF3 for regulation based on their binding (Figure 21, C-D) and expression profiles (Figure 22, C-D). Similarly, these two genes have more potent ISRE in response to IFNα, but following IFNγ stimulation, both ISRE and GAS might be potent. And we could predict IRF1 is the main complex in response to both IFNs and GAF and GAF-like (in case of IFNα) and GAF (in case of IFNγ) are less potent (Figure 45). However, additional experiments are required for more evidence. IRF9 as a gene possessing single ISRE and GAS is anticipated to be regulated using the mechanism in which ISGF3, GAF and GAF-like are the crucial TFs in response to IFNα and ISRE has greater potency. In response to IFNγ, GAF is likely the main TF over STAT1/IRF9, with IRF1 playing no role in either IFN response according to its binding profiles (Figure 23-C). Both ISRE and GAS might have the same potency in response to IFNγ, (Figure 45) but further evidence is required. We must consider that the specific time points selected for treating cells with IFNα or IFNγ may account for the observed weak or undetectable IRF9 binding (such a ETV7, GBP3) or IRF1 binding (such as IRF9) particularly in response to IFNα or IFNγ for certain genes. It is possible that IRF9 or IRF1 binding occurs at other time points, such as 4h following IFNα treatment, or 8h upon IFNγ stimulation, which were not included as distinct time points in our study. Furthermore, certain genes may require only a subset of transcription factor complexes due to the high accessibility of their binding sites or more straightforward regulatory mechanisms (Long et al., 2023).

The next gene in the single ISRE and GAS group is DDX58, and based on the binding profiles (Figure 27-A), expression patterns (Figure 28-A) and the luciferase assay results in WT cells (Figure 31-F) it is predicted to have more potent ISRE than GAS in response to IFNα and ISGF3 is the predominant TF, and IRF1, GAF and GAF-like have less potency. In contrast, IRF1, STAT1/IRF9 and GAF might be the main contributors following IFNγ treatment (Figure 45). Nonetheless, more evidence is needed for further proof. In addition to our composite genes with single ISRE and GAS elements described above, other ISGs such as GBP1 also has been found to be regulated by both IFNs through its functional ISRE and GAS sites in its proximal promoter region and ISRE plays a more important role in response to both IFNs (Honkala et al., 2019; Naschberger et al., 2004; Decker et al., 1989; Lew et al., 1991).

Another discovery we made was identifying ISRE+GAS-composite genes with multiple ISREs in their promoters, such as PARP14, DDX60, and NMI. PARP14 contains one GAS flanked by one ISRE site, which creates an overlapping ISRE site in the middle (Figure S2-AI) that plays a crucial role as the main transcriptional element. It appears that optimal promoter activity necessitates the presence of the overlapping ISRE which is predominantly bound to ISGF3 and IRF1 in response to IFNα and IFNγ, respectively (Figure 45). Likewise, it has been shown that the promoter of human CCl2 gene comprises one and a half GAS, and the half GAS plays a significant role in interacting with the STAT1 (Hüntelmann et al., 2014). Furthermore, it has been documented that the ISG15 promoter contains one and a half ISRE motifs, which are functionally activated and are essential in the regulation of ISG15 gene expression, responding to IFNs (Buonamici et al., 2005; N. Reich et al., 1987; Ritchie & Zhang, 2004).

Among the ISRE+GAS-composite genes with multiple ISRE and GAS sites, DDX60 is another example containing two ISRE sites and one GAS. Our luciferase reporter assay revealed that while the second ISRE (ISRE2) is functional, its efficacy is suboptimal compared to ISRE1 in response to IFNα and IFNγ (ISRE2 is shown in smaller size in Figure 45). Before, the presence of two or more ISREs in the promoter of DDX60 in both mice and humans has been shown (Goubau et al., 2015). Like what we observed here, a study by Konan et al. demonstrated that the promoter of the Indoleamine 2,3-dioxygenase (INDO) gene, which is induced in host cells following protozoan infections, comprises two ISRE sites essential for the optimal activation of INDO in response to IFNγ (Konan & Taylor, 1996). Additionally, Bluyssen and colleagues' research on the hamster ISG-54 K gene, revealed that this gene features two ISREs (ISRE-I and ISRE-II) in its promoter, positioned adjacently with no spacing between them. However, through mutation analysis, it was found that ISRE-I exhibited greater activity than ISRE-II in response to IFNα aligning with our observation that ISRE1 in DDX60 showed more potency (H. A. Bluyssen et al., 1994). Furthermore, an investigation into the mice Ifit1 gene promoter revealed two ISRE sites positioned 19 base pairs apart. In IFNAR−/− MEFs infected with West Nile virus (WNV), it was demonstrated that both ISREs were necessary for the optimal expression of Ifit1 and could not function independently which suggested a synergistic interaction between the two ISREs in an IFN-I independent manner (Cui et al., 2021). The valuable findings of the study conducted by Georgakopoulos-Soares et al. showed that the presence of different copy numbers of one transcription factor binding site can affect positively or negatively the level of gene expression.

Aline with this observation, DDX60 with two ISREs in its promoter indicated a high expression level, especially in response to IFNα in WT cells. (Figure 26-B) (Georgakopoulos-Soares et al., 2023). Besides the presence of two ISREs in the promoter of DDX60, another intriguing phenomenon was discovered. Although the promoter region of DDX60 contains a GAS site, its functionality appears to be lacking. This observation raises the possibility of the existence of inactive cis-elements within the promoter area of ISGs. Such a scenario suggests that while the necessary sequence elements may be present, their regulatory potential remains unutilized, indicating a more complex regulatory landscape governing the expression of DDX60. In mammals, it has been demonstrated that TFs predominantly target specific DNA binding sites. However, these interactions often do not directly contribute to the regulation of gene expression and the reasons for these observations are still not clear (Savic et al., 2015). Furthermore, akin to our findings, the study conducted by Castro et al. explored the expression of the LMP2 gene, an IFN-induced gene, in rainbow trout, a fish species. LMP2 possesses two ISREs and one GAS element in its promoter. Through the cloning of promoter fragments containing solely GAS element or fragments containing GAS element along with mutated ISRE into a luciferase reporter plasmid, they observed that neither of the fragments exhibited a response to rainbow trout IFNγ or IFNα. This highlights that, like DDX60, the induction of LMP2 can occur independently of GAS elements in response to IFNs (Castro et al., 2008). Since DDX60 is an ISG that can be induced through its ISRE elements, our observations confirmed that similar to ISRE-only containing genes, ISGF3 (in case of IFNα) and IRF1 and possibly STAT1/IRF9 (in case of IFNγ) are the potent TFs in DDX60 gene expression (Figure 45) (Sekrecka et al., 2023).

In addition to DDX60, NMI possesses two ISRE sites along with a GAS motif. However, analyzing the ISRE and GAS sequences by site-directed mutagenesis in combination with luciferase assay in WT cells revealed that the second ISRE (ISRE(2)) in the promoter of NMI is not active. And, ISGF3 and IRF1 are the potent TFs in response to IFNα and IFNγ, respectively. Additionally, based on the increased promoter activity in the mutated GAS constructs as compared to WT constructs in WT cells (Figure 31-E), it was predicted that GAS has an inhibitory effect on ISRE(1) (Figure 45).

Based on the existing knowledge presenting multiple binding sites especially overlapping binding sites in the non-coding region can lead to a competition between TFs that target those

binding sites (Parab et al., 2022). This can influence the accessibility of the DNA and ultimately modulate gene expression (Tseng et al., 2021). Moreover, previous studies have shown that in the two close transcriptional binding sites, once the TF binds to one transcriptional binding site it can block the other site from being bound by TF (Ezer et al., 2014). However, In case of NMI, the GAS and ISRE(1) elements exhibited a separation of over 200 base pairs which remains uncertain whether this considerable distance contributes to the inhibitory impact of GAS on ISRE and hinders the optimal binding of transcription factors to the ISRE(1) site.

STAT1 and IRF1 genes with distal ISRE/GAS organization feature both ISRE and GAS sites in their distal regulatory region. While the STAT1 gene possesses an ISRE in its proximal promoter, the proximal promoter of the IRF1 contains a GAS. Regardless of the presence of GAS2 in the distal region of IRF1 gene, based on the binding profiles (Figure 29-B), it is suggested that GAS1 and GAS3 are the involved motifs in the transcriptional regulation. Moreover, proximal promoter of IRF1 was found to have an only GAS site which aligns with the findings from numerous investigations (Lallemand et al., 1997; Feng et al., 2021). Based on the expression patterns and promoter activity of the STAT1 gene, even in the constructs containing mutated proximal ISRE (Figure 40), and the observed promoter activity being higher in the proximal region compared to the distal region for IRF1 (Figure 31-H), a looping mechanism is proposed for the transcriptional regulation of STAT1 and IRF1. According to luciferase assay outcomes distal ISRE and GAS have greater potency than proximal ISRE in STAT1 gene in response to both IFNs and ISGF3 is the major TF in response to IFNα and GAF and STAT1/IRF9 are the dominant complexes upon IFNγ stimulation. Despite the functionality of distal regulatory region in IRF1, we propose that the high response of proximal promoter correlates with the importance of proximal GAS in the regulation of this gene in response to both types of IFN. Moreover, in case of IRF1 gene, we predict that IRF1 complex has no role based on the lack of IRF1 binding after IFNα and IFNγ (Figure 29-B) and ISGF3, GAF and GAF-like are the key TFs after IFNα treatment, whereas, GAF might be more potent than STAT1/IRF9 in response to IFNγ (Figure 45). This is also in agreement with the binding of GAF to GAS as a pivotal TF of the IRF1 gene in response to IFNγ (Michalska et al., 2018). However, Further exploration is necessary to gain a deeper understanding of the functions of distal ISRE and GAS sites in IRF1 gene.

Among different groups of ISRE/GAS composite genes based on the compositions of ISRE and GAS described above, the group characterized by a single ISRE and GAS element is expected to demonstrate the most predominant regulatory mechanism. This expectation arises from the dual involvement of both ISRE and GAS elements in responding to both types of IFN suggesting a robust and versatile transcriptional response compared to other groups.

Despite grouping ISRE+GAS-composite genes based on the composition of ISRE and GAS, we still can observe similarities between them. For instance, DDX60, characterized by multiple ISRE and GAS and DDX58, which features a single ISRE and GAS for both it is suggested that the ISRE element exerts greater potency in their promoters compared to GAS. On the other and, within categorized groups, variations are evident. For instance, despite belonging to the category of multiple ISRE and GAS sites, NMI and DDX60 exhibited distinct characteristics. In the promoter of DDX60, the GAS site is inactive, whereas in NMI's promoter, the ISRE (2) site is inactive (Figure 45).

Collectively, we propose diverse transcriptional mechanisms for ISRE+GAS composite genes. Regardless of similarities in ISRE/GAS distances or the presence of multiple or single ISRE and GAS motifs, these ISRE+GAS-composite genes demonstrate variable transcriptional regulatory mechanisms. This indicates that the specific arrangement and context of ISRE and GAS elements within the promoter regions of these genes can lead to differential transcriptional responses. Elucidating these complexities is essential for comprehending how these genes integrate signals and modulate their expression in response to IFNs.

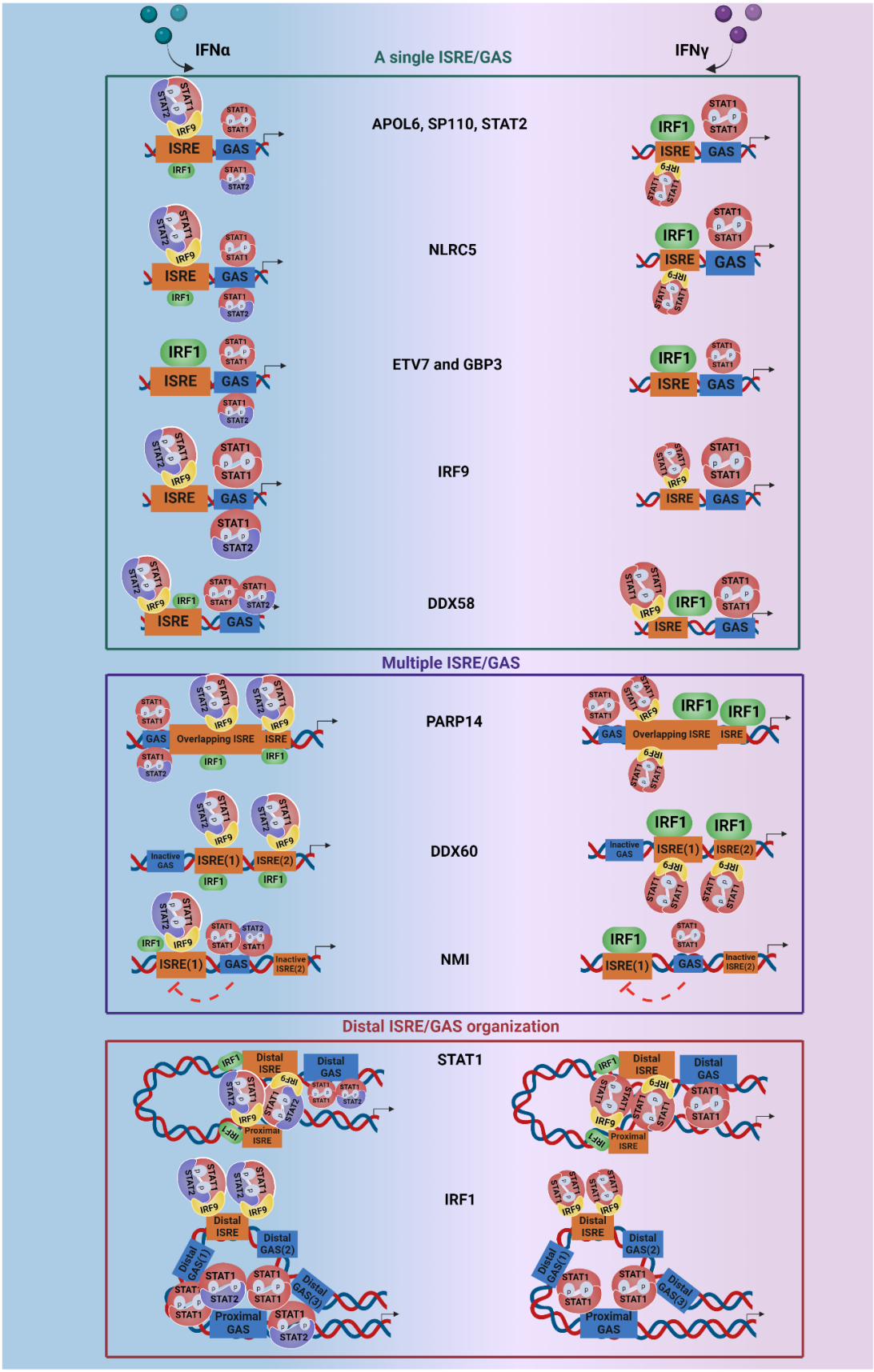

See description is on the next page.

Figure 45. Different transcriptional mechanisms of ISRE+GAS composite genes based on the composition of ISRE and GAS in response to IFNα and IFNγ.

13 pre-selected composite genes are divided to 3 major groups based on the composition of ISRE and GAS including single ISRE and GAS (green border), multiple ISRE and GAS (purple border) and distal organization (red border). The more potent complexes are depicted with larger sizes in response to IFNs. The enlarged size of the motifs indicates their greater potency. ISREs are demonstrated by orange boxes and GAS elements are indicated by blue boxes. The dashed red line indicates the inhibitory effect of GAS on ISRE. The IFNα response is demonstrated by the blue color on the left side of the figure and IFNγ response is shown by the bright purple color on the right side of the figure.

5.4 The Role Of ISRE+GAS-Composite Genes In The Antiviral Response

ISGs employ a variety of strategies and mechanisms to combat viral infections. These include the degradation of viral RNA, inhibition of protein translation, and targeting multiple stages of the viral life cycle. By using these different approaches, ISGs can effectively disrupt viral replication and propagation (E. Yang & Li, 2020)**.** To date**,** the antiviral responses have been examined in different cell types including humans and mice. For instance, Wang et al. showed the protection of infected WT mESC-FBs (mice differentiated fibroblasts from embryonic stem cells) with CHIKV virus (chikungunya virus) after IFNα treatment. (R. Wang et al., 2014)**.** Similarly, studies have shown that HDV (hepatitis delta virus)-infected HLCs cells (human pluripotent stem cell (hPSC)-derived hepatocyte-like cells) exhibit increased expression of ISGs when treated with IFNα2b, which subsequently reduces the viral infection (Lange et al., 2023). In addition to wild-type cells, several studies have explored the antiviral response in cells lacking STAT1. According to research conducted by Yamauchi et al., IFNα-treated STAT1KO Huh7.5 cells demonstrated the ability to effectively combat HCV infection through the activation of ISRE-containing genes (Yamauchi et al., 2016). Blaszczyk et al. conducted another study where IFNα treatment of hST2-U3C cells (which are STAT1-null with overexpressed STAT2) resulted in an antiviral response to EMCV or VSV infection, mediated by the STAT2/IRF9 complex (Blaszczyk et al., 2015). Furthermore, the role of IRF1 and IRF9 in induction of ISGs involved in the antiviral functions was also investigated. In a study published by Kimura et al., IRF9-deficient murine EF cells showed no antiviral response to IFNα, and these responses were impaired after IFNγ treatment following encephalomyocarditis virus (EMCV) infection. Likewise, both IFNα and IFNγ responses were disrupted after VSV and HSV infection in IRF9KO cells. They also examined antiviral responses in mice EFs that lacked both IRF9 and IRF1 and observed similar results as IRF9KO cells (Kimura et al., 1996). Moreover, research on IRF1 deficient mice has demonstrated their susceptibility to EMCV and mycobacterium bovis (BCG) in response to IFNs which

subsequently confirmed the essential role of IRF1 for providing antiviral responses (Kimura et al., 1994; Kamijo et al., 1994).

In this study, we evaluated the antiviral responses of WT, STAT1KO, and IRF1.9dKO Huh7.5 cells 24 and 72 hours after IFNβ and IFNγ stimulation. Accordingly, IFNβ-treated WT cells exhibited a more prolonged and stronger antiviral response against VSV for both 24 and 72h time points as compared to IFNβ-treated STAT1KO cells (Figure 43, A-B). This correlates with the involvement of an ISRE/GAS-dependent mechanism in which both ISRE and GAS elements are functionally active, whereas, in STAT1KO cells, only ISRE-dependent mechanism is contributed by which only ISRE-containing ISGs are involved. Nevertheless, in WT cells, 24h of IFNβ treatment showed a more prolonged antiviral response than 72h stimulation. This is in line with the reduction of ISGs expression after 72h stimulation with IFNα (Sekrecka et al., 2023). Furthermore, the IFNγ-treated WT cells (Figure 43, C-D) were able to combat the viral infection after 24h treatment, while, extending the treatment to 72 hours did not provide any viral protection. This finding is in agreement with the low induction of ISGs including ISRE+GAS-composite genes (Figure 19-B) in response to IFNγ 72h post-treatment (Sekrecka et al., 2023). IFNβ-treated STAT1KO cells demonstrated antiviral responses (Figure 43, A-B) for both 24 and 72h time points, corresponding with the expression of ISRE+GAS-composite genes in STAT1KO cells upon IFNα stimulation (Figure 19-A). Likewise, this observation aligns with the findings of our previous study by Sekrecka et al., where ISRE-only and ISRE+GAS-composite-containing genes exhibited expression in response to IFNα in STAT1KO cells, correlating with the engagement of the STAT2/IRF9 complex (Sekrecka et al., 2023). Similarly, the findings of a study led by Nowicka, have shown that ISRE-only containing genes are transcriptionally induced in IFNα-treated STAT1KO Huh7.5 cell lines in a STAT2/IRF9 dependent manner (Nowicka et al., 2023). Moreover, the study published by Abdul-Sater et al. revealed that the IFN-α/β-induced STAT2/IRF9 complex plays a crucial role in the expression of ISRE-containing genes in the absence of STAT1 and provides protection against the Dengue virus (Abdul-Sater et al., 2015). In contrast to IFNβ-treated STAT1KO cells, STAT1KO cells did not show protection against VSV in response to IFNγ at both 24 and 72h time points (Figure 43, C-D). This corresponds with the lack of ISGs induction including ISRE+GAS-composite genes after IFNγ treatment in STAT1KO cells (Sekrecka et al., 2023). Another observation we made is that IRF1.9dKO cells did not exhibit any antiviral responses to IFNβ and IFNγ at either time point (Figure 43). This highlighted that

GAS-dependent mechanism is not potent enough to produce an effective antiviral response. This is in agreement with low expression of ISGs comprising ISRE+GAS-composite genes (Figure 19) and ISRE-only containing genes in IRF1.9dKO cells upon treatment with IFNα and IFNγ (Sekrecka et al., 2023)**.** Moreover, despite the expression of GAS-only containing genes under these conditions, no viral protection was observed. This finding aligns with the role of GAS-only genes in other biological processes, such as RNA biosynthesis (Sekrecka et al., 2023). Overall, antiviral activities strongly depend on ISRE- and ISRE+GAS composite-dependent mechanisms, involving ISGF3, IRF1, STAT2/IRF9 and possibly STAT1/IRF9 complexes, whereas GAS-only containing genes only play a minor role in antiviral responses.

References

Abdul-Sater, A. A., Majoros, A., Plumlee, C. R., Perry, S., Gu, A. D., Lee, C., Shresta, S., Decker, T., & Schindler, C. (2015). Different STAT transcription complexes drive early and delayed responses to type I Interferons. *Journal of Immunology (Baltimore, Md. : 1950)*, *195*(1), 210–216. https://doi.org/10.4049/jimmunol.1401139

Abou El Hassan, M., Huang, K., Eswara, M. B. K., Xu, Z., Yu, T., Aubry, A., Ni, Z., Livne-bar, I., Sangwan, M., Ahmad, M., & Bremner, R. (2017). Properties of STAT1 and IRF1 enhancers and the influence of SNPs. *BMC Molecular Biology*, *18*, 6. https://doi.org/10.1186/s12867-017-0084-1

Abou El Hassan, M., Huang, K., Xu, Z., Yu, T., & Bremner, R. (2018). Frequent interferon regulatory factor 1 (IRF1) binding at remote elements without histone modification. *The Journal of Biological Chemistry*, *293*(26), 10353–10362. https://doi.org/10.1074/jbc.RA118.002889

Adams, T. E., Hansen, J. A., Starr, R., Nicola, N. A., Hilton, D. J., & Billestrup, N. (1998). Growth hormone preferentially induces the rapid, transient expression of SOCS-3, a novel inhibitor of cytokine receptor signaling. *The Journal of Biological Chemistry*, *273*(3), 1285–1287. https://doi.org/10.1074/jbc.273.3.1285

Alexander, W. S. (2002). Suppressors of cytokine signalling (SOCS) in the immune system. *Nature Reviews. Immunology*, *2*(6), 410–416. https://doi.org/10.1038/nri818

Ali, S., Mann-Nüttel, R., Schulze, A., Richter, L., Alferink, J., & Scheu, S. (2019). Sources of Type I Interferons in Infectious Immunity: Plasmacytoid Dendritic Cells Not Always in the Driver's Seat. *Frontiers in Immunology*, *10*, 778. https://doi.org/10.3389/fimmu.2019.00778

Alsamman, K., & El-Masry, O. S. (2018). Interferon regulatory factor 1 inactivation in human cancer. *Bioscience Reports*, *38*(3), BSR20171672. https://doi.org/10.1042/BSR20171672

Andrews, S. (2010). *FASTQC. A quality control tool for high throughput sequence data | BibSonomy*. https://www.bibsonomy.org/bibtex/f230a919c34360709aa298734d63dca3

Antonczyk, A., Krist, B., Sajek, M., Michalska, A., Piaszyk-Borychowska, A., Plens-Galaska, M., Wesoly, J., & Bluyssen, H. A. R. (2019). Direct Inhibition of IRF-Dependent Transcriptional Regulatory Mechanisms Associated With Disease. *Frontiers in Immunology*, *10*, 1176. https://doi.org/10.3389/fimmu.2019.01176

Arimoto, K.-I., Miyauchi, S., Stoner, S. A., Fan, J.-B., & Zhang, D.-E. (2018). Negative regulation of type I IFN signaling. *Journal of Leukocyte Biology*. https://doi.org/10.1002/JLB.2MIR0817-342R

Arnold, M. M., Barro, M., & Patton, J. T. (2013). Rotavirus NSP1 mediates degradation of interferon regulatory factors through targeting of the dimerization domain. *Journal of Virology*, *87*(17), 9813–9821. https://doi.org/10.1128/JVI.01146-13

Au-Yeung, N., Mandhana, R., & Horvath, C. M. (2013). Transcriptional regulation by STAT1 and STAT2 in the interferon JAK-STAT pathway. *JAK-STAT*, *2*(3), e23931. https://doi.org/10.4161/jkst.23931

Awasthi, N., Liongue, C., & Ward, A. C. (2021). STAT proteins: A kaleidoscope of canonical and non-canonical functions in immunity and cancer. *Journal of Hematology & Oncology*, *14*(1), 198. https://doi.org/10.1186/s13045-021-01214-y

Balkhi, M. Y., Fitzgerald, K. A., & Pitha, P. M. (2008). Functional regulation of MyD88-activated interferon regulatory factor 5 by K63-linked polyubiquitination. *Molecular and Cellular Biology*, *28*(24), 7296–7308. https://doi.org/10.1128/MCB.00662-08

Barrat, F. J., Crow, M. K., & Ivashkiv, L. B. (2019). Interferon target-gene expression and epigenomic signatures in health and disease. *Nature Immunology*, *20*(12), 1574–1583. https://doi.org/10.1038/s41590-019-0466-2

Begitt, A., Krause, S., Cavey, J. R., Vinkemeier, D. E., & Vinkemeier, U. (2023). A family-wide assessment of latent STAT transcription factor interactions reveals divergent dimer repertoires. *The Journal of Biological Chemistry*, *299*(5), 104703. https://doi.org/10.1016/j.jbc.2023.104703

Berry, C. M., Hertzog, P. J., & Mangan, N. E. (2012). Interferons as Biomarkers and Effectors: Lessons Learned from Animal Models. *Biomarkers in Medicine*, *6*(2), 159–176. https://doi.org/10.2217/bmm.12.10

Bilu, Y., & Barkai, N. (2005). The design of transcription-factor binding sites is affected by combinatorial regulation. *Genome Biology*, *6*(12), R103. https://doi.org/10.1186/gb-2005-6-12-r103

Blaszczyk, K., Nowicka, H., Kostyrko, K., Antonczyk, A., Wesoly, J., & Bluyssen, H. A. R. (2016). The unique role of STAT2 in constitutive and IFN-induced transcription and antiviral responses. *Cytokine & Growth Factor Reviews*, *29*, 71–81. https://doi.org/10.1016/j.cytogfr.2016.02.010

Blaszczyk, K., Olejnik, A., Nowicka, H., Ozgyin, L., Chen, Y.-L., Chmielewski, S., Kostyrko, K., Wesoly, J., Balint, B. L., Lee, C.-K., & Bluyssen, H. A. R. (2015). STAT2/IRF9 directs a prolonged ISGF3-like transcriptional response and antiviral activity in the absence of STAT1. *The Biochemical Journal*, *466*(3), 511–524. https://doi.org/10.1042/BJ20140644

Blondel, D., Maarifi, G., Nisole, S., & Chelbi-Alix, M. K. (2015). Resistance to Rhabdoviridae Infection and Subversion of Antiviral Responses. *Viruses*, *7*(7), 3675–3702. https://doi.org/10.3390/v7072794

Bluyssen, A. R., Durbin, J. E., & Levy, D. E. (1996). ISGF3 gamma p48, a specificity switch for interferon activated transcription factors. *Cytokine & Growth Factor Reviews*, *7*(1), 11–17. https://doi.org/10.1016/1359-6101(96)00005-6

Bluyssen, H. A., Muzaffar, R., Vlieststra, R. J., Van Der Made, A. C., Leung, S., Stark, G. R., Kerr, I. M., Trapman, J., & Levy, D. E. (1995). Combinatorial association and abundance of components of interferon-stimulated gene factor 3 dictate the selectivity of interferon responses. *Proceedings of the National Academy of Sciences*, *92*(12), 5645–5649. https://doi.org/10.1073/pnas.92.12.5645

Bluyssen, H. A., Vlietstra, R. J., van der Made, A., & Trapman, J. (1994). The interferon-stimulated gene 54 K promoter contains two adjacent functional interferon-stimulated response elements of different strength, which act synergistically for maximal interferon-alpha inducibility. *European Journal of Biochemistry*, *220*(2), 395–402. https://doi.org/10.1111/j.1432-1033.1994.tb18636.x

Bluyssen, HansA. R., & Levy, D. E. (1997). Stat2 Is a Transcriptional Activator That Requires Sequence-specific Contacts Provided by Stat1 and p48 for Stable Interaction with DNA. *Journal of Biological Chemistry*, *272*(7), 4600–4605. https://doi.org/10.1074/jbc.272.7.4600

Boisson-Dupuis, S., Kong, X.-F., Okada, S., Cypowyj, S., Puel, A., Abel, L., & Casanova, J.-L. (2012a). Inborn errors of human STAT1: Allelic heterogeneity governs the diversity of immunological and infectious phenotypes. *Current Opinion in Immunology*, *24*(4), 364–378. https://doi.org/10.1016/j.coi.2012.04.011

Bowie, A. G., & Unterholzner, L. (2008). Viral evasion and subversion of pattern-recognition receptor signalling. *Nature Reviews Immunology*, *8*(12), 911–922. https://doi.org/10.1038/nri2436

Braunstein, J., Brutsaert, S., Olson, R., & Schindler, C. (2003). STATs dimerize in the absence of phosphorylation. *The Journal of Biological Chemistry*, *278*(36), 34133–34140. https://doi.org/10.1074/jbc.M304531200

Brierley, M. M., & Fish, E. N. (2005). Functional relevance of the conserved DNA-binding domain of STAT2. *The Journal of Biological Chemistry*, *280*(13), 13029–13036. https://doi.org/10.1074/jbc.M500426200

Bucciol, G., Moens, L., Ogishi, M., Rinchai, D., Matuozzo, D., Momenilandi, M., Kerrouche, N., Cale, C. M., Treffeisen, E. R., Al Salamah, M., Al-Saud, B. K., Lachaux, A., Duclaux-Loras, R., Meignien, M., Bousfiha, A., Benhsaien, I., Shcherbina, A., Roppelt, A., COVID Human Genetic Effort, … Meyts, I. (2023). Human inherited complete STAT2 deficiency underlies inflammatory viral diseases. *The Journal of Clinical Investigation*, *133*(12), e168321. https://doi.org/10.1172/JCI168321

Buonamici, S., Li, D., Mikhail, F. M., Sassano, A., Platanias, L. C., Colamonici, O., Anastasi, J., & Nucifora, G. (2005). EVI1 abrogates interferon-alpha response by selectively blocking PML induction. *The Journal of Biological Chemistry*, *280*(1), 428–436. https://doi.org/10.1074/jbc.M410836200

Castro, R., Martin, S. A. M., Bird, S., Lamas, J., & Secombes, C. J. (2008). Characterisation of gamma-interferon responsive promoters in fish. *Molecular Immunology*, *45*(12), 3454–3462. https://doi.org/10.1016/j.molimm.2008.03.015

Cham, C. M., Ko, K., & Niewold, T. B. (2012). Interferon Regulatory Factor 5 in the Pathogenesis of Systemic Lupus Erythematosus. *Clinical and Developmental Immunology*, *2012*, 780436. https://doi.org/10.1155/2012/780436

Chatterjee-Kishore, M., Wright, K. L., Ting, J. P.-Y., & Stark, G. R. (2000). How Stat1 mediates constitutive gene expression: A complex of unphosphorylated Stat1 and IRF1 supports transcription of the LMP2 gene. *The EMBO Journal*, *19*(15), 4111. https://doi.org/10.1093/emboj/19.15.4111

Chen, M., Cheng, A., Chen, Y. Q., Hymel, A., Hanson, E. P., Kimmel, L., Minami, Y., Taniguchi, T., Changelian, P. S., & O'Shea, J. J. (1997). The amino terminus of JAK3 is necessary and sufficient for binding to the common gamma chain and confers the ability to transmit interleukin 2-mediated signals. *Proceedings of the National Academy of Sciences of the United States of America*, *94*(13), 6910–6915. https://doi.org/10.1073/pnas.94.13.6910

Chen, W., & Royer, W. E. (2010). Structural insights into interferon regulatory factor activation. *Cellular Signalling*, *22*(6), 883–887. https://doi.org/10.1016/j.cellsig.2009.12.005

Cheon, H., Holvey-Bates, E. G., Schoggins, J. W., Forster, S., Hertzog, P., Imanaka, N., Rice, C. M., Jackson, M. W., Junk, D. J., & Stark, G. R. (2013). IFNβ-dependent increases in STAT1, STAT2, and IRF9 mediate resistance to viruses and DNA damage. *The EMBO Journal*, *32*(20), 2751–2763. https://doi.org/10.1038/emboj.2013.203

Cheon, H., & Stark, G. R. (2009). Unphosphorylated STAT1 prolongs the expression of interferon-induced immune regulatory genes. *Proceedings of the National Academy of Sciences of the United States of America*, *106*(23), 9373–9378. https://doi.org/10.1073/pnas.0903487106

Chowdhury, F. Z., & Farrar, J. D. (2013). STAT2: A shape-shifting anti-viral super STAT. *JAK-STAT*, *2*(1), e23633. https://doi.org/10.4161/jkst.23633

Coccia, E. M., Stellacci, E., Orsatti, R., Benedetti, E., Giacomini, E., Marziali, G., Valdez, B. C., & Battistini, A. (2002). Protein inhibitor of activated signal transducer and activator of transcription (STAT)-1 (PIAS-1) regulates the IFN-gamma response in macrophage cell lines. *Cellular Signalling*, *14*(6), 537–545. https://doi.org/10.1016/s0898-6568(01)00272-8

Colonna, M., Krug, A., & Cella, M. (2002). Interferon-producing cells: On the front line in immune responses against pathogens. *Current Opinion in Immunology*, *14*(3), 373–379. https://doi.org/10.1016/s0952-7915(02)00349-7

Cui, D., Espínola, E. E., Arora, K., & Brinton, M. A. (2021). Two Interferon-Stimulated Response Elements Cooperatively Regulate Interferon-Stimulated Gene Expression in West Nile Virus-Infected IFNAR-/- Mouse Embryo Fibroblasts. *Journal of Virology*, *95*(22), e0104021. https://doi.org/10.1128/JVI.01040-21

Darnell, J. E. (1997). STATs and gene regulation. *Science (New York, N.Y.)*, *277*(5332), 1630–1635. https://doi.org/10.1126/science.277.5332.1630

Davis, C. A., Hitz, B. C., Sloan, C. A., Chan, E. T., Davidson, J. M., Gabdank, I., Hilton, J. A., Jain, K., Baymuradov, U. K., Narayanan, A. K., Onate, K. C., Graham, K., Miyasato, S. R., Dreszer, T. R., Strattan, J. S., Jolanki, O., Tanaka, F. Y., & Cherry, J. M. (2018). The Encyclopedia of DNA elements (ENCODE): Data portal update. *Nucleic Acids Research*, *46*(D1), D794–D801. https://doi.org/10.1093/nar/gkx1081

de Veer, M. J., Holko, M., Frevel, M., Walker, E., Der, S., Paranjape, J. M., Silverman, R. H., & Williams, B. R. (2001). Functional classification of interferon-stimulated genes identified using microarrays. *Journal of Leukocyte Biology*, *69*(6), 912–920.

Decker, T., Kovarik, P., & Meinke, A. (1997). GAS elements: A few nucleotides with a major impact on cytokine-induced gene expression. *Journal of Interferon & Cytokine Research: The Official Journal of the International Society for Interferon and Cytokine Research*, *17*(3), 121–134. https://doi.org/10.1089/jir.1997.17.121

Decker, T., Lew, D. J., Cheng, Y. S., Levy, D. E., & Darnell, J. E. (1989). Interactions of alpha- and gamma-interferon in the transcriptional regulation of the gene encoding a guanylate-binding protein. *The EMBO Journal*, *8*(7), 2009–2014.

Decker, T., Lew, D. J., Mirkovitch, J., & Darnell, J. E. (1991). Cytoplasmic activation of GAF, an IFN-gamma-regulated DNA-binding factor. *The EMBO Journal*, *10*(4), 927–932. https://doi.org/10.1002/j.1460-2075.1991.tb08026.x

Decout, A., Katz, J. D., Venkatraman, S., & Ablasser, A. (2021). The cGAS–STING pathway as a therapeutic target in inflammatory diseases. *Nature Reviews Immunology*, *21*(9), 548–569. https://doi.org/10.1038/s41577-021-00524-z

Delgoffe, G. M., & Vignali, D. A. A. (2013). STAT heterodimers in immunity: A mixed message or a unique signal? *JAK-STAT*, *2*(1). https://doi.org/10.4161/jkst.23060

Di Domizio, J., & Cao, W. (2013). Fueling Autoimmunity: Type I Interferon in Autoimmune Diseases. *Expert Review of Clinical Immunology*, *9*(3), 10.1586/eci.12.106. https://doi.org/10.1586/eci.12.106

Duncan, C. J. A., & Hambleton, S. (2021). Human Disease Phenotypes Associated with Loss and Gain of Function Mutations in STAT2: Viral Susceptibility and Type I Interferonopathy. *Journal of Clinical Immunology*, *41*(7), 1446–1456. https://doi.org/10.1007/s10875-021-01118-z

Ebersbach, C., Beier, A.-M. K., Thomas, C., & Erb, H. H. H. (2021). Impact of STAT Proteins in Tumor Progress and Therapy Resistance in Advanced and Metastasized Prostate Cancer. *Cancers*, *13*(19), 4854. https://doi.org/10.3390/cancers13194854

Ehret, G. B., Reichenbach, P., Schindler, U., Horvath, C. M., Fritz, S., Nabholz, M., & Bucher, P. (2001a). DNA binding specificity of different STAT proteins. Comparison of in vitro specificity with natural target sites. *The Journal of Biological Chemistry*, *276*(9), 6675–6688. https://doi.org/10.1074/jbc.M001748200

El Fiky, A., Pioli, P., Azam, A., Yoo, K., Nastiuk, K. L., & Krolewski, J. J. (2008). Nuclear transit of the intracellular domain of the interferon receptor subunit IFNaR2 requires Stat2 and Irf9. *Cellular Signalling*, *20*(7), 1400–1408. https://doi.org/10.1016/j.cellsig.2008.03.006

Escalante, C. R., Yie, J., Thanos, D., & Aggarwal, A. K. (1998). Structure of IRF-1 with bound DNA reveals determinants of interferon regulation. *Nature*, *391*(6662), 103–106. https://doi.org/10.1038/34224

Ewels, P., Magnusson, M., Lundin, S., & Käller, M. (2016). MultiQC: Summarize analysis results for multiple tools and samples in a single report. *Bioinformatics (Oxford, England)*, *32*(19), 3047–3048. https://doi.org/10.1093/bioinformatics/btw354

Ezer, D., Zabet, N. R., & Adryan, B. (2014). Homotypic clusters of transcription factor binding sites: A model system for understanding the physical mechanics of gene expression. *Computational and Structural Biotechnology Journal*, *10*(17), 63–69. https://doi.org/10.1016/j.csbj.2014.07.005

Farlik, M., Reutterer, B., Schindler, C., Greten, F., Vogl, C., Müller, M., & Decker, T. (2010). Nonconventional Initiation Complex Assembly by STAT and NF-κB Transcription Factors Regulates Nitric Oxide Synthase Expression. *Immunity*, *33*(1), 25–34. https://doi.org/10.1016/j.immuni.2010.07.001

Feng, H., Zhang, Y.-B., Gui, J.-F., Lemon, S. M., & Yamane, D. (2021a). Interferon regulatory factor 1 (IRF1) and anti-pathogen innate immune responses. *PLoS Pathogens*, *17*(1), e1009220. https://doi.org/10.1371/journal.ppat.1009220

Fensterl, V., Chattopadhyay, S., & Sen, G. C. (2015). No Love Lost Between Viruses and Interferons. *Annual Review of Virology*, *2*(1), 549–572. https://doi.org/10.1146/annurev-virology-100114-055249

Fink, K., & Grandvaux, N. (2013). STAT2 and IRF9: Beyond ISGF3. *JAK-STAT*, *2*(4), e27521. https://doi.org/10.4161/jkst.27521

Fink, K., Martin, L., Mukawera, E., Chartier, S., De Deken, X., Brochiero, E., Miot, F., & Grandvaux, N. (2013). IFNβ/TNFα synergism induces a non-canonical STAT2/IRF9-dependent pathway

triggering a novel DUOX2 NADPH oxidase-mediated airway antiviral response. *Cell Research*, *23*(5), 673–690. https://doi.org/10.1038/cr.2013.47

Firmbach-Kraft, I., Byers, M., Shows, T., Dalla-Favera, R., & Krolewski, J. J. (1990). Tyk2, prototype of a novel class of non-receptor tyrosine kinase genes. *Oncogene*, *5*(9), 1329–1336.

Fitzgerald-Bocarsly, P., & Feng, D. (2007). The role of type I interferon production by dendritic cells in host defense. *Biochimie*, *89*(6–7), 843–855. https://doi.org/10.1016/j.biochi.2007.04.018

Forero, A., Ozarkar, S., Li, H., Lee, C. H., Hemann, E. A., Nadjsombati, M. S., Hendricks, M. R., So, L., Green, R., Roy, C. N., Sarkar, S. N., von Moltke, J., Anderson, S. K., Gale, M., & Savan, R. (2019). Differential Activation of the Transcription Factor IRF1 Underlies the Distinct Immune Responses Elicited by Type I and Type III Interferons. *Immunity*, *51*(3), 451-464.e6. https://doi.org/10.1016/j.immuni.2019.07.007

Frucht, D. M., Fukao, T., Bogdan, C., Schindler, H., O'Shea, J. J., & Koyasu, S. (2001). IFN-gamma production by antigen-presenting cells: Mechanisms emerge. *Trends in Immunology*, *22*(10), 556–560. https://doi.org/10.1016/s1471-4906(01)02005-1

Gao, J., Morrison, D. C., Parmely, T. J., Russell, S. W., & Murphy, W. J. (1997). An interferon-gamma-activated site (GAS) is necessary for full expression of the mouse iNOS gene in response to interferon-gamma and lipopolysaccharide. *The Journal of Biological Chemistry*, *272*(2), 1226–1230. https://doi.org/10.1074/jbc.272.2.1226

Garg, A. D., Dudek, A. M., & Agostinis, P. (2013). Cancer immunogenicity, danger signals, and DAMPs: What, when, and how? *BioFactors (Oxford, England)*, *39*(4), 355–367. https://doi.org/10.1002/biof.1125

Garvin, A. J., Khalaf, A. H. A., Rettino, A., Xicluna, J., Butler, L., Morris, J. R., Heery, D. M., & Clarke, N. M. (2019). GSK3β-SCFFBXW7α mediated phosphorylation and ubiquitination of IRF1 are required for its transcription-dependent turnover. *Nucleic Acids Research*, *47*(9), 4476–4494. https://doi.org/10.1093/nar/gkz163

Gaudino, S. J., & Kumar, P. (2019). Cross-Talk Between Antigen Presenting Cells and T Cells Impacts Intestinal Homeostasis, Bacterial Infections, and Tumorigenesis. *Frontiers in Immunology*, *10*, 360. https://doi.org/10.3389/fimmu.2019.00360

Ge, S. X., Son, E. W., & Yao, R. (2018). iDEP: An integrated web application for differential expression and pathway analysis of RNA-Seq data. *BMC Bioinformatics*, *19*(1), 534. https://doi.org/10.1186/s12859-018-2486-6

Georgakopoulos-Soares, I., Deng, C., Agarwal, V., Chan, C. S. Y., Zhao, J., Inoue, F., & Ahituv, N. (2023). Transcription factor binding site orientation and order are major drivers of gene regulatory activity. *Nature Communications*, *14*(1), 2333. https://doi.org/10.1038/s41467-023-37960-5

Ghislain, J. J., & Fish, E. N. (1996). Application of genomic DNA affinity chromatography identifies multiple interferon-alpha-regulated Stat2 complexes. *The Journal of Biological Chemistry*, *271*(21), 12408–12413. https://doi.org/10.1074/jbc.271.21.12408

Ghislain, J. J., Wong, T., Nguyen, M., & Fish, E. N. (2001). The interferon-inducible Stat2:Stat1 heterodimer preferentially binds in vitro to a consensus element found in the promoters of a subset of interferon-stimulated genes. *Journal of Interferon & Cytokine Research: The Official Journal of the International Society for Interferon and Cytokine Research*, *21*(6), 379–388. https://doi.org/10.1089/107999001750277853

Ghoreschi, K., Laurence, A., & O'Shea, J. J. (2009). Janus kinases in immune cell signaling. *Immunological Reviews*, *228*(1), 273–287. https://doi.org/10.1111/j.1600-065X.2008.00754.x

Gil, M. P., Salomon, R., Louten, J., & Biron, C. A. (2006). Modulation of STAT1 protein levels: A mechanism shaping CD8 T-cell responses in vivo. *Blood*, *107*(3), 987. https://doi.org/10.1182/blood-2005-07-2834

Göder, A., Ginter, T., Heinzel, T., Stroh, S., Fahrer, J., Henke, A., & Krämer, O. H. (2021). STAT1 N-terminal domain discriminatively controls type I and type II IFN signaling. *Cytokine*, *144*, 155552. https://doi.org/10.1016/j.cyto.2021.155552

Golding, B., Tsokos, G. C., Fleisher, T., Muchmore, A. V., & Blaese, R. M. (1986). The role of nonactivated and interferon-gamma activated monocytes in regulating normal and SLE patient B cell responses to TNP-Brucella abortus. *Journal of Immunology (Baltimore, Md.: 1950)*, *137*(1), 103–107.

Goubau, D., van der Veen, A. G., Chakravarty, P., Lin, R., Rogers, N., Rehwinkel, J., Deddouche, S., Rosewell, I., Hiscott, J., & Reis e Sousa, C. (2015). Mouse superkiller-2-like helicase DDX60 is dispensable for type I IFN induction and immunity to multiple viruses. *European Journal of Immunology*, *45*(12), 3386–3403. https://doi.org/10.1002/eji.201545794

Gough, D. J., Messina, N. L., Hii, L., Gould, J. A., Sabapathy, K., Robertson, A. P. S., Trapani, J. A., Levy, D. E., Hertzog, P. J., Clarke, C. J. P., & Johnstone, R. W. (2010). Functional crosstalk between type I and II interferon through the regulated expression of STAT1. *PLoS Biology*, *8*(4), e1000361. https://doi.org/10.1371/journal.pbio.1000361

Gu, Z., Eils, R., & Schlesner, M. (2016). Complex heatmaps reveal patterns and correlations in multidimensional genomic data. *Bioinformatics*, *32*(18), 2847–2849. https://doi.org/10.1093/bioinformatics/btw313

Gupta, S., Yan, H., Wong, L. H., Ralph, S., Krolewski, J., & Schindler, C. (1996). The SH2 domains of Stat1 and Stat2 mediate multiple interactions in the transduction of IFN-alpha signals. *The EMBO Journal*, *15*(5), 1075–1084.

Hadjadj, J., Castro, C. N., Tusseau, M., Stolzenberg, M.-C., Mazerolles, F., Aladjidi, N., Armstrong, M., Ashrafian, H., Cutcutache, I., Ebetsberger-Dachs, G., Elliott, K. S., Durieu, I., Fabien, N., Fusaro, M., Heeg, M., Schmitt, Y., Bras, M., Knight, J. C., Lega, J.-C., … Rieux-Laucat, F. (2020). Early-onset autoimmunity associated with SOCS1 haploinsufficiency. *Nature Communications*, *11*(1), 5341. https://doi.org/10.1038/s41467-020-18925-4

Hambleton, S., Goodbourn, S., Young, D. F., Dickinson, P., Mohamad, S. M. B., Valappil, M., McGovern, N., Cant, A. J., Hackett, S. J., Ghazal, P., Morgan, N. V., & Randall, R. E. (2013). STAT2 deficiency and susceptibility to viral illness in humans. *Proceedings of the National Academy of Sciences of the United States of America*, *110*(8), 3053–3058. https://doi.org/10.1073/pnas.1220098110

Hartman, S. E., Bertone, P., Nath, A. K., Royce, T. E., Gerstein, M., Weissman, S., & Snyder, M. (2005). Global changes in STAT target selection and transcription regulation upon interferon treatments. *Genes & Development*, *19*(24), 2953–2968. https://doi.org/10.1101/gad.1371305

Haspel, R. L., & Darnell, J. E. (1999). A nuclear protein tyrosine phosphatase is required for the inactivation of Stat1. *Proceedings of the National Academy of Sciences of the United States of America*, *96*(18), 10188–10193. https://doi.org/10.1073/pnas.96.18.10188

Heim, M. H. (1999). The Jak-STAT pathway: Cytokine signalling from the receptor to the nucleus. *Journal of Receptor and Signal Transduction Research*, *19*(1–4), 75–120. https://doi.org/10.3109/10799899909036638

Heinz, S., Benner, C., Spann, N., Bertolino, E., Lin, Y. C., Laslo, P., Cheng, J. X., Murre, C., Singh, H., & Glass, C. K. (2010). Simple combinations of lineage-determining transcription factors prime cis-regulatory elements required for macrophage and B cell identities. *Molecular Cell*, *38*(4), 576–589. https://doi.org/10.1016/j.molcel.2010.05.004

Higgins, P. G. (1984). Interferons. *Journal of Clinical Pathology*, *37*(2), 109–116. https://doi.org/10.1136/jcp.37.2.109

Honkala, A. T., Tailor, D., & Malhotra, S. V. (2019). Guanylate-Binding Protein 1: An Emerging Target in Inflammation and Cancer. *Frontiers in Immunology*, *10*, 3139. https://doi.org/10.3389/fimmu.2019.03139

Hu, T., Yeh, J. E., Pinello, L., Jacob, J., Chakravarthy, S., Yuan, G.-C., Chopra, R., & Frank, D. A. (2015). Impact of the N-Terminal Domain of STAT3 in STAT3-Dependent Transcriptional Activity. *Molecular and Cellular Biology*, *35*(19), 3284–3300. https://doi.org/10.1128/MCB.00060-15

Hüntelmann, B., Staab, J., Herrmann-Lingen, C., & Meyer, T. (2014a). A Conserved Motif in the Linker Domain of STAT1 Transcription Factor Is Required for Both Recognition and Release from High-Affinity DNA-Binding Sites. *PloS One*, *9*, e97633. https://doi.org/10.1371/journal.pone.0097633

Imam, H., Kim, G.-W., Mir, S. A., Khan, M., & Siddiqui, A. (2020). Interferon-stimulated gene 20 (ISG20) selectively degrades N6-methyladenosine modified Hepatitis B Virus transcripts. *PLoS Pathogens*, *16*(2), e1008338. https://doi.org/10.1371/journal.ppat.1008338

Ivashkiv, L. B., & Donlin, L. T. (2014). Regulation of type I interferon responses. *Nature Reviews. Immunology*, *14*(1), 36–49. https://doi.org/10.1038/nri3581

Iversen, M. B., & Paludan, S. R. (2010). Mechanisms of type III interferon expression. *Journal of Interferon & Cytokine Research: The Official Journal of the International Society for Interferon and Cytokine Research*, *30*(8), 573–578. https://doi.org/10.1089/jir.2010.0063

J. Hertzog, P., Y. Hwang, S., & Kola, I. (1994). Role of interferons in the regulation of cell proliferation, differentiation, and development. *Molecular Reproduction and Development*, *39*(2), 226–232. https://doi.org/10.1002/mrd.1080390216

Jain, M., Singh, M. K., Shyam, H., Mishra, A., Kumar, S., Kumar, A., & Kushwaha, J. (2021). Role of JAK/STAT in the Neuroinflammation and its Association with Neurological Disorders. *Annals of Neurosciences*, *28*(3–4), 191–200. https://doi.org/10.1177/09727531211070532

Jefferies, C. A. (2019). Regulating IRFs in IFN Driven Disease. *Frontiers in Immunology*, *10*, 325. https://doi.org/10.3389/fimmu.2019.00325

Jiang, Z., Wei, F., Zhang, Y., Wang, T., Gao, W., Yu, S., Sun, H., Pu, J., Sun, Y., Wang, M., Tong, Q., Gao, C., Chang, K.-C., & Liu, J. (2021). IFI16 directly senses viral RNA and enhances RIG-I transcription and activation to restrict influenza virus infection. *Nature Microbiology*, *6*(7), 932–945. https://doi.org/10.1038/s41564-021-00907-x

Jordan, M. B. (2023). Loss of STAT2 may be dangerous in a world filled with viruses. *The Journal of Clinical Investigation*, *133*(12), e170886. https://doi.org/10.1172/JCI170886

Josset, L., Tchitchek, N., Gralinski, L. E., Ferris, M. T., Eisfeld, A. J., Green, R. R., Thomas, M. J., Tisoncik-Go, J., Schroth, G. P., Kawaoka, Y., Pardo-Manuel de Villena, F., Baric, R. S., Heise, M. T., Peng, X., & Katze, M. G. (2014). Annotation of long non-coding RNAs expressed in Collaborative Cross founder mice in response to respiratory virus infection reveals a new class of interferon-stimulated transcripts. *RNA Biology*, *11*(7), 875–890. https://doi.org/10.4161/rna.29442

Jounai, N., Kobiyama, K., Takeshita, F., & Ishii, K. J. (2012). Recognition of damage-associated molecular patterns related to nucleic acids during inflammation and vaccination. *Frontiers in Cellular and Infection Microbiology*, *2*, 168. https://doi.org/10.3389/fcimb.2012.00168

Kalvakolanu, D. V. (2003). Alternate interferon signaling pathways. *Pharmacology & Therapeutics*, *100*(1), 1–29. https://doi.org/10.1016/s0163-7258(03)00070-6

Kamijo, R., Harada, H., Matsuyama, T., Bosland, M., Gerecitano, J., Shapiro, D., Le, J., Koh, S. I., Kimura, T., & Green, S. J. (1994). Requirement for transcription factor IRF-1 in NO synthase induction in macrophages. *Science (New York, N.Y.)*, *263*(5153), 1612–1615. https://doi.org/10.1126/science.7510419

Kang, K., Robinson, G. W., & Hennighausen, L. (2013). Comprehensive meta-analysis of Signal Transducers and Activators of Transcription (STAT) genomic binding patterns discerns cell-specific cis-regulatory modules. *BMC Genomics*, *14*, 4. https://doi.org/10.1186/1471-2164-14-4

Karamouzis, M. V., Konstantinopoulos, P. A., & Papavassiliou, A. G. (2007). Roles of CREB-binding protein (CBP)/p300 in respiratory epithelium tumorigenesis. *Cell Research*, *17*(4), 324–332. https://doi.org/10.1038/cr.2007.10

Kaur, A., & Fang, C.-M. (2020). An overview of the human immune system and the role of interferon regulatory factors (IRFs). *Progress In Microbes & Molecular Biology*, *3*(1), Article 1. https://doi.org/10.36877/pmmb.a0000129

Kaushal, A. (2023). *[Review Article] Cyclic GMP-AMP synthase- Stimulator of Interferon Genes Signaling and their Agonistic / Antagonistic Values*. https://doi.org/10.32388/VDSV59

Kawai, T., & Akira, S. (2006). TLR signaling. *Cell Death and Differentiation*, *13*(5), 816–825. https://doi.org/10.1038/sj.cdd.4401850

Kawasaki, T., & Kawai, T. (2014). Toll-Like Receptor Signaling Pathways. *Frontiers in Immunology*, *5*. https://doi.org/10.3389/fimmu.2014.00461

Kershaw, N. J., Murphy, J. M., Lucet, I. S., Nicola, N. A., & Babon, J. J. (2013). Regulation of Janus Kinases by SOCS proteins. *Biochemical Society Transactions*, *41*(4), 1042–1047. https://doi.org/10.1042/BST20130077

Kiefer, K., Oropallo, M. A., Cancro, M. P., & Marshak-Rothstein, A. (2012). Role of type I interferons in the activation of autoreactive B cells. *Immunology and Cell Biology*, *90*(5), 498–504. https://doi.org/10.1038/icb.2012.10

Kim, H. S., & Lee, M.-S. (2007). STAT1 as a key modulator of cell death. *Cellular Signalling*, *19*(3), 454–465. https://doi.org/10.1016/j.cellsig.2006.09.003

Kimura, T., Kadokawa, Y., Harada, H., Matsumoto, M., Sato, M., Kashiwazaki, Y., Tarutani, M., Tan, R. S., Takasugi, T., Matsuyama, T., Mak, T. W., Noguchi, S., & Taniguchi, T. (1996). Essential and non-redundant roles of p48 (ISGF3 gamma) and IRF-1 in both type I and type II interferon responses, as revealed by gene targeting studies. *Genes to Cells: Devoted to Molecular & Cellular Mechanisms*, *1*(1), 115–124. https://doi.org/10.1046/j.1365-2443.1996.08008.x

Kimura, T., Nakayama, K., Penninger, J., Kitagawa, M., Harada, H., Matsuyama, T., Tanaka, N., Kamijo, R., Vilcek, J., & Mak, T. W. (1994). Involvement of the IRF-1 transcription factor in antiviral responses to interferons. *Science (New York, N.Y.)*, *264*(5167), 1921–1924. https://doi.org/10.1126/science.8009222

Kolde, R. (2019). *pheatmap: Pretty Heatmaps.* [Computer software].

Konan, K. V., & Taylor, M. W. (1996). Importance of the two interferon-stimulated response element (ISRE) sequences in the regulation of the human indoleamine 2,3-dioxygenase gene. *The Journal of Biological Chemistry*, *271*(32), 19140–19145. https://doi.org/10.1074/jbc.271.32.19140

Kopitar-Jerala, N. (2017). The Role of Interferons in Inflammation and Inflammasome Activation. *Frontiers in Immunology*, *8*, 873. https://doi.org/10.3389/fimmu.2017.00873

Kumar, K. P., McBride, K. M., Weaver, B. K., Dingwall, C., & Reich, N. C. (2000). Regulated Nuclear-Cytoplasmic Localization of Interferon Regulatory Factor 3, a Subunit of Double-Stranded RNA-Activated Factor 1. *Molecular and Cellular Biology*, *20*(11), 4159. https://doi.org/10.1128/mcb.20.11.4159-4168.2000

Kumatori, A., Yang, D., Suzuki, S., & Nakamura, M. (2002). Cooperation of STAT-1 and IRF-1 in interferon-gamma-induced transcription of the gp91(phox) gene. *The Journal of Biological Chemistry*, *277*(11), 9103–9111. https://doi.org/10.1074/jbc.M109803200

Lallemand, C., Bayat-Sarmadi, M., Blanchard, B., & Tovey, M. G. (1997). Identification of a novel transcriptional regulatory element common to the p53 and interferon regulatory factor 1 genes. *The Journal of Biological Chemistry*, *272*(47), 29801–29809. https://doi.org/10.1074/jbc.272.47.29801

Lanford, R. E., Guerra, B., Lee, H., Chavez, D., Brasky, K. M., & Bigger, C. B. (2006). Genomic response to interferon-alpha in chimpanzees: Implications of rapid downregulation for hepatitis C kinetics. *Hepatology (Baltimore, Md.)*, *43*(5), 961–972. https://doi.org/10.1002/hep.21167

Lange, F., Garn, J., Anagho, H. A., Vondran, F. W. R., von Hahn, T., Pietschmann, T., & Carpentier, A. (2023). Hepatitis D virus infection, innate immune response and antiviral treatments in stem cell-derived hepatocytes. *Liver International: Official Journal of the International Association for the Study of the Liver*, *43*(10), 2116–2129. https://doi.org/10.1111/liv.15655

Langmead, B., & Salzberg, S. L. (2012). Fast gapped-read alignment with Bowtie 2. *Nature Methods*, *9*(4), 357–359. https://doi.org/10.1038/nmeth.1923

Layish, B., Goli, R., Flick, H., Huang, S.-W., Zhang, R. Z., Kvaratskhelia, M., & Kane, M. (2023). Virus specificity and nucleoporin requirements for MX2 activity are affected by GTPase function and capsid-CypA interactions. *bioRxiv*, 2023.11.16.567336. https://doi.org/10.1101/2023.11.16.567336

Lazear, H. M., Schoggins, J. W., & Diamond, M. S. (2019). Shared and Distinct Functions of Type I and Type III Interferons. *Immunity*, *50*(4), 907–923. https://doi.org/10.1016/j.immuni.2019.03.025

Lee, A. J., & Ashkar, A. A. (2018). The Dual Nature of Type I and Type II Interferons. *Frontiers in Immunology*, *9*, 2061. https://doi.org/10.3389/fimmu.2018.02061

Lee, C.-J., An, H.-J., Cho, E. S., Kang, H. C., Lee, J. Y., Lee, H. S., & Cho, Y.-Y. (2020). Stat2 stability regulation: An intersection between immunity and carcinogenesis. *Experimental & Molecular Medicine*, *52*(9), 1526–1536. https://doi.org/10.1038/s12276-020-00506-6

Lee, M., & Rhee, I. (2017). Cytokine Signaling in Tumor Progression. *Immune Network*, *17*(4), 214–227. https://doi.org/10.4110/in.2017.17.4.214

Leonard, W. J. (2001). Role of Jak kinases and STATs in cytokine signal transduction. *International Journal of Hematology*, *73*(3), 271–277. https://doi.org/10.1007/BF02981951

Levy, D. E., & Darnell, J. E. (2002). Stats: Transcriptional control and biological impact. *Nature Reviews. Molecular Cell Biology*, *3*(9), 651–662. https://doi.org/10.1038/nrm909

Levy, D. E., Kessler, D. S., Pine, R., & Darnell, J. E. (1989). Cytoplasmic activation of ISGF3, the positive regulator of interferon-alpha-stimulated transcription, reconstituted in vitro. *Genes & Development*, *3*(9), 1362–1371. https://doi.org/10.1101/gad.3.9.1362

Lew, D. J., Decker, T., Strehlow, I., & Darnell, J. E. (1991). Overlapping elements in the guanylate-binding protein gene promoter mediate transcriptional induction by alpha and gamma interferons. *Molecular and Cellular Biology*, *11*(1), 182–191. https://doi.org/10.1128/mcb.11.1.182-191.1991

Li, G., Zhao, X., Zheng, Z., Zhang, H., Wu, Y., Shen, Y., & Chen, Q. (2024). cGAS-STING pathway mediates activation of dendritic cell sensing of immunogenic tumors. *Cellular and Molecular Life Sciences: CMLS*, *81*(1), 149. https://doi.org/10.1007/s00018-024-05191-6

Li, P., Shi, M.-L., Shen, W.-L., Zhang, Z., Xie, D.-J., Zhang, X.-Y., He, C., Zhang, Y., & Zhao, Z.-H. (2017). Coordinated regulation of IFITM1, 2 and 3 genes by an IFN-responsive enhancer through long-range chromatin interactions. *Biochimica et Biophysica Acta. Gene Regulatory Mechanisms*, *1860*(8), 885–893. https://doi.org/10.1016/j.bbagrm.2017.05.003

Li, X., Leung, S., Qureshi, S., Darnell, J. E., & Stark, G. R. (1996a). Formation of STAT1-STAT2 heterodimers and their role in the activation of IRF-1 gene transcription by interferon-alpha. *The Journal of Biological Chemistry*, *271*(10), 5790–5794. https://doi.org/10.1074/jbc.271.10.5790

Li, X., Wang, F., Xu, X., Zhang, J., & Xu, G. (2021). The Dual Role of STAT1 in Ovarian Cancer: Insight Into Molecular Mechanisms and Application Potentials. *Frontiers in Cell and Developmental Biology*, *9*. https://doi.org/10.3389/fcell.2021.636595

Liao, Y., Smyth, G. K., & Shi, W. (2014). featureCounts: An efficient general purpose program for assigning sequence reads to genomic features. *Bioinformatics*, *30*(7), 923–930. https://doi.org/10.1093/bioinformatics/btt656

Liu, S.-Y., Aliyari, R., Chikere, K., Li, G., Marsden, M. D., Smith, J. K., Pernet, O., Guo, H., Nusbaum, R., Zack, J. A., Freiberg, A. N., Su, L., Lee, B., & Cheng, G. (2013). Interferon-inducible cholesterol-25-hydroxylase broadly inhibits viral entry by production of 25-hydroxycholesterol. *Immunity*, *38*(1), 92–105. https://doi.org/10.1016/j.immuni.2012.11.005

Liu, W., Zhang, S., & Wang, J. (2022). IFN-γ, should not be ignored in SLE. *Frontiers in Immunology*, *13*. https://doi.org/10.3389/fimmu.2022.954706

Long, T., Bhattacharyya, T., Repele, A., Naylor, M., Nooti, S., Krueger, S., & Manu, null. (2023). The contributions of DNA accessibility and transcription factor occupancy to enhancer activity during cellular differentiation. *bioRxiv: The Preprint Server for Biology*, 2023.02.22.529579. https://doi.org/10.1101/2023.02.22.529579

Lou, Y.-J., Pan, X.-R., Jia, P.-M., Li, D., Xiao, S., Zhang, Z.-L., Chen, S.-J., Chen, Z., & Tong, J.-H. (2009). IRF-9/STAT2 [corrected] functional interaction drives retinoic acid-induced gene G expression independently of STAT1. *Cancer Research*, *69*(8), 3673–3680. https://doi.org/10.1158/0008-5472.CAN-08-4922

Love, M. I., Huber, W., & Anders, S. (2014). Moderated estimation of fold change and dispersion for RNA-seq data with DESeq2. *Genome Biology*, *15*(12), 550. https://doi.org/10.1186/s13059-014-0550-8

Ma, B., Chen, K., Liu, P., Li, M., Liu, J., Sideras, K., Sprengers, D., Biermann, K., Wang, W., IJzermans, J. N. M., Cao, W., Kwekkeboom, J., Peppelenbosch, M. P., & Pan, Q. (2019). Dichotomal functions of phosphorylated and unphosphorylated STAT1 in hepatocellular carcinoma. *Journal of Molecular Medicine (Berlin, Germany)*, *97*(1), 77–88. https://doi.org/10.1007/s00109-018-1717-7

Maher, S. G., Romero-Weaver, A. L., Scarzello, A. J., & Gamero, A. M. (2007). Interferon: Cellular executioner or white knight? *Current Medicinal Chemistry*, *14*(12), 1279–1289. https://doi.org/10.2174/092986707780597907

Majoros, A., Platanitis, E., Kernbauer-Hölzl, E., Rosebrock, F., Müller, M., & Decker, T. (2017). Canonical and Non-Canonical Aspects of JAK–STAT Signaling: Lessons from Interferons for Cytokine Responses. *Frontiers in Immunology*, *8*, 29. https://doi.org/10.3389/fimmu.2017.00029

Manivasagam, S., & Klein, R. S. (2021). Type III Interferons: Emerging Roles in Autoimmunity. *Frontiers in Immunology*, *12*, 764062. https://doi.org/10.3389/fimmu.2021.764062

Martinez-Moczygemba, M., Gutch, M. J., French, D. L., & Reich, N. C. (1997). Distinct STAT structure promotes interaction of STAT2 with the p48 subunit of the interferon-alpha-stimulated transcription factor ISGF3. *The Journal of Biological Chemistry*, *272*(32), 20070–20076. https://doi.org/10.1074/jbc.272.32.20070

Matsumoto, A., Masuhara, M., Mitsui, K., Yokouchi, M., Ohtsubo, M., Misawa, H., Miyajima, A., & Yoshimura, A. (1997). CIS, a cytokine inducible SH2 protein, is a target of the JAK-STAT5 pathway and modulates STAT5 activation. *Blood*, *89*(9), 3148–3154.

Matsumoto, M., Tanaka, N., Harada, H., Kimura, T., Yokochi, T., Kitagawa, M., Schindler, C., & Taniguchi, T. (1999). Activation of the transcription factor ISGF3 by interferon-gamma. *Biological Chemistry*, *380*(6), 699–703. https://doi.org/10.1515/BC.1999.087

Matta, B., Song, S., Li, D., & Barnes, B. J. (2017). Interferon regulatory factor signaling in autoimmune disease. *Cytokine*, *98*, 15–26. https://doi.org/10.1016/j.cyto.2017.02.006

Megger, D. A., Philipp, J., Le-Trilling, V. T. K., Sitek, B., & Trilling, M. (2017). Deciphering of the Human Interferon-Regulated Proteome by Mass Spectrometry-Based Quantitative Analysis Reveals Extent and Dynamics of Protein Induction and Repression. *Frontiers in Immunology*, *8*, 1139. https://doi.org/10.3389/fimmu.2017.01139

Meissl, K., Simonović, N., Amenitsch, L., Witalisz-Siepracka, A., Klein, K., Lassnig, C., Puga, A., Vogl, C., Poelzl, A., Bosmann, M., Dohnal, A., Sexl, V., Müller, M., & Strobl, B. (2020). STAT1 Isoforms Differentially Regulate NK Cell Maturation and Anti-tumor Activity. *Frontiers in Immunology*, *11*, 2189. https://doi.org/10.3389/fimmu.2020.02189

Meng, C., Guo, L.-B., Liu, X., Chang, Y.-H., & Lin, Y. (2017). Targeting STAT1 in Both Cancer and Insulin Resistance Diseases. *Current Protein & Peptide Science*, *18*(2), 181–188. https://doi.org/10.2174/1389203718666161117114735

Mengie Ayele, T., Tilahun Muche, Z., Behaile Teklemariam, A., Bogale Kassie, A., & Chekol Abebe, E. (2022). Role of JAK2/STAT3 Signaling Pathway in the Tumorigenesis, Chemotherapy Resistance, and Treatment of Solid Tumors: A Systemic Review. *Journal of Inflammation Research*, *15*, 1349–1364. https://doi.org/10.2147/JIR.S353489

Meraro, D., Hashmueli, S., Koren, B., Azriel, A., Oumard, A., Kirchhoff, S., Hauser, H., Nagulapalli, S., Atchison, M. L., & Levi, B. Z. (1999). Protein-protein and DNA-protein interactions affect the activity of lymphoid-specific IFN regulatory factors. *Journal of Immunology (Baltimore, Md.: 1950)*, *163*(12), 6468–6478.

Meyer, O. (2009). Interferons and autoimmune disorders. *Joint Bone Spine*, *76*(5), 464–473. https://doi.org/10.1016/j.jbspin.2009.03.012

Meyer, T., & Vinkemeier, U. (2004). Nucleocytoplasmic shuttling of STAT transcription factors. *European Journal of Biochemistry*, *271*(23–24), 4606–4612. https://doi.org/10.1111/j.1432-1033.2004.04423.x

Michalska, A., Blaszczyk, K., Wesoly, J., & Bluyssen, H. A. R. (2018). A Positive Feedback Amplifier Circuit That Regulates Interferon (IFN)-Stimulated Gene Expression and Controls Type I and Type II IFN Responses. *Frontiers in Immunology*, *9*. https://doi.org/10.3389/fimmu.2018.01135

Mielcarska, M. B., Bossowska-Nowicka, M., & Toka, F. N. (2020). Cell Surface Expression of Endosomal Toll-Like Receptors-A Necessity or a Superfluous Duplication? *Frontiers in Immunology*, *11*, 620972. https://doi.org/10.3389/fimmu.2020.620972

Miyamoto, M., Fujita, T., Kimura, Y., Maruyama, M., Harada, H., Sudo, Y., Miyata, T., & Taniguchi, T. (1988). Regulated expression of a gene encoding a nuclear factor, IRF-1, that specifically binds to IFN-beta gene regulatory elements. *Cell*, *54*(6), 903–913. https://doi.org/10.1016/s0092-8674(88)91307-4

Morris, A., Beresford, G. W., Mooney, M. R., & Boss, J. M. (2002). Kinetics of a gamma interferon response: Expression and assembly of CIITA promoter IV and inhibition by methylation. *Molecular and Cellular Biology*, *22*(13), 4781–4791. https://doi.org/10.1128/MCB.22.13.4781-4791.2002

Morris, R., Kershaw, N. J., & Babon, J. J. (2018). The molecular details of cytokine signaling via the JAK/STAT pathway. *Protein Science: A Publication of the Protein Society*, *27*(12), 1984–2009. https://doi.org/10.1002/pro.3519

Morrow, A. N., Schmeisser, H., Tsuno, T., & Zoon, K. C. (2011). A novel role for IFN-stimulated gene factor 3II in IFN-γ signaling and induction of antiviral activity in human cells. *Journal of Immunology (Baltimore, Md.: 1950)*, *186*(3), 1685–1693. https://doi.org/10.4049/jimmunol.1001359

Mostafavi, S., Yoshida, H., Moodley, D., LeBoité, H., Rothamel, K., Raj, T., Ye, C. J., Chevrier, N., Zhang, S.-Y., Feng, T., Lee, M., Casanova, J.-L., Clark, J. D., Hegen, M., Telliez, J.-B., Hacohen, N., De Jager, P. L., Regev, A., Mathis, D., … Immunological Genome Project Consortium. (2016). Parsing the Interferon Transcriptional Network and Its Disease Associations. *Cell*, *164*(3), 564–578. https://doi.org/10.1016/j.cell.2015.12.032

Mowen, K., & David, M. (1998). Role of the STAT1-SH2 Domain and STAT2 in the Activation and Nuclear Translocation of STAT1*. *Journal of Biological Chemistry*, *273*(46), 30073–30076. https://doi.org/10.1074/jbc.273.46.30073

Muckenhuber, M., Seufert, I., Müller-Ott, K., Mallm, J.-P., Klett, L. C., Knotz, C., Hechler, J., Kepper, N., Erdel, F., & Rippe, K. (2023). Epigenetic signals that direct cell type–specific interferon beta response in mouse cells. *Life Science Alliance*, *6*(4), e202201823. https://doi.org/10.26508/lsa.202201823

Müller, M., Laxton, C., Briscoe, J., Schindler, C., Improta, T., Darnell, J. E., Stark, G. R., & Kerr, I. M. (1993). Complementation of a mutant cell line: Central role of the 91 kDa polypeptide of ISGF3 in the interferon-alpha and -gamma signal transduction pathways. *The EMBO Journal*, *12*(11), 4221–4228. https://doi.org/10.1002/j.1460-2075.1993.tb06106.x

Naka, T., Narazaki, M., Hirata, M., Matsumoto, T., Minamoto, S., Aono, A., Nishimoto, N., Kajita, T., Taga, T., Yoshizaki, K., Akira, S., & Kishimoto, T. (1997). Structure and function of a new STAT-induced STAT inhibitor. *Nature*, *387*(6636), 924–929. https://doi.org/10.1038/43219

Nan, Y., Wu, C., & Zhang, Y.-J. (2017). Interplay between Janus Kinase/Signal Transducer and Activator of Transcription Signaling Activated by Type I Interferons and Viral Antagonism. *Frontiers in Immunology*, *8*, 1758. https://doi.org/10.3389/fimmu.2017.01758

Naschberger, E., Werner, T., Vicente, A. B., Guenzi, E., Töpolt, K., Leubert, R., Lubeseder-Martellato, C., Nelson, P. J., & Stürzl, M. (2004). Nuclear factor-kappaB motif and interferon-alpha-stimulated response element co-operate in the activation of guanylate-binding protein-1 expression by inflammatory cytokines in endothelial cells. *Biochemical Journal*, *379*(Pt 2), 409–420. https://doi.org/10.1042/BJ20031873

Negishi, H., Fujita, Y., Yanai, H., Sakaguchi, S., Ouyang, X., Shinohara, M., Takayanagi, H., Ohba, Y., Taniguchi, T., & Honda, K. (2006). Evidence for licensing of IFN-gamma-induced IFN regulatory factor 1 transcription factor by MyD88 in Toll-like receptor-dependent gene induction program. *Proceedings of the National Academy of Sciences of the United States of America*, *103*(41), 15136–15141. https://doi.org/10.1073/pnas.0607181103

Nguyen, H., Ramana, C. V., Bayes, J., & Stark, G. R. (2001). Roles of phosphatidylinositol 3-kinase in interferon-gamma-dependent phosphorylation of STAT1 on serine 727 and activation of gene expression. *The Journal of Biological Chemistry*, *276*(36), 33361–33368. https://doi.org/10.1074/jbc.M105070200

Nicholas, C., & Lesinski, G. (2011). *The Jak-STAT Signal Transduction Pathway in Melanoma*. https://doi.org/10.5772/18876

Nicola, N. A., & Greenhalgh, C. J. (2000). The suppressors of cytokine signaling (SOCS) proteins: Important feedback inhibitors of cytokine action. *Experimental Hematology*, *28*(10), 1105–1112. https://doi.org/10.1016/s0301-472x(00)00525-7

Novatt, H., Theisen, T. C., Massie, T., Massie, T., Simonyan, V., Voskanian-Kordi, A., Renn, L. A., & Rabin, R. L. (2016). Distinct Patterns of Expression of Transcription Factors in Response to Interferonβ and Interferonλ1. *Journal of Interferon & Cytokine Research: The Official Journal of the International Society for Interferon and Cytokine Research*, *36*(10), 589–598. https://doi.org/10.1089/jir.2016.0031

Nowicka, H., Sekrecka, A., Blaszczyk, K., Kluzek, K., Chang, C.-Y., Wesoly, J., Lee, C.-K., & Bluyssen, H. A. R. (2023). ISGF3 and STAT2/IRF9 Control Basal and IFN-Induced Transcription through Genome-Wide Binding of Phosphorylated and Unphosphorylated Complexes to Common ISRE-Containing ISGs. *International Journal of Molecular Sciences*, *24*(24), 17635. https://doi.org/10.3390/ijms242417635

Odendall, C., Dixit, E., Stavru, F., Bierne, H., Franz, K. M., Durbin, A. F., Boulant, S., Gehrke, L., Cossart, P., & Kagan, J. C. (2014). Diverse intracellular pathogens activate type III interferon expression from peroxisomes. *Nature Immunology*, *15*(8), 717–726. https://doi.org/10.1038/ni.2915

Odendall, C., & Kagan, J. C. (2015). The unique regulation and functions of type III interferons in antiviral immunity. *Current Opinion in Virology*, *12*, 47–52. https://doi.org/10.1016/j.coviro.2015.02.003

Oh, S., & Hwang, E. S. (2014). The role of protein modifications of T-bet in cytokine production and differentiation of T helper cells. *Journal of Immunology Research*, *2014*, 589672. https://doi.org/10.1155/2014/589672

Olszewski, M. A., Gray, J., & Vestal, D. J. (2006). In silico genomic analysis of the human and murine guanylate-binding protein (GBP) gene clusters. *Journal of Interferon & Cytokine Research: The Official Journal of the International Society for Interferon and Cytokine Research*, *26*(5), 328–352. https://doi.org/10.1089/jir.2006.26.328

Osterlund, P. I., Pietilä, T. E., Veckman, V., Kotenko, S. V., & Julkunen, I. (2007). IFN regulatory factor family members differentially regulate the expression of type III IFN (IFN-lambda) genes. *Journal of Immunology (Baltimore, Md.: 1950)*, *179*(6), 3434–3442. https://doi.org/10.4049/jimmunol.179.6.3434

Panda, D., Gjinaj, E., Bachu, M., Squire, E., Novatt, H., Ozato, K., & Rabin, R. L. (2019). IRF1 Maintains Optimal Constitutive Expression of Antiviral Genes and Regulates the Early Antiviral Response. *Frontiers in Immunology*, *10*, 1019. https://doi.org/10.3389/fimmu.2019.01019

Parab, L., Pal, S., & Dhar, R. (2022). Transcription factor binding process is the primary driver of noise in gene expression. *PLoS Genetics*, *18*(12), e1010535. https://doi.org/10.1371/journal.pgen.1010535

Parrini, M., Meissl, K., Ola, M. J., Lederer, T., Puga, A., Wienerroither, S., Kovarik, P., Decker, T., Müller, M., & Strobl, B. (2018). The C-Terminal Transactivation Domain of STAT1 Has a Gene-Specific Role in Transactivation and Cofactor Recruitment. *Frontiers in Immunology*, *9*, 2879. https://doi.org/10.3389/fimmu.2018.02879

Paul, A., Ismail, M. N., Tang, T. H., & Ng, S. K. (2023). Phosphorylation of interferon regulatory factor 9 (IRF9). *Molecular Biology Reports*, *50*(4), 3909–3917. https://doi.org/10.1007/s11033-023-08253-3

Paul, A., Tang, T. H., & Ng, S. K. (2018). Interferon Regulatory Factor 9 Structure and Regulation. *Frontiers in Immunology*, *9*, 1831. https://doi.org/10.3389/fimmu.2018.01831

Perng, Y.-C., & Lenschow, D. J. (2018). ISG15 in antiviral immunity and beyond. *Nature Reviews. Microbiology*, *16*(7), 423–439. https://doi.org/10.1038/s41579-018-0020-5

Pestka, S., Krause, C. D., & Walter, M. R. (2004). Interferons, interferon-like cytokines, and their receptors. *Immunological Reviews*, *202*, 8–32. https://doi.org/10.1111/j.0105-2896.2004.00204.x

Piaszyk-Borychowska, A., Széles, L., Csermely, A., Chiang, H.-C., Wesoły, J., Lee, C.-K., Nagy, L., & Bluyssen, H. A. R. (2019). Signal Integration of IFN-I and IFN-II With TLR4 Involves Sequential

Recruitment of STAT1-Complexes and NFκB to Enhance Pro-inflammatory Transcription. *Frontiers in Immunology*, *10*, 1253. https://doi.org/10.3389/fimmu.2019.01253

Pilz, A., Ramsauer, K., Heidari, H., Leitges, M., Kovarik, P., & Decker, T. (2003). Phosphorylation of the Stat1 transactivating domain is required for the response to type I interferons. *EMBO Reports*, *4*(4), 368–373. https://doi.org/10.1038/sj.embor.embor802

Pitha, P. M. (Ed.). (2007). *Interferon: The 50th anniversary*. Springer.

Platanitis, E., & Decker, T. (2018). Regulatory Networks Involving STATs, IRFs, and NFκB in Inflammation. *Frontiers in Immunology*, *9*, 2542. https://doi.org/10.3389/fimmu.2018.02542

Platanitis, E., Demiroz, D., Schneller, A., Fischer, K., Capelle, C., Hartl, M., Gossenreiter, T., Müller, M., Novatchkova, M., & Decker, T. (2019). A molecular switch from STAT2-IRF9 to ISGF3 underlies interferon-induced gene transcription. *Nature Communications*, *10*(1), 2921. https://doi.org/10.1038/s41467-019-10970-y

Qian, J., Zheng, H., Huangfu, W.-C., Liu, J., Carbone, C. J., Leu, N. A., Baker, D. P., & Fuchs, S. Y. (2011). Pathogen recognition receptor signaling accelerates phosphorylation-dependent degradation of IFNAR1. *PLoS Pathogens*, *7*(6), e1002065. https://doi.org/10.1371/journal.ppat.1002065

R Core Team. (2021). *R: A Language and Environment for Statistical Computing* [Computer software].

Raftery, N., & Stevenson, N. J. (2017). Advances in anti-viral immune defence: Revealing the importance of the IFN JAK/STAT pathway. *Cellular and Molecular Life Sciences: CMLS*, *74*(14), 2525–2535. https://doi.org/10.1007/s00018-017-2520-2

Ramachandran, A., & Horvath, C. M. (2009). Paramyxovirus Disruption of Interferon Signal Transduction: STATus Report. *Journal of Interferon & Cytokine Research*, *29*(9), 531–537. https://doi.org/10.1089/jir.2009.0070

Ramírez, F., Ryan, D. P., Grüning, B., Bhardwaj, V., Kilpert, F., Richter, A. S., Heyne, S., Dündar, F., & Manke, T. (2016). deepTools2: A next generation web server for deep-sequencing data analysis. *Nucleic Acids Research*, *44*(W1), W160-165. https://doi.org/10.1093/nar/gkw257

Ramsauer, K., Farlik, M., Zupkovitz, G., Seiser, C., Kröger, A., Hauser, H., & Decker, T. (2007). Distinct modes of action applied by transcription factors STAT1 and IRF1 to initiate transcription of the IFN-gamma-inducible gbp2 gene. *Proceedings of the National Academy of Sciences of the United States of America*, *104*(8), 2849–2854. https://doi.org/10.1073/pnas.0610944104

Randal, M., & Kossiakoff, A. A. (2001). The structure and activity of a monomeric interferon-gamma:alpha-chain receptor signaling complex. *Structure (London, England: 1993)*, *9*(2), 155–163. https://doi.org/10.1016/s0969-2126(01)00567-6

Ranjbar, S., Haridas, V., Jasenosky, L. D., Falvo, J. V., & Goldfeld, A. E. (2015). A Role for IFITM Proteins in Restriction of Mycobacterium tuberculosis Infection. *Cell Reports*, *13*(5), 874–883. https://doi.org/10.1016/j.celrep.2015.09.048

Rauch, I., Rosebrock, F., Hainzl, E., Heider, S., Majoros, A., Wienerroither, S., Strobl, B., Stockinger, S., Kenner, L., Müller, M., & Decker, T. (2015). Noncanonical Effects of IRF9 in Intestinal Inflammation: More than Type I and Type III Interferons. *Molecular and Cellular Biology*, *35*(13), 2332–2343. https://doi.org/10.1128/MCB.01498-14

Ravi Sundar Jose Geetha, A., Fischer, K., Babadei, O., Smesnik, G., Vogt, A., Platanitis, E., Müller, M., Farlik, M., & Decker, T. (2024). Dynamic control of gene expression by ISGF3 and IRF1 during IFNβ and IFNγ signaling. *The EMBO Journal*, *43*(11), 2233–2263. https://doi.org/10.1038/s44318-024-00092-7

Reich, N. C. (2007). STAT dynamics. *Cytokine & Growth Factor Reviews*, *18*(5–6), 511–518. https://doi.org/10.1016/j.cytogfr.2007.06.021

Reich, N. C. (2013). STATs get their move on. *JAK-STAT*, *2*(4), e27080. https://doi.org/10.4161/jkst.27080

Reich, N., Evans, B., Levy, D., Fahey, D., Knight, E., & Darnell, J. E. (1987). Interferon-induced transcription of a gene encoding a 15-kDa protein depends on an upstream enhancer element. *Proceedings of the National Academy of Sciences of the United States of America*, *84*(18), 6394–6398. https://doi.org/10.1073/pnas.84.18.6394

Reikine, S., Nguyen, J. B., & Modis, Y. (2014). Pattern Recognition and Signaling Mechanisms of RIG-I and MDA5. *Frontiers in Immunology*, *5*, 342. https://doi.org/10.3389/fimmu.2014.00342

Remling, L., Gregus, A., Wirths, O., Meyer, T., & Staab, J. (2023). A novel interface between the N-terminal and coiled-coil domain of STAT1 functions in an auto-inhibitory manner. *Cell Communication and Signaling: CCS*, *21*(1), 170. https://doi.org/10.1186/s12964-023-01124-1

Rengachari, S., Groiss, S., Devos, J. M., Caron, E., Grandvaux, N., & Panne, D. (2018). Structural basis of STAT2 recognition by IRF9 reveals molecular insights into ISGF3 function. *Proceedings of the National Academy of Sciences of the United States of America*, *115*(4), E601–E609. https://doi.org/10.1073/pnas.1718426115

Resende, M., Cardoso, M. S., Ribeiro, A. R., Flórido, M., Borges, M., Castro, A. G., Alves, N. L., Cooper, A. M., & Appelberg, R. (2017). Innate IFN-γ-Producing Cells Developing in the Absence of IL-2 Receptor Common γ-Chain. *Journal of Immunology (Baltimore, Md.: 1950)*, *199*(4), 1429–1439. https://doi.org/10.4049/jimmunol.1601701

Ritchie, K. J., & Zhang, D.-E. (2004). ISG15: The immunological kin of ubiquitin. *Seminars in Cell & Developmental Biology*, *15*(2), 237–246. https://doi.org/10.1016/j.semcdb.2003.12.005

Rogers, R. S., Horvath, C. M., & Matunis, M. J. (2003). SUMO modification of STAT1 and its role in PIAS-mediated inhibition of gene activation. *The Journal of Biological Chemistry*, *278*(32), 30091–30097. https://doi.org/10.1074/jbc.M301344200

RONNI, T., MATIKAINEN, S., LEHTONEN, A., PALVIMO, J., DELLIS, J., VAN EYLEN, F., GOETSCHY, J.-F., HORISBERGER, M., CONTENT, J., & JULKUNEN, I. (1998). The Proximal Interferon-Stimulated Response Elements Are Essential for Interferon Responsiveness: A Promoter Analysis of the Antiviral MxA Gene. *Journal of Interferon & Cytokine Research*, *18*(9), 773–781. https://doi.org/10.1089/jir.1998.18.773

Rosain, J., Neehus, A.-L., Manry, J., Yang, R., Le Pen, J., Daher, W., Liu, Z., Chan, Y.-H., Tahuil, N., Türel, Ö., Bourgey, M., Ogishi, M., Doisne, J.-M., Izquierdo, H. M., Shirasaki, T., Le Voyer, T., Guérin, A., Bastard, P., Moncada-Vélez, M., … Bustamante, J. (2023). Human IRF1 governs macrophagic IFN-γ immunity to mycobacteria. *Cell*, *186*(3), 621-645.e33. https://doi.org/10.1016/j.cell.2022.12.038

Rusinova, I., Forster, S., Yu, S., Kannan, A., Masse, M., Cumming, H., Chapman, R., & Hertzog, P. J. (2013). Interferome v2.0: An updated database of annotated interferon-regulated genes. *Nucleic Acids Research*, *41*(Database issue), D1040-1046. https://doi.org/10.1093/nar/gks1215

Sajid, M., Ullah, H., Yan, K., He, M., Feng, J., Shereen, M. A., Hao, R., Li, Q., Guo, D., Chen, Y., & Zhou, L. (2021). The Functional and Antiviral Activity of Interferon Alpha-Inducible IFI6 Against Hepatitis B Virus Replication and Gene Expression. *Frontiers in Immunology*, *12*, 634937. https://doi.org/10.3389/fimmu.2021.634937

Samuel, C. E. (2001). Antiviral Actions of Interferons. *Clinical Microbiology Reviews*, *14*(4), 778–809. https://doi.org/10.1128/cmr.14.4.778-809.2001

Savic, D., Roberts, B. S., Carleton, J. B., Partridge, E. C., White, M. A., Cohen, B. A., Cooper, G. M., Gertz, J., & Myers, R. M. (2015). Promoter-distal RNA polymerase II binding discriminates active from inactive CCAAT/ enhancer-binding protein beta binding sites. *Genome Research*, *25*(12), 1791–1800. https://doi.org/10.1101/gr.191593.115

Scarzello, A. J., Romero-Weaver, A. L., Maher, S. G., Veenstra, T. D., Zhou, M., Qin, A., Donnelly, R. P., Sheikh, F., & Gamero, A. M. (2007). A Mutation in the SH2 Domain of STAT2 Prolongs Tyrosine Phosphorylation of STAT1 and Promotes Type I IFN-induced Apoptosis. *Molecular Biology of the Cell*, *18*(7), 2455. https://doi.org/10.1091/mbc.E06-09-0843

Schindler, C., Levy, D. E., & Decker, T. (2007). JAK-STAT signaling: From interferons to cytokines. *The Journal of Biological Chemistry*, *282*(28), 20059–20063. https://doi.org/10.1074/jbc.R700016200

Schmidt, D., & Müller, S. (2002). Members of the PIAS family act as SUMO ligases for c-Jun and p53 and repress p53 activity. *Proceedings of the National Academy of Sciences of the United States of America*, *99*(5), 2872–2877. https://doi.org/10.1073/pnas.052559499

Schoggins, J. W. (2014). Interferon-stimulated genes: Roles in viral pathogenesis. *Current Opinion in Virology*, *6*, 40–46. https://doi.org/10.1016/j.coviro.2014.03.006

Schoggins, J. W. (2019). Interferon-Stimulated Genes: What Do They All Do? *Annual Review of Virology*, *6*(1), 567–584. https://doi.org/10.1146/annurev-virology-092818-015756

Schoggins, J. W., & Rice, C. M. (2011). Interferon-stimulated genes and their antiviral effector functions. *Current Opinion in Virology*, *1*(6), 519–525. https://doi.org/10.1016/j.coviro.2011.10.008

Schoggins, J. W., Wilson, S. J., Panis, M., Murphy, M. Y., Jones, C. T., Bieniasz, P., & Rice, C. M. (2011). A diverse range of gene products are effectors of the type I interferon antiviral response. *Nature*, *472*(7344), 481–485. https://doi.org/10.1038/nature09907

Schreiber, G. (2020). The Role of Type I Interferons in the Pathogenesis and Treatment of COVID-19. *Frontiers in Immunology*, *11*, 595739. https://doi.org/10.3389/fimmu.2020.595739

Seegert, D., Strehlow, I., Klose, B., Levy, D. E., Schindler, C., & Decker, T. (1994). A novel interferon-alpha-regulated, DNA-binding protein participates in the regulation of the IFP53/tryptophanyl-tRNA synthetase gene. *The Journal of Biological Chemistry*, *269*(11), 8590–8595.

Seif, F., Khoshmirsafa, M., Aazami, H., Mohsenzadegan, M., Sedighi, G., & Bahar, M. (2017). The role of JAK-STAT signaling pathway and its regulators in the fate of T helper cells. *Cell Communication and Signaling*, *15*(1), 23. https://doi.org/10.1186/s12964-017-0177-y

Sekrecka, A., Kluzek, K., Sekrecki, M., Boroujeni, M. E., Hassani, S., Yamauchi, S., Sada, K., Wesoly, J., & Bluyssen, H. A. R. (2023). Time-dependent recruitment of GAF, ISGF3 and IRF1 complexes shapes IFNα and IFNγ-activated transcriptional responses and explains mechanistic and functional overlap. *Cellular and Molecular Life Sciences: CMLS*, *80*(7), 187. https://doi.org/10.1007/s00018-023-04830-8

Sen, G. C. (2001). Viruses and Interferons. *Annual Review of Microbiology*, *55*(1), 255–281. https://doi.org/10.1146/annurev.micro.55.1.255

Shah, M., & Choi, S. (2016). Interferon Regulatory Factor. In S. Choi (Ed.), *Encyclopedia of Signaling Molecules* (pp. 1–10). Springer New York. https://doi.org/10.1007/978-1-4614-6438-9_101496-1

Shuai, K. (2006). Regulation of cytokine signaling pathways by PIAS proteins. *Cell Research*, *16*(2), 196–202. https://doi.org/10.1038/sj.cr.7310027

Silva-Gomes, S., Decout, A., & Nigou, J. (2015). Pathogen-Associated Molecular Patterns (PAMPs). In M. Parnham (Ed.), *Encyclopedia of Inflammatory Diseases* (pp. 1–16). Springer. https://doi.org/10.1007/978-3-0348-0620-6_35-1

Stanifer, M. L., Guo, C., Doldan, P., & Boulant, S. (2020). Importance of Type I and III Interferons at Respiratory and Intestinal Barrier Surfaces. *Frontiers in Immunology*, *11*, 608645. https://doi.org/10.3389/fimmu.2020.608645

Steen, H. C., & Gamero, A. M. (2012). The Role of Signal Transducer and Activator of Transcription-2 in the Interferon Response. *Journal of Interferon & Cytokine Research*, *32*(3), 103. https://doi.org/10.1089/jir.2011.0099

Steen, H. C., & Gamero, A. M. (2013). STAT2 phosphorylation and signaling. *JAK-STAT*, *2*(4), e25790. https://doi.org/10.4161/jkst.25790

Steen, H. C., Nogusa, S., Thapa, R. J., Basagoudanavar, S. H., Gill, A. L., Merali, S., Barrero, C. A., Balachandran, S., & Gamero, A. M. (2013). Identification of STAT2 serine 287 as a novel regulatory phosphorylation site in type I interferon-induced cellular responses. *The Journal of Biological Chemistry*, *288*(1), 747–758. https://doi.org/10.1074/jbc.M112.402529

Stewart, M. D., Choi, Y., Johnson, G. A., Yu-Lee, L., Bazer, F. W., & Spencer, T. E. (2002). Roles of Stat1, Stat2, and interferon regulatory factor-9 (IRF-9) in interferon tau regulation of IRF-1. *Biology of Reproduction*, *66*(2), 393–400. https://doi.org/10.1095/biolreprod66.2.393

Strehlow, I., Seegert, D., Frick, C., Bange, F. C., Schindler, C., Böttger, E. C., & Decker, T. (1993). The gene encoding IFP 53/tryptophanyl-tRNA synthetase is regulated by the gamma-interferon activation factor. *The Journal of Biological Chemistry*, *268*(22), 16590–16595.

Sundararaj, S., & Casarotto, M. G. (2021). Molecular interactions of IRF4 in B cell development and malignancies. *Biophysical Reviews*, *13*(6), 1219–1227. https://doi.org/10.1007/s12551-021-00825-6

Sung, P. S., Cheon, H., Cho, C. H., Hong, S.-H., Park, D. Y., Seo, H.-I., Park, S.-H., Yoon, S. K., Stark, G. R., & Shin, E.-C. (2015). Roles of unphosphorylated ISGF3 in HCV infection and interferon responsiveness. *Proceedings of the National Academy of Sciences of the United States of America*, *112*(33), 10443–10448. https://doi.org/10.1073/pnas.1513341112

Suprunenko, T., & Hofer, M. J. (2016). The emerging role of interferon regulatory factor 9 in the antiviral host response and beyond. *Cytokine & Growth Factor Reviews*, *29*, 35–43. https://doi.org/10.1016/j.cytogfr.2016.03.002

Takaoka, A., Tamura, T., & Taniguchi, T. (2008). Interferon regulatory factor family of transcription factors and regulation of oncogenesis. *Cancer Science*, *99*(3), 467–478. https://doi.org/10.1111/j.1349-7006.2007.00720.x

Takeuchi, O., & Akira, S. (2010). Pattern Recognition Receptors and Inflammation. *Cell*, *140*(6), 805–820. https://doi.org/10.1016/j.cell.2010.01.022

Tan, S. L., & Katze, M. G. (1999). The emerging role of the interferon-induced PKR protein kinase as an apoptotic effector: A new face of death? *Journal of Interferon & Cytokine Research: The Official Journal of the International Society for Interferon and Cytokine Research*, *19*(6), 543–554. https://doi.org/10.1089/107999099313677

Tanaka, N., Ishihara, M., Lamphier, M. S., Nozawa, H., Matsuyama, T., Mak, T. W., Aizawa, S., Tokino, T., Oren, M., & Taniguchi, T. (1996). Cooperation of the tumour suppressors IRF-1 and p53 in response to DNA damage. *Nature*, *382*(6594), 816–818. https://doi.org/10.1038/382816a0

Taniguchi, T., Lamphier, M. S., & Tanaka, N. (1997). IRF-1: The transcription factor linking the interferon response and oncogenesis. *Biochimica Et Biophysica Acta*, *1333*(1), M9-17. https://doi.org/10.1016/s0304-419x(97)00014-0

Taylor, M. W. (2014a). Interferons. *Viruses and Man: A History of Interactions*, 101–119. https://doi.org/10.1007/978-3-319-07758-1_7

Tessitore, A., Pastore, L., Rispoli, A., Cilenti, L., Toniato, E., Flati, V., Farina, A. R., Frati, L., Gulino, A., & Martinotti, S. (1998). Two gamma-interferon-activation sites (GAS) on the promoter of the human intercellular adhesion molecule (ICAM-1) gene are required for induction of transcription by IFN-gamma. *European Journal of Biochemistry*, *258*(3), 968–975. https://doi.org/10.1046/j.1432-1327.1998.2580968.x

Testoni, B., Völlenkle, C., Guerrieri, F., Gerbal-Chaloin, S., Blandino, G., & Levrero, M. (2011). Chromatin dynamics of gene activation and repression in response to interferon alpha (IFN(alpha)) reveal new roles for phosphorylated and unphosphorylated forms of the transcription factor STAT2. *The Journal of Biological Chemistry*, *286*(23), 20217–20227. https://doi.org/10.1074/jbc.M111.231068

The ENCODE Project Consortium. (2012). An integrated encyclopedia of DNA elements in the human genome. *Nature*, *489*(7414), 57–74. https://doi.org/10.1038/nature11247

Thorvaldsdóttir, H., Robinson, J. T., & Mesirov, J. P. (2013). Integrative Genomics Viewer (IGV): High-performance genomics data visualization and exploration. *Briefings in Bioinformatics*, *14*(2), 178–192. https://doi.org/10.1093/bib/bbs017

Tolomeo, M., Cavalli, A., & Cascio, A. (2022). STAT1 and Its Crucial Role in the Control of Viral Infections. *International Journal of Molecular Sciences*, *23*(8). https://doi.org/10.3390/ijms23084095

Trapani, J. A., Dawson, M., Apostolidis, V. A., & Browne, K. A. (1994). Genomic organization of IFI16, an interferon-inducible gene whose expression is associated with human myeloid cell differentiation: Correlation of predicted protein domains with exon organization. *Immunogenetics*, *40*(6), 415–424. https://doi.org/10.1007/BF00177824

Tremblay, B. J.-M. (2021). *universalmotif: Import, Modify, and Export Motifs with R.* [Computer software].

Tseng, C.-C., Wong, M.-C., Liao, W.-T., Chen, C.-J., Lee, S.-C., Yen, J.-H., & Chang, S.-J. (2021). Genetic Variants in Transcription Factor Binding Sites in Humans: Triggered by Natural Selection and Triggers of Diseases. *International Journal of Molecular Sciences*, *22*(8), 4187. https://doi.org/10.3390/ijms22084187

Tsukahara, T., Kim, S., & Taylor, M. W. (2006). REFINEMENT: A search framework for the identification of interferon-responsive elements in DNA sequences – a case study with ISRE and GAS. *Computational Biology and Chemistry*, *30*(2), 134–147. https://doi.org/10.1016/j.compbiolchem.2006.01.002

Wack, A., Terczyńska-Dyla, E., & Hartmann, R. (2015). Guarding the frontiers: The biology of type III interferons. *Nature Immunology*, *16*(8), 802–809. https://doi.org/10.1038/ni.3212

Walker, F. C., Sridhar, P. R., & Baldridge, M. T. (2021). Differential roles of interferons in innate responses to mucosal viral infections. *Trends in Immunology*, *42*(11), 1009–1023. https://doi.org/10.1016/j.it.2021.09.003

Wang, B., Thurmond, S., Zhou, K., Sánchez-Aparicio, M. T., Fang, J., Lu, J., Gao, L., Ren, W., Cui, Y., Veit, E. C., Hong, H., Evans, M. J., O'Leary, S. E., García-Sastre, A., Zhou, Z. H., Hai, R., & Song, J. (2020). Structural basis for STAT2 suppression by flavivirus NS5. *Nature Structural & Molecular Biology*, *27*(10), 875–885. https://doi.org/10.1038/s41594-020-0472-y

Wang, P.-X., Zhang, R., Huang, L., Zhu, L.-H., Jiang, D.-S., Chen, H.-Z., Zhang, Y., Tian, S., Zhang, X.-F., Zhang, X.-D., Liu, D.-P., & Li, H. (2015). Interferon regulatory factor 9 is a key mediator of hepatic ischemia/reperfusion injury. *Journal of Hepatology*, *62*(1), 111–120. https://doi.org/10.1016/j.jhep.2014.08.022

Wang, R., Wang, J., Acharya, D., Paul, A. M., Bai, F., Huang, F., & Guo, Y.-L. (2014). Antiviral Responses in Mouse Embryonic Stem Cells: Implications for Targeting G4 DNA as a novel therapeutic approach*. *Journal of Biological Chemistry*, *289*(36), 25186–25198. https://doi.org/10.1074/jbc.M113.537746

Wang, W., Yin, Y., Xu, L., Su, J., Huang, F., Wang, Y., Boor, P. P. C., Chen, K., Wang, W., Cao, W., Zhou, X., Liu, P., van der Laan, L. J. W., Kwekkeboom, J., Peppelenbosch, M. P., & Pan, Q. (2017). Unphosphorylated ISGF3 drives constitutive expression of interferon-stimulated genes to protect against viral infections. *Science Signaling*, *10*(476), eaah4248. https://doi.org/10.1126/scisignal.aah4248

Wang, Y., Song, Q., Huang, W., Lin, Y., Wang, X., Wang, C., Willard, B., Zhao, C., Nan, J., Holvey-Bates, E., Wang, Z., Taylor, D., Yang, J., & Stark, G. R. (2021). A virus-induced conformational switch of STAT1-STAT2 dimers boosts antiviral defenses. *Cell Research*, *31*(2), 206–218. https://doi.org/10.1038/s41422-020-0386-6

Welsby, I., Hutin, D., Gueydan, C., Kruys, V., Rongvaux, A., & Leo, O. (2014). PARP12, an Interferon-stimulated Gene Involved in the Control of Protein Translation and Inflammation. *The Journal of Biological Chemistry*, *289*(38), 26642–26657. https://doi.org/10.1074/jbc.M114.589515

Wen, Z., Zhong, Z., & Darnell, J. E. (1995). Maximal activation of transcription by Stat1 and Stat3 requires both tyrosine and serine phosphorylation. *Cell*, *82*(2), 241–250. https://doi.org/10.1016/0092-8674(95)90311-9

Wienerroither, S., Shukla, P., Farlik, M., Majoros, A., Stych, B., Vogl, C., Cheon, H., Stark, G. R., Strobl, B., Müller, M., & Decker, T. (2015). Cooperative Transcriptional Activation of Antimicrobial Genes by STAT and NF-κB Pathways by Concerted Recruitment of the Mediator Complex. *Cell Reports*, *12*(2), 300–312. https://doi.org/10.1016/j.celrep.2015.06.021

Wong, L. H., Sim, H., Chatterjee-Kishore, M., Hatzinisiriou, I., Devenish, R. J., Stark, G., & Ralph, S. J. (2002). Isolation and characterization of a human STAT1 gene regulatory element. Inducibility by interferon (IFN) types I and II and role of IFN regulatory factor-1. *The Journal of Biological Chemistry*, *277*(22), 19408–19417. https://doi.org/10.1074/jbc.M111302200

Wu, M., Pei, Z., Long, G., Chen, H., Jia, Z., & Xia, W. (2023). Mitochondrial antiviral signaling protein: A potential therapeutic target in renal disease. *Frontiers in Immunology*, *14*, 1266461. https://doi.org/10.3389/fimmu.2023.1266461

Xie, D., Boyle, A. P., Wu, L., Zhai, J., Kawli, T., & Snyder, M. (2013). Dynamic trans-acting factor colocalization in human cells. *Cell*, *155*(3), 713–724. https://doi.org/10.1016/j.cell.2013.09.043

Xie, T., Feng, M., Dai, M., Mo, G., Ruan, Z., Wang, G., Shi, M., & Zhang, X. (2019). Cholesterol-25-hydroxylase Is a Chicken ISG That Restricts ALV-J Infection by Producing 25-hydroxycholesterol. *Viruses*, *11*(6), 498. https://doi.org/10.3390/v11060498

Xu, D., & Qu, C.-K. (2008). Protein tyrosine phosphatases in the JAK/STAT pathway. *Frontiers in Bioscience: A Journal and Virtual Library*, *13*, 4925–4932. https://doi.org/10.2741/3051

Xu, L., Zhou, X., Wang, W., Wang, Y., Yin, Y., Laan, L. J. W. van der, Sprengers, D., Metselaar, H. J., Peppelenbosch, M. P., & Pan, Q. (2016). IFN regulatory factor 1 restricts hepatitis E virus replication by activating STAT1 to induce antiviral IFN-stimulated genes. *FASEB Journal: Official Publication of the Federation of American Societies for Experimental Biology*, *30*(10), 3352–3367. https://doi.org/10.1096/fj.201600356R

Yamane, D., Feng, H., Rivera-Serrano, E. E., Selitsky, S. R., Hirai-Yuki, A., Das, A., McKnight, K. L., Misumi, I., Hensley, L., Lovell, W., González-López, O., Suzuki, R., Matsuda, M., Nakanishi, H., Ohto-Nakanishi, T., Hishiki, T., Wauthier, E., Oikawa, T., Morita, K., … Lemon, S. M. (2019). Basal expression of interferon regulatory factor 1 drives intrinsic hepatocyte resistance to multiple RNA viruses. *Nature Microbiology*, *4*(7), 1096–1104. https://doi.org/10.1038/s41564-019-0425-6

Yamauchi, S., Takeuchi, K., Chihara, K., Honjoh, C., Kato, Y., Yoshiki, H., Hotta, H., & Sada, K. (2016). STAT1 is essential for the inhibition of hepatitis C virus replication by interferon-λ but not by interferon-α. *Scientific Reports*, *6*, 38336. https://doi.org/10.1038/srep38336

Yang, E., Henriksen, M. A., Schaefer, O., Zakharova, N., & Darnell, J. E. (2002). Dissociation time from DNA determines transcriptional function in a STAT1 linker mutant. *The Journal of Biological Chemistry*, *277*(16), 13455–13462. https://doi.org/10.1074/jbc.M112038200

Yang, E., & Li, M. M. H. (2020). All About the RNA: Interferon-Stimulated Genes That Interfere With Viral RNA Processes. *Frontiers in Immunology*, *11*, 605024. https://doi.org/10.3389/fimmu.2020.605024

Yang, E., Wen, Z., Haspel, R. L., Zhang, J. J., & Darnell, J. E. (1999). The Linker Domain of Stat1 Is Required for Gamma Interferon-Driven Transcription. *Molecular and Cellular Biology*, *19*(7), 5106–5112.

Yang, R., Mele, F., Worley, L., Langlais, D., Rosain, J., Benhsaien, I., Elarabi, H., Croft, C. A., Doisne, J.-M., Zhang, P., Weisshaar, M., Jarrossay, D., Latorre, D., Shen, Y., Han, J., Ogishi, M., Gruber, C., Markle, J., Al Ali, F., … Casanova, J.-L. (2020). Human T-bet Governs Innate and Innate-like Adaptive IFN-γ Immunity against Mycobacteria. *Cell*, *183*(7), 1826-1847.e31. https://doi.org/10.1016/j.cell.2020.10.046

Yeh, T. C., & Pellegrini, S. (1999). The Janus kinase family of protein tyrosine kinases and their role in signaling. *Cellular and Molecular Life Sciences: CMLS*, *55*(12), 1523–1534. https://doi.org/10.1007/s000180050392

You, M., Yu, D.-H., & Feng, G.-S. (1999). Shp-2 Tyrosine Phosphatase Functions as a Negative Regulator of the Interferon-Stimulated Jak/STAT Pathway. *Molecular and Cellular Biology*, *19*(3), 2416–2424.

Yu, G., Wang, L.-G., Han, Y., & He, Q.-Y. (2012). clusterProfiler: An R package for comparing biological themes among gene clusters. *Omics: A Journal of Integrative Biology*, *16*(5), 284–287. https://doi.org/10.1089/omi.2011.0118

Yuasa, K., & Hijikata, T. (2016). Distal regulatory element of the STAT1 gene potentially mediates positive feedback control of STAT1 expression. *Genes to Cells: Devoted to Molecular & Cellular Mechanisms*, *21*(1), 25–40. https://doi.org/10.1111/gtc.12316

Yuasa, K., Takeda, S., & Hijikata, T. (2012). A conserved regulatory element located far downstream of the gls locus modulates gls expression through chromatin loop formation during myogenesis. *FEBS Letters*, *586*(19), 3464–3470. https://doi.org/10.1016/j.febslet.2012.07.074

Zhang, R., Chen, K., Peng, L., & Xiong, H. (2012). Regulation of T helper cell differentiation by interferon regulatory factor family members. *Immunologic Research*, *54*(1–3), 169–176. https://doi.org/10.1007/s12026-012-8328-0

Zhang, R., Li, Z., Tang, Y.-D., Su, C., & Zheng, C. (2021). When human guanylate-binding proteins meet viral infections. *Journal of Biomedical Science*, *28*, 17. https://doi.org/10.1186/s12929-021-00716-8

Zhang, S.-M., Zhu, L.-H., Chen, H.-Z., Zhang, R., Zhang, P., Jiang, D.-S., Gao, L., Tian, S., Wang, L., Zhang, Y., Wang, P.-X., Zhang, X.-F., Zhang, X.-D., Liu, D.-P., & Li, H. (2014). Interferon regulatory factor 9 is critical for neointima formation following vascular injury. *Nature Communications*, *5*, 5160. https://doi.org/10.1038/ncomms6160

Zhang, T., Kee, W. H., Seow, K. T., Fung, W., & Cao, X. (2000). The coiled-coil domain of Stat3 is essential for its SH2 domain-mediated receptor binding and subsequent activation induced by epidermal growth factor and interleukin-6. *Molecular and Cellular Biology*, *20*(19), 7132–7139. https://doi.org/10.1128/MCB.20.19.7132-7139.2000

Zheng, H., Qian, J., Varghese, B., Baker, D. P., & Fuchs, S. (2011). Ligand-Stimulated Downregulation of the Alpha Interferon Receptor: Role of Protein Kinase D2. *Molecular and Cellular Biology*, *31*(4), 710–720. https://doi.org/10.1128/MCB.01154-10

Zhong, M., Henriksen, M. A., Takeuchi, K., Schaefer, O., Liu, B., ten Hoeve, J., Ren, Z., Mao, X., Chen, X., Shuai, K., & Darnell, J. E. (2005). Implications of an antiparallel dimeric structure of nonphosphorylated STAT1 for the activation-inactivation cycle. *Proceedings of the National Academy of Sciences of the United States of America*, *102*(11), 3966–3971. https://doi.org/10.1073/pnas.0501063102

Zhou, D., Chen, L., Yang, K., Jiang, H., Xu, W., & Luan, J. (2017). SOCS molecules: The growing players in macrophage polarization and function. *Oncotarget*, *8*(36), 60710–60722. https://doi.org/10.18632/oncotarget.19940

Zhou, M.-J., Chen, F.-Z., Chen, H.-C., Wan, X.-X., Zhou, X., Fang, Q., & Zhang, D.-Z. (2017). ISG15 inhibits cancer cell growth and promotes apoptosis. *International Journal of Molecular Medicine*, *39*(2), 446–452. https://doi.org/10.3892/ijmm.2016.2845

List of Figures

(Introduction)

(Material and Method)

(Results)

(Discussion)

Supplementary Figures

List of Tables

(Introduction)

(Material and Method)

(Results)

Supplementary Tables

Supplementary material

		IFNα								IFNγ									
				Log2FC/per Time point								Log2FC/per Time point							
Nr	Gene	Peak score	padj	2h	4h	8h	24h	48h	72h	Peak score	padj	2h	4h	8h	24h	48h	72h	ISRE	GAS
1	ACY3	583.64	4.17E-10	0.16	0.99	2.09	1.22	1.3	1.59	614.97	1.44E-64	0.39	1.7	2.91	3.49	3.04	2.43	GC-TTT-CGG-TTT-CT	TTC-CCT-GAA-G
2	ANXA2R	606.3	1.44E-07	2.13	2.76	1.58	0.8	0.73	0.81	643.86	2.69E-08	2.34	2.77	2.5	1.61	1.24	1.17	GG-TTT-CT-TTT-CT	AT-TTC-CCG-GAA-A
3	APOL1	172.86	3.05E-129	3.15	7.62	9.4	6.14	5.37	5.54	374.23	1.30E-295	3.58	6.61	8.78	10.14	9.83	9.19	AC-TTT-CAC-TTT-C	GC-TGC-TGG-GAA-G
4	APOL2	633.78	1.11E-167	1.2	3.49	3.28	1.52	1.41	1.42	582.04	0	1.07	3.01	3.42	2.73	2.17	1.64	AC-TTTCACTTTCC	TGC-TGG-GAA-G
5	APOL6	768.04	1.43E-233	3.83	5.55	4.76	3.05	2.68	2.87	765.08	5.89E-115	3.45	4.89	5.1	4.77	4.24	3.61	AC-TTT-CAG-TTT-CC	TTC-CTG-GAA-G
6	BCL2L14	133.65	5.47E-04	0.08	2.09	1.75	1.03	0.82	0.44	190.65	2.63E-02	0.67	1.15	2	1.26	0.79	0.1	GG-TTT-CTC-TTT-C	GT-TTC-CAG-GAA-A
7	C1R	111.96	2.44E-09	0.32	0.84	1.23	0.8	0.43	0.53	113.29	0	0.49	1.22	2.25	3.41	3.72	3.41	AG-TTT-TGG-TTT-T	TTC-CCG-GAG-GA
8	C1RL	471.11	0.00028	0.43	0.6	0.43	0.22	0.18	0.4	519	0.00000	0.36	0.62	0.7	0.7	0.73	0.55	CC-TTT-CTC-TTC-C	AT-TTC-CAG-GAA-C
9	C2	465.59	3.17E-13	0.21	0.54	0.56	0.27	-0.04	-0.01	529.87	8.82E-27	0.16	0.38	0.68	0.96	1.1	0.87	GG-TTT-TAC-TTC-C	ATT-TTC-GG-GAA-GT
10	CASP1	144.77	2.25E-44	2.5	4.77	6.47	3.48	2.71	2.66	212.44	2.50E-105	1.21	3.87	5.98	7.2	6.64	6.03	AC-TTT-CAG-TTT-C	TG-TTC-CAA-GAA-C
11	CASP8	272.45	6.78E-65	0.18	1.31	1.7	0.67	0.71	0.65	235.52	1.47E-52	0.2	1.19	1.52	1.23	0.88	0.81	GG-TTT-CTG-TTT-C	TT-TTC-CAA-GAA-G
12	CD274	507.55	1.74E-129	2.81	6.72	3.96	1.45	0.99	1.8	471.97	3.84E-65	3.25	5.46	5.78	5.2	4	2.98	AC-TTT-CTG-TTT-CA	TTC-ACC-GAA
13	CFB	458.47	3.47E-08	1.05	1.64	1.16	0.95	0.75	0.51	451.33	1.53E-02	0.74	1.04	1.06	0.92	0.93	0.78	AG-TTT-CTG-TTT-C	ATG-TTC-CGG-GAA-A
14	CSF1	549.3	2.63E-121	2.26	2.72	1.4	1.06	1.11	1.36	568.64	1.60E-31	2.24	2.43	2.36	2.14	1.86	1.45	AC-TTT-CAC-TTT-CC	TTC-CCA-TAA-A
15	CTSO	117.95	3.78E-21	0.17	0.86	1.17	0.27	-0.1	-0.21	141.95	9.59E-38	0.24	1.01	1.76	1.5	0.98	0.56	TC-TTT-CGG-TTC-C	C-TTC-CGG-GTA
16	CXCL10	259.84	2.49E-52	1.12	3.57	5.24	1.8	0.9	1.38	82.75	2.93E-107	2.55	4.47	6.08	5.75	5.04	4.2	GG-TTT-CAC-TTT-CC	TTC-AA-GAA-A
17	DDX58	720.61	0	1.71	4.42	4.76	3.54	3.38	3.41	394.67	4.19E-16	0.19	1.31	1.63	1.18	1.04	0.82	AG-TTT-CG-TTT-CC	TTC-CTA-TAA-A
18	DDX60	731.65	0	-0.43	7.3	9.5	8.71	8.87	8.96	485.97	1.27E-36	0.26	3.76	6.13	7.3	7.03	6.19	GG-TTT-CAG-TTT-CC/AG-TTT-CGG-TTT-CC	TTC-CAC-GAA-A

19	DTX3L	749.38	0	2.83	4.2	4.03	3.31	3.17	3.28	797.82	4.61E-95	2.05	3.45	3.69	3.35	2.86	2.36	AG-TTT-CGC-TT-CC	TGC-CGG-GAA
20	EPSTI1	412.54	5.10E-96	0	8.15	10.21	8.2	7.98	8.3	162.07	7.36E-46	0	3.55	7.24	8.84	8.31	7.41	AG-TTT-CGG-TTT-CT	TTC-TGA-GAA-A
21	ETV6	250.37	4.29E-24	0.29	1.19	0.95	-0.14	-0.1	0.09	295.4	9.49E-10	-0.01	0.59	0.92	0.3	0.11	-0.06	CC-TTT-CAG-TTT-C	TC-TTC-CAG-GAA-G
22	ETV7	304.54	3.40E-32	1.99	6.23	6.83	2.6	1.35	0.81	620.73	1.01E-43	3.69	6.63	7.81	7.49	6.72	5.23	TC-TTT-CGT-TTT-CG	TTC-CCG-GAA-G
23	GBP3	259.61	1.35E-25	0.58	4.68	6.21	3.19	3.29	3.2	297.92	1.05E-68	2	4.75	6.95	8.27	7.56	6.9	AC-TTT-CAG-TTT-CA	TTC-CTT-GAA-A
24	GSDMD	306.07	1.48E-25	0.22	0.66	0.97	0.32	0.29	0.25	188.36	2.48E-29	0.21	0.64	0.95	0.98	0.77	0.5	AG-TTT-CAC-TTT-T	TTC-CGG-GAG-G
25	IFI35	344.97	1.30E-57	0.5	2.3	3.61	2.07	2.05	1.91	244.5	4.44E-64	0.15	1.35	2.49	3.55	3	2.24	AC-TTT-CA-TTT-CC	TTC-ACGAA-A
26	IFI6	740.13	0	3.39	7.54	9.43	10.51	11.14	11.34	384.84	1.27E-145	0.14	0.84	2.79	5.51	6.88	6.94	AG-TTT-CAT-TTT-C	TC-TGC-CTG-TAAA
27	IFIT3	686.16	9.60E-199	3.59	7.31	6.7	5.12	4.77	4.99	496.35	4.95E-74	2.34	4.35	5.08	4.9	4.3	3.54	GG-TTT-CAT-TTT-C	T-TTC-TTG-TAA-TT
28	IFIT5	645.53	3.47E-297	1.8	4.27	3.57	3	2.81	2.83	283.61	6.62E-62	0.78	2.16	2.05	1.66	1.33	0.93	AG-TTT-CGG-TTT-C	C-TTC-TCG-GCA-GC
29	IFITM3	700.62	0	1.54	3.74	5.13	5.64	5.77	5.88	275.15	0	0.16	1.25	2.7	4.12	4.04	3.29	AG-TTT-CGG-TTT-CT	TGC-CAG-GAA-A
30	IL15	354.23	3.31E-11	0.25	2.49	2.37	0.67	0.36	0.65	332.93	8.68E-23	0.48	2.86	3.32	2.94	2.47	2.19	TC-TTT-CTC-TTT-C	TT-TTC-CCC-GAA-A
31	IRF1	718.52	0	4.37	4.08	1.67	0.96	0.91	1.11	746.97	2.70E-156	5.35	5.37	5.21	4.59	3.97	3.19	GG-TTT-CGG-TTT-CT	TTC-CCC-GAA/ TTC-CCG-GAA-A/ TTC-GCG-GAA-A/ TTC-CAG-GAA-G
32	IRF2	497.96	4.89E-12	0.65	1.62	1.28	0.67	0.56	0.6	482.1	6.23E-08	0.74	1.23	1.36	1.25	1.07	0.9	AA-TTT-CAT-TTT-CG	TTC-CGA-GAA-A
33	IRF9	793.34	3.99E-25	3.91	4.23	3.7	3.7	3.62	3.64	805.53	4.66E-12	3.05	3.31	3.32	3.43	3.1	2.89	AG-TTT-CAG-TT-CT	TTC-TGG-GAA-A
34	ISG15	848.96	0	2.76	5.79	7.29	7.31	7.29	7.14	581.56	6.58E-91	0.37	1.48	2.74	3.83	3.27	2.42	AG-TTT-CGG-TTT-C	CC-TTC-TAG-TAA-C
35	ISG20	501.01	4.32E-146	0.08	1.91	2.96	1.46	1.6	1.57	260.17	5.04E-93	0.16	0.78	1.65	2.13	1.75	1.24	C-TTT-GAC-TTT-GT	CA-TTC-CAA-TAA-A
36	LGALS3BP	488.83	0	0.33	3.09	5.24	5.67	5.85	6.07	277.08	0	0.38	1.43	3.26	5.12	5.73	5.58	AC-TTT-CGA-TTT-CC	TTC-TG-GAA-A
37	MDK	242.77	5.01E-20	0.05	0.15	0.39	0.48	0.6	0.7	136.09	3.37E-108	0.07	0.09	0.21	0.74	1.06	1.02	C-TTT-CAC-TTT-CT	T-TTG-GGG-GAA-CC
38	MX1	783.98	0	4.8	8.41	9.91	9.67	9.6	9.59	267.45	0	0.67	3.04	4.97	5.52	5.37	4.9	GG-TTT-CA-TTT-CT	T-TTC-TG-GAA-ACC
39	MYD88	765.34	9.09E-234	0.69	2.05	2.47	1.11	0.9	0.79	520.74	1.82E-32	0.39	0.77	1.03	0.86	0.64	0.38	GC-TTT-CGC-TTT-CC	TTC-TCG-GAA-A

40	NLRC5	662.85	0	7.62	10.73	11.66	7.18	6.97	6.86	725.89	0	8.08	11.4	12.53	12.23	11.92	11.26	AC-TTT-CAG-TTT-CG	TTC-TCG-GCA-G
41	NMI	653.92	7.42E-222	0.82	2.6	3.16	1.29	1.22	1.21	473.37	3.71E-149	0.75	2.33	3	2.72	2.29	1.85	AA-TTT-CAC-TTT-CG/TG-TTT-CAA-TTT-CC	TTC-CGG-GAA-G
42	OAS3	741.03	0	3.35	8.14	10.18	9.95	10.1	10.29	434.03	1.43E-25	-0.72	2.33	4.18	5.69	5.77	5.66	GG-TTT-GCT-TTT-C	TTC-CAA-TAA-AA
43	PARP14	761.94	0	1.53	5.05	6.22	4.24	3.9	4.02	676.01	3.15E-143	0.69	3.73	5.05	4.78	4.04	3.28	GC-TTT-CG-TTT-CC/TC-TTT-CGC-TTT-CG	TTC-CAG-GAA-A
44	PHF11	569.65	1.87E-35	0.47	1.5	2.05	1.11	1.04	1.13	78.94	5.52E-12	0.33	0.95	1.16	1.23	0.91	0.67	GG-TTT-CGT-TTT-CT	TTC-CGG-GAT
45	PLSCR1	794.7	0	1.53	3.33	4.14	3.45	3.34	3.42	430.99	1.76E-44	0.41	1.27	1.82	1.48	0.81	0.58	GG-TTT-CG-TTT-CC	TTC-TGA-GAA-G
46	PRKD2	552.94	5.98E-169	0.07	2	2.52	1.08	1.03	0.92	381.82	6.80E-31	-0.11	0.67	1.19	0.98	0.73	0.55	AG-TTT-CAC-TTT-C	C-TTC-CTG-GAT
47	RTP4	435.11	1.76E-34	2.57	7.26	6.91	3.91	3.99	4.33	228.83	9.95E-15	-1.42	4.64	5.74	5.64	5.07	3.97	AG-TTT-CTG-TTT-C	TC-TTC-TGA-GAA-G
48	RNF213	651.7	5.02E-151	0.01	0.56	2.47	1.47	1.17	1.31	320.87	1.12E-52	-0.19	0.05	0.66	0.96	0.7	0.51	GA-TTT-CAC-TTT-C	CCC-TTC-CAG-GAA
49	SAMD9	565.55	1.22E-235	4.22	9.5	10.45	8.75	8.89	9	206.58	6.43E-13	1.97	3.94	5.82	5.93	5.36	5.06	AG-TTT-CA-TTT-CT	GTT-TTC-CCC-ACA
50	SP110	798.13	1.53E-229	1.4	5.11	6.33	4.85	4.84	4.92	361.29	3.60E-54	0.62	2.64	4.02	3.65	2.85	2.44	AC-TTT-CAC-TTT-TC	TTC-TCG-GAA-G
51	SP140L	435.11	4.86E-20	-0.1	0.87	1.44	0.43	0.67	0.72	202.48	1.30E-14	-0.2	0.37	1.01	1.08	0.87	0.74	AC-TTT-CAC-TTT-T	C-TCC-CG-GAAG
52	STAT1	747.18	0	1.84	3.17	3.87	3.18	3.13	3.11	717.57	5.06E-100	2.01	3.08	3.75	3.51	3.13	2.65	AG-TTT-CGC-TTT-CC/ AC-TTT-CGC-TTTT	TTC-CCC-GAA-A
53	STAT2	703.23	9.07E-137	1.45	2.92	3.39	1.61	1.33	1.33	655.11	2.08E-125	0.55	1.6	2.22	1.99	1.54	1.05	AG-TTT-CGG-TT-CC	TTC-TC-GAA-A
54	STX17	417.61	1.4E-15	-0.14	0.41	0.76	0.26	0.1	0.18	205.5	2.42E-10	-0.14	0.3	0.57	0.55	0.3	0.35	GG-TTT-CGT-TTT-T	CT-TTA-TTG-GAA-GCT
55	TRIM22	507.77	1.58E-78	0.74	3.65	6.06	2.69	1.98	2.31	178.96	4.96E-11	0.79	1.04	2.57	3.57	3.41	2.27	AC-TTT-CG-TTT-CT	TTC-TGA-GAA-T
56	TMEM140	751	5.41E-66	0.5	1.41	1.04	0.26	0.19	0.29	676.69	3.77E-29	0.19	0.87	0.94	0.42	0.18	-0.01	AC-TTT-CG-TTT-CC	TTC-TG-GAA
57	USP18	806.57	0	0.34	3.19	4.46	3.12	3.08	3.14	459.62	1.01E-08	0	0.51	0.78	0.88	0.75	0.51	AG-TTT-CGC-TTT-CC	TTC-CCC-GCA
58	ZC3HAV1	675.38	0	1.73	3.68	1.64	1.45	1.33	1.32	594.99	0	1.08	2.55	2.24	1.39	1.09	0.97	GC-TTT-TAG-TTT-C	CT-TTC-CGG-GAA-T
59	ZNFX1	148.65	6.15E-116	1.62	3.48	2.54	1.83	1.64	1.76	492.67	9.12E-72	0.8	1.65	1.59	1.42	1.11	0.77	AC-TTT-CGG-TTT-C	CTC-TGC-CCG-TAA-G
60	NAPA	770.57	9.94E-55	0.17	0.64	1.07	0.51	0.36	0.34	644.15	1.95E-11	0.07	0.14	0.22	0.15	0.17	0.06	GG-TTT-CCT-TTT-C	AA-TTC-CGG-GAA-G
61	OSMR	505.03	1.52E-38	0.8	1.22	0.82	0.51	0.45	0.51	394.85	2.47E-04	0	0.18	0.23	0.24	0.13	0.13	GT-TTT-CGG-TTT-C	TT-TTC-CAG-TAA-C

62	RIPK1	246.02	1.85E-11	0.5	0.74	0.36	0.04	0	0.06	333.92	0.00147	0.28	0.49	0.45	0.18	0.07	0.05	AC-TTT-CG-TTT-CC	GC-TTC-CCG-GAA-G
63	C5	215.5	1.76E-13	0.27	0.5	0.55	0.37	0.19	0.34	212.76	0.00000	0.02	0.09	0.15	0.25	0.05	0.07	TG-TTT-TAG-TTC-C	AG-TTC-CTG-TAA-A
64	PNPT1	789.76	0	0.05	1.25	2.42	1.36	1.2	1.18	114.03	2.84E-04	0	0.04	0.16	0.26	0.19	0.1	AG-TTT-CG-TTT-CC	T-TTA-CTG-TAA-AT
65	HDAC9	438.98	5.00E-02	0.28	0.75	1.03	1.08	0.94	1.05	394.93	NE	NE	NE	NE	NE	NE	NE	AG-TTT-CTC-TTT-CC	TCT-TTC-TCA-GAA-AC
66	HERC5	751.44	0	0.22	5.46	7.74	5.23	5.17	5.38	193.82	NE	NE	NE	NE	NE	NE	NE	TG-TTT-CG-TTT-TC	GT-TTC-CTC-GAA-A
67	IFI27	321.63	1.66E-63	0.72	2.72	4.65	5.06	5.08	5.45	179.14	NE	NE	NE	NE	NE	NE	NE	AG-TTT-CGG-TTT-C	GT-TTC-CTG-GAA-A
68	IFI44	426.66	5.05E-125	0	7.54	10.26	9.47	9.32	9.91	104.38	NE	NE	NE	NE	NE	NE	NE	AG-TTT-CAG-TTT-C	AT-TTA-TAG-TAA-A
69	RASGRP3	401.83	1.69E-28	-0.27	1.75	2.3	0.87	1.01	1.05	200.65	NE	NE	NE	NE	NE	NE	NE	GG-TTT-GC-TTT-TC	GA-TTC-TGA-GAA-A
70	RSAD2	702.97	7.48E-226	2.59	9.86	11.48	8.05	7.72	8.03	203.57	NE	NE	NE	NE	NE	NE	NE	AC-TTT-CAG-TTT-C	TTT-TGC-TGG-GAA-G
71	ZNF107	476.64	8.20E-35	0.13	1.88	1.46	0.64	0.5	0.51	84	NE	NE	NE	NE	NE	NE	NE	GG-TTT-CAC-TTT-A	C-TTC-CGG-GAT
72	EDEM2	452.19	1.88E-16	0	0.06	0.27	0.35	0.63	0.72	547.89	NE	NE	NE	NE	NE	NE	NE	CC-TCT-CAC-TTC-C	GA-TTC-CCG-GAA-G
73	FMR1	370.19	4.72E-14	0.01	0.42	0.66	0.1	0.07	0.02	177.21	NE	NE	NE	NE	NE	NE	NE	CG-TTT-CGG-TTT-C	TTC-CCA-GCA-G
74	BTC	124.32	1.45E-05	0.24	1.12	1.96	1.17	0.73	1.06	NB	NE	NE	NE	NE	NE	NE	NE	AG-TTT-CG-TTT-CC	TTC-CAG-GCA-C
75	CAVIN2	220.56	7.14E-34	-0.58	1.17	0.63	0.46	0.25	0.33	NB	NE	NE	NE	NE	NE	NE	NE	TG-TTT-CTT-TTT-C	GT-ATC-CAG-GAA-A
76	IFIH1	691.96	0	5.37	9.85	10.72	8.97	8.82	9	NB	NE	NE	NE	NE	NE	NE	NE	GG-TTT-CTG-TTT-C	CTGCTGGGAA
77	IFITM1	334.72	2.65E-37	0	5.8	8.82	7.51	5.12	4.69	NB	NE	NE	NE	NE	NE	NE	NE	CG-TTT-CAG-TTT-C	AC-TTC-TGA-GAA-A
78	LAMP3	160.63	3.52E-51	4.39	6.66	9.51	5.54	5.11	4.69	NB	NE	NE	NE	NE	NE	NE	NE	GG-TTT-CG-TTT-CT	GC-TTC-TCA-TAA-G
79	PML	531.07	2.22E-282	1.43	3.85	3.74	2.46	2.21	2.16	NB	NE	NE	NE	NE	NE	NE	NE	AG-TTT-CGA-TTC-T	T-TTA-CCG-TAA-GT
80	TRIM5	608.79	2.72E-72	0.02	1.01	1.64	0.82	0.79	0.72	NB	NE	NE	NE	NE	NE	NE	NE	TC-TTT-CAC-TTT-C	TGT-TTC-CC-GAA-G
81	TRIP12	462.02	1.55E-17	0.06	0.27	0.52	0.2	0.08	0.11	NB	NE	NE	NE	NE	NE	NE	NE	AG-TTT-CCA-TTT-C	TTC-CGG-GGA-ACC
82	INTS12	303.99	1.38E-03	0.02	0.63	0.59	0.13	0.02	0.11	NB	NE	NE	NE	NE	NE	NE	NE	AG-TTT-CTG-TTT-C	C-TTC-CAA-TAA-AC
83	KBTBD2	191.5	1.54E-07	0.17	0.54	0.14	0	-0.02	0.04	NB	NE	NE	NE	NE	NE	NE	NE	TC-TTT-CCG-TTT-C	CGC-TTC-CCG-TCA-C

84	LRP10	183.93	3.28E-35	0.32	0.62	0.87	0.76	0.9	0.9	NB	NE	NE	NE	NE	NE	NE	NE	AG-TTT-CAG-TTT-G	AT-TTC-CTG-GAG-GT
85	CHMP5	261.51	1.72E-16	0.05	0.38	0.8	0.33	0.2	0.09	NB	NE	NE	NE	NE	NE	NE	NE	GG-TTT-CGC-TTT-C	C-TTC-GG-GAA-AGC
86	WARS1	202.87	3.36E-06	0.1	0.33	0.48	0.01	0.2	0.2	687.81	2.44E-291	0.24	1.28	2.54	2.19	1.2	0.65	TC-TTT-CAG-TTT-C	GT-TTC-TGA-GAA-T
87	COQ8B	315.01	0.50547	0.26	0.32	0.24	0.06	0.08	0	520.53	7.57E-06	0.39	0.81	0.92	0.33	0.31	0.06	AG-TCT-CTG-TTC-C	CAT-TTC-CCA-GAA-C
88	MVB12A	671.58	0.00087	0.02	0.3	0.19	0.24	0.35	0.48	572.56	4.97E-12	0	0.14	0.01	0.49	0.85	0.73	GT-TTT-CAG-TTT-C	AGT-TTC-CCA-GAA-A
89	CARD16	137.17	NE	NE	NE	NE	NE	NE	NE	170.25	2.37E-09	-3.76	1.73	2.02	3.32	3	3.02	AC-TTT-CAG-TTT-C	TG-TTC-CAA-GAA-C

Table S1. List of 89 IFNα and/or IFNγ induced ISRE+GAS-composite genes.

The ISRE+GAS composite genes were categorized into distinct groups according to their peak scores>100, padj values <0.05, and Log2FC >0.5 observed at least in one time point in response to IFNα and/or IFNγ. Genes highlighted in pink represent those exhibiting peak scores, padj <0.05, and Log2FC >0.5 at least in one time point in response to both IFNα and IFNγ. Genes highlighted in green represent those genes showing peak scores and padj values <0.05 and Log2FC >0.5 at least in one time point in response to IFNα. Blue-highlighted genes are characterized by the absence of padj values <0.05 and Log2FC >0.5 in response to IFNγ. Genes shown in yellow denote those lacking peak scores, padj values <0.05, and Log2FC >0.5 in response to IFNγ. Orange-highlighted genes indicate those exhibiting peak scores, padj <0.05, and Log2FC >0.5 at least in one time point only in response IFNγ. Finally, genes highlighted in red lack padj values <0.05 and Log2FC >0.5 in response to IFNα. Genes in the pink panel are common IFNα/IFNγ induced genes. Genes in the green, blue, and yellow panels are classified as IFNα-induced genes, while those in the orange and red panels are identified as IFNγ-induced genes. Genes marked in red in the pink panel are the 30 pre-selected composite genes for the further characterization. NB: No Binding , NE: No Expression


Consensus Coverage
A
APOL6
ISRE
GAS
pxPG (digested by SmaI) - Apol6 (2) (Gibson/Homology Cloning ligation product)
REV P_APOL6_C6_WT_H01_2021-12-04_B.ab1
B
DDX60
GAS
ISRE(1)
ISRE(2)
pXPG (digested by SmaI) - DDX60_PROMOTER REGION Copy (digested by NcoI, XhoI) ...
REV DDX60_WT_C8_C06_2022-03-18_B.ab1
C
NLRC5
GAS
ISRE
pxPG (digested by SmaI) - NLRC5_4th attempt (Gibson/Homology Cloning ligation pro...
REV NLRC5_4thattempt_C2_G08_2023-03-03_D.ab1
D(I)
DDX58
ISRE
pXPG (digested by SmaI) - DDX58_promoter region (Gibson/Homology Cloning ligatio...
REV DDX58_WT_C2_A06_2022-04-21_B.ab1
D(II)
DDX58
GAS
pXPG (digested by SmaI) - DDX58_promoter region (Gibson/Homology Cloning ligatio...
REV DDX58_WT_C2_A06_2022-04-21_B.ab1
E(I)
NMI
ISRE(1)
pXPG (digested by SmaI) - NMI (reversed) (digested by NcoI, Bsp19I, XhoI, PaeR7I, Sfr...
REV p-NMI-C6-WT_5.11_H06_2021-11-26_B.ab1
E(II)
NMI
GAS
pXPG (digested by SmaI) - NMI (reversed) (digested by NcoI, Bsp19I, XhoI, PaeR7I, Sfr...
REV p-NMI-C6-WT_5.11_H06_2021-11-26_B.ab1
E(III)
NMI
ISRE(2)
pXPG (digested by SmaI) - NMI (reversed) (digested by NcoI, Bsp19I, XhoI, PaeR7I, Sfr...
REV p-NMI-C6-WT_5.11_H06_2021-11-26_B.ab1

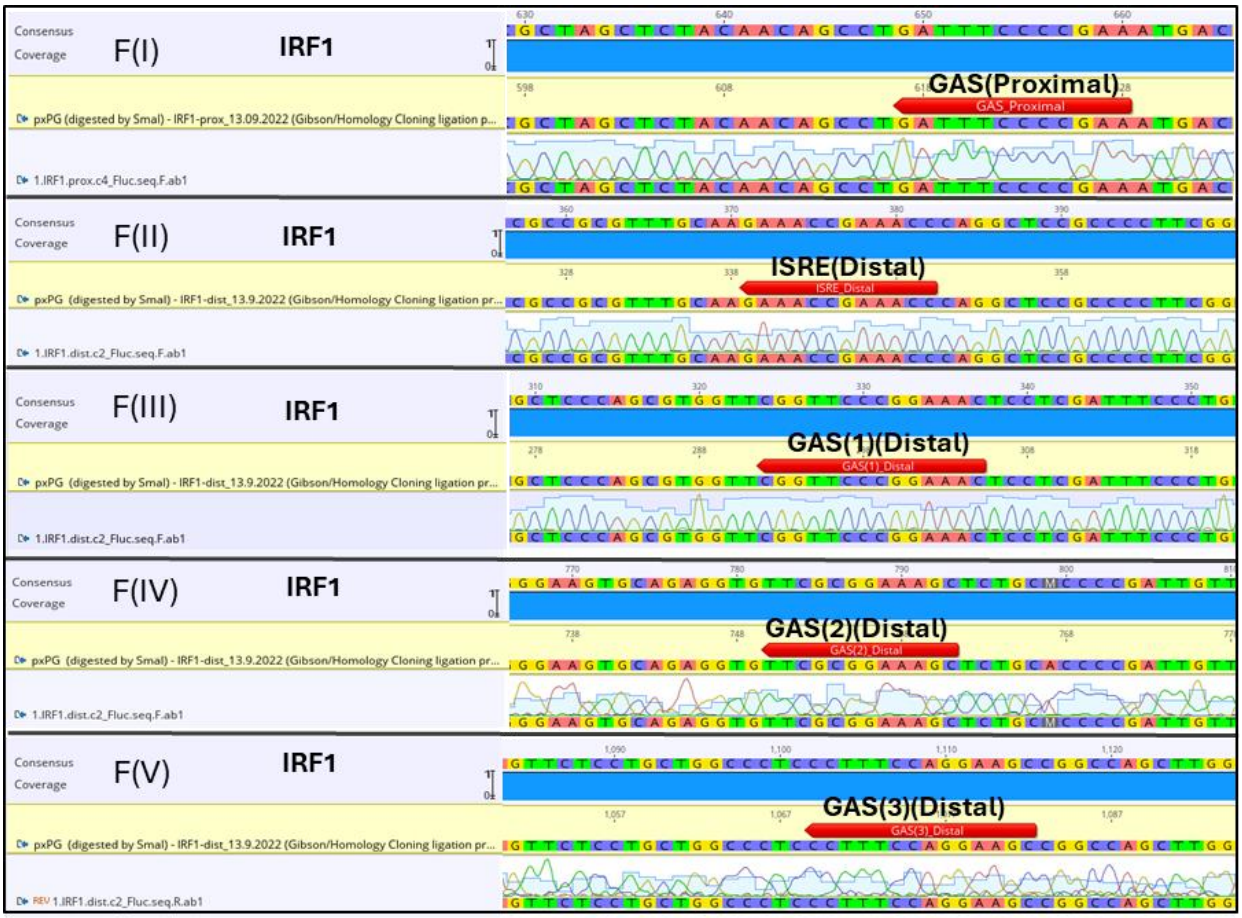

Figure S1. A data snapshot from the Geneious Prime program displaying wild-type ISRE and GAS motifs within promoter fragments. The Sanger sequencing outcome underwent a comparison with constructs generated in- silico.

The red boxes indicate ISRE or GAS motifs in the in-silico model. Confirmation via Sanger sequencing of the successful integration of wild-type (WT) promoters were achieved for APOL6 (A), DDX60 (B), NLRC5 (C), DDX58 with (DI-DII), NMI (EI, EII and EIII), along with IRF1(FI,FII, FIII, FIV and FV)

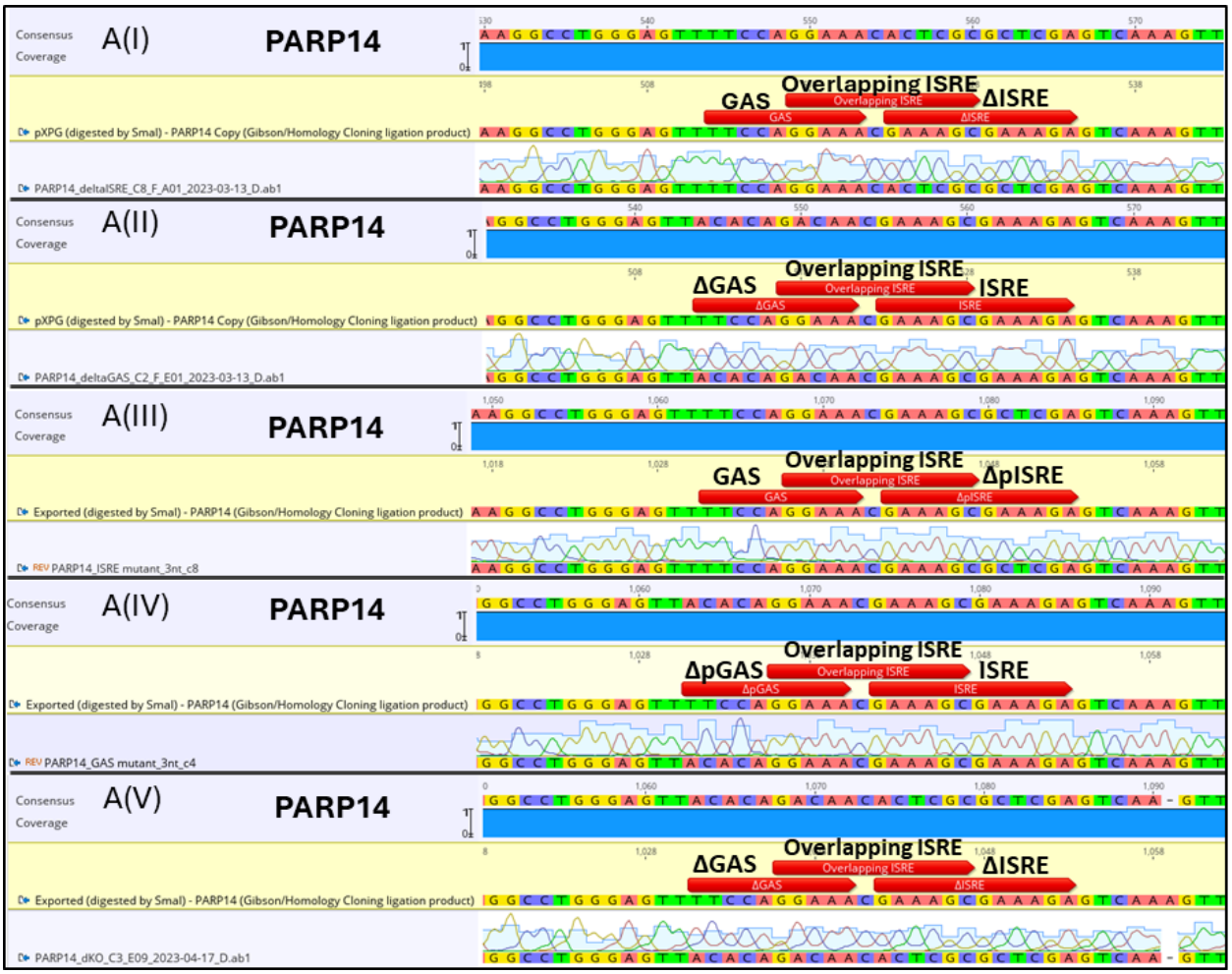
Consensus
Coverage
A(I)
PARP14
Overlapping ISRE
GAS
ΔISRE
pXPG (digested by SmaI) - PARP14 Copy (Gibson/Homology Cloning ligation product)
PARP14_deltaISRE_C8_F_A01_2023-03-13_D.ab1
A(II)
PARP14
ΔGAS
Overlapping ISRE
ISRE
pXPG (digested by SmaI) - PARP14 Copy (Gibson/Homology Cloning ligation product)
PARP14_deltaGAS_C2_F_E01_2023-03-13_D.ab1
A(III)
PARP14
GAS
Overlapping ISRE
ΔpISRE
Exported (digested by SmaI) - PARP14 (Gibson/Homology Cloning ligation product)
REV PARP14_ISRE mutant_3nt_c8
A(IV)
PARP14
ΔpGAS
Overlapping ISRE
ISRE
Exported (digested by SmaI) - PARP14 (Gibson/Homology Cloning ligation product)
REV PARP14_GAS mutant_3nt_c4
A(V)
PARP14
ΔGAS
Overlapping ISRE
ΔISRE
Exported (digested by SmaI) - PARP14 (Gibson/Homology Cloning ligation product)
PARP14_dKO_C3_E09_2023-04-17_D.ab1

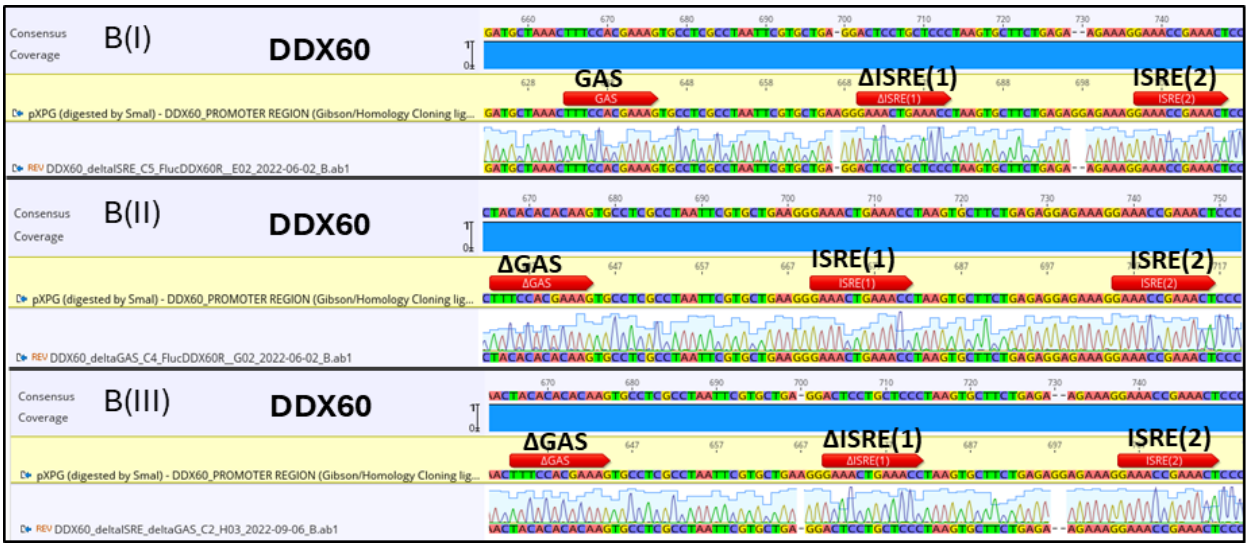
Consensus
Coverage
B(I)
DDX60
GAS
ΔISRE(1)
ISRE(2)
pXPG (digested by SmaI) - DDX60_PROMOTER REGION (Gibson/Homology Cloning lig...
REV DDX60_deltaISRE_C5_FlucDDX60R__E02_2022-06-02_B.ab1
B(II)
DDX60
ΔGAS
ISRE(1)
ISRE(2)
pXPG (digested by SmaI) - DDX60_PROMOTER REGION (Gibson/Homology Cloning lig...
REV DDX60_deltaGAS_C4_FlucDDX60R__G02_2022-06-02_B.ab1
B(III)
DDX60
ΔGAS
ΔISRE(1)
ISRE(2)
pXPG (digested by SmaI) - DDX60_PROMOTER REGION (Gibson/Homology Cloning lig...
REV DDX60_deltaISRE_deltaGAS_C2_H03_2022-09-06_B.ab1

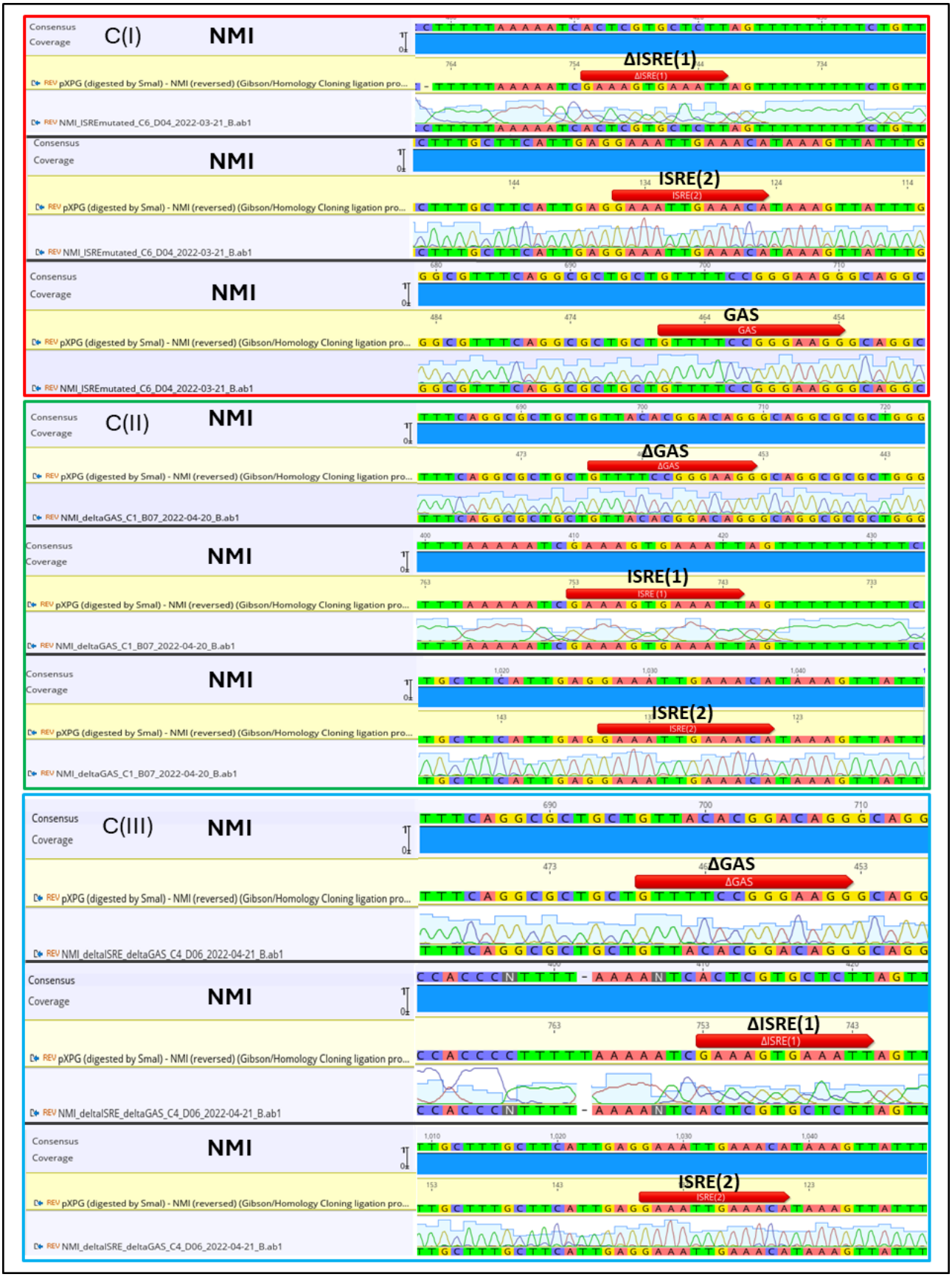
C(I)
NMI
ΔISRE(1)
ISRE(2)
GAS
C(II)
ΔGAS
ISRE(1)
ISRE(2)
C(III)
ΔGAS
ΔISRE(1)
ISRE(2)
Consensus
Coverage
pXPG (digested by SmaI) - NMI (reversed) (Gibson/Homology Cloning ligation pro...
NMI_ISREmutated_C6_D04_2022-03-21_B.ab1
NMI_deltaGAS_C1_B07_2022-04-20_B.ab1
NMI_deltaISRE_deltaGAS_C4_D06_2022-04-21_B.ab1

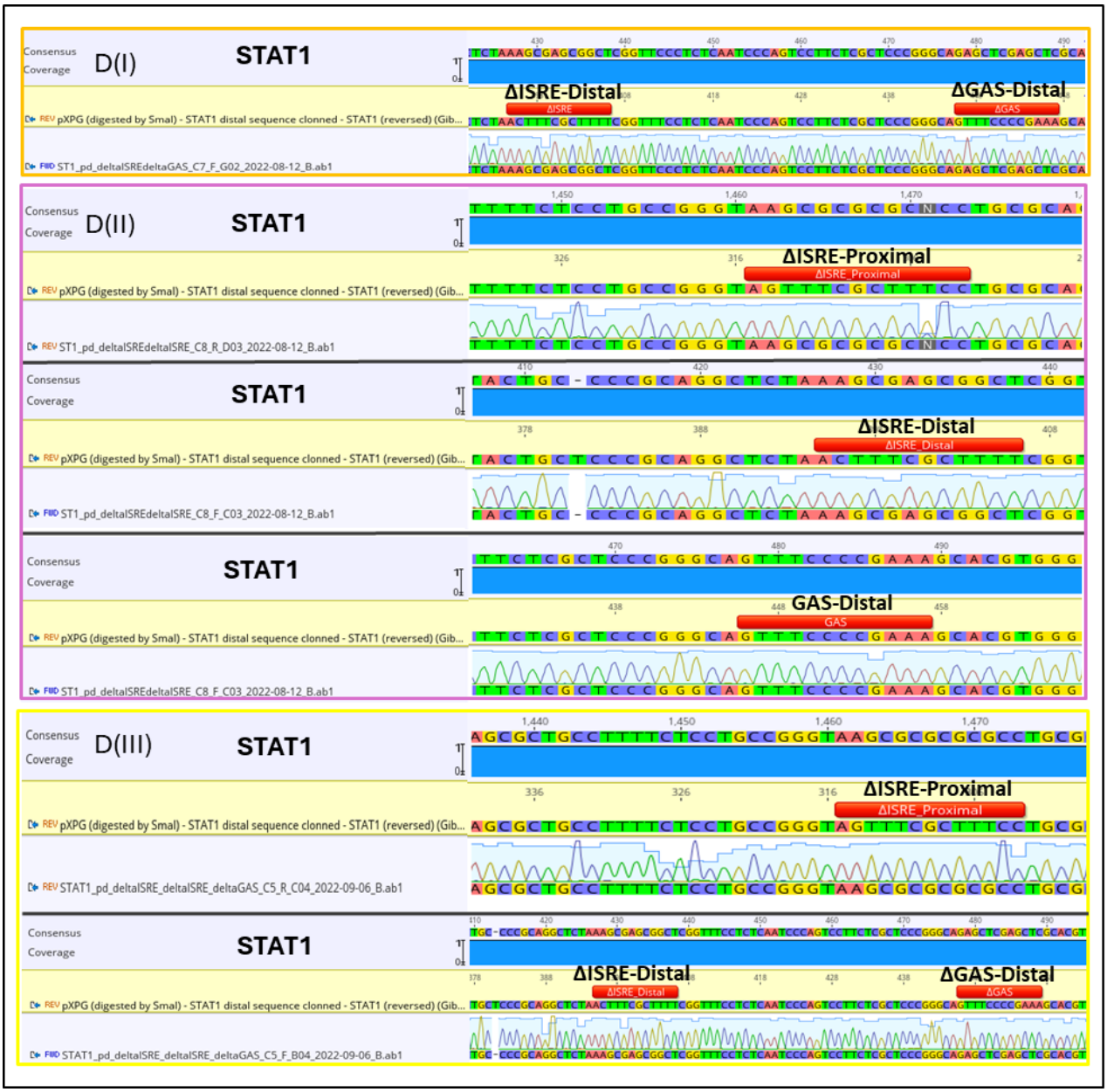

Figure S2. A data snapshot from the Geneious Prime program displaying mutations in ISRE and GAS motifs within the promoter fragments. The Sanger sequencing outcome underwent a comparison with constructs generated in- silico.

The red boxes indicate ISRE or GAS motifs in the in-silico model. Mutated ISRE or GAS motifs denoted by Δ. Confirmation via Sanger sequencing of the successful mutations in ISRE and GAS of PARP14 (AI-AV), DDX60 (BI,BII and BIII), NMI (CI, CII and CIII), STAT1(DI, DII and DIII) were achieved. For NMI and STAT1's promoter, constructs are delineated by border colors. For NMI (C): The red border signifies ΔISRE(1) constructs with unchanged ISRE(2) and GAS, green indicates ΔGAS constructs with unchanged ISRE(1) and ISRE(2), and blue represents constructs with simultaneous ΔISRE(1)/ΔGAS and unchanged ISRE(2). Regarding STAT1 (D): The orange border denotes constructs with distal ΔISRE/ΔGAS, purple illustrates distal ΔISRE/proximal ΔISRE constructs with unchanged distal GAS, and yellow signifies constructs with simultaneous distal ΔISRE/ΔGAS/proximal ΔISRE.

Abbreviations

ACE2- angiotensin converting enzyme-2

APC - antigen-presenting cell

ATRA-all-trans retinoic acid

BMDM - bone marrow-derived macrophages

CARD -caspase activation and recruitment domain

CCD - coiled-coil domain

cDC - classical dendritic cell(s)

cGAMP -cyclic guanosine monophosphate–adenosine monophosphate

cGAS -cyclic GMP-AMP synthase

ChIP - chromatin immunoprecipitation

CHIKV- chikungunya virus

DAMP - damage-associated molecular pattern

DBD - DNA-binding domain

DC - dendritic cell

EMCV- encephalomyocarditis virus

ESCs-embryonic stem cells

FDR - False Discovery Rate

GAF - γ-activated factor

GAS - γ-activated sequence

HCV-hepatitis C virus

HDV- hepatitis D virus

HEV-hepatitis E virus

HSPs- Heat Shock Proteins

IFN- interferon

IFNAR1 - IFNα-receptor subunit 1

IFNGR1- IFNγ-receptor subunit 1

IKKϵ -inhibitor of κB kinase

IL - interleukin

IRE - IRF-response elements

IRF – interferon regulatory factor

ISG - IFN-stimulated gene

ISGF3 - interferon-stimulated gene factor 3

ISRE - interferon-stimulated response element

JAK - Janus kinase

LPS – lipopolysaccharide

MAVS -mitochondrial antiviral-signaling protein

MDA5-melanoma differentiation-associated gene 5

MEFs-mouse embryonic fibroblasts

MHC -major histocompatibility complex

MTb-mycobacterium tuberculosis

MyD88-myeloid differentiation primary response protein 88

Mϕ – macrophage

NK - natural killer

NLS - nuclear localization signal

NO-nitric oxide

NTD- N-terminal domain

PAMP - pathogen-associated molecular patterns

PBMCs-human peripheral blood mononuclear cells

pDC - plasmacytoid dendritic cell(s)

PIAS-protein inhibitors of activated STATs

PKD2-protein kinase D2

PRR - pattern recognition receptors

PTPs-nuclear protein tyrosine phosphatases

RIG-G-retinoic acid-induced Gene G

RIG-I-retinoic acid-inducible gene-I

SH2 - Src homology 2 domain

SOCS - suppressor of cytokine signaling

STAT - signal transducer and activator of transcription

STING-stimulator of interferon genes

SUMO-small ubiquitin-related modifier

TAD - transactivation domain

TBK1-TANK-binding kinase 1

TF - transcription factor

Th1- T helper 1

TLR - toll-like receptor

TRAF6-tumor necrosis factor receptor-associated factor 6

TSS-transcription start site

TYK- tyrosine-kinase

U-ISGF3 - unphosphorylated Interferon-Stimulated Gene Factor 3

U-STAT - unphosphorylated-STAT

VSV - vesicular stomatitis Indiana virus

WT - wild-type

WNV - west nile virus

List of publications

1.Agata Sekrecka, Katarzyna Kluzek, Michal Sekrecki, Mahdi Eskandarian Boroujeni, **Sanaz Hasani**, Shota Yamauchi, Kiyonao Sada, Joanna Wesoly, Hans Bluyssen, **Time-dependent recruitment of GAF, ISGF3 and IRF1 complexes shapes IFNα and IFNγ-activated transcriptional responses and explains mechanistic and functional overlap. Cell. Mol. Life Sci. 80, 187, DOI: 10.1007/s00018-023-04830-8, (2023)**

2. Mahdi Eskandarian Boroujeni, Agata Sekrecka, Aleksandra Antonczyk, **Sanaz Hassani**, Michal Sekrecki, Hanna Nowicka, Natalia Lopacinska, Arta Olya, Katarzyna Kluzek, Joanna Wesoly, Hans A R Bluyssen. **Dysregulated Interferon Response and Immune Hyperactivation in Severe COVID-19: Targeting STATs as a Novel Therapeutic Strategy, Frontiers in Immunology, 13:888897; DOI: 10.3389/fimmu.2022.888897, (2022)**

3. Mahdi Eskandarian Boroujeni, Leila Simani, Hans A R Bluyssen, Hamid Reza Samadikhah, Soheila Zamanlui Benisi, **Sanaz Hassani**, Nader Akbari Dilmaghani, Mobina Fathi, Kimia Vakili, Gholam-Reza Mahmoudiasl , Hojjat Allah Abbaszadeh, Meysam Hassani Moghadda, Mohammad-Amin Abdollahifar, Abbas Aliaghaei, **Inflammatory Response Leads to Neuronal Death in Human Post-Mortem Cerebral Cortex in Patients with COVID-19, ACS Chem Neurosci. 12(12):2143-2150. DOI: 10.1021/acschemneuro, (2021)**

4. **Sanaz Hassani**, Agata Sekrecka, Michal Sekrecki, Katarzyna Kluzek, Yu-Ling Hsiao, Chien Kuo Lee, Anna Zimniewicz, Joanna Wesoly, Hans AR Bluyssen,

Mechanisms Governing ISRE+GAS Composite Gene Expression in Response to IFN-I and IFN-II.

Manuscript in progress.

Funding

This study was funded by grant number UMO-2016/23/B/NZ2/00623, which is focused on "Characterization of a Novel Intracellular Amplifier Circuit Regulating Long-Term Responsiveness to Type I and Type II IFNs."

The project was directed by Professor Hans Bluysse.

Acknowledgments

I am deeply grateful to my supervisor, Prof. Hans Bluyssen, for his consistent support, insightful guidance, and encouragement throughout my PhD journey. His expertise and mentorship have been invaluable in shaping my research and academic growth.

I would like to thank all my colleagues for their constant support and collaborative approach. Their willingness to share knowledge and offer assistance has significantly enriched my research experience. I would particularly like to extend my gratitude to Dr. Agata Sekrecka, Dr. Michał Sekrecka and Dr. Katarzyna Kluzek for their contributions, assistance and support.

I would also like to convey my appreciation to my friend Arta Olya, who patiently responded to my questions and supported me during tough times.

A heartfelt thank you goes to Prof. Lee and his team in Taipei for providing the invaluable opportunity to expand my expertise and knowledge. Especially, I would like to thank Yu-ling for her exceptional support and dedication. Their role in fostering a warm and welcoming atmosphere within the lab was instrumental in creating an environment where I could not only work effectively but also enjoy myself.

در نهایت، از صمیم قلب از والدین و خواهرم به خاطر محبت، تشویق، صبر بی‌پایان، درک و ایمانشان به من سپاسگزارم .فداکاری‌ها و ایثار آنها انگیزه‌ام را تقویت کرده و الهام‌بخش من در تلاش برای دستیابی به برتری در تحصیلاتم بوده است .از تأیید و انگیزه دائمی آنها که در رسیدن به اهدافم نقش اساسی داشته است، عمیقاً قدردانی می‌کنم .همچنین، از همسرم مهدی، برای حضور ثابت و حمایت‌های عاطفی‌اش در طول دوران دکتری‌ام به شدت سپاسگزارم .تشویق‌های مداوم و همراهی ثابت او بی‌قیمت بوده و در زمان‌های دشوار به من قدرت و آرامش داده است .حمایت او منبع دائمی الهام و انگیزه بوده .

Summary

IFNs are a group of cytokines responsible for performing antiviral activities. However, their critical function in differentiation and physiological processes is undeniable. IFN-I, IFN-II and IFN-III are the three main categories of IFNs and they act through binding cell-surface receptors. After interaction with their cell surface receptors, they trigger a kinase activation cascade, resulting in the dimerization of a specific group of proteins known as signal transducers and activators of transcription (STATs) including STAT1 and STAT2. Subsequently, GAF (STAT1 homodimer) and GAF-like (STAT1/STAT2 heterodimer) are able to induce GAS-containing ISGs (Interferon-stimulated genes) while ISGF3 (STAT1/STAT2/IRF9) and IRF1 activate the ISRE-containing ISGs. It is worth mentioning that IFN-I activates GAF, GAF-like, ISGF3 and IRF1, while IFN-II promotes the activation of GAF and IRF1. In addition to ISGs containing ISRE or GAS, the third group, known as ISRE+GAS-composite ISGs has a critical role in the immune system's adaptability against viral infections.

In this study, we examined transcriptional regulation of the ISRE+GAS composite genes in response to IFNα and IFNγ. Using high-throughput technologies like RNA-seq and ChIP-seq performed on Huh7.5 cells we identified a list of 89 ISRE+GAS-composite genes induced by IFNα or IFNγ. We also provided a list of 30 IFNα and IFNγ-commonly induced ISRE+GAS-composite genes in which genes were grouped by the ISRE/GAS distances.

Furthermore, based on the pSTAT1, pSTAT2, IRF9 and IRF1 binding profiles and gene expression patterns of these 30 ISRE+GAS-composite genes we further proved that there is no correlation between the ISRE/GAS distances or organization and their transcriptional regulation.

Additionally, our analysis using RNA-seq, ChIP-seq, and qPCR data from STAT1KO Huh7.5 cells further confirmed that the STAT2/IRF9 complex is the transcription factor responsible for regulating the expression of ISRE+GAS-composite genes in response to IFNα. Likewise, according to the binding profiles in WT cells and expression patterns of 13 pre-selected ISRE+GAS-composite genes in WT, STAT1, STAT2, IRF9, IRF1 and IRF1.9dKO cells, we were able to identify different mechanisms that govern the transcriptional regulation of ISRE+GAS-composite genes and further proved the switch ability between ISRE and GAS.

Site-directed mutagenesis (SDM) in combination with promoter-luciferase expression analysis conducted in WT and different KO Huh7.5 cells has provided evidence that ISRE is the most potent element in the promoter of ISRE+GAS-composite genes, especially in response to IFNα and the GAF, GAF-like, ISGF3, STAT1/IRF9, and IRF1 complexes work in close collaboration, even in the absence of direct interactions.

Antiviral assay results provided additional confirmation that ISRE-only and ISRE+GAS-composite ISGs are more effective compared to GAS-only containing genes in triggering antiviral responses and contribute to a more robust and efficient defense against viral infections.

Streszczenie

Interferony to grupa cytokin o aktywności przeciwwirusowej. Pełnią one również kluczową rolę w różnicowaniu komórek i procesach fizjologicznych. IFN-I, IFN-II i IFN-III to trzy główne kategorie interferonów, które działają poprzez wiązanie się z receptorami na powierzchni komórek. Po interakcji z receptorami na powierzchni komórek uruchamiają kaskadę aktywacji kinaz, co prowadzi do dimeryzacji specyficznej grupy białek, znanych jako przekaźniki sygnału i aktywatory transkrypcji (STAT), w tym STAT1 i STAT2. Następnie GAF (homodimer STAT1) i kompleks GAF-podobny (heterodimer STAT1/STAT2) są w stanie indukować ISG zawierające GAS (geny stymulowane przez interferon), podczas gdy ISGF3 (STAT1/STAT2/IRF9) i IRF1 aktywują ISG zawierające ISRE. Warto wspomnieć, że IFN-I aktywuje GAF, kompleks GAF-podobny, ISGF3 i IRF1, podczas gdy IFN-II promuje aktywację GAF i IRF1. Oprócz ISG zawierających ISRE lub GAS, trzecia grupa genów: ISG zawierające oba elementy, ISRE oraz GAS, odgrywa krytyczną rolę w adaptacji układu odpornościowego w odpowiedzi na infekcje wirusowe.

W tej pracy zbadaliśmy regulację transkrypcyjną genów zawierających ISRE+GAS w odpowiedzi na IFNα i IFNγ. Korzystając z technologii wysokoprzepustowych, takich jak RNA-seq i ChIP-seq, wykonanych na komórkach Huh7.5, zidentyfikowaliśmy listę 89 genów kompozytowych ISRE+GAS indukowanych przez IFNα lub IFNγ. Dostarczyliśmy również listę 30 genów ISRE+GAS indukowanych wspólnie przez IFNα i IFNγ, w których geny zostały pogrupowane według odległości ISRE/GAS.

Ponadto, na podstawie wiązania pSTAT1, pSTAT2, IRF9 i IRF1 oraz profiliekspresji tych 30 genów kompozytowych ISRE+GAS, udowodniliśmy, że nie ma korelacji między odległościami ISRE/GAS ani ich organizacją a ich regulacją transkrypcyjną.

Dodatkowo, nasza analiza danych RNA-seq, ChIP-seq i qPCR z komórek STAT1KO Huh7.5 potwierdziła, że kompleks STAT2/IRF9 jest czynnikiem transkrypcyjnym odpowiedzialnym za regulację ekspresji genów ISRE+GAS w odpowiedzi na IFNα. Podobnie, zgodnie z profilami wiązania w komórkach WT oraz profilami ekspresji 13 wybranych genów ISRE+GAS w komórkach WT, STAT1, STAT2, IRF9, IRF1 i IRF1.9dKO, byliśmy w stanie zidentyfikować różne mechanizmy rządzące regulacją transkrypcyjną genów zawierających ISRE+GAS i udowodnić zdolność przełączania się między ISRE a GAS.

Mutageneza ukierunkowana na określone miejsce (SDM), w połączeniu z analizą ekspresji lucyferazy promotora, przeprowadzona w komórkach WT oraz KO Huh7.5 dostarczyła dowodów, że ISRE jest najpotężniejszym elementem w promotorze genów ISRE+GAS, szczególnie w odpowiedzi na IFNα, a kompleksy GAF, GAF-podobny, ISGF3, STAT1/IRF9 i IRF1 ściśle ze sobą współpracują, nawet w przypadku braku bezpośrednich interakcji.

Wyniki testów przeciwwirusowych dostarczyły dodatkowego potwierdzenia, że ISG zawierające tylko ISRE oraz zawierające ISRE+GAS są skuteczniejsze w wywoływaniu odpowiedzi przeciwwirusowych, w porównaniu do genów zawierających tylko GAS, i przyczyniają się do silniejszej i efektywniejszej obrony przed infekcjami wirusowymi.